



# Prévisibilité des phénomènes convectifs intenses de l'échelle convective à l'échelle du climat régional

Olivier Nuissier

## ► To cite this version:

Olivier Nuissier. Prévisibilité des phénomènes convectifs intenses de l'échelle convective à l'échelle du climat régional. Météorologie. Institut National Polytechnique de Toulouse, 2016. tel-03374404

HAL Id: tel-03374404

<https://hal.science/tel-03374404>

Submitted on 12 Oct 2021

**HAL** is a multi-disciplinary open access archive for the deposit and dissemination of scientific research documents, whether they are published or not. The documents may come from teaching and research institutions in France or abroad, or from public or private research centers.

L'archive ouverte pluridisciplinaire **HAL**, est destinée au dépôt et à la diffusion de documents scientifiques de niveau recherche, publiés ou non, émanant des établissements d'enseignement et de recherche français ou étrangers, des laboratoires publics ou privés.

**Mémoire pour l'obtention du diplôme  
d'habilitation à diriger des recherches**

Présenté à L'INSTITUT POLYTECHNIQUE DE TOULOUSE  
Spécialité : Sciences de l'Univers, de l'Environnement et de l'Espace

par

**Olivier NUISSIER**

Chercheur du Développement Durable  
CNRM (UMR3589, Météo-France & CNRS)

**Titre :**

**Prévisibilité des phénomènes convectifs intenses  
de l'échelle convective à l'échelle du climat régional**

*Soutenue le 10 mai 2016 devant le jury composé de :*

**JURY**

**Véronique Ducrocq  
Sylvain Coquillat  
Heini Wernli  
Bodo Ahrens  
Cyrille Flamant**

**Directrice de recherche  
Rapporteur  
Rapporteur  
Rapporteur  
Examinateur**

Centre National de Recherches Météorologiques  
42, Avenue G. Coriolis, 31057 Toulouse, France



# Table des matières

<b>1 Curriculum Vitae</b>	<b>5</b>
1.1 Position actuelle et parcours professionnel . . . . .	5
1.2 Publications majeures pour la soutenance de l'habilitation à diriger des recherches	6
1.3 Activités . . . . .	105
1.3.1 Encadrement de chercheurs ayant permis l'obtention d'un diplôme . . . . .	105
1.3.2 Implication dans des projets nationaux et internationaux . . . . .	105
1.3.3 Autres activités . . . . .	106
1.4 Publications . . . . .	106
1.4.1 Publications dans des revues à comité de lecture . . . . .	106
1.4.2 Communications lors de congrès, conférences, séminaires, etc . . . . .	108
<b>2 Synthèse des travaux de recherche</b>	<b>113</b>
2.1 Introduction . . . . .	113
2.2 Connaissance et modélisation des systèmes précipitants intenses . . . . .	116
2.2.1 Connaissance et modélisation à méso-échelle des cyclones tropicaux . . . . .	116
2.2.2 Connaissance et modélisation des orages stationnaires des régions méditerranéennes . . . . .	120
2.2.3 Conclusions . . . . .	127
2.3 Régionalisation climatique des systèmes précipitants en régions méditerranéennes	129
2.3.1 Caractérisation des environnements météorologiques associés aux pluies intenses en Méditerranée . . . . .	129
2.3.2 Evolution des épisodes de pluies intenses dans la perspective d'un changement climatique . . . . .	134
2.3.3 Conclusions . . . . .	137
2.4 Prévisibilité à l'échelle convective des pluies intenses en Méditerranée . . . . .	139
2.4.1 Quantification des incertitudes de prévision : une approche en prévision d'ensemble (PE) . . . . .	139
2.4.2 Méthodes dédiées de prévisions d'ensemble pour l'échelle convective . .	140
2.4.3 Evaluation de systèmes de PE à l'échelle convective dédiés à la campagne HyMeX . . . . .	148
2.4.4 Conclusions . . . . .	151
<b>3 Synthèse et perspectives</b>	<b>153</b>



# Chapitre 1

## Curiculum Vitae

Olivier Nuissier,

40 ans,

Chargé de recherche du Développement Durable 1<sup>ere</sup> classe

CNRM

UMR3589, Météo-France & CNRS

42 av Coriolis

31057 TOULOUSE Cedex 1

olivier.nuissier@meteo.fr

### Diplômes

2003 : Thèse de l'Université Paul Sabatier, Toulouse III soutenue le 26 février 2003 (encadrement Frank ROUX) : "Simulations numériques de cyclones tropicaux à l'aide du modèle Meso-NH". Mention très honorable<sup>1</sup>

1999 : DEA Physique Chimie et Environnement, Institut National Pylotechnique de Toulouse. Mention Bien.

1998 : Maîtrise de Physique, Université des Antilles et de la Guyane, Guadeloupe. Mention Assez Bien.

1997 : License de Physique, Université des Antilles et de la Guyane, Guadeloupe.

1996 : DEUG Sciences de la Matière, Université des Antilles et de la Guyane, Guadeloupe.

### 1.1 Position actuelle et parcours professionnel

- **Janvier 2007-présent** : Chargé de Recherche du MEDDE affecté au CNRM-GAME (Météo-France et CNRS, UMR3589).
- *Octobre 2005-Octobre 2006* : Séjour Post-doctoral au CNRM-GAME, dans le cadre du projet national CYPRIM (Cyclogenèse et Précipitation Intenses en Méditerranée).

---

1. La mention "avec Félicitations du jury" n'est plus attribuée au sein de l'école Doctorale des Sciences de l'Univers, de l'Environnement et de l'Espace de l'Université Paul Sabatier

- Janvier 2005-Octobre 2005 : Séjour Post-doctoral au CNRM-GAME, dans le cadre du Projet Intégré du 6ème Programme Cadre Européen FLOODsite.
- Janvier-Octobre 2004 : Séjour Post-doctoral à l'Université de Miami, Rosenstiel School of Marine and Atmospheric Science, Floride, USA.
- Septembre 2001 : Visite scientifique au Hurricane Research Division, Miami, Floride, USA.

## 1.2 Publications majeures pour la soutenance de l'habilitation à diriger des recherches

- Bresson, E., Ducrocq, V., **Nuissier, O.**, Ricard, D. and de Saint-Aubin, C. (2012), Idealized numerical simulations of quasi-stationary convective systems over the Northwestern Mediterranean complex terrain. *Q.J.R. Meteorol. Soc.*, 138 : 1751–1763. doi : 10.1002/qj.1911
- Ducrocq, V., **Nuissier O.**, Ricard D., Lebeaupin C. and Thouvenin T., 2008 : A numerical study of three catastrophic precipitating events over southern France. II : Mesoscale triggering and stationarity factors. *Q.J.R. Meteorol. Soc.*, 134 : 131-145.
- Nuissier, O.**, Ducrocq V., Ricard D., Lebeaupin C. and Anquetin S., 2008 : A numerical study of three catastrophic precipitating events over southern France. I : Numerical framework and synoptic ingredients. *Q.J.R. Meteorol. Soc.*, 134, 111-130.
- Nuissier, O.**, Joly, B., Joly, A., Ducrocq, V. and Arbogast, P., 2011 : A statistical downscaling to identify the large-scale circulation patterns associated with heavy precipitation events over southern France. *Q.J.R. Meteorol. Soc.*, 137, 1812–1827.
- Nuissier, O.**, Joly, B., Vié, B., and Ducrocq, V. : Uncertainty of lateral boundary conditions in a convection-permitting ensemble : a strategy of selection for Mediterranean heavy precipitation events, *Nat. Hazards Earth Syst. Sci.*, 12, 2993-3011, doi :10.5194/nhess-12-2993-2012, 2012.
- Vié, B., Molinié, G., **Nuissier, O.**, Vincendon, B., Ducrocq, V., Boultier, F., and Richard, E. : Hydro-meteorological evaluation of a convection-permitting ensemble prediction system for Mediterranean heavy precipitating events, *Nat. Hazards Earth Syst. Sci.*, 12, 2631-2645, doi :10.5194/nhess-12-2631-2012, 2012.

## A numerical study of three catastrophic precipitating events over southern France. II: Mesoscale triggering and stationarity factors

V. Ducrocq,\* O. Nuissier, D. Ricard, C. Lebeaupin and T. Thouvenin  
CNRM/GMME, Météo-France, Toulouse, France

**ABSTRACT:** In the western Mediterranean basin, large amounts of precipitation can accumulate in less than a day when a Mesoscale Convective System (MCS) stays over the same area for several hours. Heavy Precipitating Events (HPEs) in this region (especially southern France) are not only characterized by significant precipitation rates (typically more than 200 mm in less than 24 or 48 hours) but also by quasi-stationary behaviour. The aim of this present study is to use realistic simulations of past events to analyze and better understand the physical mechanisms which lead to the stationarity of HPEs over southern France using a high-resolution (2.5 km) non-hydrostatic mesoscale atmospheric model. We focused on three HPEs: 13–14 October 1995 (the Cévennes case), 12–13 November 1999 (the Aude case) and 8–9 September 2002 (the Gard case).

The experimental design for simulating realistic structures and evolutions of the HPEs with the Meso-NH model has been presented in a companion paper. In that study, the evolution of the synoptic patterns in which the HPEs occurred were analysed. In this paper, the importance of mesoscale ingredients, such as the moist and conditionally unstable low-level jet (LLJ), is examined in terms of their ability to focus the deep convection over the same area for several hours. The Cévennes case is typical of a so-called ‘Cévenole’ event in France for which orographic forcing is the primary mechanism which acts to continuously generate convective cells upwind of the Massif Central. The unusual location of the Gard event is explained by a cold pool induced by the evaporation of precipitation which acts as a relief-like feature to force the conditionally unstable and moist LLJ to rise. This constitutes a quasi-stationary forcing as the cold pool is blocked in the Rhône Valley. For the third case, diabatic cooling and the Massif Central act to enhance the precipitation but have almost no impact on the location of the anchoring point of the precipitating system. Copyright © 2008 Royal Meteorological Society

KEY WORDS mesoscale convective systems; quasi-stationary behaviour; heavy precipitation; low-level cold pool

Received 21 August 2006; Revised 2 July 2007; Accepted 17 September 2007

### 1. Introduction

The continuous formation of convective cells in a specific area while older cells are dissipating downstream is the condition for which a Mesoscale Convective System (MCS) becomes stationary. This process first requires a triggering mechanism to release the convective available potential energy (CAPE) stored in the atmosphere, then a mechanism is needed to focus the convection over a relatively small area (Chappell, 1986). The synoptic-scale ingredients (upper-level potential vorticity (PV) anomalies, high atmospheric moisture content, CAPE, etc.) supply mass and energy for the convective activity, while other mesoscale factors contribute to continuously focus the necessary lifting to trigger and/or maintain the convection over the same region.

In the western Mediterranean region, the sea and the orography combine to form a strong surface component

which acts on the genesis and the evolution of MCSs. The sea provides the moisture supply to the moderate to strong, southerly to easterly, low-level flow that feeds the heavy precipitation events. The role of sensible and latent-heat fluxes from the Mediterranean Sea has been investigated by Buzzi *et al.* (1998) for the Piedmont flood event (1994). They found for their case-study that the Mediterranean mainly modulates the intensity and not the location of the convective precipitation. Similar results have been found in a recent numerical study by Lebeaupin *et al.* (2006) for three intense flash-flood episodes over southern France, which revealed that even though a uniform increase (or decrease) of Mediterranean sea-surface temperatures (SSTs) by a few degrees intensifies (or weakens) convection, fine-scale SST anomalies do not have any significant impact on the short-range forecast of convection and low-level jets (LLJs). Besides, the role of orography in triggering heavy precipitation over western Mediterranean regions has been well documented (e.g. Smith, 1979; Houze, 1993; Lin, 1993; Buzzi *et al.*, 1998; Buzzi and Foschini, 2000; Lin

\*Correspondence to: Dr V. Ducrocq, CNRM/GMME/ MICADO, 42 av. G. Coriolis, 31057 Toulouse Cedex, France.  
E-mail: veronique.ducrocq@meteo.fr

*et al.*, 2001; Rotunno and Ferretti, 2001; Pradier *et al.*, 2002; Bousquet and Smull, 2003; Georgis *et al.*, 2003, among others). All these studies have noted the importance of having a very moist and conditionally unstable LLJ impinging upon the mountain range foothills. The more the LLJ is perpendicular to the mountain range, the higher is the occurrence of heavy orographic rainfall. The CAPE stored in the atmosphere could be thus released only if the orographic lifting is strong enough to bring air parcels to their level of free convection. Considering both synoptic-scale forced and unforced cases, recent numerical studies (Buzzi *et al.*, 1998; Ferretti *et al.*, 2002; Stein, 2002) have emphasized that suppression of orography significantly reduces total simulated rainfall, clearly showing the orography as the first-order cause of floods. Buzzi *et al.* (1998) emphasized the feedback between latent heat release and orographic forcing that can determine the type of orographic flow regime (via ‘effective’ Froude number changes), thus influencing the larger-scale flow. Other studies also insist on the role played by the low-level convergence in producing heavy precipitation. Diagnostic studies and numerical experiments (cf. Ramis *et al.*, 1994, 1998) have revealed the importance of the meso-high induced over northeastern Spain where the Pyrenees chain causes a blocking effect under southerly flow. Low pressure centred just south of the region can help to enhance the offshore wind component and thus help to focus more convection over the coastal areas of northeastern Spain (Romero *et al.*, 2000). For the two severe convective events studied over eastern Spain, the importance of the surface meso-low driven by latent heat release, as well as lee cyclogenesis induced by the Atlas mountains, were shown to be providing low-level convergence over the Mediterranean Sea and thus enhancing upslope winds over eastern Spain.

In addition, there is also evidence of precipitation or convective feedbacks which interact with orography to contribute to rainfall enhancement. For convective systems, the evaporative/sublimative cooling produced by the falling precipitation reaching the sub-cloud layer may serve as an additional mechanism for convective cell formation. Both the combined effect of cold air outflows and orographic forcing have to be taken into account in the generation and evolution of quasi-stationary convective systems. Chu and Lin (2000) and Chen and Lin (2005a, 2005b) have shown this interaction through idealized simulations of a conditionally unstable flow over a two-dimensional mountain ridge. For one of their regimes, the density current resulting from the evaporation of precipitation may trigger new cells far upstream of the mountain, thus focusing the convective activity in this region.

As in many other western Mediterranean regions, southern France is prone to devastating flash floods during the autumn season. Two severe episodes occurred on 8–9 September 2002 (the Gard case) and 12–13 November 1999 (the Aude case). The precipitation total reached 690 mm in only 24 hours near the city of Alès (Gard department) in 2002, and more than 500 mm fell in the same period in Lézignan-Corbières (Aude

department) in 1999, both leading to the deaths of several tens of people and to several billion Euros in damages. A third case, which was less intense but more typical and representative of flash-flood episodes over southern regions of the Massif Central, occurred on 13–14 October 1995 (the Cévennes case) and is also investigated in this study. Note that the Gard event was not only characterized by persistent torrential precipitation, but also by an unusual location of the rainfall maximum, upstream of the Massif Central foothills. In part I of this study (Nuissier *et al.*, 2008), 10 km resolution numerical simulations were used to identify the main synoptic-scale ingredients responsible for favouring the development and the evolution of these three flash-flood events. Some synoptic-scale similarities and differences between the studied flash-flood events were described and discussed. The Gard and Aude episodes had a strong trough or a closed cyclone at upper levels, just west of the flooded regions. In addition to these common precursors aloft, a large supply of low-level moist air was being advected and convergence was enhanced by either a slow-moving cold front approaching from the west (the Gard case) or by a near-stationary low located to the southwest (the Aude case). Moreover, the best 2.5 km simulations were evaluated by comparing them against observations in order to corroborate that realistic simulations of the heavy precipitation events were being obtained and could be used to study the events in this companion paper. The purpose of this paper is to better explain the fine-scale processes relative to the internal dynamics of the simulated MCSs based on these fine-scale simulations. It is important to stress here that, in this study, we focused only on the stationarity stage of the convective systems with the goal of pointing out the physical mechanisms leading to the stationarity of these heavy precipitating systems over a specific location and, in particular, for the Gard event which occurred over an unusual region well upstream of the foothills.

Section 2 of this paper thus gives a detailed analysis of the high-resolution numerical experiments and details the key mesoscale factors leading to the sustaining of the MCSs at the same location over several hours. In section 3, further sensitivity experiments are discussed which confirm our hypotheses on the role of the orography and the convection itself in favouring the stationarity of these HPEs.

## 2. Detailed analysis of the mesoscale and convective-scale ingredients

Besides the synoptic-scale meteorological precursors described in part I which were conducive to heavy precipitation (upper-level divergence, upper-level PV anomalies, slow-moving patterns, etc.), there are also mesoscale and convective-scale factors that operate in making a MCS stationary. Among the various theories for explaining quasi-stationary behaviour of convective systems, there is, in particular, the Chappell (1986) conceptual scheme in which convective cells are forced to repeatedly

trigger over a given area and are generally transported downstream by the mean tropospheric flow. If new convective cells can regenerate at a rate compensating the advective speed of the older cells, then quasi-stationarity of the MCS occurs. Our goal in this study is to identify the different mesoscale processes leading to continuous regeneration of convection, based on the most realistic numerical simulations of our case-studies. The fine-scale patterns of the low-level conditions relative to the anchoring area during the mature stationary phase will be examined. We then take advantage of differences between MDA and REF2.5 simulations (Nuissier *et al.*, 2008) in terms of intensity (the Cévennes case) or location (the Gard event) which arise due to differences in their initial conditions. This analysis will permit us to underline some of these key mesoscale ingredients leading to the triggering and maintenance of a MCS at the same location. In order to point out the location of deep convective triggering and to suggest physical mechanisms explaining this location, backward trajectories are examined. Then

heat/water budgets associated with the simulated MCSs are used to explain the differences in the triggering mechanisms during the stationarity phase.

### 2.1. Low-level jet, convective instability and moisture inflow

Figures 1, 2 and 3 reflect that the simulations reproduce, on average for all three cases, a mesoscale environment conducive to deep convection, i.e. there is a moderate to strong southeasterly LLJ strengthening over the Gulf of Lion. The figures also depict two other important mesoscale ingredients (strong values of CAPE and lower-level water vapour flux) which are directly combined with the LLJ to focus the most active convection over the same area for several hours. For the three cases, the most active part of the MCSs (see simulated radar reflectivities in Figures 11(a), 16(a) and 19(a) of part I) was just downstream of the location where the low-level water vapour flux, CAPE, and the LLJ were simultaneously the strongest. Moreover, the focus of these low-level

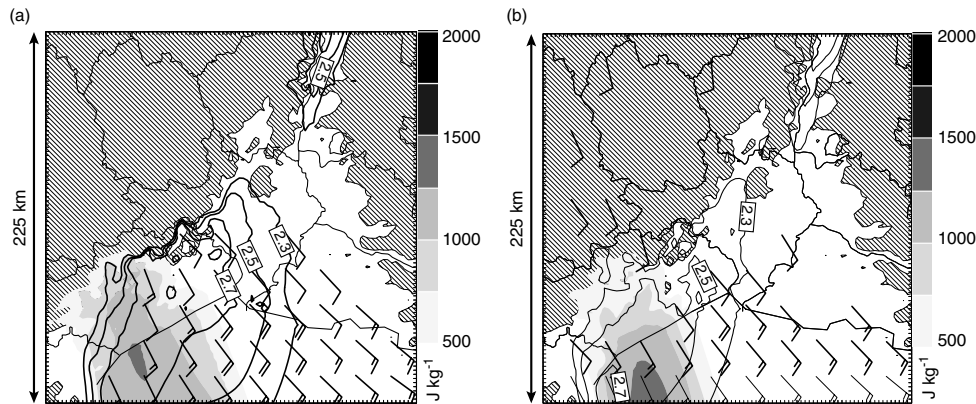


Figure 1. Simulated CAPE (shading) based on the most unstable parcel and water vapour flux integrated from the surface to 3 km altitude (solid contours,  $10^2 \text{ kg s}^{-1} \text{ m}^{-2}$ ) for the Cévennes case at (a) 03 UTC on 14 October, and (b) 06 UTC on 14 October 1995. Winds (barbs) at 10 m above ground level  $>5 \text{ m s}^{-1}$  are shown. Orography above 250 m is hatched.

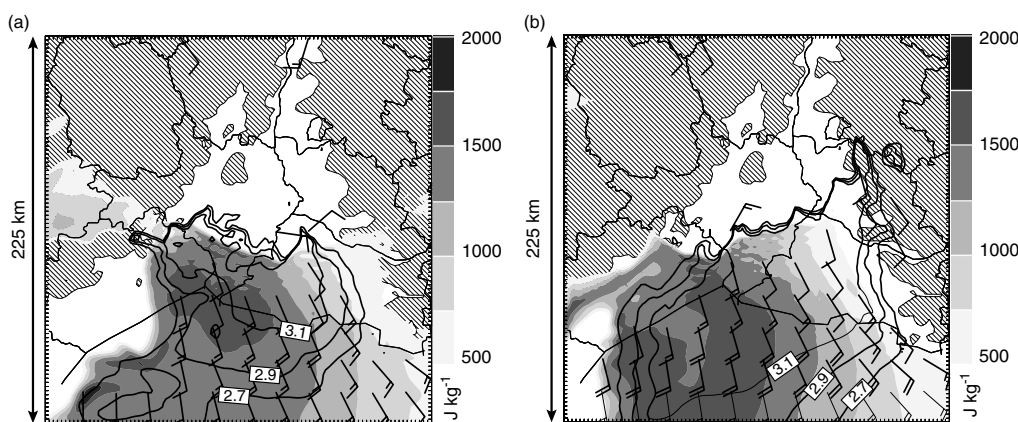


Figure 2. As Figure 1, but for the Gard case at (a) 18 UTC on 8 September and (b) 00 UTC on 9 September 2002.

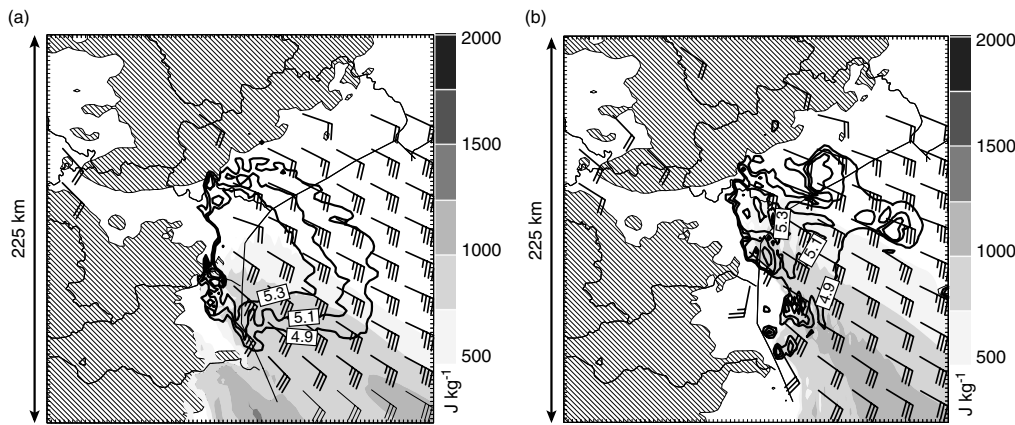


Figure 3. As Figure 1, but for the Aude case at (a) 21 UTC on 12 November and (b) 00 UTC on 13 November 1999.

mesoscale ingredients over the same area for several hours (Figures 1, 2 and 3) due to stationary large-scale conditions seems to be a key factor for sustaining the deep convective activity at the same location.

#### 2.1.1. Cévennes case

For the Cévennes case (Figure 1), the model simulated a moderate southerly low-level flow of about  $12 \text{ m s}^{-1}$ , extending from the sea inland over the Hérault department and which was co-located with the maximum low-level water vapour inflow. The strongest values of conditional instability of about  $1400 \text{ J kg}^{-1}$  were found directly south of Hérault and also upstream of the LLJ.

#### 2.1.2. Gard case

Conditional instability for the Gard event appeared to be at least as strong as in the Cévennes case, although of rather different spatial extent. Indeed, values of CAPE greater than  $1500 \text{ J kg}^{-1}$  covered a large part of the Gulf of Lion, locally reaching  $1800 \text{ J kg}^{-1}$  just south of the Gard department. Such strong conditional instability is explained by the slow-moving cold front (part I) which enhanced the convergence of the low-level moisture flow upstream of the Rhône valley. For the Gard case, Figure 2 also indicates a LLJ which was comparable in orientation and intensity to that simulated for the Cévennes case.

#### 2.1.3. Aude case

The LLJ simulated for the Aude case was at least twice as strong as those simulated for the Cévennes and Gard events and peaked near  $30 \text{ m s}^{-1}$  at the edge of the Aude department (Figure 3). Weaker values of CAPE were simulated for the Aude event than for the Cévennes and Gard cases, but they were counterbalanced by a very intense low-level moisture inflow of approximately  $600 \text{ kg s}^{-1} \text{ m}^{-2}$ . The low pressure system located over Spain (Figure 24(b) of part I) generated strong northward

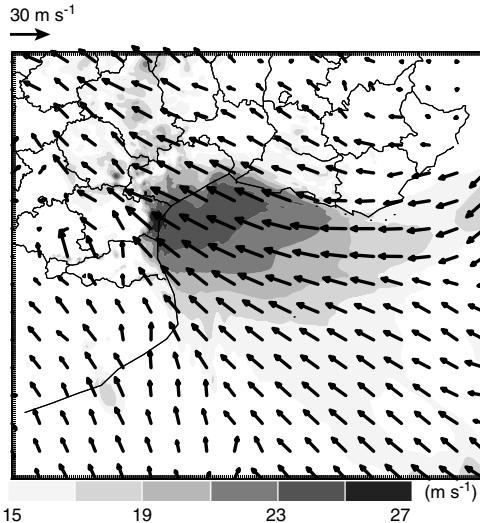


Figure 4. Simulated horizontal wind at 30 m above ground level for the Aude case at 21 UTC on 12 November 1999; shading represents horizontal winds  $>15 \text{ m s}^{-1}$ .

advection of warm and moist air giving significant low-level convergence of the moisture flux which maintained the convective activity over the Aude department. Furthermore, an interesting feature for the Aude case was the possible enhancement of the LLJ due to deflection effects, especially around the southern edge of the Alps (Figure 4).

## 2.2. Differences in initial conditions

#### 2.2.1. Cévennes case

During the morning and afternoon of 13 October 1995, an influx of maritime air occurred over the vicinity of the Massif Central, followed by convection off the Mediterranean coast, resulting in a moistening of the low troposphere. Nearly saturated air at 2 m was measured by the

mesonet stations along the Mediterranean coast and the eastern part of the Massif Central. The MDA procedure, applied at 22 UTC, included this information within the initial state of the MDA simulation. Figure 5(a) depicts the difference of the precipitable water (PW) and CAPE between the initial states obtained from the MDA procedure and the ARPEGE large-scale analysis (REF2.5) for the Cévennes case. While the large-scale analysis depicted less conditionally unstable and drier conditions at low levels, the MDA initial conditions resulted in an increase of the PW by up to 10 mm over the key region of the Massif Central foothills. Due at least in part to moister low levels, the CAPE was substantially increased (about  $2000 \text{ J kg}^{-1}$ ) over the Cévennes region (i.e. where the convective system developed). Stronger available convective energy favoured more intense and deeper updraughts than those simulated by the MDA experiment compared to the shallow and weak updraughts of the Ref. 2.5 experiment. Moreover, the area of maximum increase in CAPE was elongated along the south-eastern Massif Central foothills and the orographic forcing might help to more easily release this convective instability stored in the troposphere. In spite of that, the main impact of inclusion of mesonet surface data for this present case was not restricted to moistening of the lower region of the troposphere and increasing the convective instability. Indeed, Figure 5(a) reveals that the low-level flow has also been modified, with enhanced low-level convergence off the Mediterranean coast. It is clear that this increased low-level convergence acted as an additional mechanism to lift air parcels to their condensation level or their level of free convection.

### 2.2.2. Gard case

Figure 5b illustrates differences in the initial conditions for the Gard case between the ARPEGE large-scale analysis (Ref. 2.5) and the improved conditions with the MDA procedure. The difference of CAPE is superimposed on the virtual potential temperature,  $\theta_v$ , field.  $\theta_v$  is a quantity which is generally related to the density of air masses and is well suited to identify the cold pool generated by convective systems.

The MDA procedure introduced a fairly strong low-level cooling in  $\theta_v$  (about  $4\text{--}5^\circ\text{C}$ ) along the Rhône Valley, due to the lower observed 2 m temperature in this area at noon. Indeed, as deep convective cells formed and progressed inland in the morning of 8 September, the 2 m temperatures decreased beneath the convective system. The previous convection had also moistened the region, as indicated by a 30% moisture surplus in the corrected initial conditions with respect to the large-scale analysis (not shown). In other words, the inclusion of mesoscale surface data contributed to a better estimation of the cooling beneath the storms, which may have acted as an additional forcing ingredient to trigger the convection. Similar to the Cévennes case, the impact of including mesoscale surface data through the MDA procedure can be also found in terms of convective

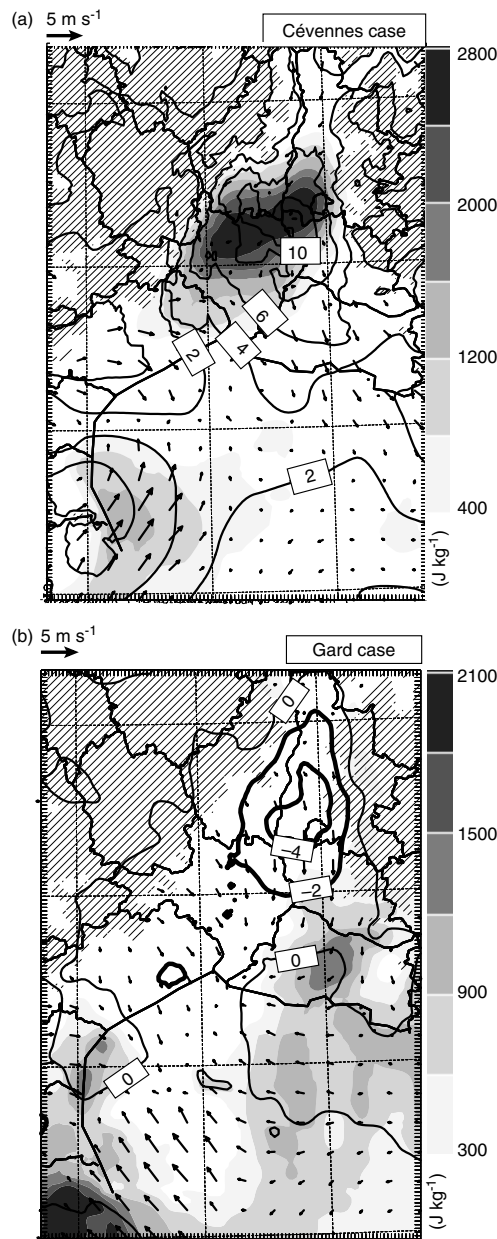


Figure 5. Difference between the initial states from the MDA procedure and the ARPEGE large-scale analysis for (a) the Cévennes case with precipitable water (solid contours), CAPE (shading) based on the most unstable parcel, and wind at 500 m above ground level (arrows), and for (b) the Gard case with CAPE (shading), virtual potential temperature ( $^{\circ}\text{C}$ , solid contours) and 10 m AGL wind (arrows).

instability. Indeed, Figure 5(b) displays an increase of CAPE of about  $800 \text{ J kg}^{-1}$  on both the eastern and the western sides of the tongue of relatively large CAPE shown in Figure 2.

### 2.3. Backward trajectories

In order to better understand the dynamic basis for the common mesoscale forcings associated with the stationarity of the case-studies, and to document the evolving vertical structure, a series of backward trajectories were performed for the different experiments. The Lagrangian trajectory tool is described in Gheusi and Stein (2002). A few Lagrangian parcels were selected inside the mature simulated MCSs near the tropopause level, i.e. at 11, 10, and 9 km altitudes, for the three cases. In all three cases, parcels taken in the upper troposphere in the cloud plume of the MCSs originated from lower levels at about 1 or 2 km above the Mediterranean Sea or Spanish coast. The rapid ascents correspond to strong upward motions within the deep convective cells which lifted the parcels from near the surface up to the tropopause. Finally, at the end of their tracks, parcels were generally transported northwards due to the mid-to-upper southerly mean flow that prevailed during these events. There are many similarities in the tracks of the Lagrangian parcels for the three cases, but differences occurred in the locations of deepest convective activity. This will be described in more detail in the following sub-sections.

#### 2.3.1. Cévennes case

For this case, the condensation occurred and the first shallow clouds formed over the sea in an area where the low-level convergence was significant as evidenced by the converging trajectories (Figure 6(a)). The cloudy cells then moved northeastwards toward the flood location. The main lift for the release of the convective instability occurred when the cells reached and impinged upon the first Massif Central relief; they became deep convective cells with strong upward motion reaching the tropopause level (Figure 6(b)). The time evolution of the convective cells within the MDA simulation (not shown) confirms that new cells repeatedly formed within the low-level convergence area or just at the first Massif Central relief which is only a few hundred metres high. Therefore, it is possible to say that in the specific Cévennes case, orographic forcing acted to continuously generate new convective cells upwind of the Massif Central and thus maintain the stationarity of the MCS over the region. This behaviour is very similar to what was found in southerly flow near the Alps (e.g. Medina and Houze, 2003).

#### 2.3.2. Gard case

For this case, the back trajectories do not show low-level convergence over the Mediterranean Sea (Figure 7(a)). This case also differs from the Cévennes case in the location of the deepest convective activity. Indeed, the associated strongest upward motions were found over the central plains of Gard, well upstream of the first relief of the Massif Central. It is argued that, for this specific case, there is another mesoscale ingredient apart from the orographic forcing leading to the continuous triggering of strong convection. A low-level cold pool (LLCP)

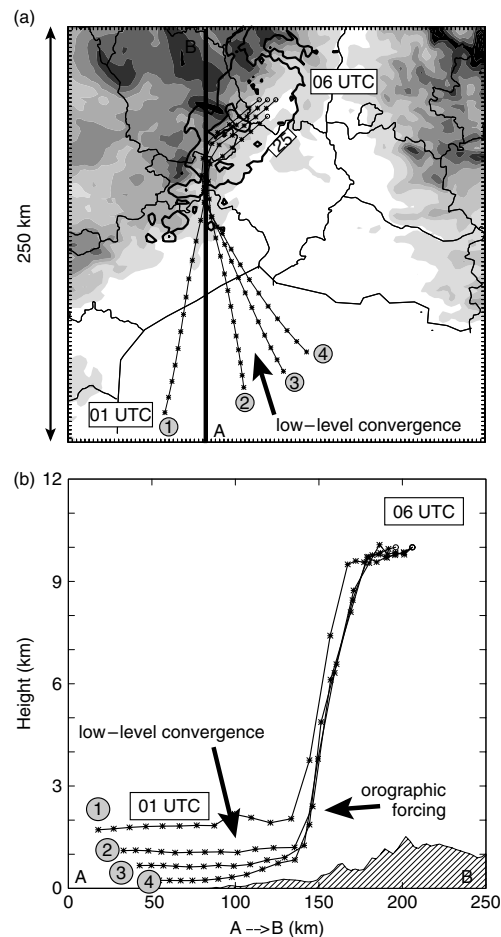


Figure 6. (a) Backward trajectories for the MDA experiment for the Cévennes case from 06 UTC to 01 UTC on 14 October 1995. 2.5 km resolution orography is shaded, with contour interval 200 m, starting at 200 m. The simulated radar reflectivity at 2 km altitude (bold contour for 25 dBZ) is at 03 UTC. (b) represents a projection of the trajectories along the vertical cross-section AB in (a). Stars on the backward trajectories are spaced at 15-minute intervals.

was analysed forming just under the simulated MCS, which is clearly visible in the simulation through the low values of  $\theta_v$  (about 4–5 °C lower than the environment; Figure 7(b)). The observed 2 m temperatures confirm the existence of this cold pool beneath the convective system. Both the simulation and the observations showed unsaturated low levels, meaning that precipitation falling in the lower troposphere could easily evaporate and thus maintain and/or strengthen the cooling beneath the storms. The LLCP played a role of a relief-like feature by blocking the warm and moist LLJ and pushing the deep convection upstream; the LLCP acted as the main mesoscale ingredient for triggering deep convection. In order to better understand the role of the LLCP, backward trajectories were also performed by following some parcels in the lower troposphere (200 m altitude) just

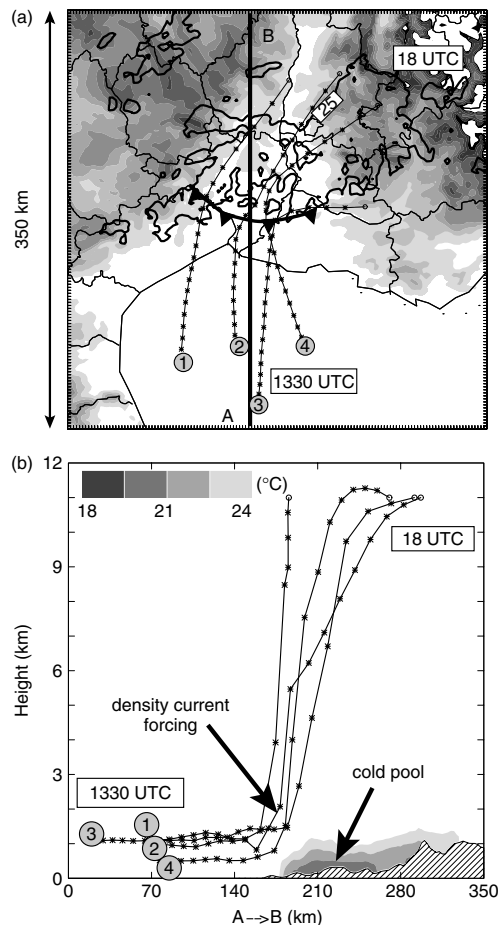


Figure 7. As Figure 6, but for the MDA experiment for the Gard case, with trajectories from 18 UTC to 1330 UTC on 8 September 2002. In (b), the shaded areas represent the simulated virtual potential temperature.

downstream of the deep convection area (Figure 8). It is clear that there was downward motion immediately above the LLCP with significant downdraughts originating in the mid-troposphere (Figure 8(b)). Furthermore, an analysis of relative humidity (not shown) in the area of origin of the parcels seen in Figure 8 indicated that mid-tropospheric dry air located farther south of the flood area could be mixed into the lower levels over the Gard region thus facilitating the rainfall evaporation.

### 2.3.3. Aude case

In some of the back trajectories obtained for the Aude case (Figure 9), strong ascent associated with deep convection occurred slightly inland over relatively flat regions. However, orography might be a source of lifting for this specific Aude case. Indeed, parcel 1 in Figure 9(b) seems to be lifted along the upslope of the small hill located near 140 km. Parcels 2 and 4 were lifted to the lee

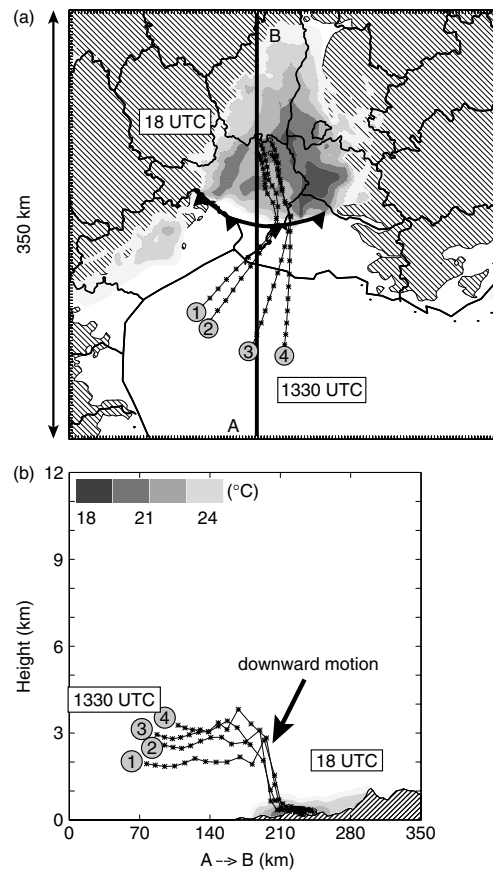


Figure 8. As Figure 6, but for the MDA experiment for the Gard case, with trajectories from 18 UTC to 1330 UTC on 8 September 2002 within the low-level cold pool. Orography above 250 m is hatched. Shaded areas in (b) represent the simulated virtual potential temperature.

of this hill, perhaps in association with a hydraulic-jump-like feature. However, despite evidence of a significant signal of synoptic forcings such as larger-scale lifting, the influence of the mesoscale ingredients discussed above will be described in more detail in the following sections.

### 2.4. Water/heat budgets of the MCS

In order to better understand the different mechanisms leading to the occurrence of the LLCP and to quantify the cooling beneath the convective system, water/heat budgets were performed within the simulated MCSs. Figure 10 shows the one-dimensional budgets of the potential temperature,  $\theta$ , for the three simulated MCSs near their mature stages and the surface virtual potential temperature,  $\theta_v$ , for only the Gard case at 18 UTC on 8 September 2002. The different terms of the budgets have been averaged over a 15-minute period in the precipitating areas associated with the MCSs.

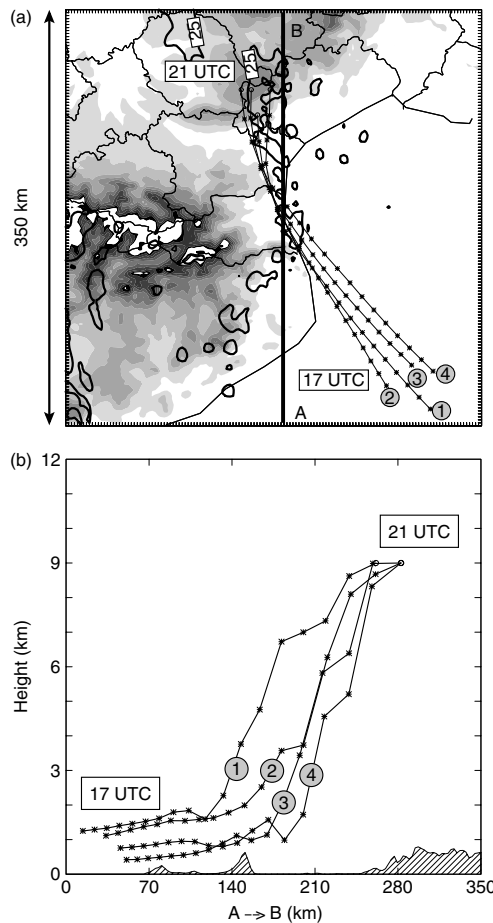


Figure 9. As Figure 6, but for the Ref. experiment for the Aude case, with trajectories from 21 UTC to 17 UTC on 12 November 1999.

Figure 10(a) shows that the main cooling observed below about 2 km altitude results from evaporation of rainfall in this region. The cooling is the most significant for the Gard case, near  $3 \text{ K h}^{-1}$  at 500 m altitude, whereas for the Cévennes event it is much less pronounced with values not exceeding  $1 \text{ K h}^{-1}$ . This is in agreement with nearly saturated low levels for the Cévennes case which do not favour evaporation of liquid water. The layer in which the cooling due to evaporation of liquid water occurs is the deepest for the Gard case. The results for the Aude case show a range in values of cooling due to rainfall evaporation between those for the previous cases. A contribution to the cooling of the melting of ice species around the freezing levels (about 2 km altitude, depending on the season) is also visible for the three cases (Figure 10(b)). Above, cooling due to sublimation of ice species is the most significant for the Cévennes case, whereas it is almost zero for the Aude case (Note that warming due to microphysical processes such as deposition and condensation is not shown in these

figures). Budgets of microphysical species (not shown here) bear out that the evaporation process is a large sink of liquid water in the lower layers for the Gard event and therefore help in creating a significant LLCP (lower  $\theta_v$ ) just beneath the MCSs (Figure 10(d)), confined in the Rhône valley between the Massif Central and the Alps.

### 3. Discussion

Based on the results of the previous simulations, it has been inferred that mesoscale ingredients such as the Massif Central relief and/or the LLCP could have been relevant for at least two of our case-studies (Gard and Cévennes). In order to compare and check the importance of these different forcings on the stationarity of our case-studies, we performed a series of sensitivity experiments considering the best simulation (MDA for the Cévennes and Gard cases; REF2.5 for the Aude case) as the control experiments (called CTRL hereafter). Two sets of sensitivity experiments were performed by modifying the Meso-NH microphysical parametrization and the orography both in the 10 and 2.5 km resolution domains. Concerning diabatic effects, we removed the evaporative cooling of liquid water in a first experiment (NOC) and then, in a second simulation, cooling of both the evaporation of liquid water and the sublimation of ice hydrometeors (snow and graupel) were switched off (NOCS).

These modifications were applied on a box centred over and including only the simulated MCSs in order to generate the least possible disturbances in the environment. As we have seen in the previous section, the simulation as well as the observations displayed almost no cooling beneath the storm, so no NOC experiment was performed for the Cévennes case. Finally, a last set of experiments were performed in which the Massif Central relief was removed (NOR), while the Alps and Pyrenees were kept as they are in the model domains.

#### 3.1. On the role of the LLCP

##### 3.1.1. Gard case

For this event, the results of the NOC and NOCS experiments differ considerably from the CTRL one. Figure 11 displays the simulated accumulated rainfall for the NOC and the CTRL experiments from 18 to 22 UTC on 8 September 2002, and the differences between the two simulations for the 10 m AGL wind and the  $\theta_v$  at 22 UTC, 8 September. Figure 11(a) shows that the simulated MCS in NOC loses its stationarity over the Gard plains and the resulting precipitation pattern is significantly shifted northwestwards over the Massif Central foothills, with a maximum rainfall amount about of 120 mm over the Ardèche department. Figure 11(b) clearly shows that the cooling induced by the evaporation of liquid water is the main mechanism leading to the maintenance of the LLCP. Indeed, the differences in  $\theta_v$

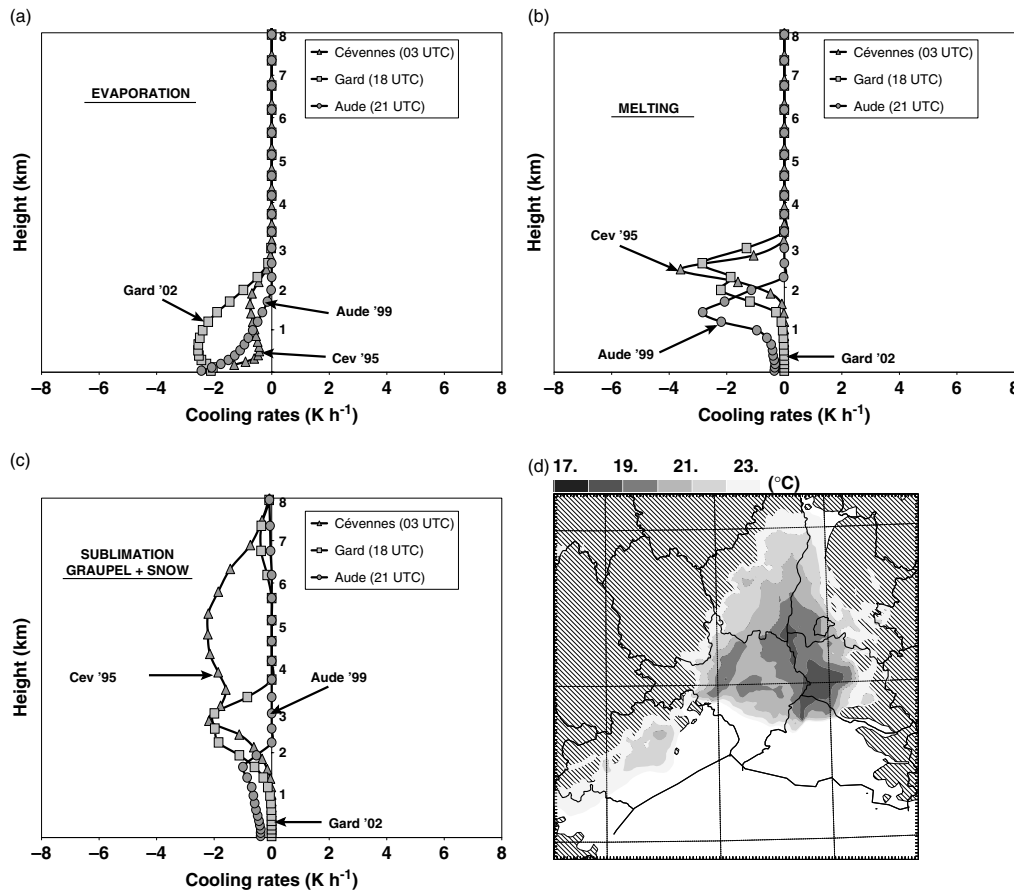


Figure 10. One-dimensional budgets of potential temperature performed over the three different precipitating systems for the simulated MCSs near the mature stage for (a) the evaporation of liquid precipitation, (b) the melting of icy species, and (c) the sublimation of graupel and snow. (d) shows the virtual potential temperature at 30 m AGL for the Gard case at 18 UTC on 8 September 2002, with orography hatched above 250 m.

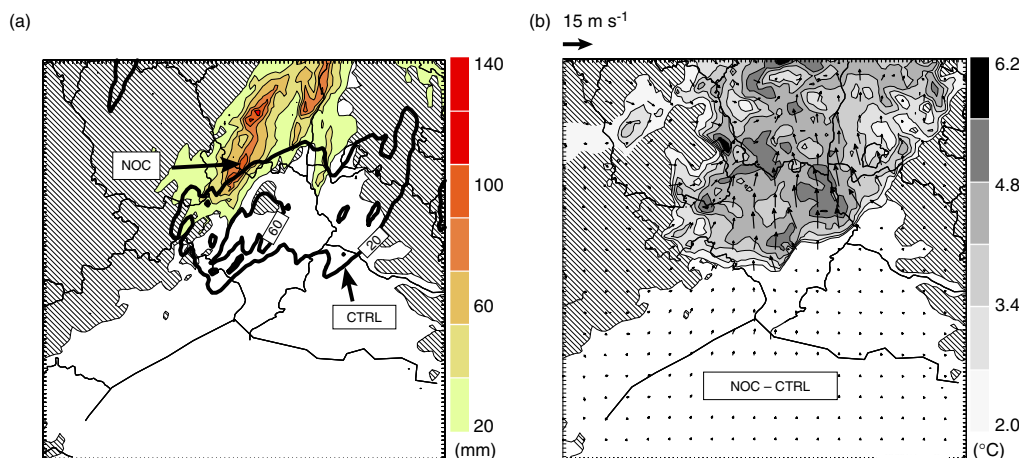


Figure 11. NOC and CTRL experiments for the Gard case: (a) the simulated accumulated rainfall from 18 to 22 UTC on 8 September 2002 (NOC shading and CTRL bold contours); (b) differences between the two experiments in  $\theta_v$  (shading) and 10 m AGL wind (arrows) at 22 UTC. Orography above 250 m is shown hatched. This figure is available in colour online at [www.interscience.wiley.com/qj](http://www.interscience.wiley.com/qj)

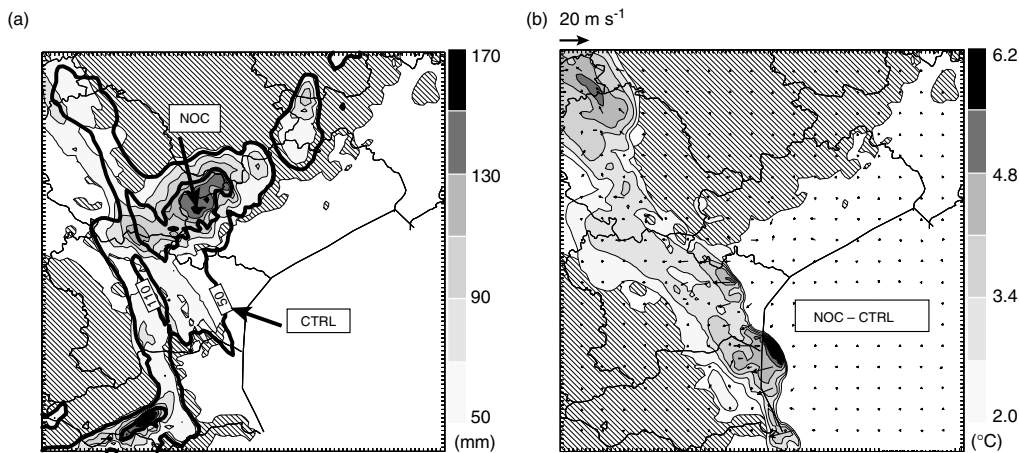


Figure 12. As Figure 11, but for the Aude case, from 12 UTC on 12 November to 00 UTC on 13 November 1999.

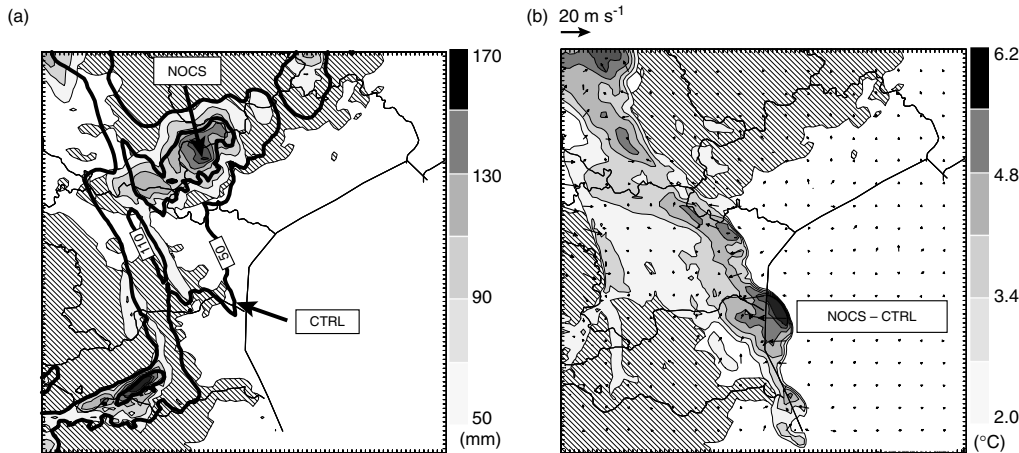


Figure 13. As Figure 12, but for the Aude case for NOCS and CTRL experiments, from 12 UTC on 12 November to 00 UTC on 13 November 1999.

between the NOC experiment and the CTRL run show a strong warming of about 4–5 °C in the lower troposphere, indicating that the NOC simulation fails to sustain any LLCP. In NOC, the warm and moist LLJ also extends further north than it did in the CTRL experiment, up to the Ardèche department (i.e. over the Massif Central flanks). Clearly, it is demonstrated through this sensitivity test that the cooling beneath the storms is the main mesoscale ingredient which makes the MCS stationary over the Gard plains rather than over the Massif Central foothills, as might be expected from climatology.

### 3.1.2. Aude case

Regarding the cooling beneath the storms, the Aude case is intermediate between the Cévennes and the Gard cases. Removing the diabatic cooling associated with the evaporation of liquid rainwater does not significantly

modify the location of the system (Figure 12(a)). Indeed, the maximum rainfall peaks moved only a few kilometres inland and this feature is associated with a slight westward extension of the LLJ (Figure 12(b)). Diabatic cooling for this specific case acts mainly to enhance the rainfall intensity by reinforcing the low-level convergence at the leading edge of the convective line. The results obtained from the NOCS experiment for the same period (Figure 13) confirm the important role played by the cooling induced by evaporation of liquid and frozen precipitation produced by the convective system itself in enhancing the rainfall amounts. Indeed, when cooling from both evaporation of liquid water and sublimation of ice hydrometeors is turned off, precipitation almost disappears over the flat areas of the Aude department and heavy rainfall persists only over the southern mountainous end of the Massif Central (Figure 13(a)).

### 3.2. On the role of orography

For the three cases, the Massif Central has been removed from the model domains to evaluate the general role of this mountain range (NOR experiments).

#### 3.2.1. Cévennes case

Figure 14(a) and (b) show significantly different precipitating structures of the MCSs in the two simulations (NOR and CTRL) for the Cévennes case. In the NOR experiment, rainy cells still form within the low-level convergence area, but their vertical extent is limited, not exceeding 6 km in altitude (not shown). Moreover, they do not form any organized or quasi-stationary MCS. Removal of the Massif Central orography (especially the southeastern flanks of the mountain) significantly reduces the rainfall totals (Figure 14(c)). NOR clearly shows the key role of the Massif Central in this specific case in forcing the LLJ to lift and its main triggering role for the heavy precipitation.

#### 3.2.2. Gard case

For the Gard case, Figure 15(a) and (b) highlight the main differences of MCS structure. In the NOR experiment, the simulated convective system leaves the Gard plains and moves northwards. At 21 UTC, 8 September 2002, the western part has dramatically weakened, and only its eastern region still exhibits intense reflectivities (Figure 15(b)). Associated with the motion of the system, the LLJ strengthens and progress further inland, up to 100 km north and northwestward, than in the CTRL run. The LLCP weakens and spreads northwestwards due to the lack of Massif Central relief (Figure 15(b)). The simulated rainfall for the NOR experiment is significantly decreased, especially over the western Gard region, where simulated precipitation reaches only about 40 mm compared to more than 100 mm in the CTRL run (Figure 15(c)). Therefore, for this specific Gard case, the NOR experiment shows that the stationarity of the MCS can be explained by: (i) the generation of the cold pool facing and blocking the warm and moist low-level jet while (ii) the cold pool in turn is maintained in place in the Rhône valley between the Massif Central and the Alps.

#### 3.3. Aude case

The impact on stationarity of removing the Massif Central relief is quite different in the Aude case than in the Cévennes and Gard cases. Indeed, at 21 UTC, 12 November 1999, the NOR experiment for the Aude case displays a significant convective line, and does not show any significant difference in the location of the convective system (Figure 16(a) and (b)). Nevertheless, simulated rainfall amounts are reduced; peak values are 210 mm in NOR against 280 mm in CTRL (Figure 16(c)). For this specific case, the Massif Central mountain probably acts to enhance the intensity of the rainfall by channelling

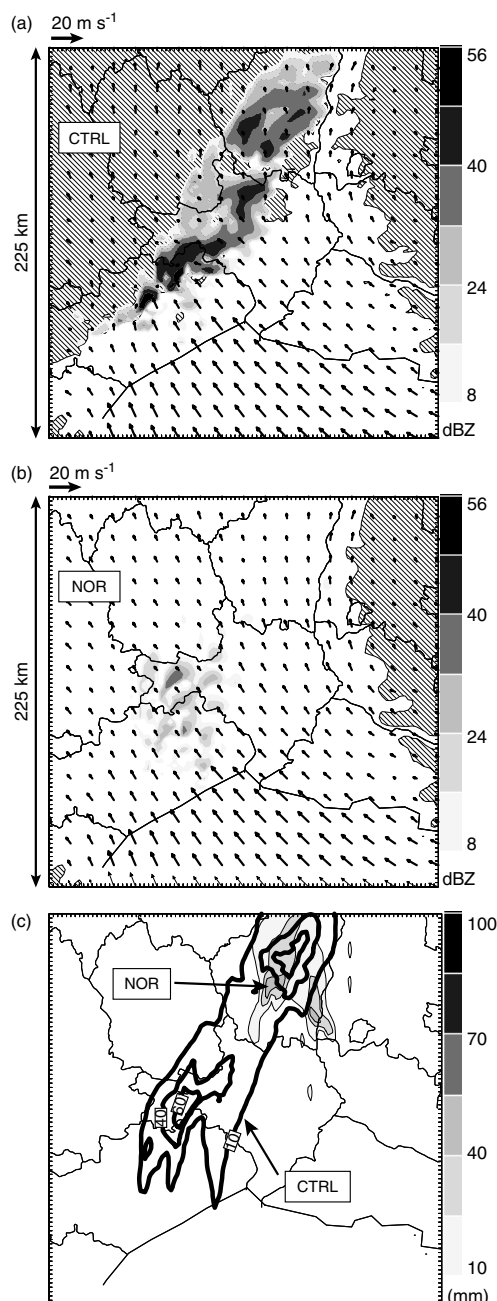


Figure 14. Simulated radar reflectivities (shading) at 2 km altitude and the 10 m AGL wind at 03 UTC on 14 October for the Cévennes case for (a) the CTRL and (b) the NOR experiments. Hatching shows the topography above 250 m. (c) displays the simulated accumulated rainfall from 00 to 06 UTC on 14 October 1995 for the NOR (shading) and the CTRL (bold contours) experiments.

the warm and moist LLJ between the eastern portion of the Pyrenees and the southern end of the Massif Central orography.

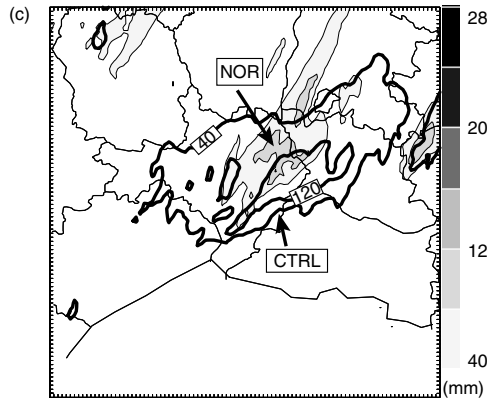
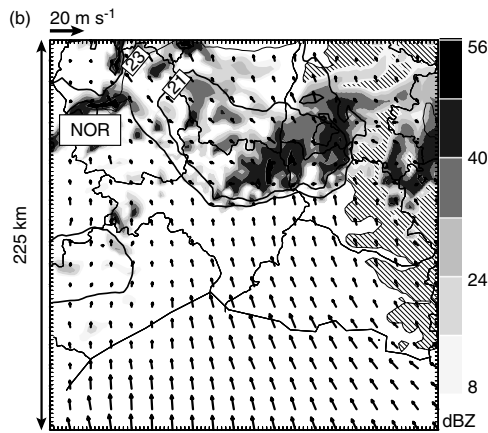
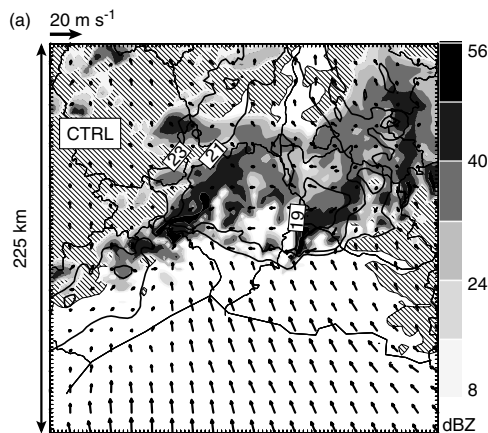


Figure 15. As Figure 14, but for the Gard case. Time for (a) and (b) is 21 UTC on 8 September 2002, and the period in (c) is from 12 to 21 UTC on 8 September.

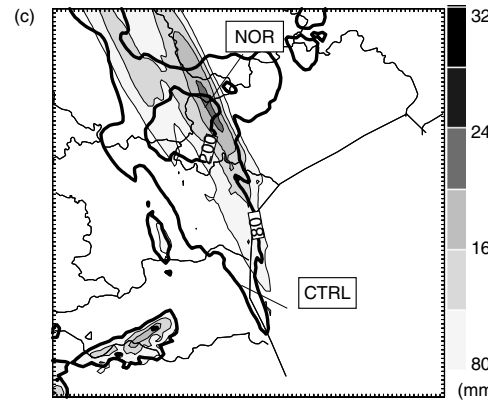
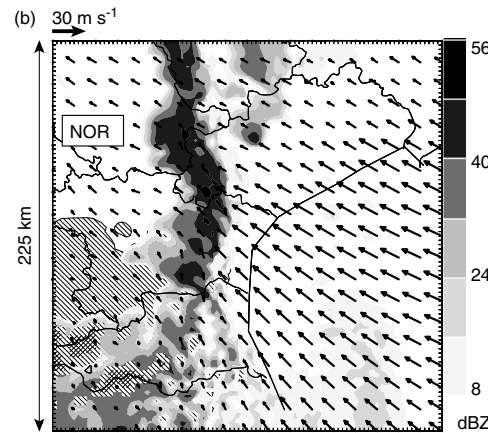
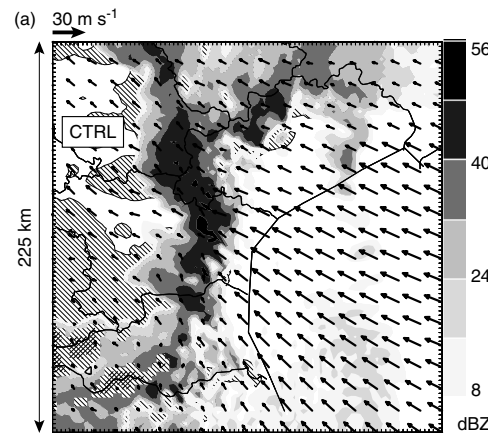


Figure 16. As Figure 14, but for the Aude case. Time for (a) and (b) is 21 UTC on 12 November 1999 and the period in (c) is from 12 UTC on 12 November to 06 UTC on 13 November.

#### 4. Synthesis and conclusions

Three representative cases of HPEs over southeastern France have been investigated in these two papers. Two extreme flash-flood episodes (with very large rainfall

totals exceeding 500 mm in 24 hours) on 8–9 September 2002 and 12–13 November 1999, respectively, and a more typical event for the Cévennes region (13–14 October 1995) have been presented. High-resolution simulations (2.5 km horizontal resolution) of these three events

using the French Meso-NH non-hydrostatic mesoscale numerical model have helped to understand the fine-scale processes relative to the internal dynamics of the convective systems and they have clearly highlighted the mechanisms leading to the stationarity of the HPEs, which has been the main goal of this present paper.

A set of numerical experiments (REF2.5) with initial conditions coming from the large-scale analysis have

been used for one test and, in another one (MDA), additional ingredients have been added using a Mesoscale Data Analysis (Nuissier *et al.*, 2008). The best simulation for each case has been used to emphasize the triggering and/or enhancing mesoscale factors for deep convection in order to understand better the physical mechanisms which lead to quasi-stationarity of these HPEs. When comparing the two sets of initial conditions for the

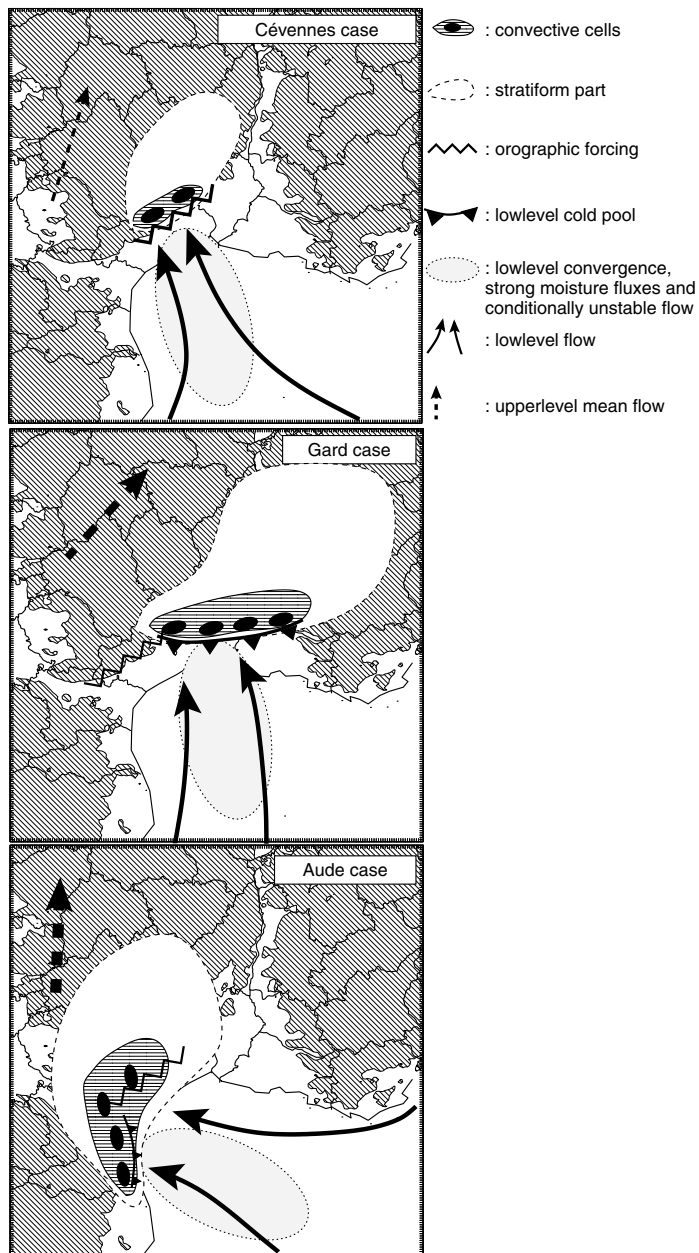


Figure 17. Schematic drawings of the precipitating structures of the MCSs and the mesoscale triggering and stationarity ingredients for the flash-flood events at Cévennes (13–14 October 1995), Gard (8–9 September 2002), and Aude (12–13 November 1999).

Cévennes case, strong moistening of the low levels (due to an influx of maritime air) significantly increased the CAPE along the southeastern Massif Central foothills (the Cévennes region) in the MDA experiment. Stronger available convective energy together with orographic forcing thus favoured more intense and deeper updraughts in this simulation. The MDA procedure impacts on the Gard case by introducing a low-level cooling of about 4–5 °C in  $\theta_v$  over the Rhône Valley due to the presence of the convective system at this time. The assimilation of mesonet surface data for this specific case introduced this cooling which is a possible mechanism for triggering further deep convection.

Figure 17 shows a synthesis for the three cases of mesoscale and convective-scale factors conducive to long-lasting back-building quasi-stationary MCSs. For all three cases, the best simulations depict a mesoscale environment conducive to deep convection, i.e. a strong easterly to southerly low-level flow strengthening over the Gulf of Lion. However, other important mesoscale ingredients such as high CAPE and low-level moisture flux are directly associated with the LLJ and act to focus the deep convection development over the same area over several hours. The low-level simulated conditions for the three cases indicate that the location of the convective part of the different MCSs is directly correlated with the area where the three mesoscale ingredients (water vapour flux, CAPE and LLJ) are simultaneously strongest. Deflection of the low-level flow by the neighbouring mountain ranges acts to enhance the LLJ and the low-level convergence. The focus of these low-level mesoscale ingredients upstream of the flood area appears to be a crucial factor for maintaining the deep convective activity at the same location.

Moreover, backward trajectories have highlighted the triggering mesoscale factors for deep convection. For the Cévennes case, the first cloudy cells form over the sea where low-level wind convergence is significant, then they are advected by the southerly flow toward the Massif Central foothills. Deep convection is triggered or enhanced when the cells reach and impinge upon the first Massif Central foothills. Therefore, orographic forcing is the primary mechanism which continuously generates new convective cells upwind of the Massif Central and thus maintains a stationary MCS over the region (Figure 17). Indeed, the surface rainfall almost disappears when the Massif Central is removed from the model domains in the NOR sensitivity experiment. For the Gard case, the rapid ascent of the parcels does not occur at the same location as the Cévennes case. Strong updraughts take place upstream of the Massif Central's foothills over the Gard plain, induced by a mesoscale ingredient other than orographic lifting. The LLCP generated by the diabatic cooling induced by evaporation/sublimation/melting of microphysical species composing the MCS appears to play a role in blocking and forcing the warm and moist southerly to easterly LLJ to ascend (Figure 17). The NOC sensitivity experiment clearly shows that the simulated surface rainfall is shifted significantly northwards over

the Massif Central foothills when the cooling associated with the evaporation of liquid rain water is removed. The Massif Central, as well as the Alps (although not explicitly demonstrated here with backward trajectories or sensitivity experiments), contributes to the stationarity of the MCS by blocking the LLCP within the Rhône valley. Finally, for the Aude case, removal of the Massif Central relief or of the diabatic cooling do not have any significant impact on the stationarity of the simulated MCS. However, these are primary low-level mesoscale ingredients which act in locally enhancing heavy precipitation over the region, in addition to the favourable larger-scale meteorological conditions aloft.

This present study dealt with three cases of HPEs and it is of course not enough to form a generalized conclusion on the mesoscale triggering and stationarity factors. A climatological study, based on mesoscale reanalysis and idealized simulations, is currently in progress in order to investigate the link between these mesoscale conducive ingredients and the location of past flash-flood events.

### Acknowledgements

This work was carried out within the framework of the FLOODSite project, funded by the EU Sixth Framework Program. We thank A. Boone for improving the English of the manuscript. We gratefully acknowledge the comments made by the anonymous reviewers that helped to significantly improve the quality of the paper.

### References

- Bousquet O, Smull BF. 2003. Observations and impacts of upstream blocking during a widespread orographic event. *Q. J. R. Meteorol. Soc.* **129**: 391–410.
- Buzzi A, Tartaglione N, Malguzzi P. 1998. Numerical simulations of the 1994 Piedmont flood: Role of orography and moist processes. *Mon. Weather Rev.* **126**: 2369–2383.
- Buzzi A, Foschini L. 2000. Mesoscale meteorological features associated with heavy precipitation in the Southern alpine region. *Meteorol. Atmos. Phys.* **72**: 131–146.
- Chappell CF. 1986. Quasi-stationary convective events. Pp 289–310 in *Mesoscale meteorology and forecasting*. Ray PS (ed). Amer. Meteorol. Soc: Boston.
- Chen CH, Lin YL. 2005a. Orographic effects on a conditionally unstable flow over an idealized three-dimensional mesoscale mountain. *Meteorol. Atmos. Phys.* **88**: 1–21.
- Chen CH, Lin YL. 2005b. Effects of moist Froude number and CAPE on a conditionally unstable flow over a mesoscale mountain ridge. *J. Atmos. Sci.* **62**: 331–350.
- Chu CM, Lin YL. 2000. Effects of orography on the generation and propagation of mesoscale convective systems in a two-dimensional unstable flow. *J. Atmos. Sci.* **57**: 3817–3837.
- Ferretti R, Low-Nam S, Rotunno R. 2002. Numerical simulations of the Piedmont flood of 4–6 November 1994. *Tellus* **52A**: 162–180.
- Georgis JF, Roux F, Chong M, Pradier S. 2003. Triple-Doppler radar analysis of the heavy rain event observed in the Lago Maggiore region during MAP IOP 2b. *Q. J. R. Meteorol. Soc.* **129**: 495–522.
- Gheusi F, Stein J. 2002. Lagrangian description of airflows using Eulerian passive tracers. *Q. J. R. Meteorol. Soc.* **128A**: 337–360.
- Houze RA. 1993. *Cloud dynamics*. International Geophysics series **53**: Academic Press.
- Lebeaupin C, Ducrocq V, Giordani H. 2006. Sensitivity of Mediterranean torrential rain events to the sea surface temperature based on high-resolution numerical forecasts. *J. Geophys. Res.* **111**(D12110): 1–19. DOI: 10.1029/2005JD006541.
- Lin YL. 1993. Orographic effects on airflow and mesoscale weather systems over Taiwan. *Terr. Atmos. Ocean Sci.* **4**: 381–420.

## 1.2. PUBLICATIONS MAJEURES POUR LA SOUTENANCE DE L'HABILITATION À DIRIGER DES RECHERCHES

- Lin YL, Chiao S, Wang TA, Kaplan ML, Weglarz RP. 2001. Some common ingredients for heavy orographic rainfall. *Weather and Forecasting* **16**: 633–660.
- Medina S, Houze RA. 2003. Air motions and precipitation growth in Alpine storms. *Q. J. R. Meteorol. Soc.* **129**: 345–371.
- Nuisier O, Ducrocq V, Ricard D, Lebeaupin C, Anquetin S. 2008. A numerical study of three catastrophic precipitating events over Southern France. I: Numerical framework and synoptic ingredients. *Q. J. R. Meteorol. Soc.* **134**: 111–130.
- Pradier S, Chong M, Roux F. 2002. Radar observations and numerical modeling of a precipitating line during MAP IOP 5. *Mon. Weather Rev.* **130**: 2533–2553.
- Ramis C, Llasat MC, Genovès A, Jansa A. 1994. The October 1987 floods in Catalonia: Synoptic and mesoscale mechanisms. *Meteorol. Appl.* **1**: 337–350.
- Ramis C, Romero R, Homar V, Alonso S, Malarcon M. 1998. Diagnosis and numerical simulation of a torrential precipitation event in Catalonia (Spain). *Meteorol. Atmos. Phys.* **69**: 1–21.
- Romero R, Doswell CA III, Ramis C. 2000. Mesoscale numerical study of two cases of long-lived quasi-stationary convective systems over eastern Spain. *Mon. Weather Rev.* **128**: 3731–3751.
- Rotunno R, Ferretti R. 2001. Mechanisms of intense Alpine rainfall. *J. Atmos. Sci.* **58**: 1732–1749.
- Smith RB. 1979. The influence of mountains on the atmosphere. *Adv. Geophys.* **21**: 87–230. Academic Press.
- Stein J. 2002. Moist airflow regimes over more or less smooth mountains. Pp 178–181 in preprints, 10th Conference on Mountain Meteorology, Park City, UT. Amer. Meteorol. Soc: Boston.

# A numerical study of three catastrophic precipitating events over southern France. I: Numerical framework and synoptic ingredients

O. Nuissier,<sup>a\*</sup> V. Ducrocq,<sup>a</sup> D. Ricard,<sup>a</sup> C. Lebeaupin<sup>a</sup> and S. Anquetin<sup>b</sup>

<sup>a</sup> CNRM/GMME, Météo-France, Toulouse, France

<sup>b</sup> Laboratoire d'étude des Transferts en Hydrologie et Environnement, Grenoble, France

**ABSTRACT:** This study examines the simulation of three torrential rain events observed on 13–14 October 1995 (the Cévennes case), 12–13 November 1999 (the Aude case) and 8–9 September 2002 (the Gard case) over the southeastern part of France using the Meso-NH non-hydrostatic mesoscale numerical model. These cases were associated with extreme Heavy Precipitation Events (HPEs) with significant precipitation amounts exceeding 500 mm in less than 24 hours. Several sets of numerical experiments were performed with 10 km and 2.5 km horizontal resolutions. In part I of this study, special attention is paid to the experimental design for obtaining realistic simulations of HPEs with the Meso-NH model, as well as the evolution of the synoptic patterns in which the rainfall events are embedded.

The best 2.5 km numerical simulations show the ability of the Meso-NH model to reproduce significant quasi-stationary rainfall events. Moreover, the model fairly reproduces the low-level mesoscale environments associated with the three HPEs. The HPEs formed in a slow-evolving synoptic environment favourable for the development of convective systems (diffluent upper-level southerly flow, PV anomalies, etc.). At lower levels, a southerly to easterly moderate to intense flow provided conditionally unstable and moist air as it moved over the relatively warm Mediterranean Sea, typical for this time of the year (late summer and autumn). The two extreme cases (Gard and Aude) differ from the more classical event (Cévennes) in terms of larger low-level moisture fluxes. Weaker values of conditional convective instability, as in the Aude case, is counterbalanced by a stronger warm and moist low-level jet. The mesoscale triggering and/or sustaining ingredients for deep convection and the physical mechanisms leading to the stationarity of these rainfall events are presented and discussed in a companion paper. Copyright © 2008 Royal Meteorological Society

KEY WORDS mesoscale convective systems; heavy precipitation; non-hydrostatic numerical model

Received 21 August 2006; Revised 2 July 2007; Accepted 17 September 2007

## 1. Introduction

The western Mediterranean region is prone to devastating flash-flood events, particularly during the autumn. In past decades, devastating flash floods have been responsible for human casualties, and the destruction of houses, buildings, roads, bridges, power and telephone lines, etc. Table I gives a non-exhaustive inventory of dramatic events which have taken place in the Mediterranean area during the last twenty years. All of the coastal areas of the western Mediterranean region are affected (see Figure 1 for geographical locations): southern France with extreme flash-flood events such as those of Vaison-la-Romaine (Sénési *et al.*, 1996), Aude (Ducrocq *et al.*, 2003a) and Gard (Ducrocq *et al.*, 2004; Delrieu *et al.*, 2005) on 22 September 1992, 12–13 November 1999 and 8–9 September 2002, respectively; the eastern Spanish coast with, for example, more than 800 mm recorded in 24 hours at Gandia on 3 November 1987 (Llasat

and Puigcerver, 1994; Fernandez *et al.*, 1995; Penarrocha *et al.*, 2002); northwestern Italy (and Sardinia) with the catastrophe of 4–5 November 1994 in the Piedmont region (Buzzi *et al.*, 1998; Doswell *et al.*, 1998; Ferretti *et al.*, 2000; Rotunno and Ferretti, 2001, among others); and even the northern African coast with the most catastrophic event of recent decades in term of human losses in Algiers on 10 November 2001 (Hamadache *et al.*, 2002).

From a climatic point of view, Frei and Schär (1998) have analyzed high-resolution rain-gauge observations of daily surface rainfall to produce a precipitation climatology extending from the Massif Central to the eastern Alps. This climatological study has shown that precipitation is particularly enhanced along the Alpine foothills, with dryer conditions over the mountain ranges. This is one reason which motivated the MAP experiment in this area (Bougeault *et al.*, 2001). However, Frei and Schär (1998) have also clearly shown that the southeastern part of the Massif Central (named Cévennes) is one of the five雨iest areas of the region. Figure 2 focuses on this region of interest and shows the number of days for which

\* Correspondence to: Dr O. Nuissier, CNRM/GMME/MICADO, 42 av. G. Coriolis, 31057 Toulouse Cedex, France.  
 E-mail: olivier.nuissier@meteo.fr

Table I. Summary of recent flash floods around the western Mediterranean.

Place	Date	Surface rainfall (mm)	Human losses	Damage costs (US \$)
Gandia (Spain)	3 Nov 1987	>800 in 24 hours		
Vaison-la Romaine (France)	22 Sep 1992	300 in 24 hours	>50	$1 \times 10^9$
Piedmont region (Italy)	4–5 Nov 1994	300 in 36 hours	>60	$12 \times 10^9$
Aude (France)	12–13 Nov 1999	630 in <48 hours	>30	$3 \times 10^6$
Algiers (Algeria)	10 Nov 2001	>260 in <24 hours	886	$4 \times 10^9$
Gard (France)	8–9 Sep 2002	>600 in 24 hours	>20	$1.5 \times 10^9$

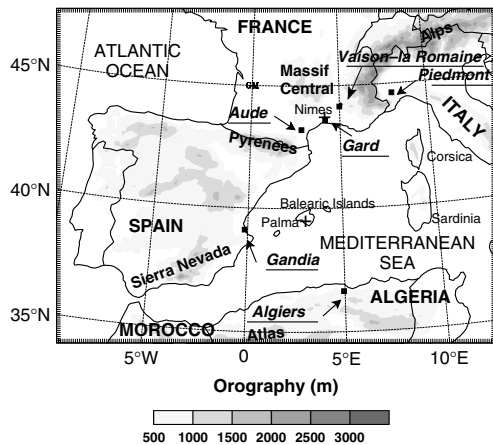


Figure 1. Topography (10 km resolution) of the western Mediterranean region, with the different locations mentioned in the text. The black squares denote a few catastrophic flash-flood events in the area. Crosses show the locations of Nîmes and Palma.

the daily surface rainfall exceeded 200 mm between 1958 and 2004 over southern France; the southern Alps, the

eastern Pyrenees, eastern Corsica and the southern Massif Central are the areas most frequently exposed to heavy precipitation. In other words, it is clear that the heaviest precipitation events occur mainly over the southeastern flanks of the mountainous regions, which are oriented perpendicular to the southerly to easterly moist low-level flow over the Mediterranean Sea.

Heavy precipitation events (HPEs) in the Mediterranean basin can be attributed to either convective or non-convective processes, or a combination of both. Large amounts of precipitation can accumulate over several days when frontal disturbances slow down and are strengthened by the relief of the Massif Central and the Alps, but also significant rainfall totals can be recorded in less than a day (typically more than 200 mm in less than 24 hours, and sometimes in only 6 hours) when a Mesoscale Convective System (MCS) stays over the same area for several hours. Most of the flash-flood events can be attributed to these quasi-stationary MCSs (Riosalido, 1990; Rivrain, 1997; Hernandez *et al.*, 1998; Romero *et al.*, 2000; Ducrocq *et al.*, 2003a, 2004). These convective systems frequently take a characteristic V-shape on infrared satellite images (Scofield, 1985) and are back-building (Bluestein and Jain, 1985). In this process, new

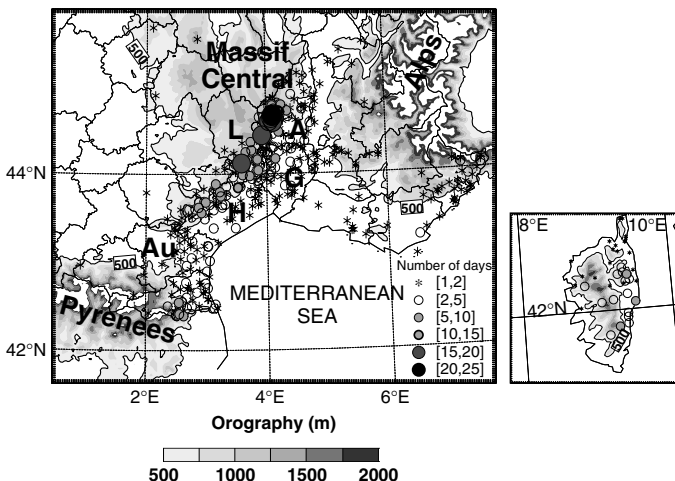


Figure 2. Number of days with daily precipitation greater than 200 mm over southern France from 1958 to 2004. The orography has a bold solid contour at the 500 m level. The thin lines delineate the departments (administrative areas of France); the Aude, Hérault, Gard, Ardèche and Lozère departments are labelled Au, H, G, A and L, respectively. The southeastern region of the Massif Central is named 'Cévennes'.

convective cells are continuously generated at the V tip, whereas older ones are gradually transported toward the V branches and dissipate downstream. The V-shape cloud pattern results from the interaction of the deep convection and the generally strong southerly to westerly diffluent flow at upper levels. To become stationary, MCSs require triggering mechanisms that release conditional convective instability at the same location over several hours. Quasi-stationary MCSs are particularly efficient in terms of rain production due to their high intensities and their spatial stationarity (Chappell, 1986; Delrieu *et al.*, 2005).

Western Mediterranean regions are favoured locations for major flash floods due to the fact that all the conducive factors for such extreme precipitating events (e.g. discussed by Lin *et al.*, 2001) can be simultaneously observed in the area. The first consists in a relatively warm Mediterranean Sea, which occurs mainly at the end of summer and the beginning of autumn. This feeds in moisture and heats the lowest levels of the troposphere through air-sea sensible and latent-heat fluxes. The second factor is the presence, in most cases, of a strong synoptic-scale trough or a closed cyclone at upper levels, just west of the threat area which generates a southerly to easterly flow that transports the warm and moist air masses from the Mediterranean Sea towards the coast and thus helps to destabilize the air column. The third factor is related to the steep and particular orography of the Mediterranean region which helps to trigger convection within the impinging moist and conditionally unstable low-level flow, but it also channels this very moist low-level jet (LLJ), inducing upwind low-level convergence which contributes to the release of conditional convective instability near the Mediterranean Sea.

The link, even though complex, between heavy precipitation and synoptic-scale troughs and cyclones (and their possible alteration by mountain ranges) has been well established in the past (Doswell *et al.*, 1998; Homar *et al.*, 1999; Massacand *et al.*, 1998). Jansa *et al.* (2001) have found that in most cases (around 90%) of heavy rain in the western Mediterranean, there is a cyclonic centre in the vicinity, usually located so that its presence favours the creation and intensification of the moist low-level flow which feeds the heavy precipitation system. Cyclone intensity could, however, vary from strong and deep systems to weak and shallow depressions, and even in some cases (10%) no cyclone is present in the vicinity.

If it is more or less obvious to clearly identify these synoptic-scale precursors inducing dynamic forcing favourable to torrential event occurrences, one of the most challenging tasks using weather numerical models is to correctly forecast when (and especially where) a MCS will occur and what will be the associated quantitative precipitation. The orography of the western Mediterranean Sea usually interacts with the synoptic flow, modifying the circulation and generating mesoscale disturbances that force and focus the convection in specific areas. For instance, Romero *et al.* (2000) showed that the development of a surface meso-low driven by latent heat release, as well as lee cyclogenesis induced

by the Atlas mountains, could have had a key role in the two severe convective cases they studied. A significant reduction of forecast errors (location, intensity, etc.) associated with Mediterranean HPEs comes through a good representation in numerical models of both the synoptic- and mesoscale ingredients, in addition to a description of terrain conditions which are likely to influence these meteorological phenomena.

As shown by Figure 2, the southeastern region of France is often affected by intense flash-flooding episodes. The goal of these two papers is therefore to analyze and document three HPEs observed over this specific region. Two of them are extreme flash-flood events with significant precipitation totals (more than 500 mm in less than 24 hours), whereas the third had its precipitation maximum placed over the region statistically most exposed to HPEs, e.g. along the Massif Central southeastern flank (Cévennes region). Even though many studies have focused on the way in which synoptic-scale conditions and terrain characteristics are conducive (or not) for triggering heavy precipitation, it is important to identify the mechanisms that lead to the formation, distribution and especially persistence over several hours of this kind of precipitation at a specific location. The main goal of our study is to use realistic structures and evolutions of three representative HPEs simulated by a convective-scale model to highlight the factors leading to the stationarity of the heavy precipitation systems which are responsible for accumulation of large rainfall amounts over southeastern France. In part I of this study, greater attention is paid to the experimental design needed to obtain realistic simulations of HPEs together with the evolution of the synoptic patterns in which the rainfall events are embedded, whereas the mesoscale and fine-scale structures of the MCSs and their environment, as well as the role of the convection and orography, are discussed in a companion paper (Ducrocq *et al.*, 2008).

Following this introduction, an overview of the meteorological phenomena is provided. The description of the experimental design is outlined in Section 3, followed by an overview of the results of the simulations in Section 4. Section 5 discusses the evolution of the synoptic patterns in which the precipitating systems are embedded. Finally, concluding remarks are presented in the last section.

## 2. The case-studies

Our study focuses on three flood events: 13–14 October 1995 (the Cévennes case), 8–9 September 2002 (the Gard case) and 12–13 November 1999 (the Aude case). The Cévennes and Gard cases occurred in the vicinity of the Massif Central, in the Ardèche and Gard departments, respectively, whereas the Aude event took place in the Aude region between the Massif Central and the eastern Pyrenees. For all three cases, most of the precipitation was induced by a quasi-stationary MCS. Although the rainfall events are described in Ducrocq *et al.* (2002, 2003a, 2004) and Delrieu *et al.* (2005), this present

section provides a detailed overview of the life cycle of the different systems adopting a uniform presentation for the three cases.

### 2.1. Cévennes case

During the morning of 13 October 1995, a moist sea-air intrusion over the Hérault and Gard departments led to nearly saturated low levels over these regions. Convective activity started around 1800 UTC on 13 October when a first MCS formed offshore. This first system (labelled MCS 1 in Figure 3(a)) contributed to the moistening of the southerly low-level flow, thus enhancing further the moisture over the region and leading to conducive conditions for the development of another MCS (labeled MCS 2 in Figure 3(a)) during the evening over the Massif Central foothills. After 2100 UTC, several convective cells formed over the sea and the Gard department and then progressed northwards while strengthening, finally merging into a single system at 2230 UTC (MCS 2). Radar images (not shown) indicate that MCS 2 was continually fed by a train of convective cells advected toward the mountainous region of Massif Central by the southerly flow. MCS 2 stayed over the Gard, Ardèche and Lozère departments for about 9 hours before moving northeastwards around 0800 UTC on 14 October while decaying (as indicated by warmer cloud tops in Figure 3(c)). At its mature stage around 0200 UTC, the cloud pattern of the MCS formed a typical V-shape on the infrared imagery, with the coldest top cloud extending between the Gard and Lozère departments (Figure 3(b)).

Figure 4(a) shows the rain amounts recorded by Météo-France's rain-gauge network for the Cévennes case from 2100 UTC on 13 October to 0800 UTC on 14 October. The heavy precipitation for that case mainly occurred along the Massif Central southeastern foothills with a peak of precipitation of about 262 mm over the northwestern portion of the Gard department. Such an accumulated rainfall distribution is typical of flash-flooding episodes over the region. Maximum precipitation was recorded over the Gardon d'Anduze river watershed, an area of about 545 km<sup>2</sup>. The maximum specific discharge recorded at the outlet of this catchment was about 2.6 m<sup>3</sup> s<sup>-1</sup> km<sup>-2</sup> at 0700 UTC on 14 October, whereas the maximum hourly precipitation was recorded around midnight (Figure 4(b)). Fortunately, little damage was observed in the region and no casualties were reported for this Cévennes case.

### 2.2. Gard case

The first convective cells associated with Gard event appeared over the Mediterranean Sea around 0400 UTC on 8 September 2002, in the warm air well ahead of the surface front that affected western France at that time. Progressing northwards, the convection started to organize while forming a MCS just south of the Gard

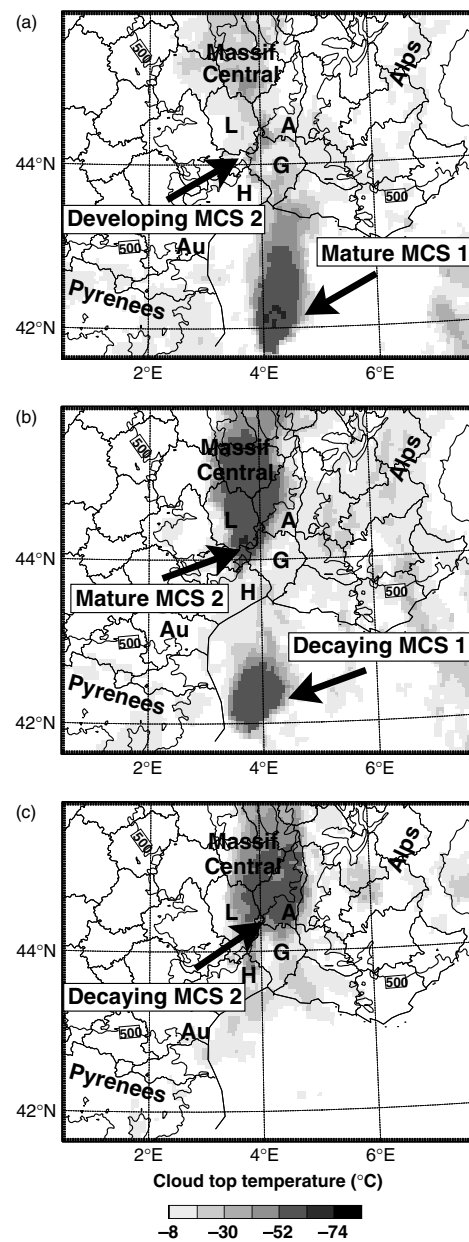


Figure 3. METEOSAT infrared brightness temperature for the Cévennes case at (a) the growing stage (21 UTC, 13 October 1995), (b) the mature stage (02 UTC, 14 October) and (c) the decaying stage (08 UTC, 14 October). The bold contour shows the 500 m level. The Au, H, G, A and L labels are as in Figure 2.

department from 0800 UTC as shown by the radar reflectivity over the region (Figure 5(a)). The convective system stayed over almost the same region from 1200 UTC on 8 September until 1200 UTC on 9 September. During its mature stage, the cloud shield took on a classical V-shape on the infrared images, with the tip of the

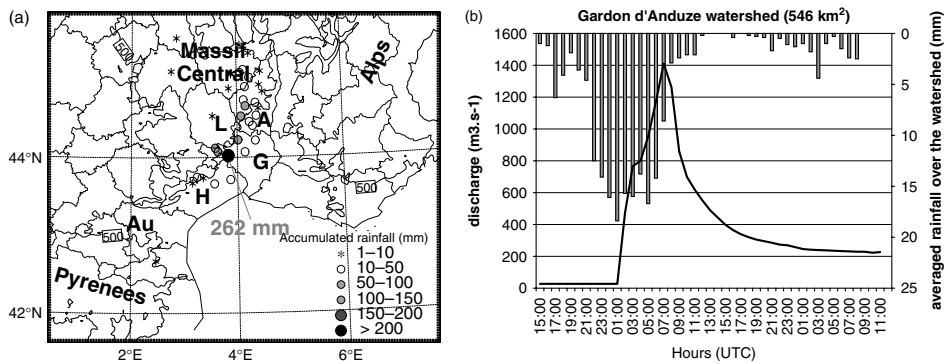


Figure 4. (a) Accumulated precipitation (mm) from Météo-France's rain-gauge network for the Cévennes case from 21 UTC, 13 October to 08 UTC, 14 October 1995. The bold contour shows the 500 m level. (b) Rainfall (grey bars) and discharge (solid curve) over the Gardon d'Anduze watershed.

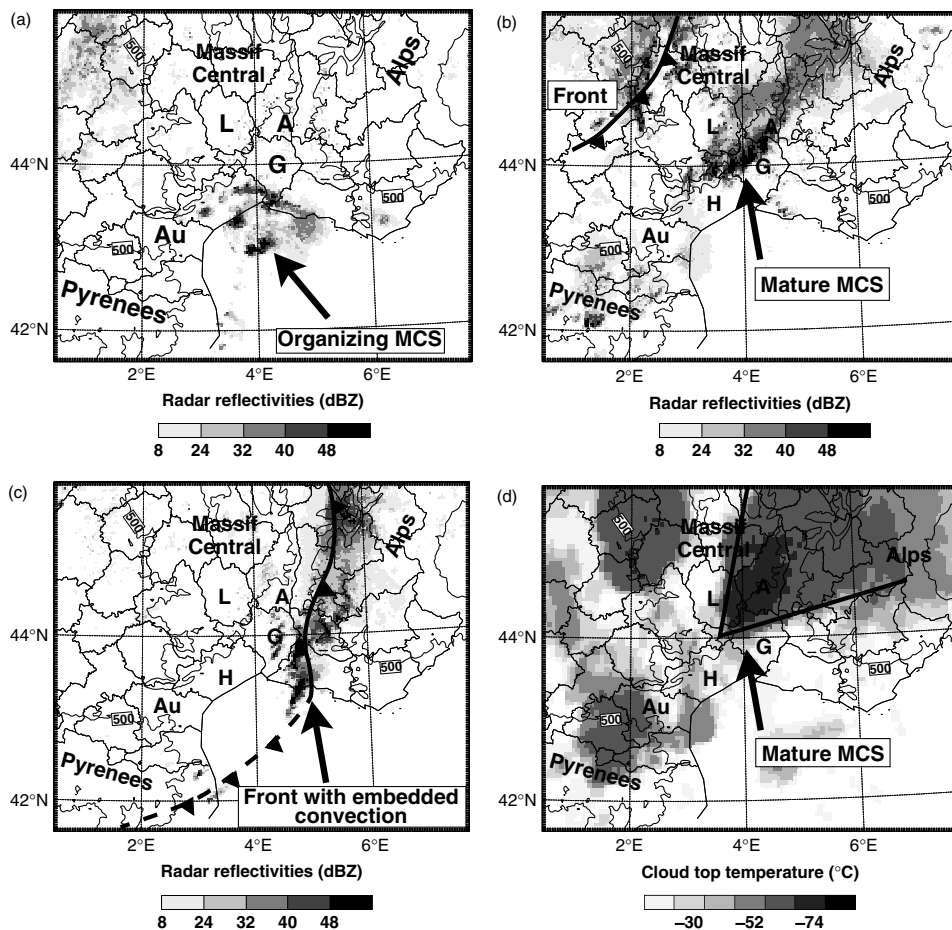


Figure 5. Composite radar reflectivities from the observations of the Gard case at (a) the growing stage (08 UTC, 8 September 2002), (b) the mature stage (2230 UTC, 8 September) and (c) the decaying stage (12 UTC, 9 September). (d) is as (b) but for METEOSAT infrared brightness temperature. The bold solid and solid/dashed lines in (b) and (c) denote the surface front (undulating in (c)). Au, H, G, A and L labels are as in Figure 2.

V facing the upper-level southwesterly flow that prevailed at that time (Figure 5(d)). Beneath the cloud shield, the convective precipitation mainly affected the Gard region (as indicated in Figure 5(b)), while the stratiform precipitation was extending farther to the north. At this time, the MCS took a southwest–northeast orientation according to the prevailing mid- to upper-level tropospheric flow. But as the upper-level trough axis tilted counterclockwise in a northwest–southeast orientation later on the night of 8 September, the convective system moved in a more north–south orientation and began a slow northwestward motion. Early in the morning of 9 September, the surface cold front approached from the west and merged with the MCS around 0400 UTC. As the cold front was progressing eastwards, the whole precipitating system again swept over the Gard department during the late morning of 9 September (Figure 5(c)).

The Gard precipitation event was an exceptional one due to many factors. Firstly, Figure 6 shows that the intensity of the event was extreme with maximum precipitation around 600–700 mm in 24 hours (from 1200 UTC on 8 September) near Alès. Secondly, the area affected by precipitation over 200 mm was considerable. This area extended over at least 3000 km<sup>2</sup> covering a large portion of the northern Gard department, as far as the Massif Central foothills in Ardèche. As emphasized by Delrieu *et al.* (2005), the episode underwent three distinct phases. In phase 1 from 0800 UTC till 2200 UTC on 8 September, the MCS developed and became stationary. The heaviest precipitation was located over the plains just north of the city of Nîmes (Gard department), i.e. a rather unusual location according to the heavy rainfall climatology (Figure 2). Maximum rainfall amounts were about 300 mm during this phase. Between 2200 UTC and 0400 UTC (phase 2), the system slowly moved north–westwards. The MCS produced rainfall amounts greater than 100 mm over this 6-hour period. Finally, after 0400 UTC (phase 3), the surface cold front approached and

swept over the region again producing sustained showers with rainfall amounts exceeding 100 mm during an 8-hour period.

The river discharges in the region were also exceptional. For the Gard and Vidourle river watersheds, peak discharges twice as high as the 10-year return period discharge were recorded (Delrieu *et al.* 2005; Chancibault *et al.*, 2006). The estimated peak discharges of the upstream watersheds of these rivers were very high ( $5\text{--}10 \text{ m}^3 \text{s}^{-1} \text{km}^{-2}$ ), locally reaching extreme values as high as  $20 \text{ m}^3 \text{s}^{-1} \text{km}^{-2}$ . Such large discharge measurements can be explained by both the spatial extent and the intensity of the heavy rainfall. This event caused damage estimated to be 1.2 billion US dollars (Huet *et al.*, 2003) and led to the deaths of 25 people (Table I).

### 2.3. Aude case

In the early afternoon of 12 November 1999, the first convective cells formed a few tens of kilometers east of the Aude coast. This area of intense precipitation (Figure 7(a)) gradually moved westwards while strengthening. Convection organized and evolved to a MCS which stayed stationary over the Aude department from 1600 UTC on 12 November until 0000 UTC on 13 November. Similar to the Cévennes and Gard cases, this system took a classical V-shape as shown on the infrared imagery in Figure 7(d), resulting from the intense diffluent flow aloft. However, beneath the upper-level cloud plume, the precipitation was organized in a narrow line with an approximate north–south orientation (Figure 7(b)). Between 0000 and 0400 UTC on 13 November, other strong convective cells coming from the Balearic Islands merged with the previous MCS. The stormy activity started to decrease after 0400 UTC as the system moved off the Aude coast while becoming less organized (Figure 7(c)).

During the Aude event, high surface rainfall amounts were recorded which in large part can be directly

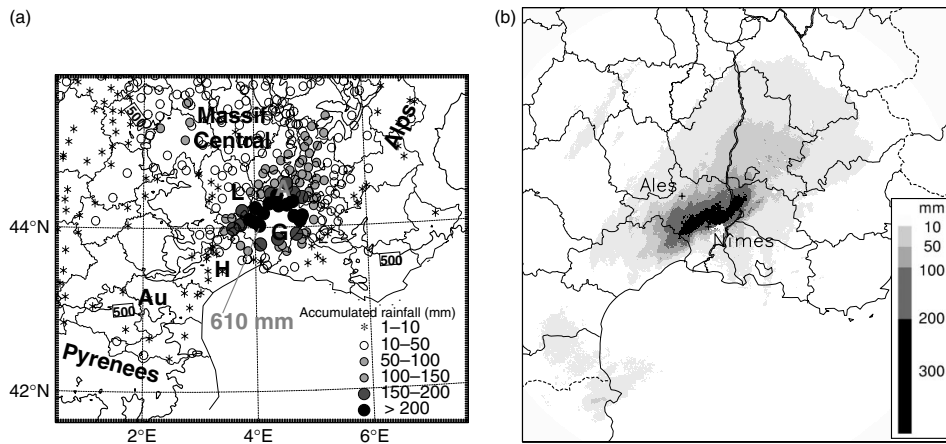


Figure 6. (a) Accumulated precipitation (mm) from Météo-France's rain-gauge network for the Gard case from 12 UTC, 8 September to 12 UTC, 9 September 2002. (b) shows the accumulated rainfall from the Nîmes radar for the same period.

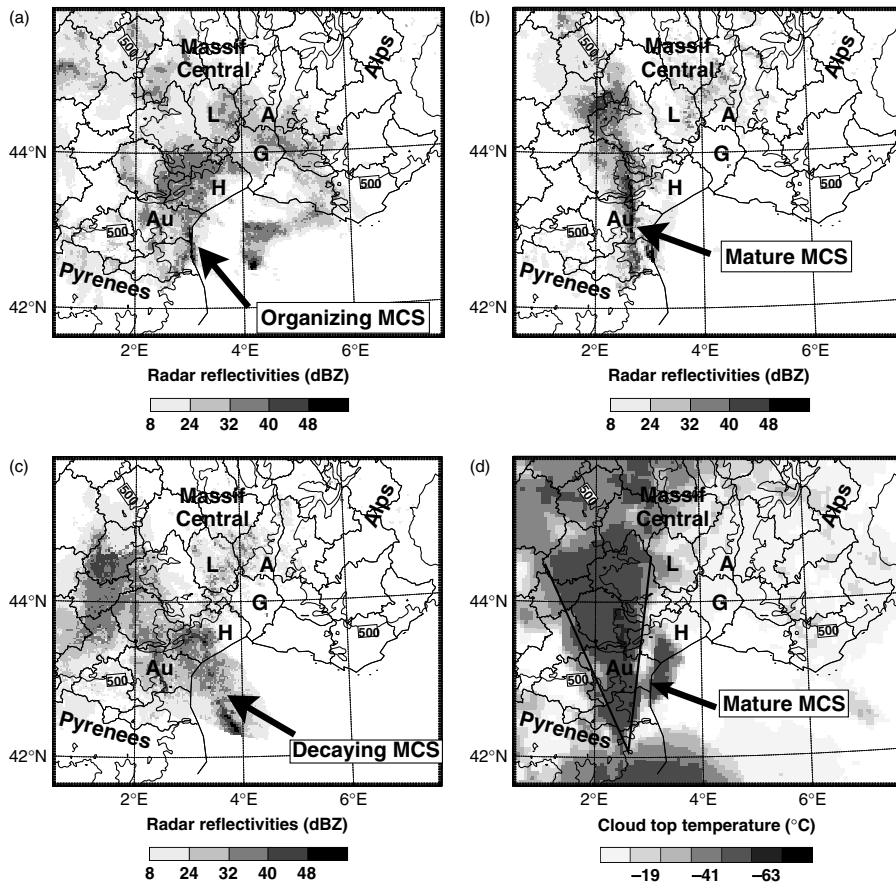


Figure 7. As Figure 5, but for the Aude case. Times are (a) 16 UTC, 12 November 1999, (b) 00 UTC, 13 November and (c) 04 UTC, 13 November. (d) is as (b) but for METEOSAT infrared brightness temperature.

attributed to the MCS mentioned above. Figure 8 shows that from 1200 UTC on 12 November until 0600 UTC the next day, 485 mm fell at Lézignan-Corbières in the Aude department. The Aude event had some strong similarities with the Gard case in terms of the spatial extent of the accumulated surface rainfall. Indeed, the area receiving more than 200 mm in 48 hours extended more than 150 km in length and about 50 km in width. This extreme rainfall event resulted in one of the century's most significant floods in the Aude region and produced remarkable flash floods in some catchments. Peak flood discharge as high as  $10 \text{ m}^3 \text{s}^{-1} \text{km}^{-2}$  were recorded from the small upstream watersheds (areas  $<100 \text{ km}^2$ ) of the Aude river (Gaume *et al.*, 2004). Strong low-level easterly winds were also recorded during this event. Surface wind gusts reached about  $35\text{--}40 \text{ m s}^{-1}$  during the morning of 12 November, and these high winds along the coast lasted at least 24 hours causing a significant surge of 4–5 feet above normal tide levels. This prevented the rivers from discharging into the

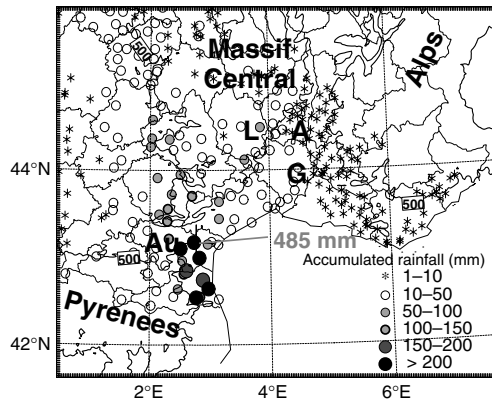


Figure 8. As Figure 4, but for the Aude case from 12 UTC, 12 November 1999 to 06 UTC, 13 November.

Mediterranean Sea, thereby aggravating the flooding. This flash-flood event was particularly deadly, resulting in the deaths of 36 people (Table I).

### 3. Description of the numerical experiments

#### 3.1. The Meso-NH model

A three-dimensional version of the French Meso-NH non-hydrostatic mesoscale numerical model (Lafore *et al.*, 1998) has been used for the simulation of the precipitating events. Meso-NH allows the simultaneous use of several nested grids in a two-way interactive mode (Clark and Farley, 1984; Stein *et al.*, 2000); the coarser grid provides the lateral boundary conditions to the finer grid, while the variables of the coarser grid are relaxed with a short relaxation time toward the finer grid's values in the overlapping area. For this study, the domain configuration has been retained which was used with success by Ducrocq *et al.* (2002) and Ricard (2005) for quantitative precipitation forecasting, by Chancibault *et al.* (2006) for hydrological response, by Brenot *et al.* (2006) based on ground GPS observations, and by Caumont *et al.* (2006) based on radar reflectivity, i.e. two two-way nested domains in the horizontal plane with horizontal grid spacings of about 10 and 2.5 km, with the 2.5 km domains ranging from  $250 \times 375$  km to  $600 \times 600$  km. The Gal-Chen and Sommerville (1975) vertical coordinate is used for 40 vertical levels; the spacing between them varies continuously with altitude, from 75 m close to the surface to 900 m aloft. The top of the domain is at 19 km altitude, and Rayleigh damping is progressively applied above 15 km altitude (i.e. the last six levels) to the perturbations of the wind components and the thermodynamical variables with respect to their large-scale values, in order to prevent spurious reflections from the upper boundary.

The prognostic variables are the three Cartesian components of velocity, the dry potential temperature, the different water mixing ratios and the turbulent kinetic energy. Pressure perturbations are determined by solving the elliptic equation obtained by combining air mass continuity and momentum conservation equations. A bulk microphysical scheme (Caniaux *et al.* 1994; Pinty and Jabouille 1998) governs the equations of the six water species: water vapour, cloud water, rain water, primary ice, snow aggregates, and graupel. Moreover, for the coarser horizontal resolutions ( $>10$  km), the subgrid-scale convection is parametrized by the Kain and Fritsch (1990, 1993) scheme, adapted to the Meso-NH model by Bechtold *et al.* (2001). The turbulence parametrization is based on a 1.5-order closure (Cuxart *et al.*, 2000). For the coarser grids, the mixing length follows the method

of Bougeault and Lacarrère (1989) and the horizontal gradients are not considered. For the finer grids, the mixing length is directly proportional to the grid volume and three-dimensional turbulent fluxes are modelled (Redelsperger and Sommeria, 1981).

#### 3.2. Experimental design

The different numerical experiments performed for each case are summarized in Table II. In order to document the larger-scale environment, a first set of simulations was performed with only the 10 km resolution domain (REF10 experiments in Table II). The initial conditions are provided by the large-scale operational analysis of the French ARPEGE NWP suite at noon. Additional simulations (not listed in Table II) were performed to test the model sensitivity to the time of the initial conditions, with the runs starting 12 hours earlier than the REF10 simulations.

In order to study the finer-scale ingredients, Meso-NH was run at about a 2.5 km resolution in order to have an explicit treatment of the convection. The REF2.5 experiments consider the same initial conditions as the REF10, but with the two interactive domains at 10 km and 2.5 km resolutions. However, in the Cévennes and Gard cases, the REF2.5 experiments failed to reproduce the key characteristics of the phenomena, so other initial conditions were investigated and tested. A Mesoscale Data Analysis (MDA) following Ducrocq *et al.* (2000, hereafter D00) was therefore used to obtain initial conditions for the MDA experiments. The fine-scale initialization procedure of D00 was applied to these two cases after the observed triggering of the convection, to take into account of the early stage of convective activity in the analysis. First, mesonet surface observations are included both in the altitude and surface optimal interpolation analyses of the Aladin model to provide the initial states of both the 10 km and 2.5 km domain. Then, a cloud and precipitation analysis, based on the radar reflectivities and Meteosat infrared brightness temperatures, drove a moisture and microphysical adjustment that was finally superimposed on the initial state of the 2.5 km domain. The adjustment is such that the vapour mixing ratio inside the cloudy areas is set to its saturated value with respect to the ambient temperature. Also, some rainwater (snow) is inserted inside the rainy areas below (above) the freezing level. (D00 provides a more complete description of this fine-scale initialization procedure.)

Table II. Initial conditions used for the simulation of different cases.

Case	REF10	REF2.5	MDA
	1 domain (10 km) from ARPEGE analysis	2 domains (10 and 2.5 km) from ARPEGE analysis	2 domains (10 and 2.5 km) from D00's full mesoscale initialization technique
Cévennes	1200 → 1200 UTC	1200 → 0600 UTC	2200 → 1200 UTC
Gard	1200 → 1200 UTC	1200 → 1200 UTC	1200 → 1200 UTC
Aude	1200 → 1200 UTC	1200 → 0600 UTC	

In order to highlight the mesoscale forcing, additional orography and microphysical parametrization sensitivity experiments were performed. The sensitivity experiments are presented in the companion paper.

#### 4. Overview of the simulations

Chancibault *et al.* (2006) have assessed the validity of the high-resolution simulations of the Gard case by simulating stream flow with the topography-based model TOPMODEL (Beven and Kirkby, 1979; Beven *et al.*, 1995) driven by Meso-NH model rainfall. They found that, for the Gard case, the MDA simulations produced more realistic peak flows, which were higher than those obtained for REF2.5 experiments. Furthermore, Ducrocq *et al.* (2002) calculated various scores to assess the high-resolution rainfall numerical forecasts for the Cévennes and Aude cases. They concluded that while the increase in resolution significantly improves the results for the Aude case (REF2.5), it was necessary to apply the MDA procedure to get a more realistic rainfall event for the Cévennes case. The best simulations at 2.5 km resolution (i.e. MDA for Cévennes and Gard cases, REF2.5 for the Aude case) identified by these previous studies are here further compared against observations to corroborate that realistic simulations of the HPEs and of their low-level mesoscale environment have been obtained and could be used to study the events which are described in the following sub-sections. As the 10 km simulations are used to characterize the evolution of the synoptic-scale environment in the following, they are also verified against the ARPEGE large-scale analyses.

##### 4.1. Cévennes case

###### 4.1.1. Upper-level synoptic-scale environment forecast

The upper-level synoptic situation is presented in Figure 9(a) at the initial time of REF10 for the Cévennes case (i.e. at 1200 UTC on 13 October 1995). The synoptic situation was characterized by a large upper-level cold low located well away from France (between 20 and 25 °W) and by a mid- to upper-level ridge centred over central Europe. Between both these large-scale structures prevailed a fair upper-level southerly flow and the associated height gradients were rather weak. Analysis of the surface pressure (not shown) reveals that anticyclonic conditions dominated over most of the convective area. Although the signal of synoptic forcing is not obvious in the Cévennes event, one can note the presence of a short-wave trough located near the Algerian coast, associated with a decreasing dynamic tropopause altitude. The dynamic tropopause height is estimated using the 1.5 PVU (Potential Vorticity Unit) surface. The low elevation of this surface indicates a stratospheric air intrusion into the troposphere, generally associated with decreasing pressure at upper levels. This configuration,

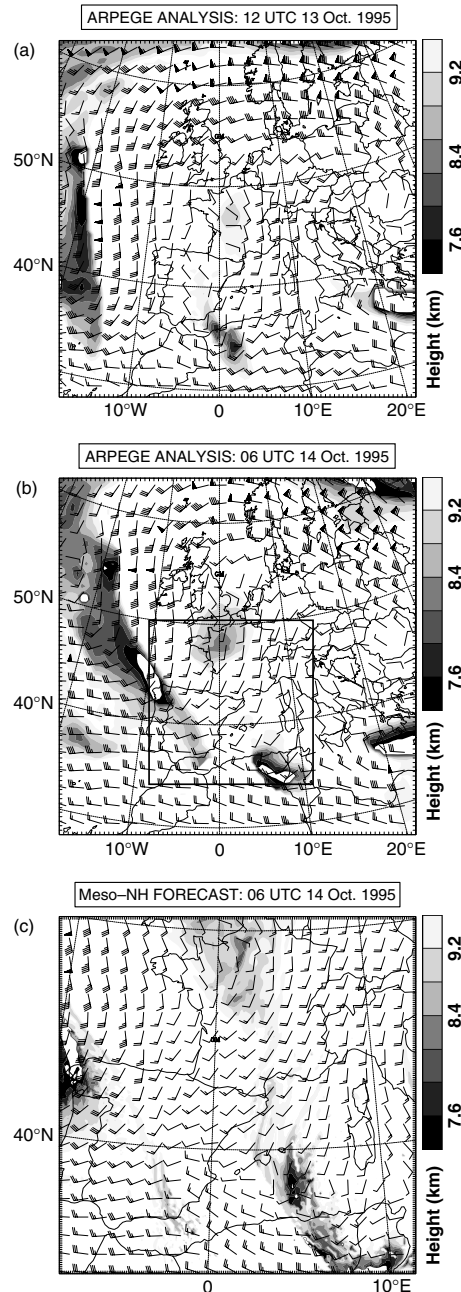


Figure 9. 500 hPa winds (barbs) and 1.5 PVU surface height (shading) for the Cévennes case: (a) and (b) are from the ARPEGE analysis and (c) is from REF10.

in addition to cold air aloft (not shown), helped to destabilize the air mass over the Mediterranean Sea.

After 12 hours of simulation (at 0600 UTC on 14 October), the Meso-NH model simulated the slow evolution of the synoptic pattern fairly well (Figure 9(c) versus 9(b)).

Indeed, coming from a southerly then from a southwest direction, the upper-level flow was still weak in the area of interest and the small short-wave trough depicted at 1200 UTC on 13 October moved very slightly eastwards. Moreover, persistence of a mid- to upper-level ridge, centred over the north of Italy and central Europe is another factor at the synoptic scale which explains the slow evolution of the synoptic pattern. Moreover, the upper-level ridge which stalled over central Europe also increased the amplitude of the upper-level trough which, in turn, may have acted to increase upper-level divergence over southern France.

#### 4.1.2. Low-level mesoscale environment forecast

It is also important to validate the simulation of the location and the strength of the low-level inflow. Figure 10(a) and (c) show the 2 m above ground level (AGL) simulated temperature and wind for the best 2.5 km simulation at 0300 UTC on 14 October 1995 for the Cévennes case. The highest surface temperatures ( $\approx 20^{\circ}\text{C}$ ) are co-located with the LLJ and reach the coast just south of the Hérault department, in good agreement with the observations (Figure 10(b) and (d)). The best simulation also reproduces quite well a moderate south to southeast low-level flow impinging upon the Massif Central foothills.

#### 4.1.3. Heavy precipitation forecast

For the Cévennes case, the simulated MCS presents itself as a southwest–northeast elongated precipitating line oriented along the Massif Central, as illustrated by the simulated radar reflectivities (Figure 11(a)). For this case, the maximum simulated radar echoes ( $\approx 45 \text{ dBZ}$ ) seem to be generated and focused over a limited area of the Massif Central foothills (not exceeding  $1400 \text{ km}^2$ ), but in a region typified by heavy precipitation (Figure 2). The model succeeds in simulating the whole life cycle of the MCS, including its decaying phase.

The observed surface rainfall for this case (Figure 11(b)) consists of an area of marked rainfall (with a peak of 176 mm in only 6 hours), extending from the Hérault to the Ardèche departments. Although the maximum simulated rainfall is underestimated (about 108 mm), the best simulation predicts both the pattern and the amounts quite well (Figure 11(d)). Also, the simulated surface rainfall in the best simulation is considerably improved over the REF10, as Meso-NH simulates a maximum rainfall amount of only 28 mm, well south of the observed location (Figure 11(c)). Furthermore, the model provides a good representation of the stationarity of the simulated precipitation event. The rainfall time series shown in Figure 12 depicts a well-defined rainfall peak with a maximum 1-hour accumulated rainfall of

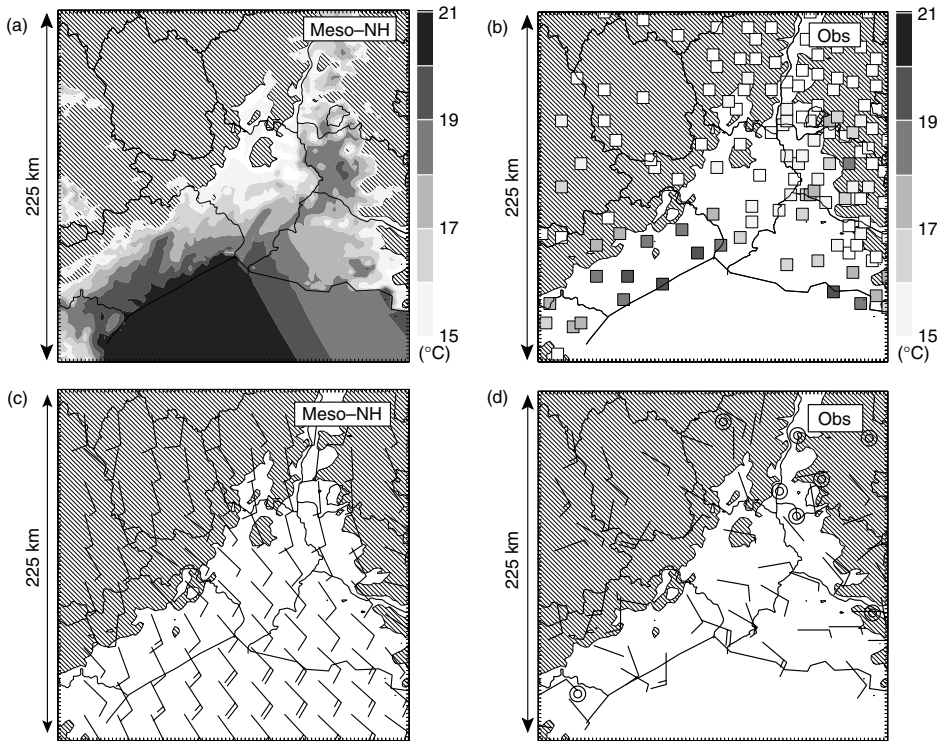


Figure 10. (a) 2 m AGL temperature (shading) and (c) 10 m AGL wind (barbs) for the Cévennes case from the MDA simulation at 0300 UTC, 14 October 1995. (b) and (d) show the corresponding observations at the same time. Orography above 250 m is shown hatched.

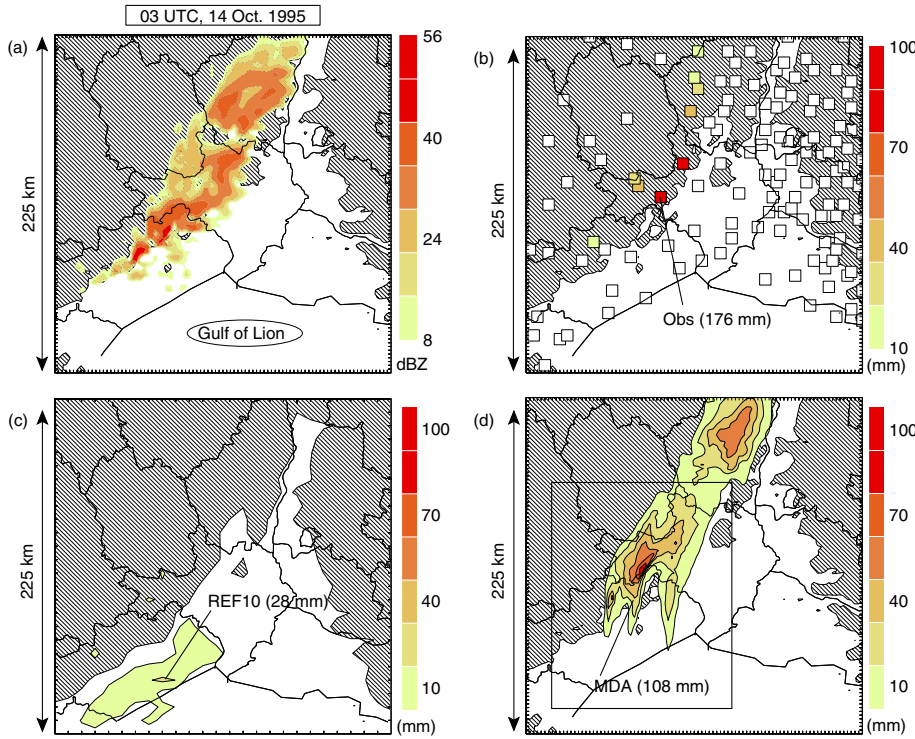


Figure 11. (a) Simulated radar reflectivities (shading) at 2 km altitude from the MDA for the Cévennes case. (b) rainfall observations from 00 to 06 UTC, 14 October 1995. (c) and (d) show the simulated accumulated rainfall (shading) over the model domain for the REF10 experiment and MDA, respectively. Hatching shows orography above 250 m. This figure is available in colour online at [www.interscience.wiley.com/qj](http://www.interscience.wiley.com/qj)

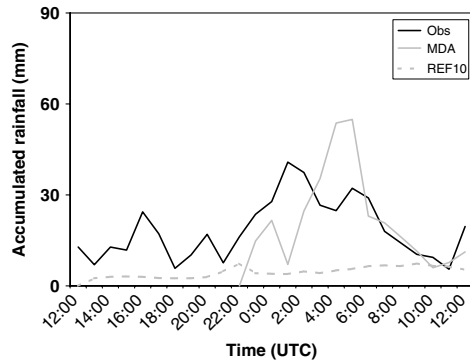


Figure 12. Maximum 1-hour accumulated precipitation for the Cévennes case in the box shown in Figure 11(d) from the REF10 (dashed grey) and MDA (solid grey) simulations and observations (solid black).

about 55 mm for the best simulation, against only 7 mm in the REF10 experiment simulation.

#### 4.2. Gard case

##### 4.2.1. Upper-level synoptic-scale environment forecast

At 1200 UTC on 8 September 2002, the meteorological situation was dominated by an upper-level cold low

centred over Ireland extending via a trough toward the Iberian Peninsula (Figure 13(a)). The trough axis, with a roughly northnortheast–southsouthwest orientation, was generating a southwesterly diffluent flow of about  $20 \text{ m s}^{-1}$  over southeastern France. Thus, contrary to the Cévennes case, the upper-level circulation was significantly more dynamic and stronger synoptic forcing prevailed for this event. Figure 13(a) also shows the presence of several PV anomalies circulating around the trough axis. Such conditions were precursors for enhancing the upper-level divergent flow over southeastern France which provided additional upward motion for convective triggering. At 0000 UTC on 9 September, the 500 hPa flow for REF10 indicated that the trough axis tilted more northwest–southeast and moved closer to France (Figure 13(b)). The upper-level flow strengthened to around  $30 \text{ m s}^{-1}$ , but the flow kept its general southwest component and its diffluent feature. As with the Cévennes case, the Meso-NH model succeeded in simulating a slow evolution of the synoptic pattern conducive to heavy precipitation (Figure 13(b) versus Figure 13(c)).

##### 4.2.2. Low-level mesoscale environment forecast

Simulated 2 m AGL temperature and 10 m wind for the Gard case at 1800 UTC on 8 September 2002 are shown in Figure 14 for the best 2.5 km simulation. The observations, as well as the best simulation, depict a warm south

#### 4.2.3. Heavy precipitation forecast

The simulated IR brightness temperature is shown in Figure 15. The simulated MCS for the Gard case is quite impressive, as the associated cloud shield extends over at least six departments (i.e. about 16 000 km<sup>2</sup>). The precipitating structure of the system shows a strong convective part anchored over the flooded location and a less intense stratiform region extending downstream (Figure 16(a)). However the most intense radar reflectivities (i.e. >45 dBZ) are located in an unusual area over the central plains of Gard, which means well upstream of the Cévennes case (Figure 16(a) versus Figure 11(a)). Also, Figure 15 displays a very realistic signature of the interaction between the deep convection and the strong southwesterly flow aloft, which is about 35 m s<sup>-1</sup> (not shown). The cloud shield has the classical V-shape in the simulated infrared imagery as in the observed METEOSAT imagery (Figure 5(d)).

Accumulated precipitation from the simulations are shown in Figure 16. Whereas the model starting from the ARPEGE large-scale analysis with low resolution (Figure 16c) did not succeed in simulating realistic rainfall amounts at the correct locations, the best simulation (Figure 16(d)) gives much better results with a simulated rainfall peaking at about 250 mm just over the central plains of Gard, in good agreement with the observations (Figure 16(b)). In contrast to the Cévennes case, for which heaviest precipitation and windward foothills were co-located, the Gard case is marked by an unusual location of maximum precipitation, well upstream of the first Massif Central foothills. The first phase (up to 22 UTC, 8 Sept. 2002) of the event is particularly well reproduced. Although an intense 1-hour accumulated surface rainfall of about 50 mm is predicted by the model (Figure 17), the simulated convective system is located too far north in the second and third phases of the event. (A detailed hydrological evaluation of this simulation can be found in Chancibault *et al.*, 2006). The following discussions of the best simulations for this specific Gard case will therefore be focused on the first phase of the event.

#### 4.3. Aude case

##### 4.3.1. Upper-level synoptic-scale environment forecast

Similar to the Gard case, the Aude event also exhibits a strong dynamic circulation and obvious upper-level forcing. At 12 UTC on 12 November 1999, a pronounced and elongated upper-level deep tropospheric trough was centred over northwestern Spain (Figure 18(a)). This pattern generated a broad and fast southerly flow over the Mediterranean Sea, from the north African coast to France. Even though the meteorological context in the Aude case seems to be characterized by a dynamic upper-level circulation similar to the Gard case, the synoptic forcing tended to be stronger, similar to those described by Maddox *et al.* (1979) and Chappell (1986). The upper-level cold low was closer to the threatened area (southern France), and the region was located just downstream

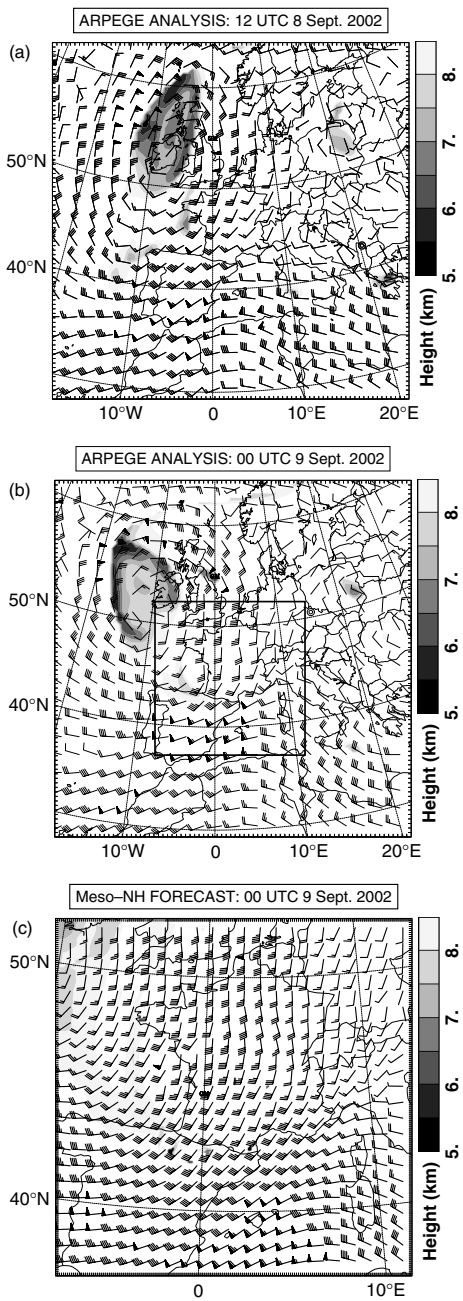


Figure 13. As Figure 9, but for the Gard case.

to southeasterly low-level flow of about 10 m s<sup>-1</sup> coming from the Mediterranean Sea. An interesting feature which is well simulated by the model is the stronger meridional surface temperature of 5–6 K just south of Gard, marking the boundary between the warm and moist low-level flow and the cold surface air mass generated beneath the precipitation system.

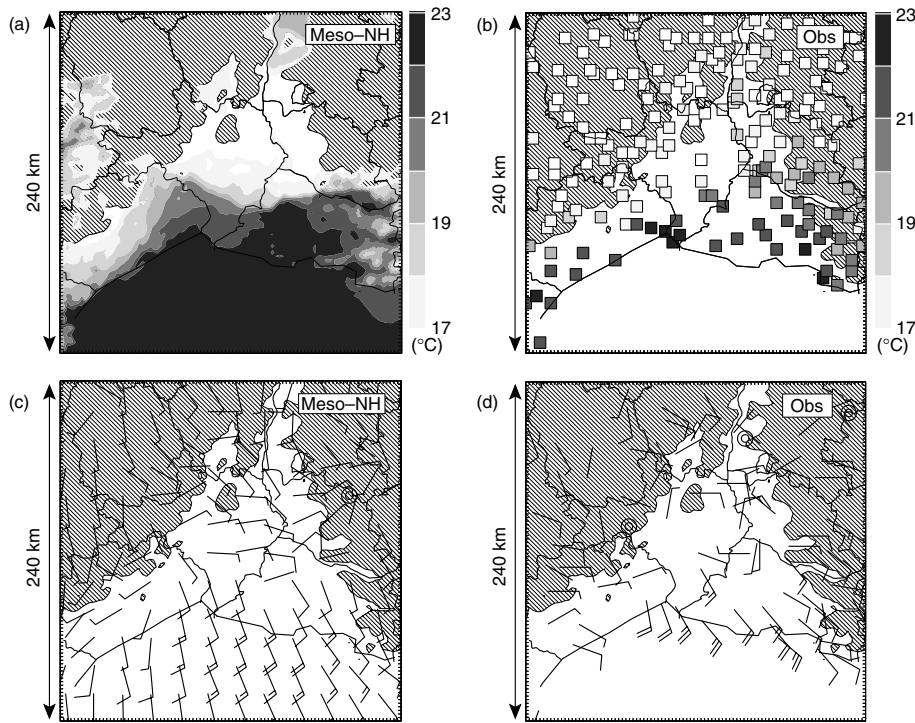


Figure 14. As Figure 10, but for the Gard case. The time is 18 UTC, 8 September 2002.

of the disturbed upper-level ‘jet-streak’. The diffluence associated with the south to southwesterly upper-level flow appeared to be strongest over northern France at 12 UTC on 12 November (Figure 18a). However, at 00 UTC, the trough axis became oriented more northwest–southeast, and southern regions of France become much more directly influenced by the upper-level diffluence. The model also succeeded in simulating fairly well the counterclockwise rotation of the trough axis (Figure 18(b) and (c)) except for later in the simulation when the motion is too fast with respect to the ARPEGE analysis. The fact that the upper-level pattern persisted and lasted through the simulation might generate favourable synoptic conditions for maintenance of convective activity over the area by providing additional upward motion.

#### 4.3.2. Low-level mesoscale environment forecast

The location of the observed very strong low-level flow is well captured by Meso-NH (Figure 19), although the simulated surface winds are slightly weaker than those observed (Figure 19(c) and (d)). The tongue of warmest surface air is well simulated as well as its spatial extent and intensity.

#### 4.3.3. Heavy precipitation forecast

As for the Gard case, the model simulates a precipitating system for the Aude event which is close to the observed

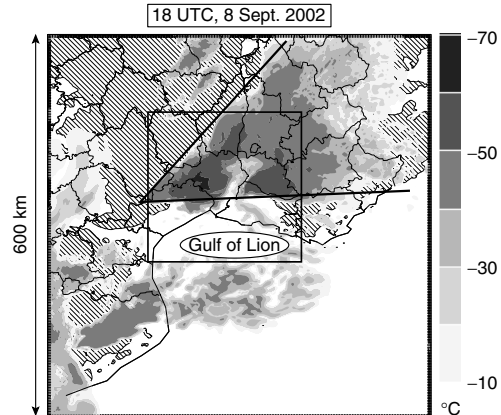


Figure 15. Simulated METEOSAT infrared brightness temperature (shading) for the Gard case from MDA. The bold solid line shows the V-shape of the system at this time and the box represents the subdomain used for Figure 16(a).

one, i.e. a south–north line of precipitation extending from the eastern edge of Pyrenees up to the southwestern part of the Massif Central (Figure 20(a)).

The Aude case is the only one for which Meso-NH is able to trigger a significant precipitation system, even starting from the REF10 simulation. Indeed, Meso-NH already succeeds fairly well in forecasting the

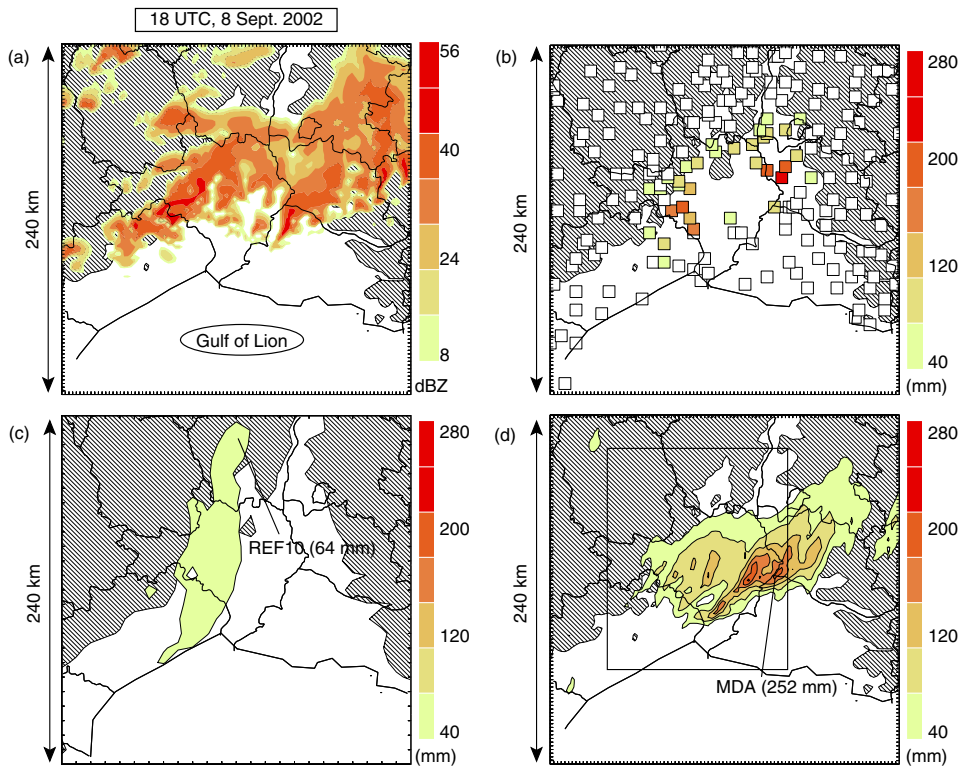


Figure 16. As Figure 11, but for the Gard case from 12 to 22 UTC, 8 September 2002. This figure is available in colour online at [www.interscience.wiley.com/qj](http://www.interscience.wiley.com/qj)

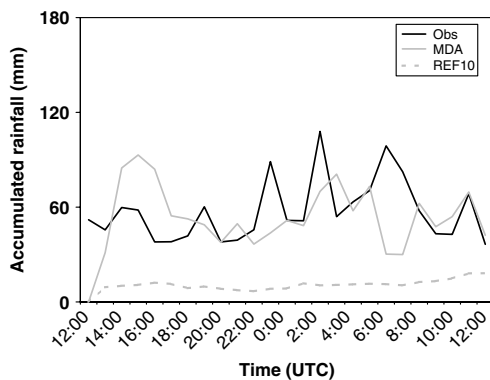


Figure 17. As Figure 12, but for the Gard case within the box shown in Figure 16(d).

location of the heavy precipitation centre over the central eastern region of the Aude department with accumulated rainfall peaking near 210 mm (Figure 20(c)). Increasing the resolution also improves the precipitation forecast with a maximum of 281 mm for the best high-resolution simulation (Figure 20(d)). Moreover, the rainfall time series shown in Figure 21 indicates a strong maximum 1-hour accumulated precipitation of about 50 mm during

the mature stage of the convective system. However, it is important to note that the model produces a slight eastward shift of the area of intense precipitation south of Aude which is weaker than the observations because the simulated trough (as mentioned above) rotates faster than the observed.

For the three cases, it is concluded that Meso-NH succeeds in reproducing realistic structures of the three HPEs since the model captures and correctly simulates the synoptic-scale environment in which the convective systems were embedded.

## 5. Detailed analysis of synoptic-scale ingredients leading to HPEs

After having evaluated the simulations for the three cases and described the upper-level dynamics favourable for the HPEs, we now emphasize the additional synoptic-scale ingredients that favour long-lasting HPEs. For that purpose, water vapour fluxes at low levels, i.e.

$$\int_{z=0}^{z=3 \text{ km}} \rho_v \mathbf{V}_h dz$$

(where  $\rho_v$  is the specific humidity and  $\mathbf{V}_h$  the horizontal wind) have been computed at the mature stages of

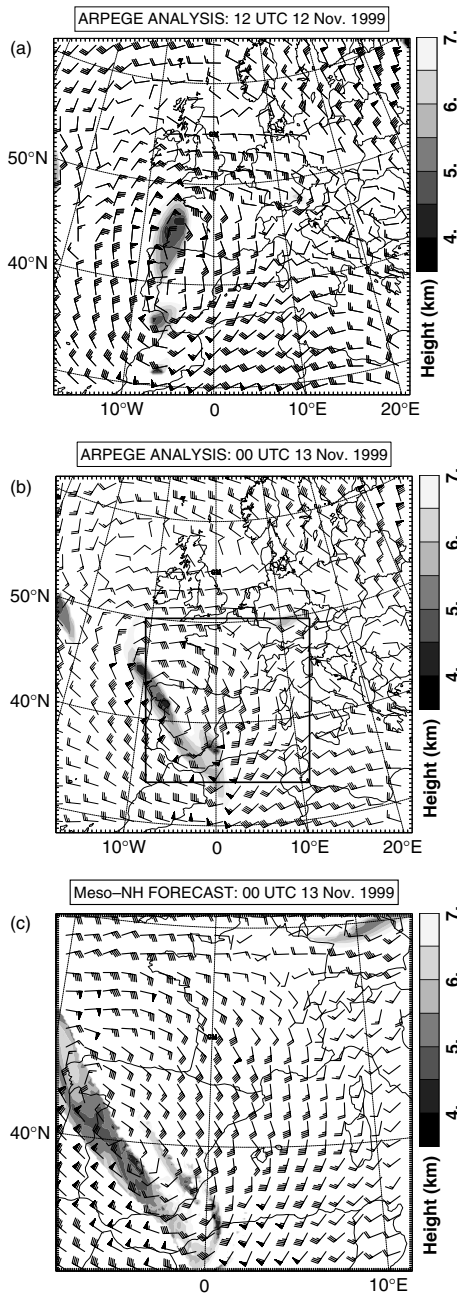


Figure 18. As Figure 9, but for the Aude case.

the convective systems, as well as composites of the simulated conditional convective instability.

### 5.1. Cévennes case

Figure 22(a) shows the spatial distribution of the simulated convective available potential energy (CAPE) at 1800 UTC on 13 October, i.e. just before the period of

heaviest rain. At this time, significant values of CAPE cover almost the entire western Mediterranean from southeastern France to North Africa (Figure 12(a)). A large area with maximum values greater than  $1500 \text{ J kg}^{-1}$  is centred just east of the Balearic Islands. Associated with these conditionally unstable air masses over the sea are large amounts of precipitable water (not shown) in the area.

In order to check whether air masses coming from areas of strong conditional convective instability feed the convective area, backward trajectories (Gheusi and Stein, 2002) have been computed. Parcels in the same vertical column as the simulated rainfall maxima (Figures 11, 16 and 20) have been taken at 1.5, 3, 5, 7 and 9 km heights and their origins six hours earlier have been determined. In Figure 22(a), the 6-hour back trajectories from 00 UTC on 14 October are superimposed. The trajectories show that parcels in the area of interest at 00 UTC were over the Mediterranean six hours earlier in the moist and strongly conditionally unstable area discussed above. This result confirms that the tongue of strong CAPE is important for feeding and sustaining the convective activity associated with the Cévennes event. Only the backward trajectory of the parcel at 1.5 km at 00 UTC departs slightly from the others, because of a more southerly flow at low levels. Trajectories are relatively short during the considered 6-hour period due to a slow and almost unidirectional mid- to upper-level flow.

Figure 22(b) reveals a tongue of significant values of water vapour flux coming from the south of Sardinia and from the Balearic Islands which reinforce the idea that, between 12 and 00 UTC, the air coming from the moist and conditionally unstable area mentioned above helps to maintain the convective activity by continuously advecting warm and moist air masses just off the French southeastern coast. It must be also stressed that this low-level synoptic pattern has more or less the same trend in the upper troposphere, i.e. the patterns evolve slowly.

### 5.2. Gard case

The synoptic environment for the Gard event has some similarities with the Cévennes event in terms of the distribution of the conditional convective instability. At 1800 UTC on 8 September, the atmosphere is quite conditionally unstable and the CAPE field is similar to that for the Cévennes episode, with the largest values (about  $1600 \text{ J kg}^{-1}$ ) located over the northwestern Mediterranean. An interesting pattern shown by the 6-hour back trajectories from 00 UTC (Figure 23(a)) is a significant veering to the southwest with altitude. Indeed, the LLJ contributes to enhance moisture advection whereas the strong mid- to upper-level flow favours northward motion of precipitation out of the triggering area. Such a wind profile is one of the factors which could maintain the rainfall activity. Moreover, as was the case for the Cévennes event, the parcels originate from the moist humid and conditionally unstable regions of the western Mediterranean (Figure 23(a)).

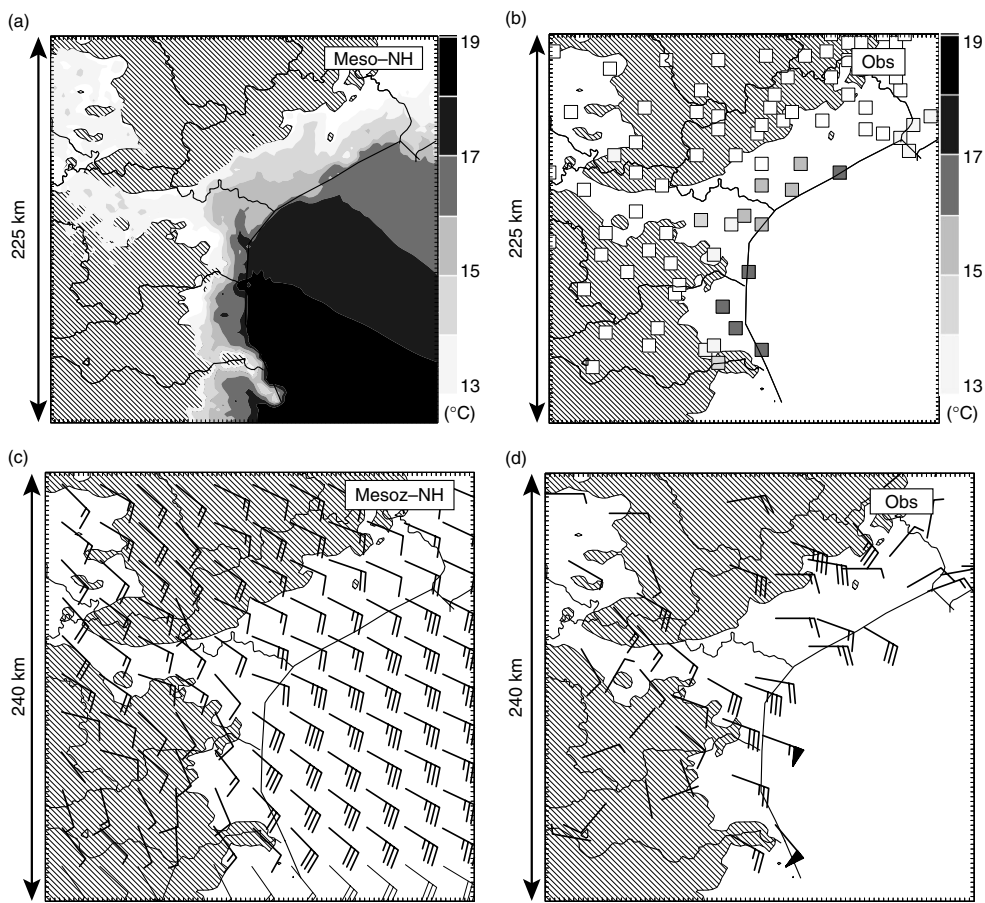


Figure 19. As Figure 10, but for the Aude case at 21 UTC, 12 November 1999.

Strong forcing also prevails at the surface for the Gard event. Indeed, as the cold front progresses slowly eastwards, the water vapour flux in the lower troposphere is increased ahead of the front with strong convergence of the flux upstream of the Rhône valley, bringing more moisture in to feed the convection in the region (Figure 23(b)). Once more, the slow approach of the cold front was a positive factor for advecting high humidity which was necessary to maintain the high precipitation rates over several hours.

### 5.3. Aude case

Finally, in contrast to the Cévenne and Gard cases, the Aude event has much weaker available conditional convective instability over the Mediterranean Sea. At 18 UTC on 12 November, the strongest values of CAPE (up to  $1500 \text{ J kg}^{-1}$ ) are located near Sardinia, i.e. away from the area of convection (Figure 24(a)).

Nevertheless, the Aude case also exhibits very pronounced low-level forcing in addition to a strong upper-level dynamic circulation already discussed in the previous section. Figure 24(b) depicts a large low-level area

of low pressure centred over the Sierra Nevada (Spain) and an anticyclone over the Italian Alps. Between these structures, a south to southeasterly jet prevails generating a very strong low-level water vapour flux of about  $650 \text{ kg s}^{-1} \text{ m}^{-2}$  in the 12 hours from 12 UTC on 12 November. On the eastern side of the low, significant northward advection of warm and moist air is probably supported by the strong low-level convergence of the moisture flux which maintains convective activity over the Aude department. As with the previous cases, the low-level synoptic pattern for the Aude event evolves very slowly as the low pressure area over Spain is nearly stationary over at least 12 hours.

## 6. Summary and concluding remarks

A description of three deep moist convective events which produced floods over southern France has been presented in this first of two linked papers. These particular cases have been selected due to their location over the southern Massif Central foothills, which is a region statistically favoured for very heavy precipitation events.

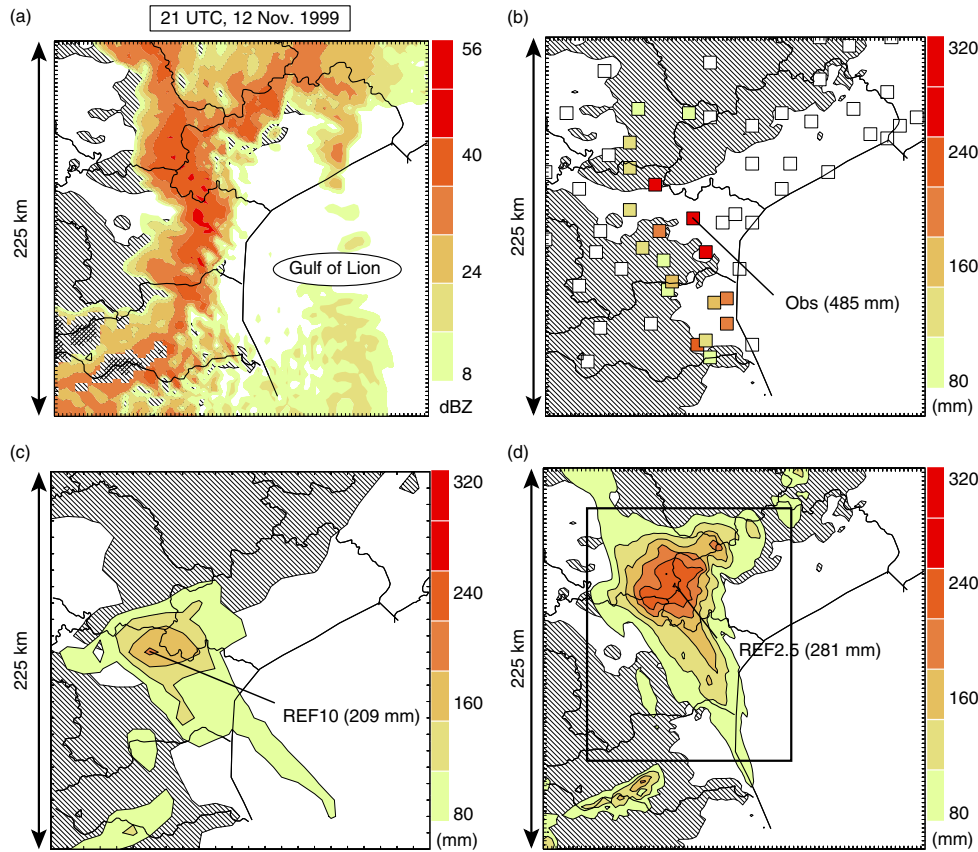


Figure 20. As Figure 11, but for the Aude case from 12 UTC, 12 November to 06 UTC, 13 November 1999. This figure is available in colour online at [www.interscience.wiley.com/qj](http://www.interscience.wiley.com/qj)

The aim of the first part of this study was to validate the best high-resolution simulations by comparing some features and the evolution from Meso-NH with the available observations. Moreover, the different synoptic ingredients which favoured the development of quasi-stationary MCSs in the case-studies have also been identified.

These numerical experiments have shown that, first, Meso-NH can reproduce and forecast significant rainfall amounts associated with convective systems with quasi-stationary behaviour (i.e. lasting several hours at the same location). Moreover, the model reproduces fairly well the low-level mesoscale environments associated with the three HPEs. Second, the meteorological synoptic-scale context was analyzed and the evolution in which each convective system was embedded was described. At the synoptic scale, the meteorological patterns for the Gard and the Aude cases were characterized by deep cyclonic circulations generating a strong diffluent southerly flow over the Mediterranean, from the North African coast to France. This upper cold low was initially to the west or to the north-west of France and moved very slowly. For the Cévennes case, although the synoptic forcing was less pronounced, a short-wave trough located off the

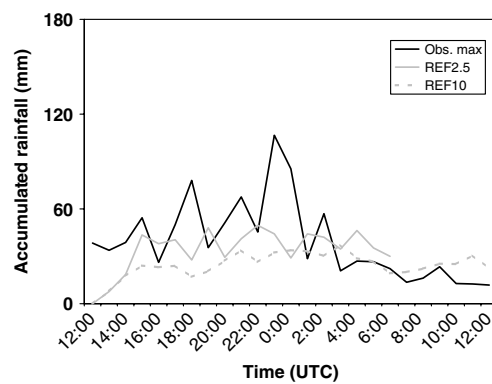


Figure 21. As Figure 12, but for the Aude case within the box shown in Figure 20(d).

North African coast most likely favoured triggering of the convection. For this last case, the synoptic conditions evolved very slowly due to a blocking high located over central Europe. The surface pattern also revealed strong forcing consisting of an anticyclone over the northern

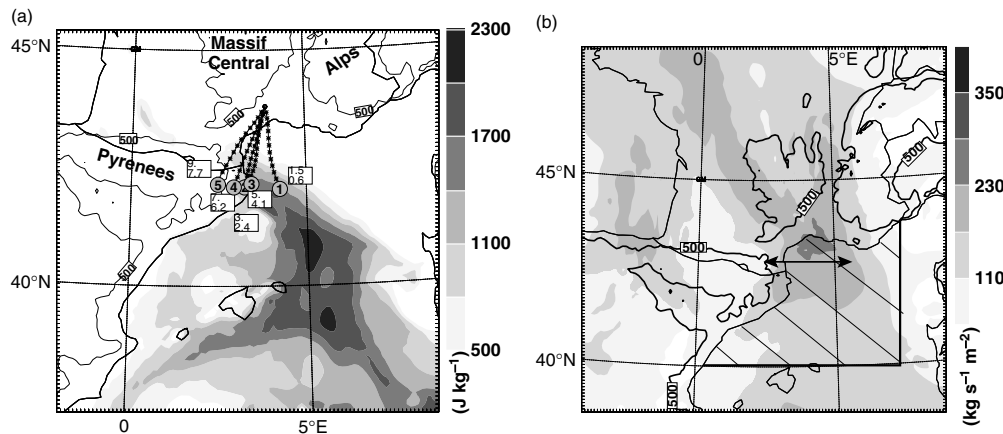


Figure 22. Low-level conducive ingredients for the best simulation for the Cévennes case: (a) simulated CAPE (shading) at 18 UTC, 13 October and (b) water vapour flux (shading) integrated between the surface and 3 km altitude, at 00 UTC, 14 October. (a) also shows 6-hour back trajectories for Lagrangian parcels starting at 00 UTC on 14 October at five heights. Lower and upper boxed labels indicate the height (km) over the flooding area at 00 UTC and at the source regions 6 hours earlier, respectively, and stars mark the parcel positions every 30 minutes. In (b), the hatched box represents the sea area over which CAPE was averaged for Figure 25, and the double-headed arrow denotes the line across which water vapour fluxes were integrated (also for Figure 25) through an area of 280 km length and 3 km height, about 70 km upstream of the flooding area. The 500 m topography contour is shown in both panels.

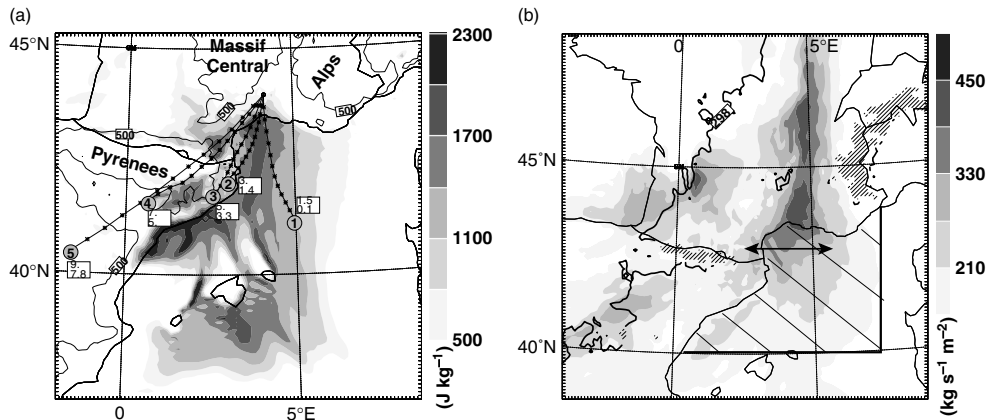


Figure 23. As Figure 22, but for the best simulation for the Gard case. Time is (a) 18 UTC, 8 September and (b) 00 UTC, 9 September 2002. Back trajectories start at 00 UTC, 9 September 2002. The bold contour in (b) denotes virtual temperature of 298 K.

Alps and a low pressure area over Spain for the Aude case, and a slow-moving surface cold front approaching the region for the Gard case. These low-level synoptic patterns induced an intense south to easterly LLJ which favoured strong low-level moisture transport and significant conditional convective instability over the flooded areas. For both extreme HPEs (i.e. Gard and Aude), the main basic ingredients for a flash-flood-producing system, as pointed out by Lin *et al.* (2001) for instance, were present to more or less the same extent for these cases: a conditionally unstable atmosphere and moist low levels in the presence of the large-scale forcing mentioned above and mesoscale lifting (i.e. orographic forcing and low-level convergence). Moreover, low-level moisture

fluxes or CAPE had larger values than those of the more classical heavy rain event (i.e. typical Cévennes cases). The conditional convective instability was weak for the Aude case but seems to be counterbalanced by large moisture fluxes (and *vice versa* for the Gard case), as can be seen in Figure 25. These slow-evolving synoptic ingredients favoured long-lasting rain over southern France in the numerical model.

However, even though synoptic-scale ingredients (upper-level PV anomalies, strong low-level moisture advection, CAPE, etc.) can provide the necessary ingredients for the convective activity, other important mesoscale factors and/or finer-scale processes contribute to continuously focus the activity over the same specific region

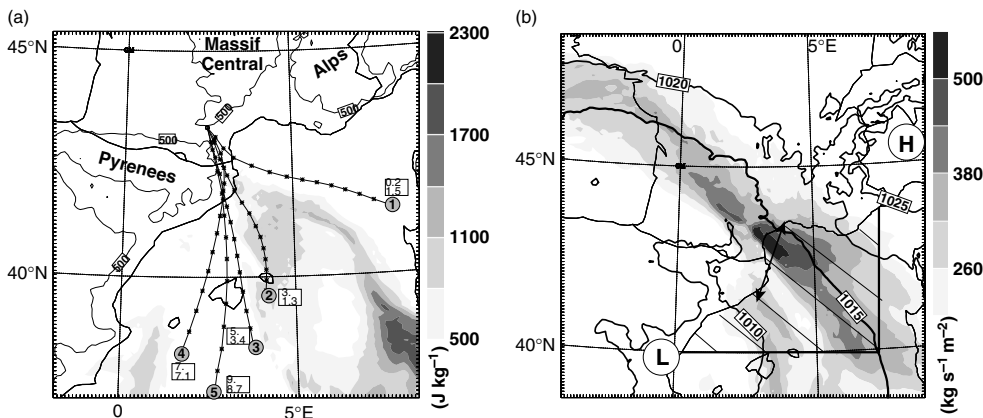


Figure 24. As Figure 22, but for the best simulation for the Aude case. Time is (a) 18 UTC, 12 November and (b) 00 UTC, 13 November 1999. In (b), L and H denote low and high pressure centres; surface isobars (bold) are also shown at 5 hPa intervals.

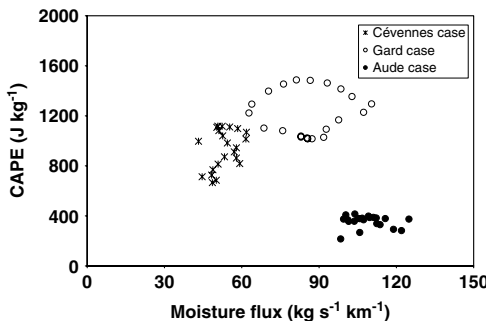


Figure 25. CAPE ( $\text{J kg}^{-1}$ ) versus water vapour flux ( $\text{kg s}^{-1} \text{km}^{-1}$ ) at times through each of the three cases. Both quantities are averaged as indicated in Figure 22.

(the necessary forced ascent to trigger and/or maintain the convection). This paper was dedicated to the evaluation of the best numerical simulation and also the identification of the synoptic-scale ingredients conducive for three flash-flood events over southern France. This, however, is not enough to explain, for instance, why heavy precipitation was located over the plain for the Gard case, i.e. about 80 km southeast of the most statistically favoured region for very heavy precipitation. Based on the best high-resolution numerical experiments with the Meso-NH model, the physical mechanisms leading to the stationarity of the three heavy precipitating systems over a specific region of southern France will be examined and discussed in a companion paper.

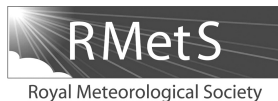
### Acknowledgements

This work has been carried out in the framework of the FLOODsite project, funding by the EU Sixth Framework Program. We thank A. Boone for improving the English of the manuscript. We gratefully acknowledge the comments made by the anonymous reviewers that helped to significantly improve the quality of the paper.

### References

- Bechtold P, Bazile E, Guichard F, Mascart P, Richard E. 2001. A mass-flux convection scheme for regional and global models. *Q. J. R. Meteorol. Soc.* **127**: 869–886.
- Beven KJ, Kirby MJ. 1979. A physically based, variable contributing area model of basin hydrology. *Hydrol. Sci. Bull.* **24**: 43–69.
- Beven KJ, Lamb R, Quinn P, Romanowicz R, Freer J. 1995. *Models of watersheds hydrology*. Water Resources Publications: Colorado, USA.
- Bluestein HB, Jain MH. 1985. Formation of mesoscale lines of precipitation: Severe squall lines in Oklahoma during the spring. *J. Atmos. Sci.* **42**: 1711–1732.
- Bougeault P, Binder P, Buzzi A, Dirks R, Houze R, Kuettner J, Smith RB, Steinacker R, Volkert H. 2001. The MAP Special Observing Period. *Bull. Am. Meteorol. Soc.* **82**: 433–460.
- Bougeault P, Lacarrère P. 1989. Parameterization of orography-induced turbulence in a meso-beta-scale model. *Mon. Weather Rev.* **117**: 1870–1888.
- Brenot H, Ducrocq V, Walpersdorf A, Champollion C, Caumont O. 2006. GPS zenith delay sensitivity evaluated from high-resolution numerical weather prediction simulations of the 8–9 September 2002 flash flood over southeastern France. *J. Geophys. Res.* **111**(D15105): DOI: 10.1029/2004JD005726.
- Buzzi A, Tartaglione N, Malguzzi P. 1998. Numerical simulations of the 1994 Piedmont flood: Role of orography and moist processes. *Mon. Weather Rev.* **126**: 2369–2383.
- Caniaux G, Redelsperger JL, Lafore JP. 1994. A numerical study of the stratiform region of a fast-moving squall line. Part I: General description and water and heat budgets. *J. Atmos. Sci.* **51**: 2046–2074.
- Caumont O, Ducrocq V, Delrieu G, Gosset M, Pinty J-P, Parent du Châtelet J, Andrieu H, Lemaitre Y, Scialom G. 2006. A radar simulator for high-resolution non-hydrostatic models. *J. Atmos. Oceanic Technol.* **20**: 1049–1067.
- Chancibault K, Anquetin S, Ducrocq V, Saulnier G-M. 2006. Hydrological evaluation of high resolution precipitation forecasts of the Gard flash-flood event (8–9 September 2002). *Q. J. R. Meteorol. Soc.* **132**: 1091–1117.
- Chappell CF. 1986. Quasi-stationary convective events. Pp 289–310 in *Mesoscale meteorology and forecasting*. Ray PS (ed). Amer. Meteorol. Soc: Boston.
- Clark TL, Farley RD. 1984. Severe downslope windstorm calculations in two and three spatial dimensions using anelastic interactive grid nesting: A possible mechanism for gustiness. *J. Atmos. Sci.* **41**: 329–350.
- Cuxart J, Bougeault P, Redelsperger J-L. 2000. A turbulence scheme allowing for mesoscale and large-eddy simulations. *Q. J. R. Meteorol. Soc.* **126**: 1–30.
- Delrieu G, Ducrocq V, Gaume E, Nicol J, Payrastre O, Yates E, Kirstetter P-E, Andrieu H, Ayral P-A, Bouvier C, Creutin J-D, Livet M, Anquetin S, Lang M, Neppel L, Obled C, Parent-du-Châtelet J, Saulnier G-M, Walpersdorf A, Wobrock W. 2005. The

- catastrophic flash-flood event of 8–9 September 2002 in the Gard region, France: A first case-study for the Mediterranean Hydro-meteorological Observatory. *J. Hydrometeorol.* **6**: 34–52.
- Doswell CA III, Ramis C, Romero R, Alonso S. 1998. A diagnostic study of three heavy precipitation episodes in the Western Mediterranean region. *Weather and Forecasting* **13**: 102–124.
- Ducrocq V, Lafore J-P, Redelsperger JL, Orain F. 2000. Initialization of a fine-scale model for convective system prediction: A case-study. *Q. J. R. Meteorol. Soc.* **126**: 3041–3066.
- Ducrocq V, Ricard D, Lafore J-P, Orain F. 2002. Storm-scale numerical rainfall prediction for five precipitating events over France: On the importance of the initial humidity field. *Weather and Forecasting* **17**: 1236–1256.
- Ducrocq V, Aulio G, Santurette P. 2003a. Les précipitations intenses et les inondations du 12 et 13 Novembre 1999 sur le sud de la France. *La Météorologie* 8th série, **42**: 18–27.
- Ducrocq V, Lebeaupin C, Thouvenin T, Giordani H. 2004. L'événement des 8–9 septembre 2002: Situation météorologique et simulation à mésoscale. *La Houille Blanche* **6**: 86–92.
- Ferretti R, Low-Nam S, Rotunno R. 2000. Numerical simulations of the Piedmont flood of 4–6 November 1994. *Tellus* **52A**(1): 162–180.
- Fernandez C, Gaertner MA, Gallardo C, Castro M. 1995. Simulation of a long-lived Meso- $\beta$  scale convective system over the Mediterranean coast of Spain. Part I: Numerical predictability. *Meteorol. Atmos. Phys.* **56**: 157–179.
- Frei C, Shär C. 1998. A precipitation climatology of the Alps from high-resolution raingauge observations. *Int. J. Climatol.* **18**: 873–900.
- Gal-Chen T, Sommerville RCJ. 1975. On the use of a coordinate transformation for the solution of the Navier–Stokes equations. *J. Comput. Phys.* **17**: 209–228.
- Gaume E, Livet M, Desbordes M, Villeneuve J-P. 2004. Hydrological analysis of the river Aude, France, flash flood on 12 and 13 November 1999. *J. Hydrol.* **286**: 135–154.
- Gheusi F, Stein J. 2002. Lagrangian description of airflows using Eulerian passive tracers. *Q. J. R. Meteorol. Soc.* **128**: 337–360.
- Hamadache B, Terchi A, Brachemi O. 2002. Study of the meteorological situation which affected the west and the centre of Algeria in general and Bab-el-oued in particular on 10 November 2001. Proceedings of fourth EGS Plinius Conference, Mallorca, Spain, CD-ROM.
- Hernandez E, Cana L, Diaz J, Garcia R, Gimeno L. 1998. Mesoscale convective complexes over Western Mediterranean area during 1990–1994. *Meteorol. Atmos. Phys.* **68**: 1–12.
- Homar V, Romero R, Ramis C, Alonso S. 1999. A case of convection development over the Western Mediterranean Sea: A study through numerical simulations. *Meteorol. Atmos. Phys.* **71**: 169–188.
- Huet P, Martin X, Prime J-L, Foin P, Laurain C, Cannard P. 2003. ‘Retour d’expérience des crues de Septembre 2002 dans les départements du Gard, de l’Hérault, du Vaucluse, des Bouches-du-Rhône, de l’Ardèche et de la Drôme’. Technical report, Ministère de l’écologie et du développement durable: Paris, France.
- Jansa A, Genoves A, Angeles Picornell M, Campins J, Riosaldo R, Carretero O. 2001. Western Mediterranean cyclones and heavy rain. Part 2: Statistical approach. *Meteorol. Appl.* **8**: 43–56.
- Kain JS, Fritsch JM. 1990. A one-dimensional entraining/detraining plume model and its application in convective parameterizations. *J. Atmos. Sci.* **47**: 2784–2802.
- Kain JS, Fritsch JM. 1993. Convective parameterization for mesoscale models: the Kain–Fritsch scheme. *Meteorol. Monogr.* **46**: 165–170.
- Lafore J-P, Stein J, Ascencio N, Bougeault P, Ducrocq V, Duron J, Fisher C, Hereil P, Mascart P, Pinty J-P, Redelsperger J-L, Richard E, Vila-Guerau de Arellano J. 1998. The Meso-NH Atmospheric Simulation System. Part I: Adiabatic formulation and control simulations. *Ann. Geophys.* **16**: 90–109.
- Lin Y-L, Chiao S, Wang T-A, Kaplan ML, Weglarz RP. 2001. Some common ingredients for heavy orographic rainfall. *Weather and Forecasting* **16**: 633–659.
- Lasat MC, Puigcerver M. 1994. Meteorological factors associated with floods in the North-eastern part of the Iberian Peninsula. *Nat. Hazards* **9**: 81–93.
- Maddox R-A, Chapell C-F, Hoxit L-R. 1979. Synoptic and meso-alpha scale aspects of flash flood events. *Bull. Am. Meteorol. Soc.* **60**: 115–123.
- Massacand AC, Wernli H, Davies HC. 1998. Heavy precipitation on the Alpine south side: An upper-level precursor. *Geophys. Res. Lett.* **25**: 1435–1438.
- Penarrocha D, Estrela M, Millan M. 2002. Classification of daily rainfall patterns in a Mediterranean area with extreme intensity levels: the Valencia region. *Int. J. Climatol.* **22**: 677–695.
- Pinty J-P, Jabouille P. 1998. A mixed-phased cloud parameterization for use in a mesoscale non-hydrostatic model: Simulations of a squall line and orographic precipitation. Pp 217–220 in Preprints, Conference on Cloud Physics, Everett, WA. Amer. Meteorol. Soc: Boston.
- Redelsperger J-L, Sommeria G. 1981. Méthode de représentation de la turbulence d’échelle inférieure à la maille pour un modèle tridimensionnel de convection nuageuse. *Boundary-Layer Meteorol.* **21**: 509–531.
- Ricard D. 2005. Modélisation à haute résolution des pluies intenses dans les Cévennes: Le système convectif des 13 et 14 Octobre 1995. *La Météorologie* 8th série, **42**: 28–38.
- Riosaldo R. 1990. Characterization of mesoscale convective systems by satellite pictures during PREVIMET MEDITERR-ANEJO-89 (In Spanish). Pp. 135–148 in Proc. Segundo Simposio Nacional de Predicción, Madrid. Available from Instituto Nacional de Meteorología, Apartado 285, 28071 Madrid, Spain.
- Rivrain J-C. 1997. Les épisodes orageux à précipitations extrêmes sur les régions méditerranéennes de la France. *Phénomènes remarquables* **4**: Météo-France: Toulouse.
- Romero R, Doswell CA III, Ramis C. 2000. Mesoscale numerical study of two cases of long-lived quasi-stationary convective systems over Eastern Spain. *Mon. Weather Rev.* **128**: 3731–3751.
- Rotunno R, Ferretti R. 2001. Mechanisms of intense Alpine rainfall. *J. Atmos. Sci.* **58**: 1732–1749.
- Scofield RA. 1985. ‘Satellite convective categories associated with heavy precipitation’. Pp 42–51 of Preprints for Sixth Conference on Hydrometeorology, 29 October 1985, Indianapolis. Amer. Meteorol. Soc: Boston.
- Sénési SP, Bougeault P, Chèze J-L, Cosentino P, Thepenier R. 1996. The Vaison-la Romaine flash flood: Mesoscale analysis and predictability issues. *Weather and Forecasting* **11**: 417–442.
- Stein J, Richard E, Lafore J-P, Pinty J-P, Ascencio N, Cosma S. 2000. Meso-NH simulations with grid-nesting and ice phase parameterization. *Meteorol. Atmos. Phys.* **72**: 203–221.



## A statistical downscaling to identify the large-scale circulation patterns associated with heavy precipitation events over southern France

O. Nuissier,\* B. Joly, A. Joly, V. Ducrocq and P. Arbogast

CNRM-GAME, Météo-France/CNRS, Toulouse, France

\*Correspondence to: O. Nuissier, CNRM/GMME/MICADO, 42 av. G. Coriolis, 31057 Toulouse, France.  
E-mail: olivier.nuissier@meteo.fr

This study assesses the potential for a detection algorithm to identify discriminating analysis-based statistical predictors of a few relevant parameters that can be used to capture heavy precipitation events (HPEs), or, at least, their associated large-scale circulation (LSC) patterns in a climate scenario. HPEs are defined from a sample combining ‘large-scale’ fields from the ECMWF ERA-40 reanalysis with local observations from the Météo-France rain-gauge network. In a first step, LSC patterns considered as significantly favouring HPE over southern France are identified and described with the greatest robustness possible. For that purpose, an objective automatic clustering of the unfiltered 500 hPa geopotential height field is performed. Four clusters are obtained. Among them, the most discriminating for heavy precipitation is characterised by a synoptic-scale deep upper-level low northwest of the area of interest, inducing a southerly flow over the western Mediterranean Sea and southern France. In a second step, other lower-scale parameters are used to refine the characteristics of the clusters. It has been found that the low-level moisture transport is a relevant low-level ingredient to regionally characterise heavy precipitation. Indeed, ‘Cévennes’ cases are related to more south to southeasterly flows over the Gulf of Lion, whereas ‘Languedoc-Roussillon’ events occurred preferentially within a more pronounced easterly wind component with two streams of low-level moisture transport. Moreover, in-depth examination of the low-level features reveals that HPEs tend to occur when the wind blows in a specific direction and for the greatest low-level moisture flux over the Gulf of Lion. Finally, the predictive skill of a detection tool for HPEs over southern France, with only synoptic-scale favourable parameters as predictors, is discussed. It is shown that this tool allows selection of HPE situations in more than 70% of cases. Copyright © 2011 Royal Meteorological Society

*Key Words:* flash floods; cluster analysis; synoptic-scale precursors

*Received 13 November 2009; Revised 18 May 2011; Accepted 20 May 2011; Published online in Wiley Online Library 1 August 2011*

*Citation:* Nuissier O, Joly B, Joly A, Ducrocq V, Arbogast P. 2011. A statistical downscaling to identify the large-scale circulation patterns associated with heavy precipitation events over southern France. *Q. J. R. Meteorol. Soc.* 137: 1812–1827. DOI:10.1002/qj.866

### 1. Introduction

The western Mediterranean region is prone to devastating flash-flood events induced by heavy precipitation events

(HPEs), particularly during the autumn season. Frei and Schär (1998) analysed high-resolution rain-gauge observations of daily surface rainfall to produce a precipitation climatology extending from the Massif Central to the eastern

## 1.2. PUBLICATIONS MAJEURES POUR LA SOUTENANCE DE L'HABILITATION À DIRIGER DES RECHERCHE

European Alps. This study showed that precipitation is particularly enhanced along the Alpine foothills, with dryer conditions over the mountains. Furthermore, Frei and Schär (1998) also clearly showed that the southeastern part of the Massif Central (also known as the Cévennes) is one of the five rainiest areas of the region. Focusing on this region of interest and considering the number of days for which the daily surface rainfall exceeded 200 mm between 1958 and 2004 over southern France, the southern Alps, the eastern Pyrenees, eastern Corsica and the southern Massif Central, it was found that these areas are the most frequently exposed to heavy precipitation (Figure 2 of Nuissier *et al.*, 2008). Some of these events may lead to violent total rainfall from a few hours up to one day and cause severe damage and even casualties. During the Gard event over southern France on 8–9 September 2002 (the Gard case), over 600 mm fell in 24 h. Such an amount over the small to medium catchments of the region had a dramatic hydrological impact (Delrieu *et al.*, 2005). In most cases, such rainfall amounts are generally produced by intense deep convection associated with quasi-stationary mesoscale convective systems (MCSs). Mesoscale ingredients are crucial in the triggering of deep convection, e.g. conditional instability, low-level convergence and moisture flux that pinpoint the deep convection development over the same area over several hours (Ducrocq *et al.*, 2008). As a major mechanism, the orographic lifting continuously generates convective cells over the upwind side of the mountain. In addition to these favourable mesoscale ingredients, some recurrent large-scale circulation (LSC) configurations are often considered to play a key role in the formation and sustaining HPEs.

The link between heavy precipitation occurring over the western Mediterranean regions and synoptic-scale troughs or surface cyclones was well established in previous case-studies. That these synoptic-scale precursors interact with the orography of the western Mediterranean Sea and induce dynamic forcing favourable to torrential event occurrences is also well established (Buzzi *et al.*, 1998; Doswell *et al.*, 1998; Massacand *et al.*, 1998; Homar *et al.*, 1999; Romero *et al.*, 2000; Jansa *et al.*, 2001). A recent study by Nuissier *et al.* (2008) of three HPEs over southern France showed the importance of upper-level synoptic ingredients such as the deep cyclonic upper-level circulation that generates a strong confluent flow over the Mediterranean Sea and a blocking located downstream over central Europe slowing down the evolution of the synoptic conditions. These synoptic patterns are generally associated with intense south to southeasterly low-level jets that favour strong low-level moisture transport towards the flooded areas. Whether these conclusions extend to all HPEs of a given region still remains open.

The study by Plaut *et al.* (2001, PSD01 hereafter) initiated a new framework to specifically address this previous point. As in many LSC identification studies, this one is based on classification methods which in PSD01 are applied to the 700 hPa geopotential height (denoted  $Z_{700}$ ) over the North Atlantic and western Europe. The LSC classes over three sub-regions of the French Alps were identified. The classification was made from a set of precipitating events defined as having daily rainfall exceeding 40 mm. Moreover, PSD01 introduced a new criterion in order to investigate whether or not a cluster is significantly ‘propitious’ to heavy rainfall. They computed the ‘discriminating power’ of a cluster, i.e. the probability of large rainfall occurrence versus the proximity to the cluster centre. Thus, they

found a classification providing patterns that are associated with heavy rainfall over the given sub-domain with high probability (between 50% and 75%). PSD01 found that large rainfalls occurring over the Alpes Maritimes region (i.e. the French southern flank of the Alps) are associated with a deep negative geopotential anomaly just south of Ireland. This feature generates a large-amplitude wave at mid-tropospheric level with strong moisture-advection southwesterly over the southern Alps. LSC classification analysis performed by PSD01 over the Alps provides an alternative method to identify HPE situations for classical quantitative rainfall analysis. There is a great interest in such results since (numerical weather prediction or climate) models suffer from a significant rise in quantitative precipitation errors at the medium range. Nevertheless, there is still a fairly high level of predictability at the space- and time-scales of the LSC patterns propitious to HPEs.

This present study broadens the scope of the PSD01 study and explores (through a statistical downscaling approach) the possible detection of intense precipitation events over southern France only from synoptic-scale propitious meteorological ingredients. This paper is divided into two parts. The first goal is to characterise in a systematic way the heavy precipitation events over southern France. Dynamic climatology methods are used in order to emphasise relationships between local intense precipitation and large-scale patterns of different meteorological parameters. The second objective of this paper is then to build a detection algorithm based on a discriminating analysis of a few relevant parameters that can be used to ‘capture’ situations propitious to HPEs, either in climate scenarios or in long-range operational forecasting. A companion paper (Beaulant *et al.*, 2011) describes such an application for a climate scenario.

Firstly, we identify and describe with the greatest possible robustness the LSC patterns favouring HPEs over southern France. Then, we intend to find statistical predictors from the properties of these LSC patterns to build a detection algorithm for HPEs over the region of interest. We expect a better description of LSC patterns and better discrimination of HPEs than in PSD01. For that purpose, a deeper and newer reanalysis dataset, as well as a higher-resolution and more extended rain-gauge network identifying rainfall events, are used.

The outline is as follows. The rain-gauge and the reanalysis database, and the statistical methodology, are first described in section 2, then an objective criterion is proposed to define HPEs. Section 3 presents the classification of the rainfall events LSC patterns and the composite analyses of the low- and upper-level synoptic signatures associated with the rainfall clusters. Section 4 discusses the predictive skill of a detection tool for HPEs over southern France, with only synoptic-scale favourable parameters as predictors. Finally, synthesis and conclusions are given in section 5.

## 2. Datatsets and methodology

### 2.1. Rainfall dataset: definition of rainfall events

Rainfall observations are provided by the Météo-France rain-gauge network and 435 stations have been used (Figure 1(b)). In this study, we consider a four-month period from 1 September to 31 December, from 1960 to 2000, to fully encompass the autumn season. Two types of rainfall events

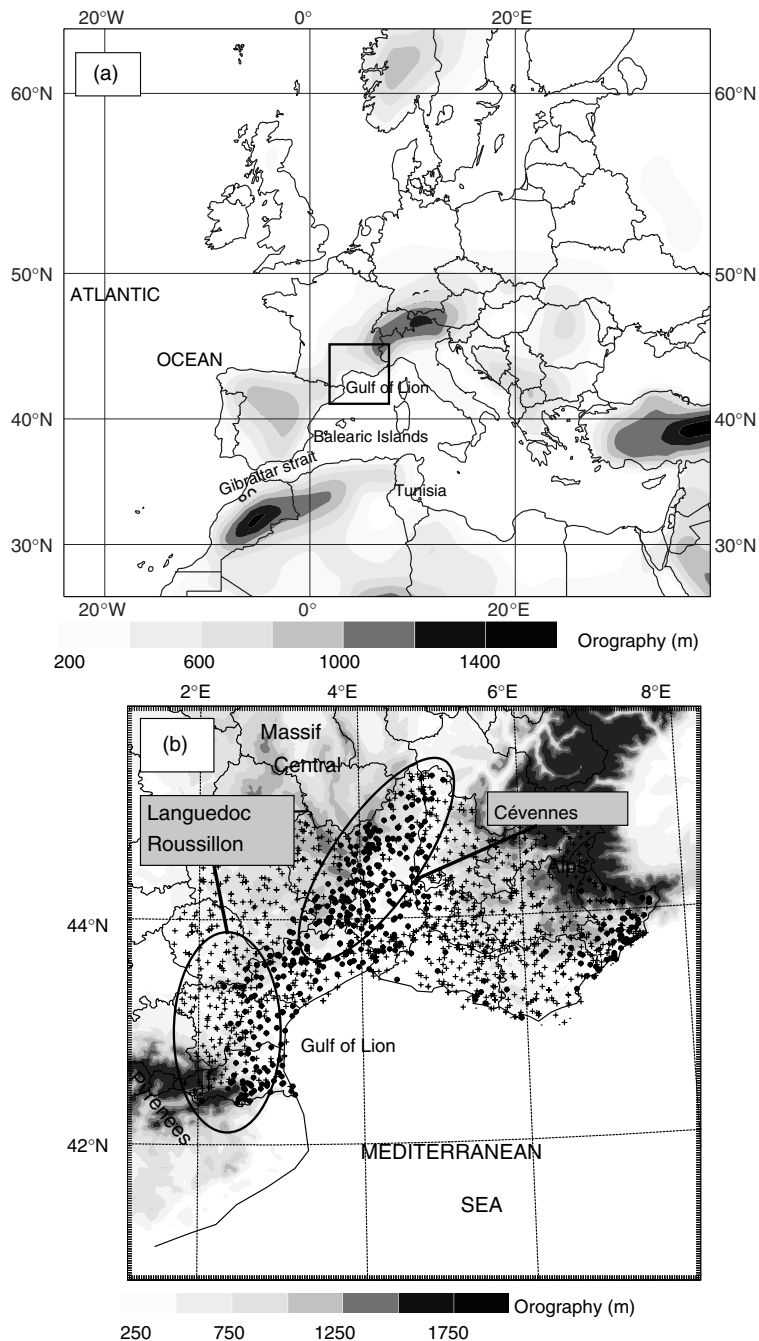


**Figure 1.** (a) Geographical domain used for circulation classification. (b) Map of rain-gauge stations used to define the precipitation events (black dots); crosses show the full rain-gauge network in the area of interest. The orography resolution is (a) 110 km and (b) 2.5 km.

are defined according to the distribution properties of the 24 h accumulated rainfall series from the rain-gauges. A first set of 1200 significant rainfall events (SREs) was made when at least two stations distant by 60 km, exceed their corresponding 97% quantile (mean value 37.5 mm and standard deviation 15.3 mm). A second set of 202 HPEs was made under the same conditions, but increasing the

quantile to 99.9% (mean value 144.6 mm and standard deviation 38.4 mm). Obviously, the set of HPEs is included in the SRE set. Both sets of events are defined as objectively as possible with statistical criteria. A quantile-based criterion has been preferred to a threshold value in order to estimate the level of ‘extremeness’ of the daily maximum precipitation as a statistical property rather than an absolute physical value.

## 1.2. PUBLICATIONS MAJEURES POUR LA SOUTENANCE DE L'HABILITATION À DIRIGER DES RECHERCHE

The second criterion on proximity between two stations has been used in order to avoid isolated HPEs.

### 2.2. LSC dataset and classification

In order to perform the classification of relevant LSCs, the 41-year reanalysis ERA-40 database is used (Uppala *et al.*, 2005). This is available from the European Centre for Medium-range Weather Forecasting (ECMWF), and the period 1960–2001 has been used. The daily analysis at 1200 UTC is employed. The geopotential height at 500 hPa ( $Z_{500}$ ) was chosen as it provides a good summary of the mid- to upper-troposphere synoptic dynamics (Vautard, 1990). The fields are interpolated and provided by the ECMWF ERA-40 reanalysis system on a regular latitude-longitude grid with  $1.5^\circ$  resolution on a domain that extends from  $24^\circ\text{W}$  to  $39^\circ\text{E}$  and from  $25.5^\circ\text{N}$  to  $63^\circ\text{N}$  (Figure 1(a)). This domain is wide enough to encompass the Mediterranean area and to account for the LSC patterns that cover the Mediterranean basin, the northern African coast and the northeastern Atlantic.

Prior to the classification step, the fields are prepared as follows. The climatological anomalies (i.e. the seasonal cycle) and a linear trend over the whole period are first removed from the data for each grid point, considering the whole period of the ERA-40 reanalysis. Then, the overall mean is removed from the detrended fields. A principal component analysis (PCA) is then performed in order to reduce the dimension of the dataset considering here only four specific months: 1 September to 31 December. The leading 20 principal components (PCs) of the  $Z_{500}$  field corresponding to the 1200 days of SRE are retained. The projection on these eigenvectors explains about 90% of the variance.

Clusters are then built from these fields using a clustering algorithm implemented in the ANAXV package provided by the Laboratoire de Météorologie Dynamique of CNRS (Michelangeli *et al.*, 1995). The core clustering algorithm, known as the  $K$ -means clustering method, is a partitioning algorithm based on the recurrence property of patterns. It is largely used in atmospheric circulation classifications because of its skill to maximise the separation between the centroids (Huth *et al.*, 2008). It determines a partition of the whole dataset that simultaneously minimises the sum of variances within each clusters and maximises the variance between clusters. The partition must also be independent from the initial seeds. It is a non-hierarchical method and, as a result, the number of classes is not *a priori* prescribed. The number of classes is automatically determined following the Michelangeli *et al.* (1995) method. Classifications with between two and nine clusters are built after the  $K$ -mean method described above. Two classifiability indices measuring variances and correlations within classes are computed for each of these classifications and compared to several random ones with the same number of classes. The most relevant classification has a maximum correlation and a minimum variance; both need to exceed the noise level provided by the random classifications. This objective technique has already been used in several studies on weather regime identification in the Northern Hemisphere (e.g. Robertson and Ghil, 1999; Kageyama *et al.*, 1999; Plaut *et al.*, 2001; Lana *et al.*, 2007) and also in the Southern Hemisphere (Solman and Menendez, 2003).

### 2.3. Synopsis of our procedure

The first goal of our study is to highlight the large and subsynoptic-scale environment patterns favourable to intense precipitation in the Mediterranean area. The second objective of the article is then to find statistical predictors based on a discriminating analysis from the different parameters identified in the previous step, in order to detect and extract LSC patterns propitious to heavy rainfall events. For that purpose, we applied a statistical procedure based on:

- (i) a dynamical clustering of LSC patterns (geopotential height at 500 hPa) to isolate the synoptic-scale upper-level features leading to SREs and HPEs,
- (ii) the identification and exploration of other low-level dynamical parameters to provide a more relevant description of the clusters associated with HPEs,
- (iii) an analysis of correlation distance distributions to assess the most discriminating ingredients for HPEs, and finally,
- (iv) an assessment of the ability of a detection algorithm to capture a HPE only from its associated synoptic-scale environment.

In step (i), the dynamical clustering is applied to the SRE dataset. As HPEs are a small subset of SREs, specific LSC for HPEs will be retrieved from the SRE classification. This approach refers to the ‘weather regime’ approach (Vautard *et al.*, 1988; Vautard, 1990; Michelangeli *et al.*, 1995) used in PSD01. After isolating the synoptic-scale upper-level features associated with HPEs, other lower-level parameters are used to refine the characteristics of the environment favourable to heavy precipitation. After a discriminating analysis in (iii), a detection algorithm is finally built in step (iv) by combining the three previous steps. This statistical procedure is constructed to select the HPEs most controlled by the synoptic-scale conditions.

### 3. Rainfall event LSC patterns

The algorithm summarised in the previous section yields a partition into four clusters. The classifiability index is above the significance threshold of 90%. It implies that classification computations always lead to the same clusters, whatever the way the classes are initialised. It has been decided, for the sake of simplicity, to use a specific nomenclature, similar to the description made in the *Grosswetterlagen* (James, 2006). Table I shows the four

Table I. Classification of synoptic types for significant rainfall in southern France, and percentage of significant rainfall events and heavy precipitation events by type (1960–2001).

Cluster	Synoptic type		
		SRE	HPE (%)
1	Cyclonic southwesterly	CSW	35.7 44.4
2	Western low (cut-off)	WL	23.0 18.2
3	Cyclonic northwesterly	CNW	15.8 3.9
4	Cyclonic southerly	CS	25.5 33.5
Total no. of events		1210	202

synoptic types; cluster CSW is the most populous with 35.7% (431 cases out of the 1200 days) of SREs, and 44.4% of HPEs; CNW contains only 15.8% (191 cases) of SREs and 3.9% of HPEs.

In a first subsection, composites, i.e. spatial averaged distributions, of upper-level fields ( $Z_{500}$  and wind speed at 300 hPa) are computed and discussed for each cluster. Secondly, we distinguish HPE and non-HPE days as two subsets of each LSC cluster: one subset gathers the days when an HPE occurred, and the other subset is made up of the SRE days with HPEs excluded. Composites are also computed for these two subsets. Moreover, other low-level parameters are used to refine the characteristics of the environment propitious to heavy precipitation.

### 3.1. SRE cluster composites

Cluster CSW is characterised by a large and strong upper-level low between Iceland and Ireland with a trough extending southwards towards the Iberian Peninsula (Figure 2(a)). The trough axis, with a weak northwest–southeast tilt, induces a strong mid- to upper-level southwesterly flow over France. The horizontal wind on the 2 PVU surface is also presented in Figure 2. The western side of the trough hosts a jet streak with wind speed reaching about  $35 \text{ m s}^{-1}$ . The areas exposed to rainfall events are below the eastern side of the trough where the weaker flow speed is about  $24\text{--}26 \text{ m s}^{-1}$ . It is worth mentioning that the anticyclonic curvature of the height contours over continental Europe suggests the presence of upper-level diffluence, which may be a source of upward motion forcing. This is a favourable synoptic-scale configuration for triggering and/or maintaining deep convective activity, consistent with the occurrence of rainfall events.

The upper-level synoptic-scale composite fields of cluster WL are shown in Figure 2(b). It depicts on its western side a large strongly tilted upper-level ridge extending from the Azores to the British Isles. France and the Iberian Peninsula are below a large trough, near an isolated low over the Bay of Biscay. This trough induces a weak mid- to upper-level southwesterly flow over the western Mediterranean. This pattern is very similar to the one occurring during anticyclonic wave breaking (Thornicroft *et al.*, 1993). Indeed, with the same southwest–northeast tilt, both the British Isles ridge and the Biscay low tend to sever themselves from the westerly flow and begin to form a block. Cluster WL is also characterised by an upper-level subtropical jet with a maximum wind speed of about  $30 \text{ m s}^{-1}$  over northwestern Africa. The upper-level Atlantic jet is weaker than in cluster CSW, and is flowing anticyclonically over Iceland and Scandinavia, far to the north.

Cluster CNW displays a well-marked upper-level trough aligned just east of the Greenwich meridian. This pattern resembles the CSW pattern, but it is slightly tilted and shifted to the east. This trough is associated with a jet-streak reaching about  $35 \text{ m s}^{-1}$  (Figure 2(c)). The flow in the area of interest is more westerly, at the southern end of the trough, with upper-level disturbances propagating eastwards.

Cluster CS has in common with clusters CSW and CNW a northwest–southeast weaker but wider trough. However, it depicts a more meridional structure. CS displays a trough–ridge pattern with a strong upper-level ridge over the Mediterranean and Central Europe. Like cluster WL, the Atlantic westerly flow is located far to the north while

the subtropical jet covers all North Africa. This pattern favours the isolation of cold air and the generation of cut-off lows over the Iberian peninsula. The ridge slows down the eastward propagation of the trough. It also enhances upper-level diffluence over southern France and the Gulf of Lion.

### 3.2. HPE composites

The above description of the upper-level features of the four clusters shows significant differences between the LSC patterns associated with rainfall events. Clusters CSW and CS both clearly depict upper-level synoptic-scale features favourable to the triggering and sustaining of deep convective activity associated with HPEs over southern France. From Table I showing the proportion of HPEs in each cluster, it can be seen that more than 75% of HPEs occur within a CSW or CS configuration. Because cluster CNW has so few HPEs associated with it (3.9%), it will not be considered further.

Figures 3 to 8 show HPE against non-HPE composites of geopotential height  $Z_{500}$ , quasi-geostrophic (QG) vertical velocity at 500 hPa, adiabatic wet-bulb potential temperature and horizontal wind and low-level moisture flux at 925 hPa for clusters CSW, WL and CS. In order to highlight the existence of significant feature differences between the HPE and non-HPE subsets, a Student *t*-test is performed at each grid point, and two levels of significance are indicated on the maps.

#### 3.2.1. CSW cluster

It has been previously pointed out that cluster CSW is characterised by a large trough extending southwards towards the Iberian peninsula. Its HPE sub-composite depicts a  $Z_{500}$  signature with a more curved and slightly deeper trough and especially a stronger anticyclonic curvature just downstream of this trough (Figure 3(a, b)). The interaction of the trough with large-scale baroclinicity implies the existence of synoptic-scale vertical motion. This active environment may ease the onset of convection: it contributes to reduce the vertical stability in ascent zones and it possibly enhances moisture convergence at lower levels (Doswell *et al.*, 1998).

The identification of upward motion areas at the synoptic scale using the QG theory can provide important guidance in determining development zones for convective systems (Caracena and Fritsch, 1983; Doswell, 1987). Indeed, the QG equations provide a convenient framework in which the vertical velocity is a solution of a second-order partial derivative equation called the  $\omega_g$  equation (Hoskins *et al.*, 1978). The source term can be partitioned into several components (the dynamical term related to the Q-vector divergence and diabatic sources). We choose to focus only on the dynamical contribution to the QG vertical velocity, as we are interested in assessing the effect of upper-level forcing contribution of the upper-level troughs.

The  $\omega_g$  composites for HPE days (Figure 3(c)) show a large meridionally elongated ascending area extending from the North African coast to the British Isles, with a maximum over the Pyrenees. The area of upward motion for the non-HPE composite (Figure 3(d)) is spatially less extended, thinner and slightly shifted further eastwards than the HPE composite. In the latter, the maximum of  $\omega_g$

## 1.2. PUBLICATIONS MAJEURES POUR LA SOUTENANCE DE L'HABILITATION À DIRIGER DES RECHERCHE

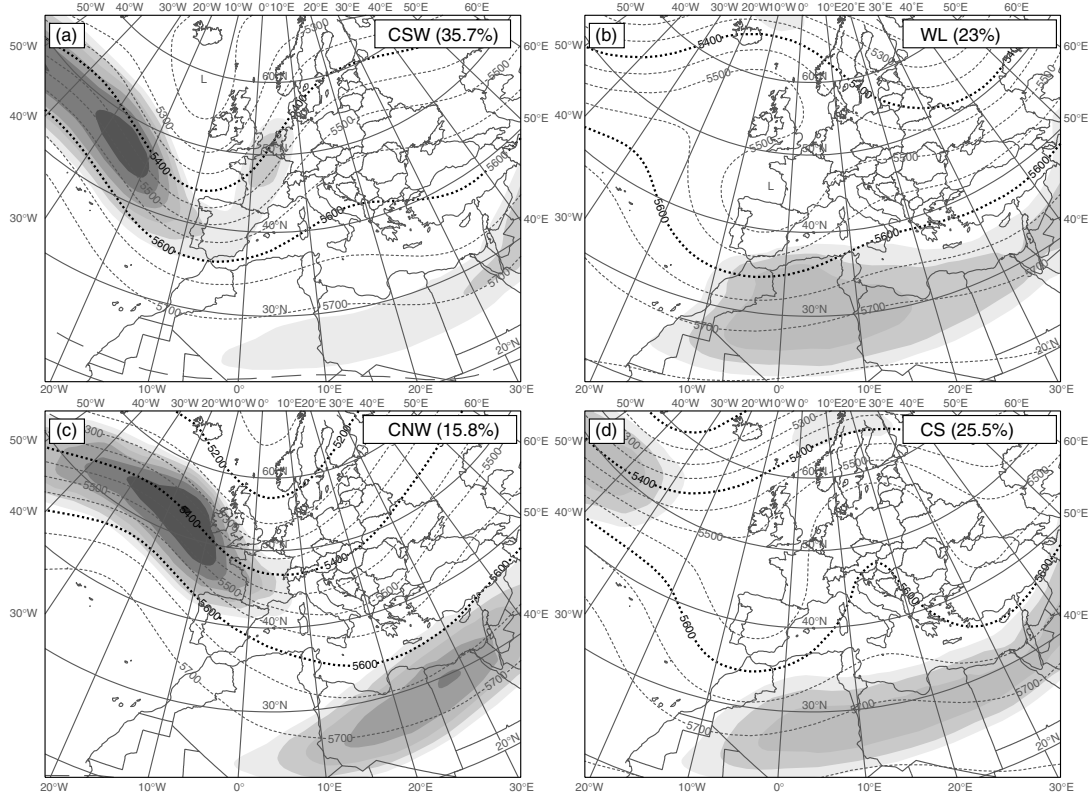


**Figure 2.** Composite maps of 500 hPa height (dashed contours with interval 50 dam) and wind speed on the 2 PVU surface (shading with interval  $2 \text{ m s}^{-1}$  above  $24 \text{ m s}^{-1}$ ) for the four LSC patterns over southern France associated with SREs from 1960 to 2001. For each type, the percentage of all SRE days is shown.

coincides with the area of the strongest significance. Such synoptic-scale upward motion upstream of southeastern France leads to a low-level cyclonic circulation. For both composites, the effects of the Iberian plateau lead to a well-established southwesterly wind in the extreme western Mediterranean (Figure 4(c, d)). However, in the HPE composite this flow looks like a more intense low-level jet along the Spanish coast, with a maximum magnitude over the French Mediterranean coast.

Diagnosis of the adiabatic wet-bulb potential temperature  $\theta'_w$  (Figure 4(a, b)) and the water vapour fluxes at the 925 hPa level are computed in order to exhibit moisture supply induced by the low-level wind. The moisture flux norm  $\|q_v \mathbf{V}_h\|$ , where  $q_v$  is the specific humidity  $\text{g kg}^{-1}$  and  $\mathbf{V}_h$  the horizontal wind ( $\text{m s}^{-1}$ ), is shown in Figure 4(e, f). Significant differences in  $\theta'_w$  between HPE and non-HPE days are depicted in Figure 4(a, b). Indeed, a maximum about  $2$  to  $3^\circ\text{C}$  warmer centred over the Eastern tip of the Pyrenees is found in the HPE composite, suggesting moist and warm air masses advected over the area. However, the area having the most significant differences between the two composites is spatially very large. It cannot clearly isolate sub-synoptic low-level structures potentially related to HPEs. This aspect is particularly obvious for cluster CSW.

The analysis of moisture flux pattern confirms that the areas of significant differences between HPE and non-HPE composites, already seen for the low-level wind field. This

is illustrated by an intense southwesterly inflow tongue only for HPEs which leads to a remarkable maximum over the Gulf of Lion.

### 3.2.2. WL cluster

The differences between HPE and non-HPE composites for LSC cluster WL are illustrated in Figures 5 and 6. Unlike the overall composite, the geopotential height reveals a closed cut-off low over the Bay of Biscay, deeper and nearly symmetric in the case of HPE composite. The non-HPE composite keeps the northeastern tilt. This results in a more southerly upper-level flow over the French Mediterranean coast during HPE days.

The quasi-geostrophic ascent zone is centred over southern France for both HPE and non-HPE composites. As for cluster CSW, a maximum is close to the flooding area. Although the shape of the ascending zone appears to be quite different over Spain and the Balearic Islands, these differences are not statistically significant.

The low-level flow is almost in phase with the upper-level one. It has a more south to southeasterly cyclonic component and it is more pronounced for the HPE composite. For cluster WL the area of maximum moisture flux in the HPE composite is large and specifically southeasterly oriented, connected with a significant inflow from near Tunisia through Sardinia and Corsica (Figure 6(c, d)). This inflow

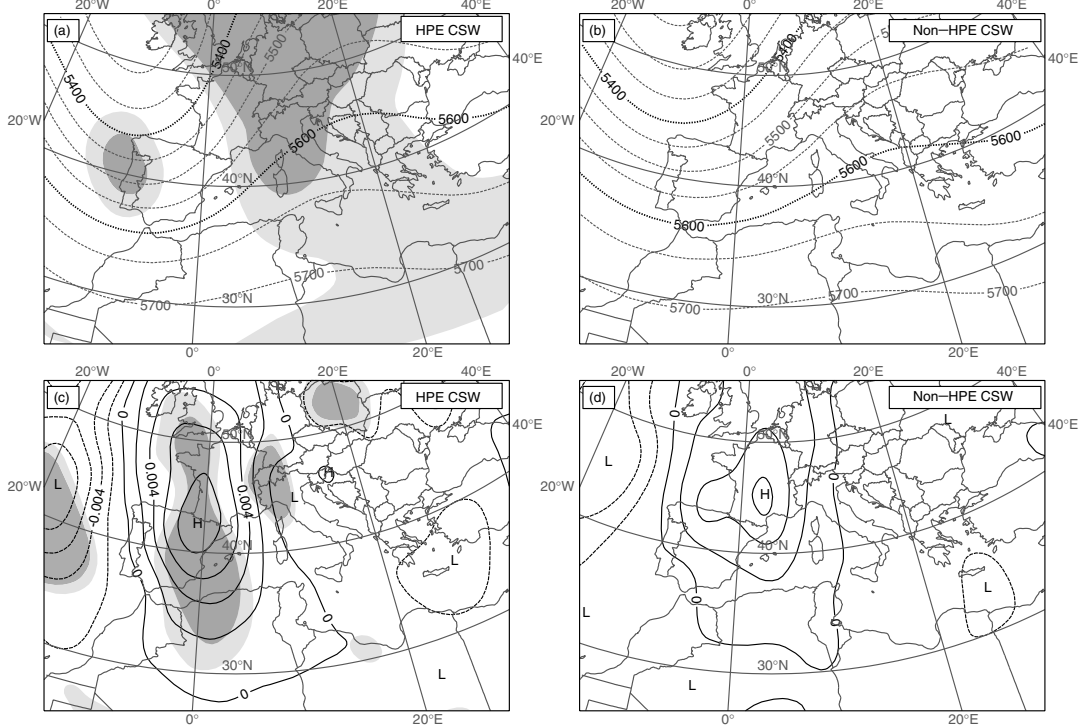


**Figure 3.** Composites for cluster CSW associated with (a, c) HPEs and (b, d) non-HPEs showing (a, b) geopotential height (m) at 500 hPa (with contour interval 25 m), (c, d) quasi-geostrophic vertical velocity  $\omega_g$  (with contour interval 2 Pa s $^{-1}$ ). In (a) and (c) the light and dark shaded areas indicate regions where the differences between the composite features are significant for the Student *t*-test at confidence levels 90% and 95%, respectively.

is then deflected near the southern Alps towards the Gulf of Lion. The moisture input from the Atlantic and the Gibraltar Strait, already seen in CSW is also present here, but less intense.

### 3.2.3. CS cluster

The ridge dominates the upper-level picture for the HPE composite of cluster CS (Figure 7). The trough over the Bay of Biscay is also deeper in the HPE composite. The dynamical forcing, as represented by the  $\omega_g$  composites, indicates, for both subsets, a maximum ascent zone shifted from southern France (in the previous clusters) towards the Balearic Isles (in the non-HPE subset) and even further southwards in the HPE subset. These differences in location and shape are found statistically significant. Over southern Italy and Sicily, upward motion in the non-HPE composite is replaced by downward motion in the HPE one. Both the 925 hPa wind field and moisture flux magnitude for the HPE composite of cluster CS clearly indicate a large moisture content in the Gulf of Lion. This southeasterly flow originates from southeastern Tunisia. The non-HPE composite displays similar low-level structures but much weaker.

### 3.3. Synoptic patterns propitious for HPE occurrence

In order to estimate the usefulness of clustering to find synoptic-scale patterns characteristic of HPEs, the concept of ‘discriminating power’ of PSD01 is applied. The idea is

to compare any weather map available in the reanalysis with each of the clusters. If the probability to be a HPE increases, as the correlation to a cluster centroid is increasing, then this cluster is qualified as ‘discriminating’ HPE. Taking any one situation in the sample, the following properties are considered:

- (i) the precipitation category of that situation, whether a HPE or a SRE occurred;
- (ii) the distance of the reanalysis field(s) of that situation to the centroids; the relevant distance is 1 minus the correlation between the fields; and
- (iii) the spatial distribution of precipitation.

Figure 9 shows the probability density functions of the spatial correlation distance of the  $Z_{500}$  height field for each population of rainfall event (HPE or SRE). Following PSD01, the closer to a given cluster centroid the density distribution maximum of a given event category is, the more discriminating is the cluster of that category.

For cluster CSW, it can be observed that the different rainfall event distributions significantly spread out on both sides of distance 0.4. Above this threshold, SREs are much more likely to occur than HPEs, with a difference peak around 1.0 distance. Below, i.e. at the closest distance to the CSW centroid, HPEs reach the overall highest probability (Figure 9(a)). Accordingly, the probability of having a HPE taking place increases as the situation looks more like the CSW centroid. As a result, cluster CSW appears as a highly discriminating pattern. For HPEs, it is the most discriminating one among the four clusters.

## 1.2. PUBLICATIONS MAJEURES POUR LA SOUTENANCE DE L'HABILITATION À DIRIGER DES RECHERCHE

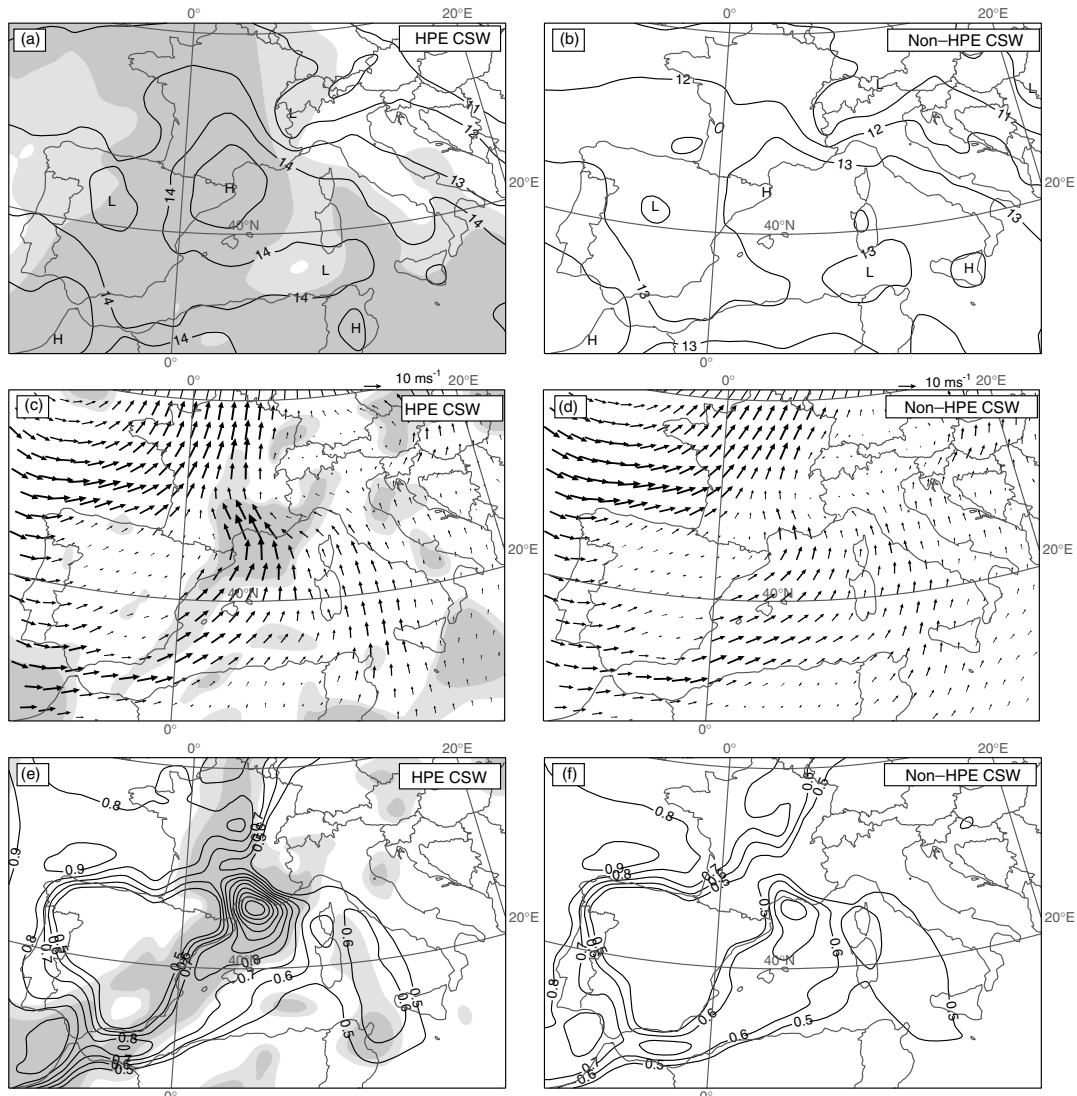


**Figure 4.** As Figure 3, but showing (a, b) adiabatic wet-bulb potential temperature ( $^{\circ}\text{C}$ ) at 925 hPa (with contour interval  $1^{\circ}\text{C}$ ), (c, d) horizontal wind (arrows) at 925 hPa, and (e, f) moisture flux magnitude (contour is  $0.1 \text{ kg m s}^{-2}$ ) at 925 hPa, respectively.

Clusters WL and CS also yield a fair separation between HPE and SRE density distribution maxima (Figure 9(b, d)); this confirms that these clusters also have discriminating properties. Conversely, cluster CNW is the only one for which the peak of HPE probability distribution is at a larger distance from the centroid than that of SRE. This suggests that  $Z_{500}$  patterns looking closely like the CNW centroid are rather unlikely to lead to intense precipitation events over the area of interest, which is also relevant information.

It is also possible to assess the relevance of the synoptic-scale clusters with respect to HPEs through simple compositing of the rain-gauge dataset. Figure 10 displays the spatial distribution of the mean daily precipitation amount associated with HPEs within each cluster. The composite for the cluster CNW is not shown, as it appears

not to be associated with intense rainfall events in that area. It can be seen that the different synoptic-scale clusters are associated with different geographical distributions of the rainfall over southern France. Moreover, the averaged rainfall amounts are also different. First, cluster CSW, containing 44.4% of the total HPEs (Table I), has its maximum of precipitation located over the Cévennes area, along the southern foothills of the Massif Central. The location is very close to the one of the overall climatology (Figure 2 of Nuissier *et al.*, 2008). A secondary peak of precipitation is also found over the southeastern part of the region of interest. Another interesting feature is that HPEs within cluster CSW do not affect the southwestern part of the region (e.g. Languedoc-Roussillon). Whereas clusters WL and CS also show some precipitation over the Cévennes region, Languedoc-Roussillon is the region most directly

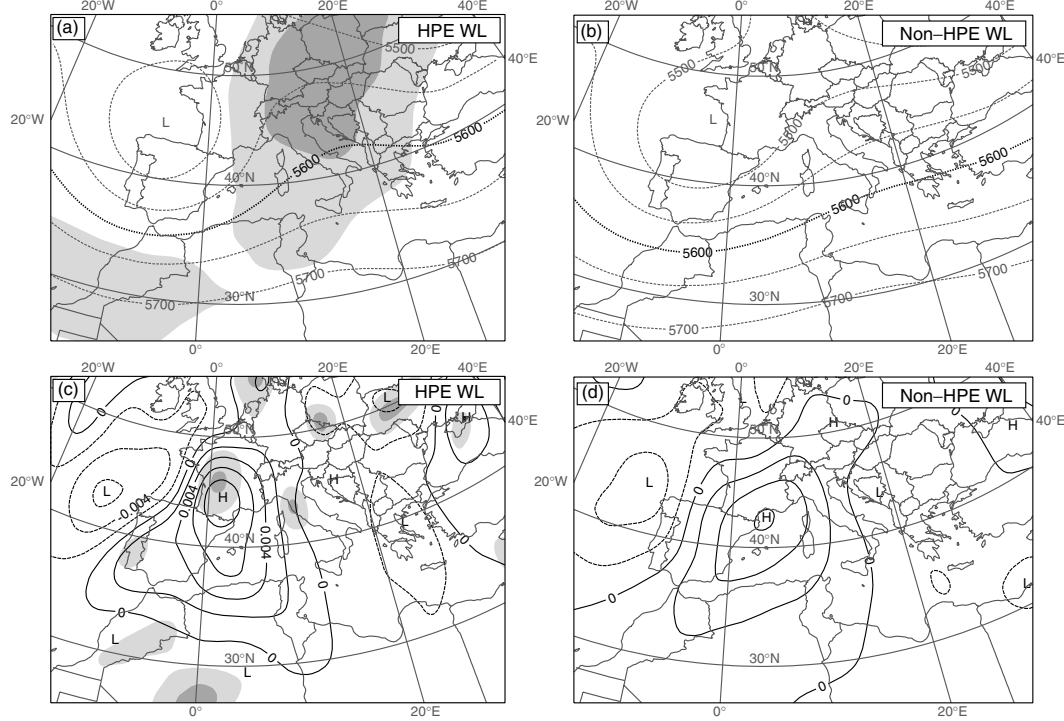


Figure 5. As Figure 3, but for the cluster WL.

concerned by the largest precipitation. The relative rainfall maximum in the southeastern area in cluster CSW does not exist in clusters WL and CS. Furthermore, it can be noted that the direction of the low-level flow is well correlated to the location of the maximum precipitation in each cluster (Figures 4, 6, 8(c)). Indeed, heavy precipitation in CSW tend to occur over the southeastern part of the Massif Central facing the southerly low-level flow. The HPEs associated with clusters WL or CS produce rainfall over the southwestern part of the area facing the southeasterly to easterly low-level flow that prevails for these clusters.

This rainfall composite analysis confirms the representativeness of our clusters and their link with the most intense precipitation events. However, and in a first step, we highlighted this relationship only for situations for which a HPE actually occurred. Therefore, on the other hand, it is an interesting issue to assess whether the reverse of this relationship is verified. This verification can be achieved through a statistical downscaling approach, i.e. evaluating the probability of a HPE to occur when synoptic-scale conditions are propitious to them. Whenever this probability is high, cluster composite patterns could be implemented as predictors of HPEs; this is further addressed in the following section.

#### 4. Predictive skill of the statistical downscaling approach

##### 4.1. Conditional correlation-distance distributions

The *conditional* frequency of occurrence of the given kind of rainfall event (SRE or HPE) is evaluated according to the correlation distance to the clusters. In other words, the

range [0, 2] of correlation distance is divided into a number of bins. With respect to the number of cases falling into a given bin, the ratio of occurrence of the rainfall events is computed. It can be also read as the marginal probability distribution of the occurrence of one kind of rainfall event versus the correlation distance to a centroid.

Figure 11 shows the resulting frequency of SRE occurrence as a function of the distance to the centroids. Clusters CSW, WL and CS discriminate SRE below a 0.7–0.8 correlation. That is to say, below this distance threshold to these cluster centroids, the frequency of occurrence of a SRE is well above the climatological frequency of 19%. The further away a case is from these three cluster centroids, the weaker the frequency of a SRE. Note that, conversely, the distance of a case to cluster CNW is only weakly relevant to the occurrence of a SRE, with a curve that remains close to the climatological frequency. Given the way the clusters were originally built, this figure is essentially a verifying reciprocal result. It validates that these three recurrent LSC patterns are representative of the synoptic-scale environment of precipitation events over southeastern France. One can note the SRE probability even exceeds 50% for a distance to clusters CSW and WL smaller than 0.2, since only one synoptic-scale field ( $Z_{500}$ ) is considered.

For HPEs (Figure 12), these same three clusters WL, CSW and CS still show a significant discriminating power with the highest probability corresponding to the lowest distance. Most remarkably, the frequency even increases much faster than for SRE when the correlation distance decreases from 0.3–0.4 to zero. At small distances, the probability of having a HPE is above 20% for clusters CSW and CS, even though at such small distances ( $\leq 0.1$ ) very few cases are collected.

## 1.2. PUBLICATIONS MAJEURES POUR LA SOUTENANCE DE L'HABILITATION À DIRIGER DES RECHERCHE

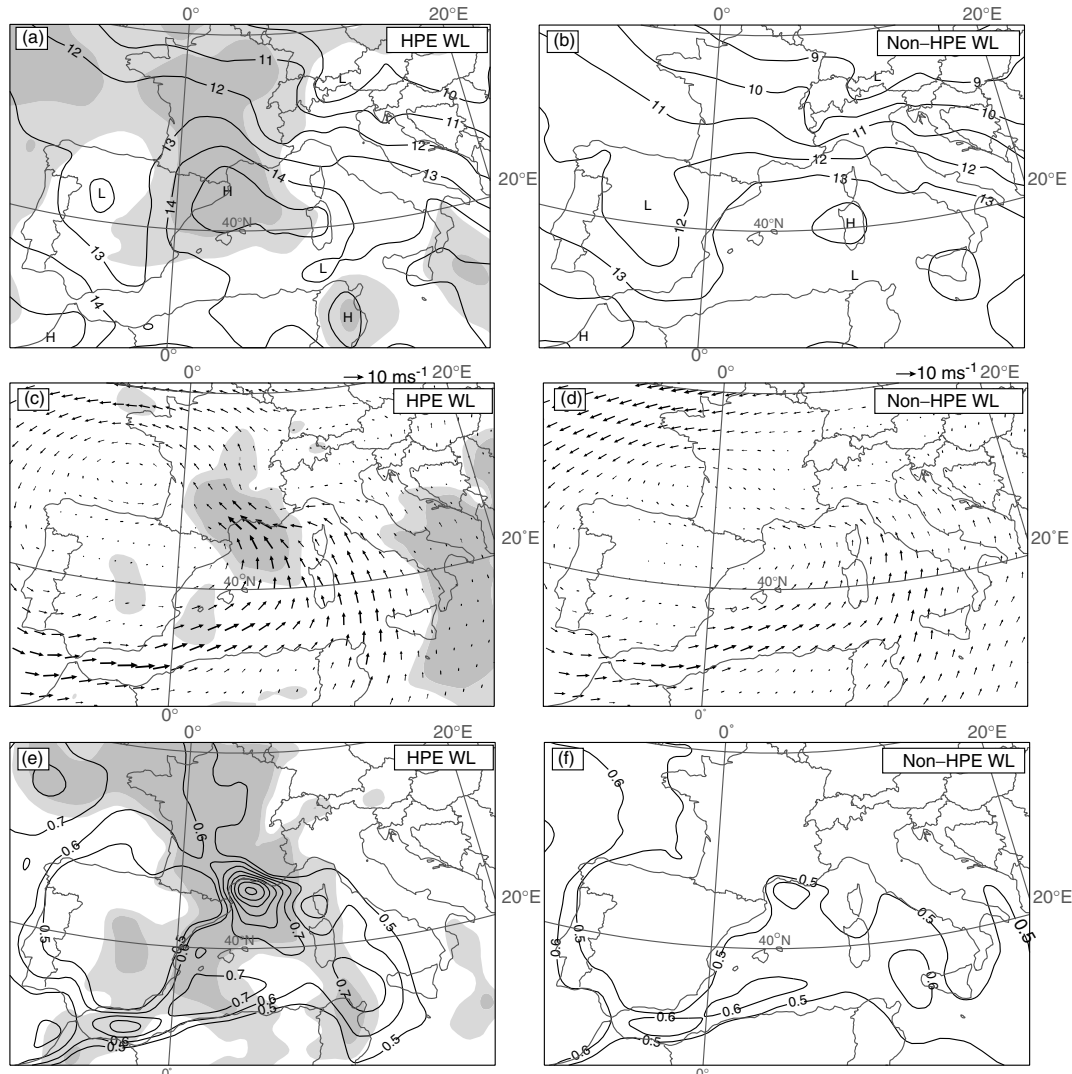


Figure 6. As Figure 4, but for the cluster WL.

The probabilities ranging from 20% to 10% are much more significant as they exceed by more than three times its standard deviation the HPE climatological frequency for a more representative number of cases. This occurs in the range of distance between 0.15 to 0.4. Within this range, clusters CSW and CS are related to a higher probability than cluster WL. These results are promising since clustering is not based on HPEs only. Indeed, by construction, clusters should discriminate SREs but not necessarily HPEs.

Concerning HPEs (Figure 12), situations close to the CNW centroid correspond to lower HPE occurrence frequency than the ones at greater distance. In this latter case, HPE frequency reaches three times the value of the climatology frequency. CNW circulations could then be interpreted as patterns inhibiting HPE. These results suggest that CNW is associated with the weakest part of rainfall events within the SREs. This can also be related to the fact that for cluster CNW the Atlantic storm-track and related

upper-level jet stream is shifted northward of the region of interest towards northern France (cf. section 3.1).

It is worth mentioning that when a pattern is close to clusters WL, CSW or CS, the probabilities reached for such a case, although well above the climatological frequency (i.e. 4%), still remain quite modest in absolute values: between 15% and 25% (except for WL, for which many fewer patterns are met at this distance). These values can be considered to be the upper limit of the skill of a forecast based on a single upper-level field.

### 4.2. Sufficient conditions for an HPE: a practical detection algorithm

In order to increase the probability to obtain a HPE, other ingredients based on the low-level conditions are added to the 500 hPa geopotential. Following the results shown in section 3.2, we focus here on fields that have provided

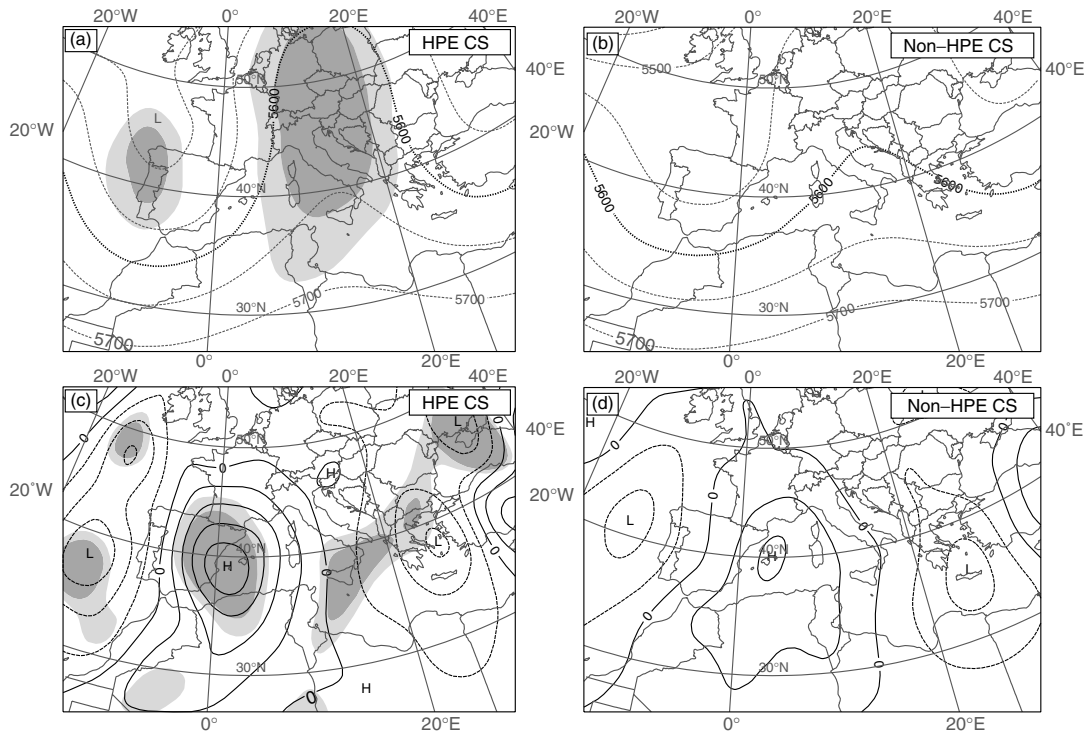


Figure 7. As Figure 3, but for the cluster CS

relevant composites of the clusters, such as the wind field at 925 hPa and the moisture flux.

The respective distributions of these parameters are built for SRE and HPE in order to highlight typical characteristics. This is performed in the domain encompassing the anomaly (small domain in Figure 1(a)).

First, the direction of the 925 hPa winds for each kind of rainfall event is considered (Figure 13). Whereas the distribution of wind directions corresponding to SREs appears to be quite flat with a large dispersion, the distribution associated with HPEs shows a well-defined single maximum shifted toward the range 110–180°. Furthermore, in the wide range 220–90°, the frequency of HPEs is virtually zero. This is supported also by the quartiles that show that more than 75% of HPEs coexist with only 45% of the SREs.

Figure 14 shows the distribution of the moisture flux maximum over the same domain. The separation between the distribution of the two kinds of rainfall events appears less visible than for the wind direction. Nonetheless, the moisture flux distribution for HPEs is clearly shifted towards larger values, as the HPE lower quartile is higher than the SRE median. For lowest values of moisture flux, the frequency of HPE occurrence dramatically drops, whereas the frequency of SREs still reaches about 10%.

These distributions of low-level parameters as analysed in ERA-40 do reveal some potential for isolating HPEs independently from the 500 hPa geopotential height and its associated clusters. These are now combined to design a detection algorithm.

The existence of sufficient conditions for having a HPE occurring over southeastern France is obtained by building a

practical detection algorithm derived from the discriminant analysis method. The considered predictors are: the 500 hPa geopotential height field, the wind direction at 925 hPa over the smaller domain in Figure 1(a) and the maximum magnitude of the moisture flux at the same level and in the same domain. A first criterion enforces directions of the 925 hPa wind within a given range limited by two thresholds  $D_1$  and  $D_2$ . A second one considers only the 925 hPa maximum moisture flux magnitude exceeding a threshold  $M_3$ . Finally, the third projects the 500 hPa height field onto the centroids of clusters CSW and CS and retains the minimum of these two correlation distances. Clusters CNW and WL are not considered here because either there are no discriminating SREs or HPEs, or they have too few cases very close to the centre. Figure 15 shows, for each set of thresholds, the empirical probability of occurrence of a HPE (solid line), and the corresponding absolute number of cases detected by picking up cases closer than a given correlation distance (dotted line). The thresholds are chosen in order to maximise the detection rate for the largest number of cases, while minimising the false alarms. The following thresholds are retained: 925 hPa wind direction between 110° and 160°, 925 hPa moisture flux magnitude larger than  $1.2 \text{ g kg}^{-1} \text{ m s}^{-1}$ . Figure 15 shows that taking a correlation distance smaller than 0.4 now yields a probability to have a HPE larger than 0.7 for a set of more than 50 potential situations (in 42 years), instead of a probability of about 0.1 with the sole geopotential height (Figure 12). When the correlation distance reaches 0.2, the probability becomes larger than 0.8, but reducing the set to about 30 potential situations. In a more or less heuristic way, we define a point in Figure 15 at a correlation distance of 0.3 below which the

## 1.2. PUBLICATIONS MAJEURES POUR LA SOUTENANCE DE L'HABILITATION À DIRIGER DES RECHERCHE

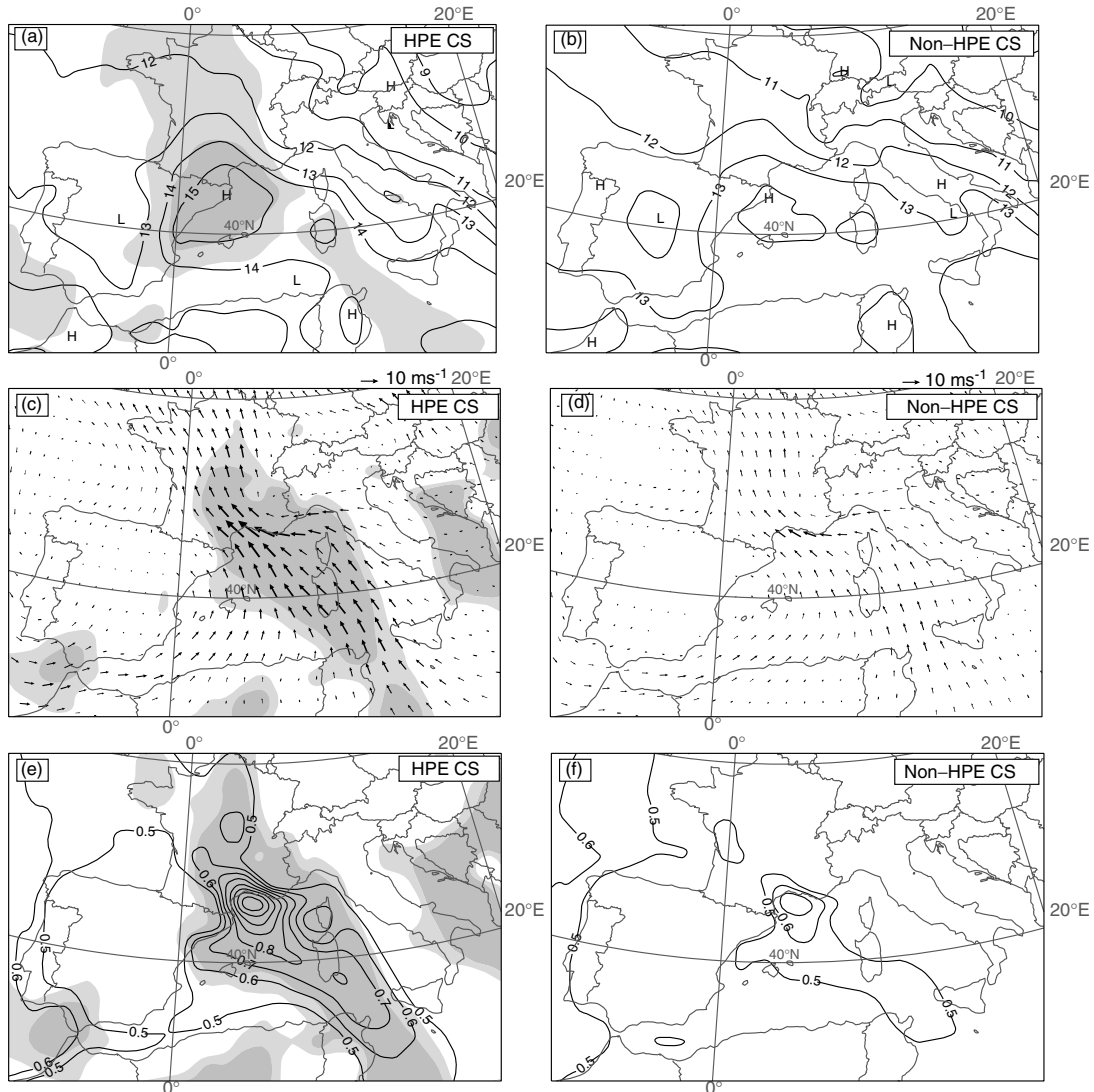


Figure 8. As Figure 4, but for the cluster CS.

HPE proportion among the detected case is optimal (71%). The number of HPEs effectively captured corresponds to 23% of the full set total (202 cases) and includes most of the extreme ones. This means that it is possible to find sufficient conditions for having a HPE with a high probability from a small set of dynamical fields.

Moreover, it is also interesting to assess the other 29% of detected cases, i.e. those that are not actually HPEs. Most of them correspond to rainfall amounts between 100 and 130 mm day $^{-1}$  (not shown), and thus are considered as significant rainfall amounts. There are very few cases yet for which precipitation is very weak. They can be related to a limitation of our procedure which does not consider any persistence criterion for the favourable synoptic-scale environment. Indeed, Nuissier *et al.* (2008) have shown that HPEs mainly occur in a slow-evolving synoptic-scale environment, and considering only one field per day cannot

permit the filtering out of more transitory events leading to smaller daily rainfall amounts.

### 5. Synthesis and conclusions

A statistical downscaling approach has been presented to characterise in an automatic way the synoptic-scale circulation patterns associated with heavy precipitation events over the southeastern regions of France. These HPEs generally occur over the southern Massif Central foothills, a region where very heavy precipitation episodes are relatively frequent. The first aim of this study was to describe the synoptic-scale features favouring HPE triggering. The second aim was to build a detection method for HPE from favourable synoptic-scale circulations.

For that purpose, the ERA-40 reanalysis available over a 42-year period and rainfall data from the Météo-France

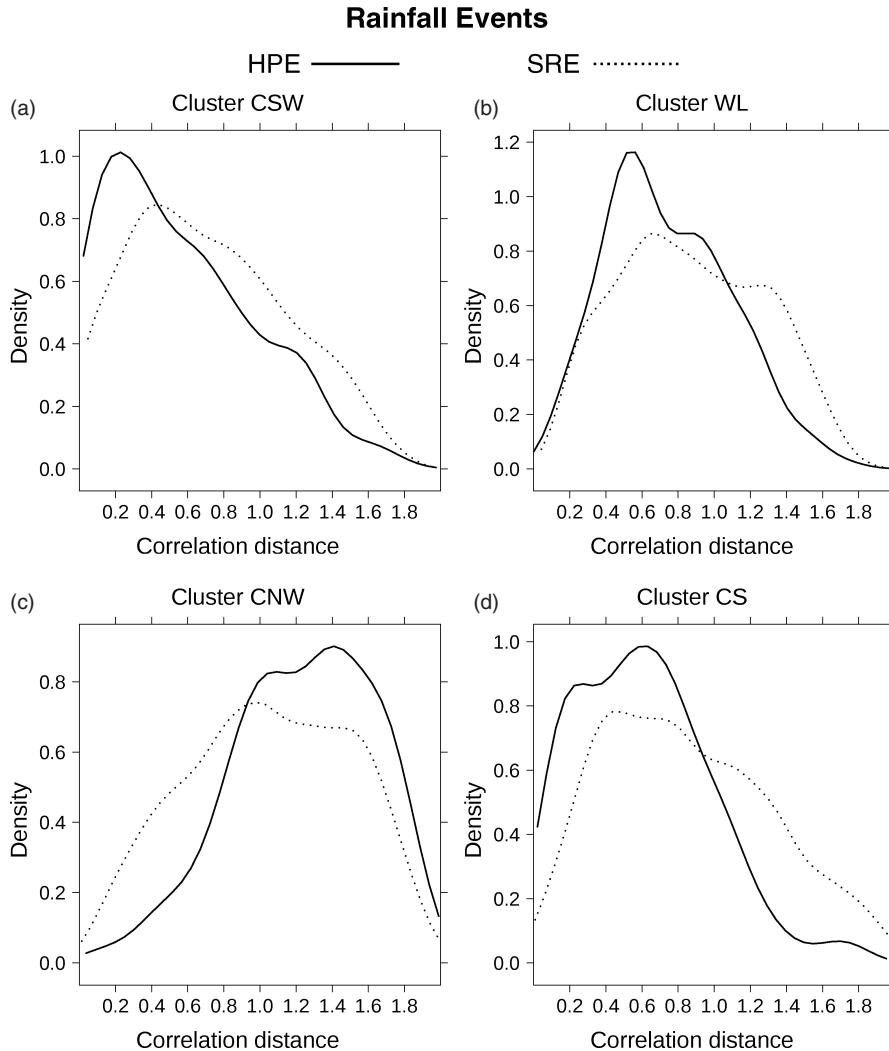


**Figure 9.** Density distributions of the HPEs (solid lines) and SREs (dotted lines) as a function of the spatial correlation distance to the centroid of clusters (a) CSW, (b) WL, (c) CNW and (d) CS.

rain-gauge network were used to extract meteorological fields typical of upper- and lower-troposphere dynamics associated with intense precipitating events. First, a dynamical clustering was performed to classify the large-scale circulations of 1200 days defined as significant rainfall events. The  $K$ -means algorithm employed, combined with self-determination of the number of clusters, leads to a partition into four clusters. Among these, two are particularly associated with HPEs, and include more than 77% of them.

This enables us to provide a meaningful meteorological description of the synoptic-scale contexts in which the different rainfall events occur. At the upper level, cluster CSW is characterised by a large and strong upper-level low centred near Ireland inducing a strong mid-to-upper level southwesterly flow over the southern regions of France. The low-level flow is from the southwest over the Atlantic Ocean and the Straits of Gibraltar and gradually veers south to southeast over the Gulf of Lion while strengthening.

Almost all the low-level moisture supply is provided by the moist flow coming from the Balearic Islands. From that standpoint, clusters WL and CS are quite different from cluster CSW as the low-level flow takes a more pronounced easterly component with two streams of low-level moisture transport; the first one comes from the Atlantic through the Gibraltar Straits (a common feature with cluster CSW), and the second one comes from near Tunisia. The presence of a strong ridge over central Europe, especially in cluster CS, appears important to enhance the low-level convergence over the Gulf of Lion with a pronounced diffluent flow aloft. The rainfall composites for each cluster are consistent with the low-level flow, with HPEs occurring mainly over the northern regions of the area of interest (e.g. the Cévennes region) in a south to southeasterly low-level flow for cluster CSW, whereas clusters WL and CS are more associated with HPEs over the Languedoc-Roussillon region (further west) embedded in a east to southeasterly low-level flow.

## 1.2. PUBLICATIONS MAJEURES POUR LA SOUTENANCE DE L'HABILITATION À DIRIGER DES RECHERCHE

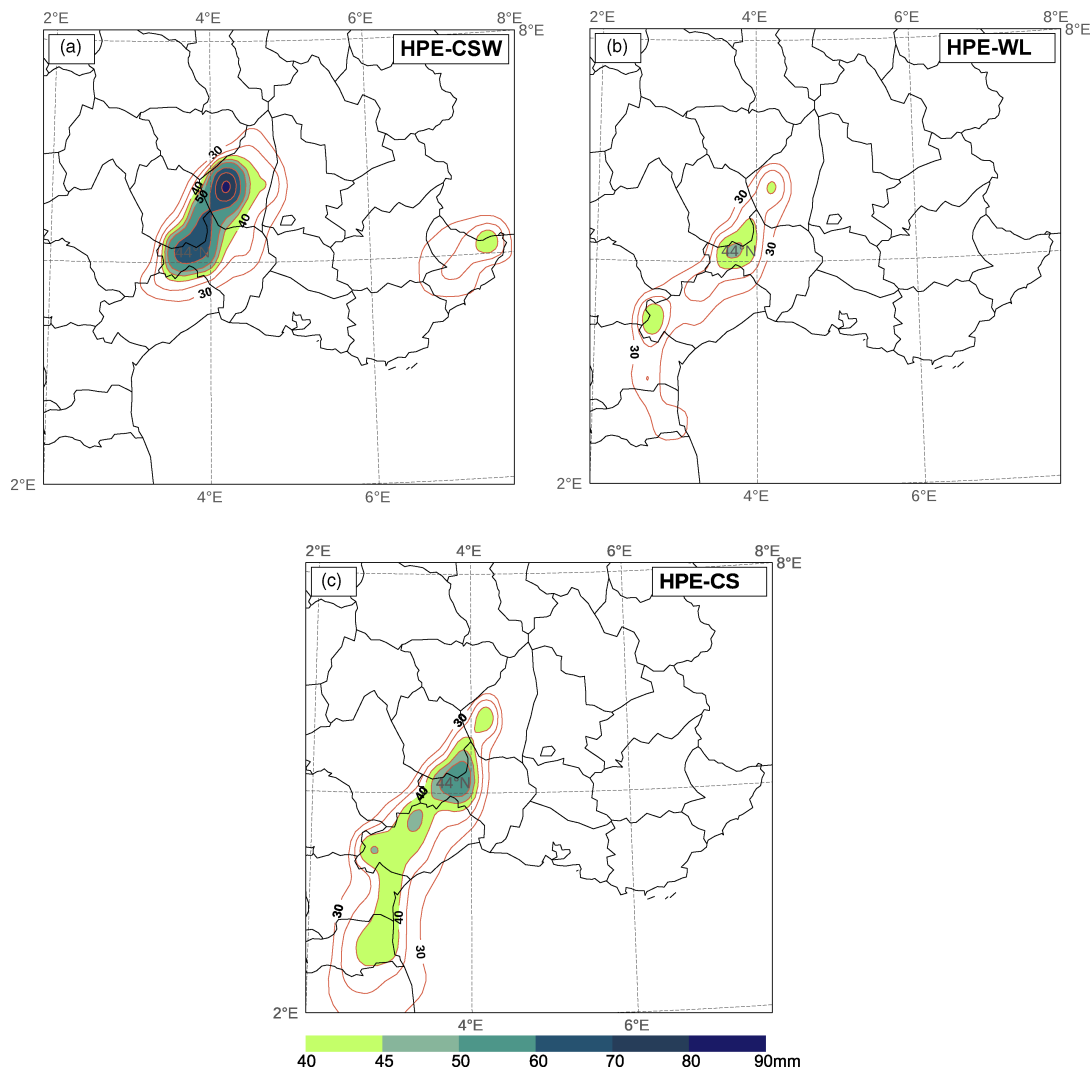


**Figure 10.** Rainfall composites (mm) associated with HPEs within (a) cluster CSW, (b) cluster WL and (c) cluster CS. Composites have been calculated using whole rain-gauge network in Figure 1(b). This figure is available in colour online at [wileyonlinelibrary.com/journal/qj](http://wileyonlinelibrary.com/journal/qj)

It has been found that cluster CSW has the strongest discriminating power with respect to high precipitation. Indeed, 500 hPa geopotential height field density distributions corresponding to HPEs are closer to the centroid of cluster CSW than both clusters WL or CS. Examination of low-level features reveals that there is a well-defined signature in cluster composites of these fields.

The density distributions of horizontal flow direction and 925 hPa maximum moisture flux magnitude show that HPEs tend to occur with wind direction in the range 110° to 180° and for the strongest values of low-level moisture flux.

A detection algorithm, combining the distance to upper-level patterns, the low-level wind direction (in the 110–180° range), and the low-level moisture flux (larger than  $1.2 \text{ g kg}^{-1} \text{ m s}^{-1}$ ) enables us to ‘predict’ a frequency of occurrence of a HPE larger than 70%, or even 80% for slightly smaller distances to the key clusters. Such properties

capture around a quarter of all HPEs over the period. The other part depends on other aspects, probably to be found at smaller scales, not yet represented in reanalyses such as ERA-40.

These results can be useful in two areas. One is the prediction of the occurrence of a HPE with sufficient lead time and sufficient certainty to mitigate the economic impact of an upcoming HPE. A second one is related to the evolution of the frequency of these events in a climate change context. In both cases, one ongoing difficulty is that direct rainfall forecasts remain too much parametrization-dependent, and so can be only indicative, especially when convection is involved. The advantage of the approach presented here is that it depends on dynamical fields only. It can provide the basis for downscaling techniques with either short- or medium-range ensemble forecasts or with climate projections. The latter aspect has indeed been employed in the framework of the CYPRIM (Cyclogenesis

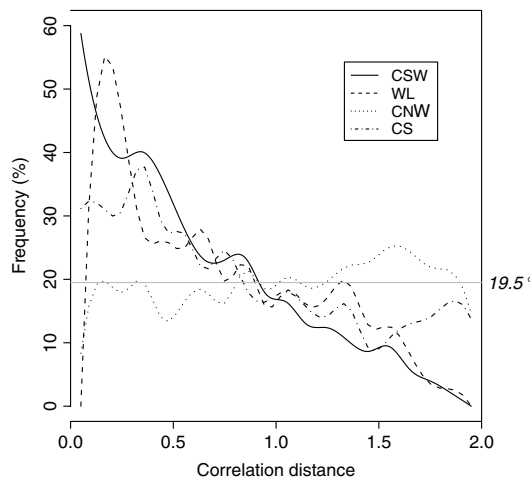


**Figure 11.** SRE occurrence ratio as a function of spatial correlation distance from the centroid of cluster CSW (solid), WL (dashed), CNW (dotted) and CS (dash-dotted). The climatological frequency is shown as the horizontal line.

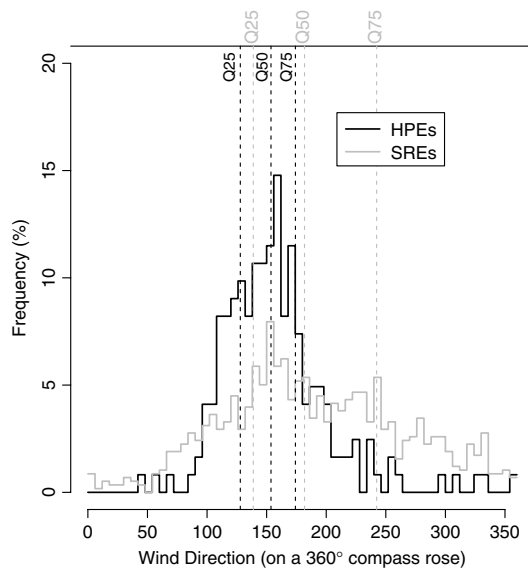


**Figure 13.** Distribution densities of horizontal wind direction at 925 hPa where the moisture flux is the strongest inside the domain shown in Figure 1(b), for HPE and SRE events. Quartile values are given by the vertical lines (Q25 for the 25% quantile, etc.)

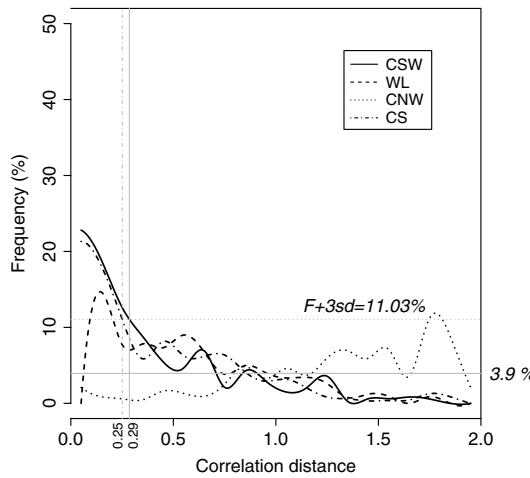


**Figure 12.** As Figure 11, but for HPEs. The usual order of magnitude for representativeness of the frequency of the observed event is given by the horizontal dotted line ( $F + 3sd = 11.04\%$ ), corresponding to three times the standard deviation (here annual) above the mean frequency of HPE occurrence.

and Intense Precipitation in the Mediterranean) project. The ‘detection’ algorithm outlined above has been applied to a coupled Mediterranean climate scenario evolution to retrieve potential HPE cases. These cases have then been simulated in detail with a convection-permitting model; the results of these studies are presented in a companion paper (Beaulant *et al.*, 2011).

#### Acknowledgements

Drs M. Déqué and D. Ricard are acknowledged for their valuable comments. The authors also gratefully acknowledge

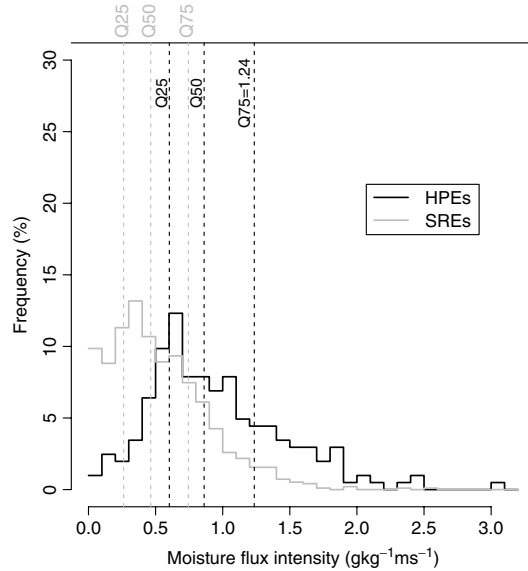


**Figure 14.** As Figure 13, but showing distributions of the maximum value of the moisture flux at 925 hPa ( $\text{g kg}^{-1} \text{m s}^{-1}$ ) inside the domain shown in Figure 1(b).

the two anonymous reviewers for their relevant comments and suggestions. This work has been carried out within the framework of the CYPRIM project, funding by ACI-FNS ‘Aléas et Changements Globaux’ and in the framework of the MEDUP project, funding by ANR ‘Vulnérabilité Milieux Climat’.

## 1.2. PUBLICATIONS MAJEURES POUR LA SOUTENANCE DE L'HABILITATION À DIRIGER DES RECHERCHE

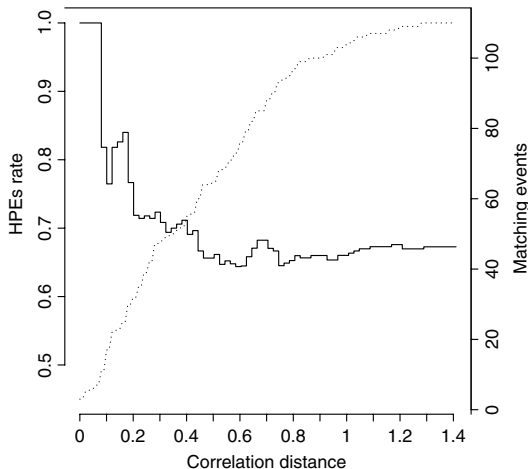


**Figure 15.** Probability of HPE occurrence (solid line) and cumulative number of detected events (dotted line) as a function of the correlation distance to centroids CSW or CS.

### References

- Beaulant A-L, Joly B, Nuissier O, Somot S, Ducrocq V, Joly A, Sevault F, Déqué M, Ricard D. 2011. Statistico-dynamical downscaling for Mediterranean heavy precipitation. *Q. J. R. Meteorol. Soc.* In press.
- Buzzi A, Tartaglione N, Malguzzi P. 1998. Numerical simulations of the 1994 Piedmont flood: Role of orography and moist processes. *Mon. Weather Rev.* **126**: 2369–2383.
- Caracena F, Fritsch JM. 1983. Focusing mechanisms in the Texas hill country flash floods of 1978. *Mon. Weather Rev.* **111**: 2319–2332.
- Delrieu G, Ducrocq V, Gaume E, Nicol J, Payrastre O, Yates E, Kirstetter PE, Andrieu H, Ayral PA, Bouvier C, Creutin JD, Livet M, Anquetin S, Lang M, Neppel L, Obled C, Parent du Châtelet J, Saulnier GM, Walpersdorf A, Wobrock W. 2005. The catastrophic flash-flood event of 8–9 September 2002 in the Gard region, France: A first case-study for the Cévennes–Vivarais Mediterranean Hydrometeorological Observatory. *J. Hydrometeorol.* **6**: 34–52.
- Doswell CA. 1987. The distinction between large-scale and mesoscale contribution to severe convection: A case-study example. *Weather and Forecasting* **2**: 3–16.
- Doswell CA III, Ramis C, Romero R, Alonso S. 1998. A diagnostic study of three heavy precipitation episodes in the western Mediterranean region. *Weather and Forecasting* **13**: 102–124.
- Ducrocq V, Nuissier O, Ricard D, Lebeaupin C, Thouvenin T. 2008. A numerical study of three catastrophic precipitating events over southern France. II: Mesoscale triggering and stationarity factors. *Q. J. R. Meteorol. Soc.* **134**: 131–145.
- Frei C, Schär C. 1998. A precipitation climatology of the Alps from high-resolution raingauge observations. *Int. J. Climatol.* **18**: 873–900.
- Homar V, Romero R, Ramis C, Alonso S. 1999. A case of convection development over the western Mediterranean Sea: A study through numerical simulations. *Meteorol. Atmos. Phys.* **71**: 169–188.
- Hoskins BJ, Draghici I, Davies HC. 1978. A new look at the  $\omega$ -equation. *Q. J. R. Meteorol. Soc.* **104**: 31–38.
- Huth R, Beck C, Philipp A, Demuzere M, Ustrnul Z, Cahynová M, Kyselý J, Tveito OE. 2008. Classification of atmospheric circulation patterns – Recent advances and applications. *Annals NY Acad. Sci.* **1146**: 105–152.
- James PM. 2006. An objective classification method for Hess and Brezowsky Grosswetterlagen over Europe. *Theor. Appl. Climatol.* **88**: 17–42.
- Jansa A, Genoves A, Angeles Picornell M, Campins J, Riosalido R, Carretero O. 2001. Western Mediterranean cyclones and heavy rain. Part 2: Statistical approach. *Meteorol. Appl.* **8**: 43–56.
- Kageyama M, D'andrea F, Ramstein G, Valdes PJ, Vautard R. 1999. Weather regimes in past climate atmospheric general circulation model simulations". *Clim. Dyn.* **15**: 773–793.
- Lana A, Campins J, Genovés A, Jansa A. 2007. Atmospheric patterns for heavy rain events in the Balearic Islands. *Adv. Geosci.* **12**: 27–32.
- Lin YL, Chiao S, Wang TA, Kaplan ML, Weglarz RP. 2001. Some common ingredients for heavy orographic rainfall. *Weather and Forecasting* **16**: 633–659.
- Massacand AC, Wernli H, Davies HC. 1998. Heavy precipitation on the Alpine south side: An upper-level precursor. *Geophys. Res. Lett.* **25**: 1435–1438.
- Michelangeli PA, Vautard R, Legras B. 1995. Weather regimes: recurrence and quasi-stationarity. *J. Atmos. Sci.* **52**: 1237–1256.
- Nuissier O, Ducrocq V, Ricard D, Lebeaupin C, Anquetin S. 2008. A numerical study of three catastrophic precipitating events over southern France. I: Numerical framework and synoptic ingredients. *Q. J. R. Meteorol. Soc.* **134**: 111–130.
- Plaut G, Schuepbach E, Doctor M. 2001. Heavy precipitation events over a few Alpine sub-regions and the links with large-scale circulation. *Clim. Res.* **17**: 285–302.
- Robertson A, Ghil M. 1999. Large-scale weather regimes and local climate over western United States. *J. Climate* **12**: 1795–1813.
- Romero R, Doswell CA III, Ramis C. 2000. Mesoscale numerical study of two cases of long-lived quasi-stationary convective systems over Eastern Spain. *Mon. Weather Rev.* **128**: 3731–3751.
- Solman SA, Menendez CG. 2003. Weather regimes in the South American sector and neighbouring oceans during winter. *Clim. Dyn.* **21**: 91–104.
- Thornicroft CD, Hoskins BJ, McIntyre M. 1993. Two paradigms of baroclinic-wave life-cycle behaviour. *Q. J. R. Meteorol. Soc.* **119**: 17–55.
- Uppala SM, Källberg PW, Simmons AJ, Andrae U, Da Costa Bechtold V, Fiorino M, Gibson JK, Haseler J, Hernandez A, Kelly GA, Li X, Onogi K, Saarinen S, Sokka N, Allan RP, Andersson E, Arpe K, Balmaseda MA, Beljaars ACM, Van De Berg L, Bidlot J, Bormann N, Caires S, Chevallier F, Dethof A, Dragosavac M, Fisher M, Fuentes M, Hagemann S, Holm E, Hoskins BJ, Isaksen L, Janssen PAEM, Jenne R, McNally AP, Mahfouf J-F, Morcrette J-J, Rayner NA, Saunders RW, Simon P, Sterl A, Trenberth KE, Untch A, Vasilevic D, Viterbo P, Woollen J. 2005. The ERA-40 re-analysis. *Q. J. R. Meteorol. Soc.* **131**: 2961–3012.
- Vautard R. 1990. Multiple weather regimes over the North Atlantic: Analysis of precursors and successors. *Mon. Weather Rev.* **118**: 2056–2081.
- Vautard R, Legras B, Déqué M. 1988. On the source of midlatitude low-frequency variability. Part I: A statistical approach to persistence. *J. Atmos. Sci.* **45**: 2811–2843.



# Uncertainty of lateral boundary conditions in a convection-permitting ensemble: a strategy of selection for Mediterranean heavy precipitation events

O. Nuissier, B. Joly, B. Vié, and V. Ducrocq

GAME/CNRM, Météo-France, URA1357, CNRS, Toulouse, France

Correspondence to: O. Nuissier (olivier.nuissier@meteo.fr)

Received: 28 February 2012 – Revised: 29 June 2012 – Accepted: 28 August 2012 – Published: 1 October 2012

**Abstract.** This study examines the impact of lateral boundary conditions (LBCs) in convection-permitting (C-P) ensemble simulations with the AROME model driven by the ARPEGE EPS (PEARP). Particular attention is paid to two torrential rainfall episodes, observed on 15–16 June 2010 (the Var case) and 7–8 September 2010 (the Gard-Ardèche case) over the southeastern part of France. Regarding the substantial computing time for convection-permitting models, a methodology of selection of a few LBCs, dedicated for C-P ensemble simulations of heavy precipitation events is evaluated. Several sensitivity experiments are carried out to evaluate the skill of the AROME ensembles, using different approaches for selection of the driving PEARP members. The convective-scale predictability of the Var case is very low and it is driven primarily by a surface low over the Gulf of Lyon inducing a strong convergent low-level flow, and accordingly advecting strong moisture supply from the Mediterranean Sea toward the flooded area. The Gard-Ardèche case is better handled in ensemble simulations as a surface cold front moved slowly eastwards while increasing the low-level water vapour ahead is well reproduced. The selection based on a cluster analysis of the PEARP members generally better performs against a random selection. The consideration of relevant meteorological parameters for the convective events of interest (i.e. geopotential height at 500 hPa and horizontal moisture flux at 925 hPa) refined the cluster analysis. It also helps in better capturing the forecast uncertainty variability which is spatially more localized at the “high-impact region” due to the selection of more mesoscale parameters.

## 1 Introduction

The northwestern Mediterranean area is frequently affected by heavy precipitation events (HPEs) that produce disastrous flash-flood events, particularly during autumn. In most cases of dramatic events, large amounts of precipitation are recorded in less than one day (typically more than 200 mm in less than 24 h, and sometimes in only 6 h) when a mesoscale convective system (MCS) develops and stays over the same area for several hours.

The ability to predict such dramatic events remains weak due to the contribution of very fine-scale processes over the northwestern Mediterranean complex terrain and their non-linear interactions with the larger scale processes. The knowledge of the large-scale meteorological environment propitious to heavy precipitation has been increased for past years. Despite a better prediction of these precursors, the forecast of the precise location of the anchoring region of the precipitating system, especially in case of extreme event, is nowadays still a challenging issue. Furthermore, a better knowledge of the forecast uncertainty is really crucial as the hydrological response of the typical small and steep Mediterranean watersheds is very sensitive to the location of the heaviest precipitation (Chancibault et al., 2006; Vincendon et al., 2010).

The recent studies by Nuissier et al. (2008, 2011) showed typical upper-level synoptic ingredients such as the deep cyclonic upper-level circulation that generates a strong diffluent flow over the Mediterranean Sea and a blocking located downstream over central Europe slowing down the evolution of these synoptic conditions. These synoptic patterns are generally associated with intense south to southeasterly low-level jets that favour strong low-level moisture transport

towards the flooded areas. In addition, mesoscale ingredients are also crucial in the triggering of deep convection (e.g. conditional instability, low-level convergence, moisture flux), pinpointing the deep convection development over the same area over several hours.

A new generation of non-hydrostatic convection-permitting (C-P) atmospheric models have been developed in the past years for operational or research purposes. The forecast of precipitation systems is significantly improved with these new-generation models due to a better representation of water cycle processes and resolved deep convection (Stein et al., 2000; Mass et al., 2002; Richard et al., 2003; Fritsch and Carbone, 2004; Ducrocq et al., 2008; Bresson et al., 2009; Bresson, 2011, among others). However, more faithful simulations do not imply systematic increased quality (e.g. in terms of quantitative precipitation forecasts) of model forecasts as measured by “grid-based” metrics (Mass et al., 2002). Convective processes are highly nonlinear and associated with very short lifespans. As a consequence, their forecasts are strongly impacted by uncertainties, e.g. emerging from the initial state of the model, from the formulation of the model and from the lateral boundary conditions which are provided by the driving model, in case of limited area models (Gebhardt et al., 2011). This meteorological uncertainty can then propagate to the hydrological forecasts, since hydrological forecasts are strongly related to precipitation forecasts (Zappa et al., 2010).

Ensemble forecasting or ensemble simulation approaches are well known tools to quantify the forecast uncertainty. Such a probabilistic methodology, thanks to available computing resources, has been introduced for operational purposes in the 1990s, using Ensemble Prediction Systems (EPSs) designed for medium-range forecasting (Molteni and Palmer, 1993; Molteni et al., 1996; Toth and Kalnay, 1997). Unfortunately, these methods designed to generate a global, large-scale ensemble cannot be easily adapted to C-P numerical weather prediction models due to strong nonlinearities and large sensitivity to initial conditions.

Recent studies make use of a wide range of techniques to build ensemble forecasts at meso- $\beta$  for regional, limited-area, convection-parameterizing (or not) models (Stensrud et al., 2000; Grimit and Mass, 2002; Nutter et al., 2004; Walser et al., 2004; Zhang et al., 2006; Hohenegger et al., 2006; Hohenegger and Schär, 2007; Kong et al., 2007, among others). For very high (e.g. kilometric)-resolution, Vié et al. (2011) examines the impact of uncertainty on convective-scale initial conditions and the uncertainty on lateral boundary conditions (LBCs) in cloud-resolving simulation with the Application of Research to Operations at Mesoscale (AROME) model at 2.5-km horizontal resolution, with special attention paid to Mediterranean heavy precipitation. They show that the uncertainty of LBC has an impact at longer range than uncertainty of mesoscale initial conditions (typically beyond 12 h), as the spread in the driving global

EPS increases. Moreover, the rate of LBC uncertainty propagation depends on the synoptic-scale meteorological conditions. Gebhardt et al. (2011) explore the use of perturbation methods within the COSMO-DE model at 2.8-km horizontal resolution, isolating uncertainty sources (e.g. model errors and LBCs). They obtain results fairly similar to Vié et al. (2011), with model perturbations always dominating the first few hours and variations of LBCs often dominating the following forecast hours.

The studies mentioned above have shown the importance of using global large-scale EPS as perturbed LBCs for C-P EPS. Furthermore, the design of a future C-P EPS will need to tackle the major uncertainty sources previously mentioned. At first glance, the approach would basically combine  $N$  global EPS members as driving LBCs and  $M$  other members representing additional perturbations generated in the C-P model, thus involving the computation of  $N \times M$  members in that configuration. Despite significant increase of computational power, a major issue for convective-scale EPS is the size of the ensemble since C-P models suffer from expansive computing time. Whereas large-scale global EPS size is typically 35–50 members, 8–15 members in C-P EPS can be the targeted size for operational implementation. A selection among the large-scale EPS members should thus be applied to drive the C-P EPS. It is based on a selection of a few representative members from global EPSs, followed by nesting of limited-area models with the retained individual large-scale solutions. The Consortium for Small-Scale Modelling Limited-area Ensemble Prediction System (COSMO-LEPS), for instance, already uses such a methodology (Marsigli et al., 2001; Molteni et al., 2001; Montani et al., 2011) but for a convection-parameterizing model.

The present work aims at addressing whether such an approach is relevant for a C-P EPS working at kilometric horizontal resolution and for short-range lead times (up to 24 h). Therefore, this paper proposes to evaluate a methodology of selection of LBCs dedicated for C-P ensemble simulations of heavy precipitation events. For that purpose, several C-P ensemble simulation experiments are carried out, with various subsets of LBCs provided by a short-range global EPS. In this approach, the C-P model is assumed to be “perfect” and that the major uncertainty sources are mainly associated with variability of the meteorological synoptic-scale patterns propagating inside the C-P numerical model.

The paper is organised as follows: Sect. 2 reports the meteorological description of the case studies. The numerical experiments set up and the methodology used are described in Sect. 3, results are presented then discussed in Sect. 4. Finally, a synthesis and concluding remarks are given in Sect. 5.

## 2 The case studies

Our study focuses on two recent flash-flooding events: 15–16 June 2010 (called hereafter the Var case) and 7–8 September 2010 (called hereafter the Gard-Ardèche case). The Gard-Ardèche case occurred over the southeastern region of Massif Central which is a typical area for very heavy precipitation from climatology. On the other hand, the Var case was an exceptional episode since it occurred in June (autumn is the favourable period) and over a region usually less exposed to heavy precipitation (southern flanks of the Alps).

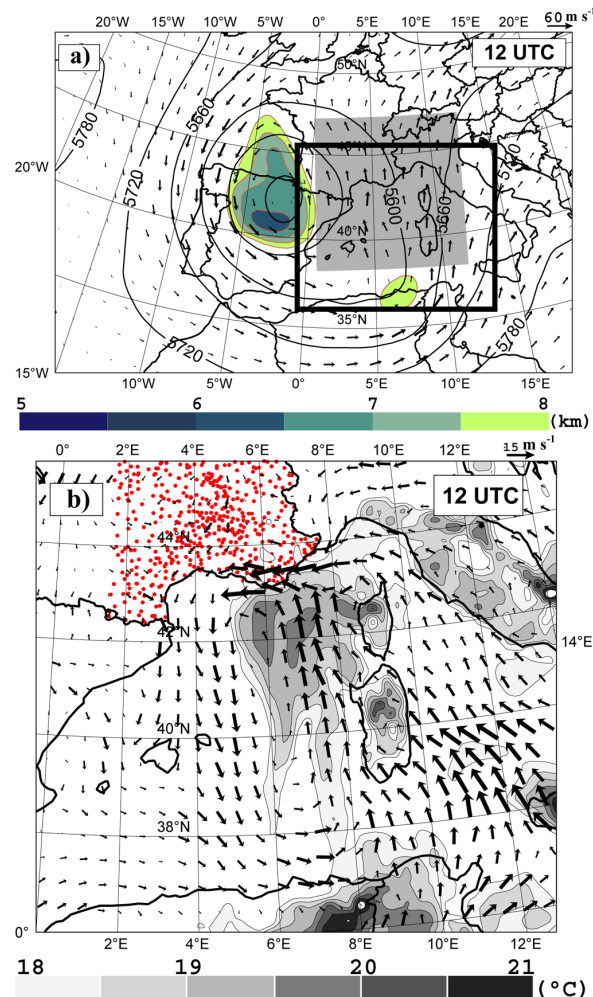
### 2.1 The Var case

Figure 1a illustrates the synoptic situation associated with the Var case in terms of the 500 hPa geopotential height, 1.5 PVU surface height, 300 hPa wind fields, 925 hPa adiabatic wet-bulb potential temperature and wind fields (derived from the ARPEGE analysis) on 15 June 2010 at 12:00 UTC. The meteorological situation was dominated by an upper-level (almost cut-off) cold low centred through the Northern Iberian peninsula and the Bay of Biscay. The main upper-level PV anomaly, shown by low elevation of the 1.5 PVU (potential vorticity unit) surface, extending southwestwards and was associated with a pronounced mid to upper-level southerly flow (Fig. 1a). In the same time at low-level, a large surface low deepened between Balearic Islands and Sardinia and led to a moderate and moist south to southeasterly low-level flow impinging upon the southern Alps foothills (Fig. 1b). This low-level circulation in addition to flow deflection around Southern Alps helped in reinforcing low-level convergence and focusing moist air masses, with high values of adiabatic wet-bulb potential temperature, towards the flooded-area (i.e. the Var region). These very favourable conditions for heavy precipitation, rather atypical for the season, lasted the entire day on 15 June.

The first convective cells associated with the Var event appeared over the Mediterranean Sea around 00:00 UTC on 15 June 2010, embedded in the southerly low-level flow. Progressing northwards, the convection started to organise forming a very intense south–north oriented line in the morning on 15 June (Fig. 2a). The convective line turned more southeast–northwest in the afternoon associated with a more easterly shift of the low-level flow (Fig. 2b). During the Var event, high surface rainfall amounts of about 460 mm in less than 24 h were recorded in Draguignan which in large part can be directly attributed to this stationary convective line (Fig. 2c). This event led to dramatic flash-flooding that caused the deaths of 25 people and considerable damages.

### 2.2 The Gard-Ardèche case

As for the Var case, the upper-level synoptic situation is presented in Fig. 3a at 12:00 UTC on 7 September 2010. The synoptic-scale situation was characterised by a large upper-



**Fig. 1.** Var case (a): 300 hPa winds (arrows), 1.5 PVU surface height (colour) and 500 hPa geopotential height (solid line) and (b): adiabatic wet-bulb potential temperature (shading) and horizontal winds at 925 hPa, from ARPEGE analysis on 15 June 2010 at 12:00 UTC. The computational domain (shading) used for AROME ensemble simulations is shown in (a). The black rectangle represents the domain seen in (b).

level cold low located away from France (i.e. near 5° W) moving gradually eastward, and by a mid- to upper-level ridge centred over Northern Italy (Fig. 3a). Between these two large-scale structures prevailed a fairly strong upper-level southwesterly flow over the southeastern regions of France. The analysis of low-level conditions (Fig. 3b) clearly depicts a strong south to southwesterly low-level jet, emerging from the Balearic Islands with high values of adiabatic wet-bulb potential temperature, bringing and focusing very moist and unstable air masses to the Massif Central foothills.

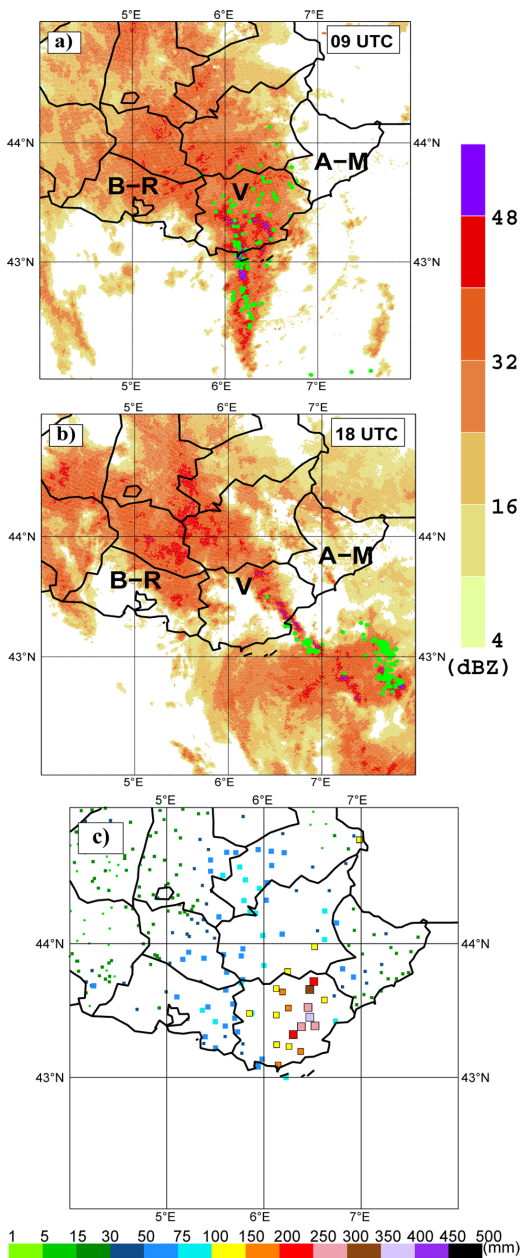


**Fig. 2.** Var case radar reflectivities composite from the observations on 15 June 2010 at (a) 09:00 UTC, and (d) 18:00 UTC, respectively. The green squares show lightning strikes observed during 3 h from the radar time. The thin lines delineate the departments (administrative areas of France); the Bouches du Rhônes, the Var and the Alpes-Maritime departments are labelled B-R, V, and A-M, respectively. (e) stands for rainfall observations from 06:00 UTC, 15 June 2010 to 06:00 UTC, 16 June 2010.

This south to southwesterly low-level jet took a more easterly component after 12:00 UTC (not shown).

A quasi-stationary mesoscale convective system (MCS) formed over the Massif Central foothills in the afternoon of 6 September and stayed over the same region until 18:00 UTC on 7 September 2010. This MCS developed within the warm air ahead of the surface front that affected western France at that time (Fig. 4a). At 18:00 UTC on 7 September, the surface cold front approached from the west and merged with the MCS, strengthening the convective activity (Fig. 4b). Moreover, the Gard-Ardèche case was characterised also by tremendous lightning activity. Although observed rainfall amounts locally exceeded 350 mm in 24 h (Fig. 4c), little damage was observed and no casualties were reported for this case.

### 3 Ensemble set up and methodology

#### 3.1 The reference convection-permitting ensemble experiment

This study is carried out with the non-hydrostatic numerical model AROME, which has been operational at Météo-France since December 2008 (Seity et al., 2011). AROME is run with a horizontal resolution of about 2.5 km. Moreover, the AROME domain used in this present study is mainly centred over the Northwestern Mediterranean Sea encompassing the French southeastern Mediterranean regions, Catalonia, Balearic Islands, Sardinia, Corsica and a part of Northern Italy and Gulf of Genoa (Fig. 1a). Such a Mediterranean domain is chosen instead of the operational one in order to better tackle the meteorological ingredients favouring heavy precipitation over Southeastern France. The vertical grid comprises 60 vertical levels. AROME is based on the non-hydrostatic dynamic core of the limited-area model ALADIN (Bénard, 2004; Bubnova et al., 1995), sharing the same physical parameterizations as the research model Meso-NH (Lafore et al., 1998). The bulk microphysics scheme following Caniaux et al. (1994) governs the prognostic equations of the six water variables (water vapour, cloud water, rain water, primary ice, graupel and snow). Shallow convection is parameterized by the EDKF scheme of Pergaud et al. (2009) and the turbulent scheme follows Cuxart et al. (2000). No deep convection parameterization is used, as it is assumed that deep convection is explicitly resolved at 2.5 km grid spacing.

AROME uses LBCs interpolated from ARPEGE forecasts (about 10 km horizontal resolution over France), with a coupling frequency of 1 h. The AROME data assimilation system uses a rapid forward sequential assimilation cycle with a 3-hourly data analysis frequency. The observations assimilated in the 3-D-VAR AROME system included those from radio soundings, screen-level stations, wind profilers, GPS, buoys, ships, and aircraft. Assimilated satellite data

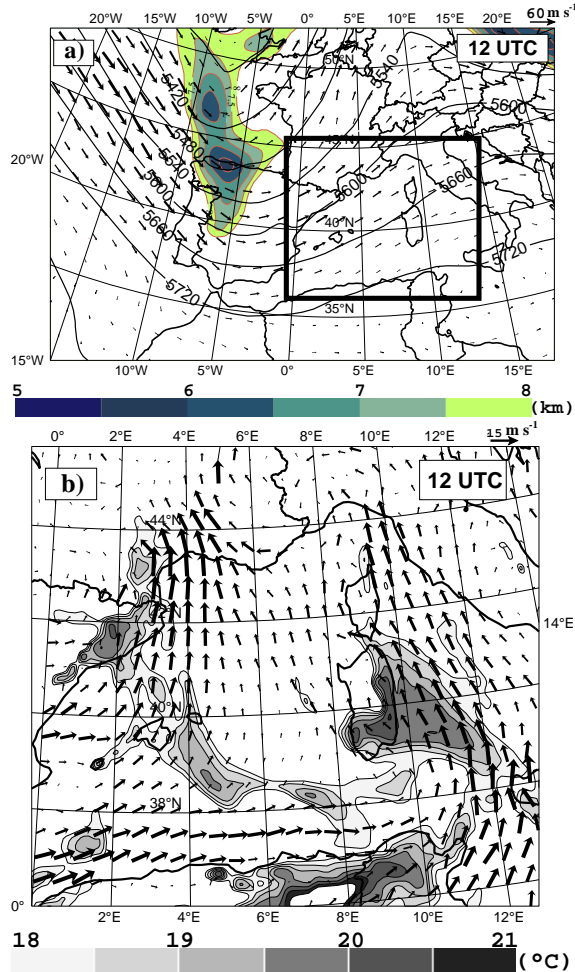


**Fig. 3.** Gard case (a): 300 hPa winds (arrows), 1.5 PVU surface height (colour) and 500 hPa geopotential height (solid line) and (b): adiabatic wet-bulb potential temperature (shading) and horizontal winds at 925 hPa, from ARPEGE analysis on 7 September 2010 at 12:00 UTC. The black rectangle represents the domain seen in (b).

included horizontal winds from atmospheric motion vectors (AMVs) and the QuickSCAT scatterometers, Advanced Microwave Sounding Unit (AMSU)-A and -B radiances from the NOAA-15, -16, -17, and the Aqua satellites, High-resolution Infrared Sounder (HIRS) radiances from NOAA-17, and clear-air Spinning Enhanced Visible and Infrared Imager (SEVIRI) radiances from the Meteosat-8 satellite. In addition, AROME assimilates Doppler radial winds from the weather radar network over France.

To carry out the C-P ensemble experiments, AROME is driven by the global short-range ARPEGE EPS (called hereafter PEARP). PEARP uses a stretched horizontal grid over the globe, allowing higher horizontal resolution over West-

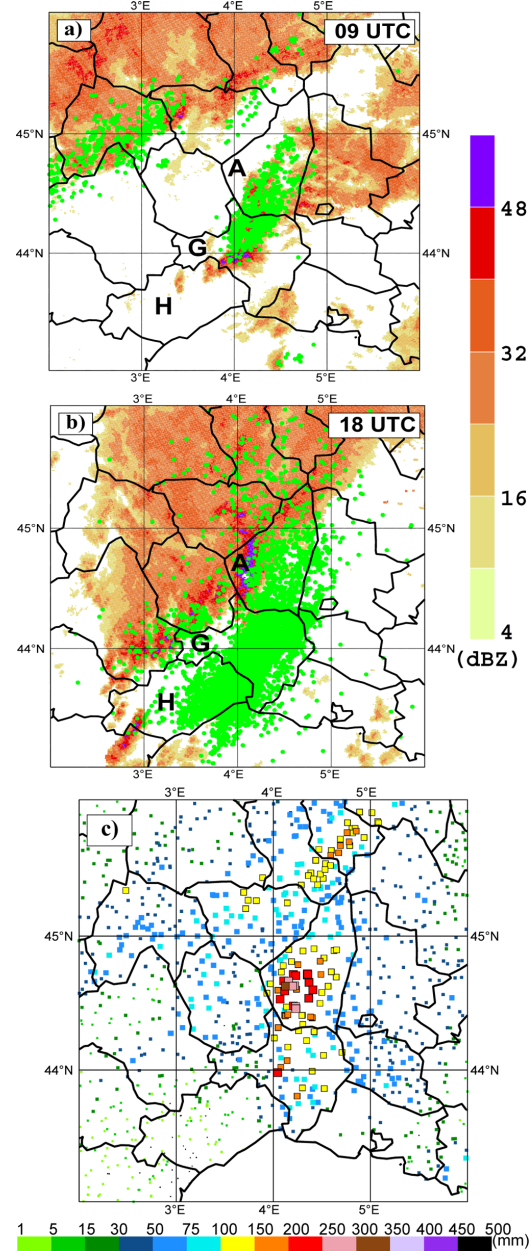


**Fig. 4.** Gard case radar reflectivities composite from the observations on 7 September 2010 at (a) 09:00 UTC, and (d) 18:00 UTC, respectively. The green squares show lightning strikes observed during 3 h from the radar time. The thin lines delineate the departments (administrative areas of France); the Bouches du Rhônes, the Var and the Alpes-Maritime departments are labelled B-R, V, and A-M, respectively. (c) stands for rainfall observations from 06:00 UTC, 7 September 2010 to 06:00 UTC, 8 September 2010.

ern Europe. The control run is similar to the ARPEGE operational deterministic system, except for its coarser grid spacing of about 15 km over France. The initial conditions for the other 34 members are obtained by adding perturbations to the control run. The perturbation method blends ensemble assimilation in ARPEGE and calculation of 12-h dry singular vectors.

A first reference ensemble simulation (called hereafter REF) is performed to analyse the convective-scale predictability of both case studies. The REF ensemble experiment used in this study has 35 members (i.e. 34 perturbed + 1 control member) and is driven by the PEARP members which also counts 35 members. In order to get the best as possible mesoscale initial state for our C-P ensemble and simultaneously examine the impact of LBC uncertainty, all members start from a unique initial condition provided by a parallel mesoscale data assimilation performed over the AROME domain. This mesoscale data assimilation cycle starts two days before the time of the events, that means on 13 June 2010 at 00:00 UTC for the Var case and on 5 September 2010 at 00:00 UTC for the Gard-Ardèche case, respectively.

### 3.2 A dedicated cluster analysis for heavy precipitation events

The approach adopted in this study lies in the idea of reducing the number of global-ensemble members driving the limited-area forecasts, still retaining a large fraction of the driving-ensemble variability. The selection technique used here consists of a dynamical clustering of the large-scale meteorological circulation patterns simulated by the 35 PEARP's members.

Based on the knowledge of the large and subsynoptic-scale environment patterns favourable to intense precipitation in the Mediterranean area (Nuissier et al., 2011), specific statistical predictors are precisely used to refine the dynamical clustering. The methodology is the following:

- i. a PEARP ensemble run, starting on given day at 00:00 UTC, is first considered. Here two forecast times are considered  $t + 9\text{ h}$  and  $t + 30\text{ h}$ .
- ii. for each PEARP member, specific meteorological parameters are extracted over a large Mediterranean domain at different levels and for various time steps,
- iii. a  $(N_v \times N_p)$  matrix is then built where  $N_p$  is the number of members and  $N_v$  is the number of parameters times the number of levels times the number of grid points times the number of forecast steps. Each variable of the matrix (i.e. column)  $v_i$  is normalised regarding to the mean and the standard deviation of all members  $p_i$ .
- iv. a cluster analysis is performed over Southern Europe (approximately  $60^\circ\text{N}$ – $30^\circ\text{N}$ ,  $10^\circ\text{W}$ – $40^\circ\text{E}$ ) and

the complete-linkage algorithm, through a hierarchical cluster analysis, is used to construct the clusters.

- v. the representative member (RM), chosen among each cluster, is the nearest element from its respective centroid and simultaneously the more distant from the other centroids. The above RMs provide both initial conditions and LBCs for the AROME model.

### 3.3 The convection-permitting ensemble simulations

To evaluate the impact of an “oriented” LBC selection against a random approach, and to assess the sensitivity of clustering to specific meteorological parameters favourable for heavy precipitation, 4 ensemble simulation experiments are carried out, in which LBCs for AROME are selected from PEARP members. The initial size of the reference ensemble is reduced down to 8 members in two experiments, either randomly selecting 7 LBCs from PEARP members (called hereafter *RAND1*, *RAND2*) or isolating 7 LBCs from a cluster analysis on PEARP members (called hereafter *CLUST-REF* and *CLUST-MOIST*). *RAND1* is a first set of 7 LBCs by drawing lots among 34 and *RAND2* is a second set. For each type of sub-ensemble, the control member is the same as in the one in the reference one. The choice of size of 8 members for our ensembles is purely subjective and corresponds to the targeted ensemble size expected for the design of the future AROME C-P EPS.

In *CLUST-REF*, the methodology for the dynamical clustering closely follows the one adapted for COSMO-LEPS (Molteni et al., 2001; Marsigli et al., 2001; Montani et al., 2003; Marsigli et al., 2005; Federico et al., 2007; Montani et al., 2011). The meteorological parameters are the geopotential height  $Z$ , the two horizontal wind components  $U$  and  $V$ , and the specific humidity  $Q$  all at 850, 700 and 500 hPa, respectively. In *CLUST-MOIST*, the dynamical core of the clustering is the same as in *CLUST-REF*, except that specific statistical predictors for heavy precipitation over the region (e.g. geopotential at 500 hPa and the moisture flux at 925 hPa) are only considered in the clustering.

Finally, a last series of ensemble simulations is considered to evaluate the added value of joining successive PEARP runs for the dynamical clustering. The use of this super-ensemble was introduced by Montani et al. (2003) and Marsigli et al. (2005), aiming at increasing the spread of the global ensemble on which the cluster analysis is performed. For that purpose, the *LAG* ensemble is driven by a set of PEARP members starting either at the forecast start time or 12 h before. It is worth noticing that all ensemble simulations are run for 30 h, starting at 00:00 UTC on 15 June 2010 or at 00:00 UTC on 7 September 2010.

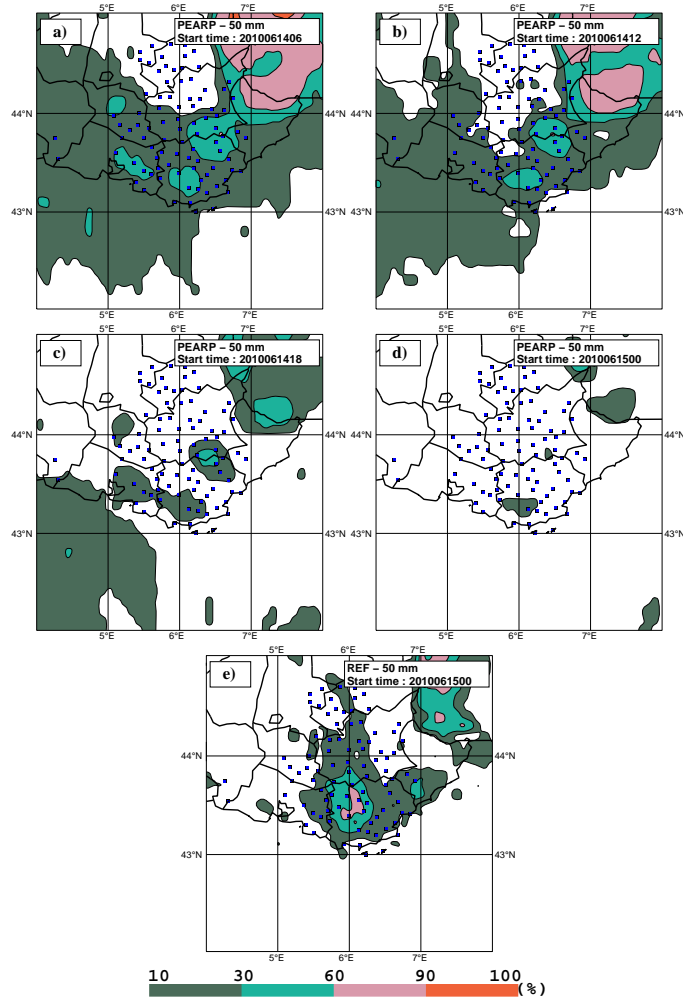


**Fig. 5.** Var case probability map for the 24-h accumulated precipitation (valid at 06:00 UTC on 16 June 2010) exceeding 50 mm and for the PEARP ensemble starting at: (a) 06:00 UTC, 14 June 2010, (b) 12:00 UTC, 14 June 2010, (c) 18:00 UTC, 14 June 2010 and (d) 00:00 UTC, 15 June 2010. (e) and (f) stand for the REF convective-permitting ensemble experiment starting at 00:00 UTC, 15 June 2010 and for the thresholds 50 and 100 mm. The squares are observations (rain-gauges) over the same threshold.

#### 4 Overall performance of ensembles

This section compares the performance of the reference C-P ensemble (i.e. REF) and the skill of the driving lower-resolution PEARP in terms of quantitative precipitation forecasts (QPFs). In order to facilitate the direct comparison between PEARP and REF, the grid point forecasts of both ensembles are aggregated over boxes of  $0.2 \times 0.2^\circ$ , averaging all the forecast values falling into the boxes. We focus primarily on the phases of heavy precipitation occurring between 15 and 16 June 2010 over southern foothills of Alps, and between 6 and 7 September 2010 over the southeastern region

of the Massif Central (see Sect. 2), adopting an uniform presentation for both cases.

##### 4.1 The Var case

The probabilistic forecasts from PEARP are presented for the Var case in Fig. 5a, b, c and d and for different starting times. The panels show the probability maps for precipitation forecasts exceeding  $50 \text{ mm day}^{-1}$ , valid for 16 June 2010 at 06:00 UTC and starting at 00:00 UTC on 15 June 2010 and at 18:00, 12:00 and 06:00 UTC on 14 June 2010. Unexpectedly, high values of probability are not obtained for the nearest time of the event, but for the longest forecast ranges.

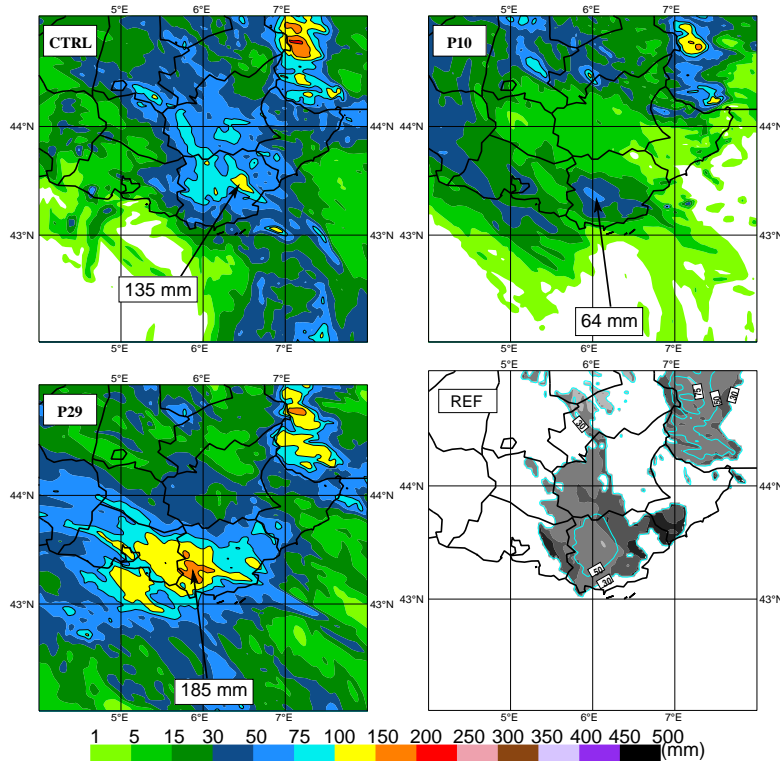


**Fig. 6.** Var case 24-h accumulated simulated precipitation for the REF convective-permitting ensemble experiment. The run is valid for 16 June 2010 at 06:00 UTC and starts on 15 June 2010 at 00:00 UTC. Precipitation maxima are pointed out over the Var department. The last panel shows the 24-h accumulated ensemble-mean (solid line) and the normalised spread (shading). The spread is not shown for precipitation below  $30 \text{ mm day}^{-1}$ .

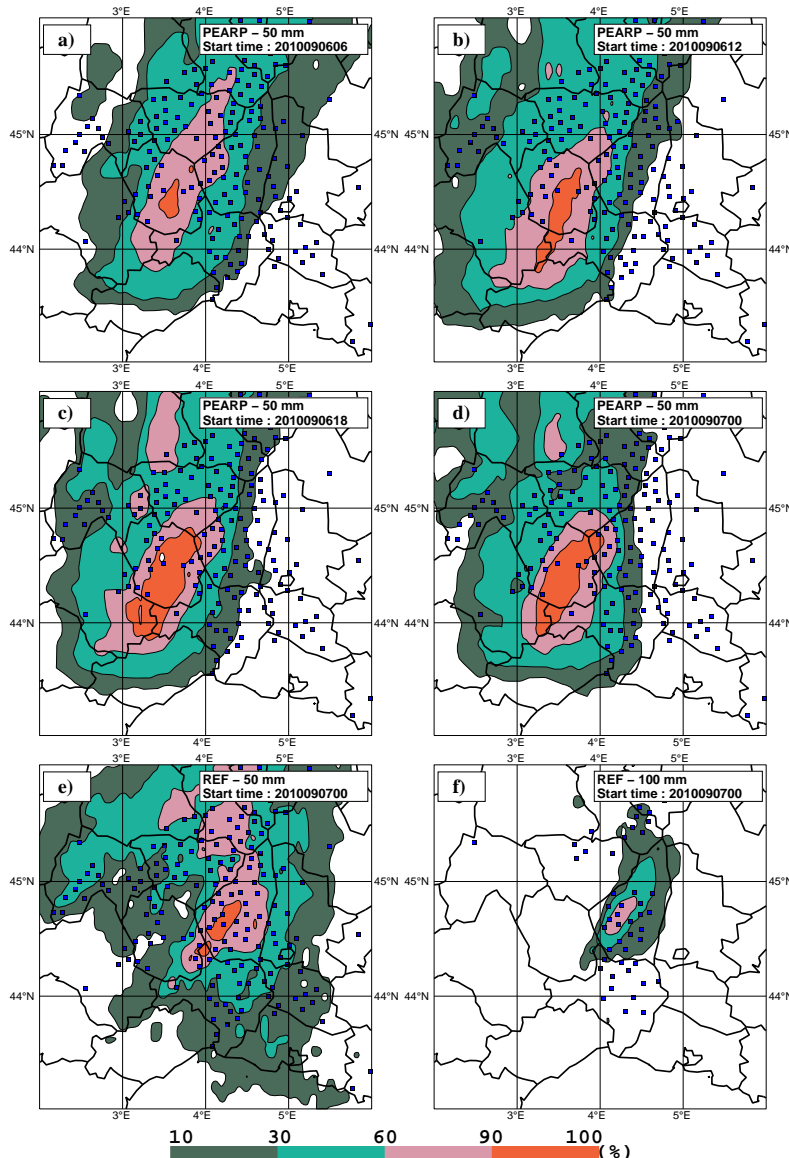
Indeed, the highest probability are located over Italy with two areas of about 70 % and 40 % over the northeastern and southwestern portion of the Var Department on 14 June 2010 at 06:00 UTC (Fig. 5a). The Var region still have significant probabilities of heavy precipitation regarding forecasts starting at 12:00 UTC on 14 June 2010, but the values strongly decrease beyond 18:00 UTC and especially for the run starting at 00:00 UTC on 15 June 2010 (Fig. 5d). Therefore, an important result for the Var case is that the best skill is not obtained for the most recent PEARP ensemble forecasts. The “oldest” runs better predict the favourable synoptic-scale meteorological ingredients. For instance, the PEARP run starting at 12:00 UTC on 14 June 2010 depicts on average more members with a stronger upper-level PV- anomaly closer to the flooded area, providing a more pronounced southerly upper-level flow over the flooded area (not shown).

Figure 5e displays the same probability maps shown for PEARP but for the REF experiment and for the thresholds 50 mm, respectively. One can remark that the REF experiment yields substantial improved QPFs. Although the areas affected by heavy precipitation are misplaced westward, the

REF ensemble simulation enables to focus and clearly isolate the heaviest precipitation amount probability over the flooded area (Fig. 5e).

Accumulated precipitation for the control and the better/worse members of REF are shown in Fig. 6. There are obvious differences and a strong variability between members, in terms of location as well as in intensity. A local maximum over the Var region of about 64 mm in 24 h is simulated by member 10 (worse), whereas 185 mm is obtained by member 29 (better). The precipitation forecasts of some members are very accurate, but no member predicts precipitation peaks of about 460 mm as observations (Fig. 6 vs. Fig. 2c). This could be due to the lack or bad representation of some very favourable ingredients (i.e. low-level moisture convergence), triggering deep convection over Mediterranean Sea.

As in Hohenegger et al. (2006), we pay attention to the assessment of the predictability for our case studies. For that purpose, the ensemble spread is used as a measure with large spread indicating poor predictability and vice versa. The spread-skill relation, i.e. more (less) spread leads to less (higher) predictability, is well established for the prediction



**Fig. 7.** Gard case probability map for the 24-h accumulated precipitation (valid at 06:00 UTC on 8 September 2010) exceeding 50 mm and for the PEARP ensemble starting at: (a) 06:00 UTC, 6 September 2010, (b) 12:00 UTC, 6 September 2010, (c) 18:00 UTC, 6 September 2010 and (d) 00:00 UTC, 7 September 2010. (e) and (f) stand for the REF convective-permitting ensemble experiment starting at 00:00 UTC, 7 September 2010 and for the thresholds 50 and 100 mm. The squares are observations (rain-gauges) over the same threshold.

of upper-air variables in the framework of global-ensemble forecasting. Although this relation is less clear as for prediction of surface fields (as some topographic effects could affect predictability), surface precipitation spread is used as a measure of predictability. The spread  $S$  is calculated as the standard deviation for the precipitation parameter  $P$ , i.e.  $S = \sqrt{\frac{1}{N-1} \sum_{i=1}^N (P_i - \bar{P})^2}$ , where  $N$  denotes the num-

ber of ensemble members and  $\bar{P}$  is the precipitation ensemble mean. Since precipitation fields can display strong variability, a normalised spread defined as  $S \times \bar{P}^{-1}$  is used. It is worth noticing that this normalised spread is rather useful, where precipitation amounts are strong but may lead to unrealistically large spread values especially at the borders of rainy areas. The last panel of Fig. 6 illustrates the 24-h

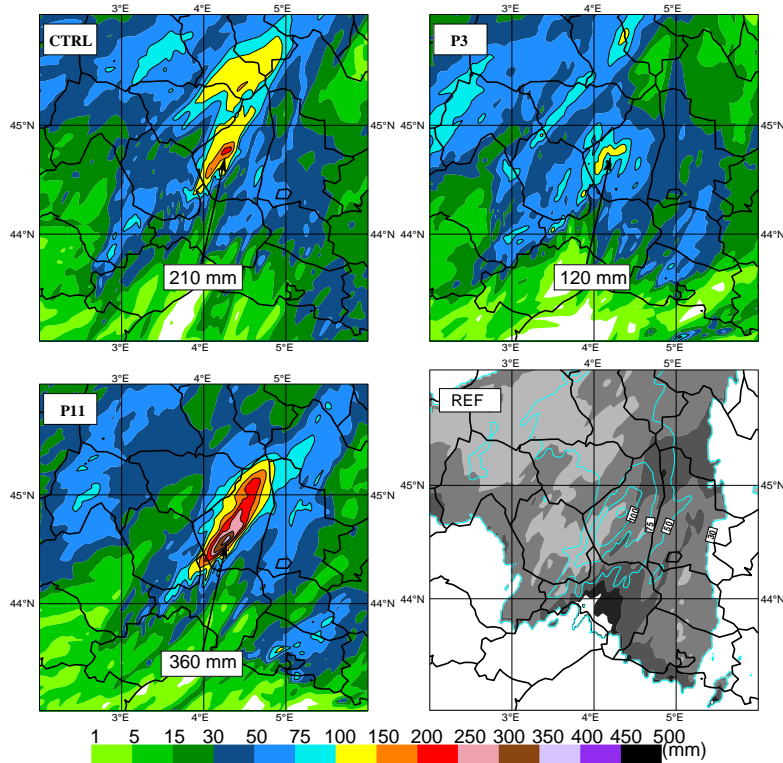


**Fig. 8.** Gard case 24-h accumulated simulated precipitation for the REF convective-permitting ensemble experiment. The run is valid for 8 September 2010 at 06:00 UTC and starts on 7 September 2010 at 00:00 UTC. Precipitation maxima are pointed out over the Gard department. The last panel shows the 24-h accumulated ensemble-mean (solid line) and the normalised spread (shading). The spread is not shown for precipitation below  $30 \text{ mm day}^{-1}$ .

ensemble mean accumulated precipitation and the associated normalised spread for REF. Normalised spread is not shown for precipitation ensemble mean values below  $30 \text{ mm day}^{-1}$ . The Var case is characterised by moderate to strong spread with values generally around 0.6 over the Var department, and peaking near 1 over the flooded area (i.e. southeastern Var). These strong values of spread in the vicinity of the strongest precipitation ensemble mean underline that the convective system is highly unpredictable.

#### 4.2 The Gard-Ardèche case

Concerning the Gard-Ardèche case, the probability for precipitation forecasts exceeding  $50 \text{ mm day}^{-1}$ , valid for 8 June 2010 at 06:00 UTC and starting at 00:00 UTC on 7 September 2010 and at 18:00, 12:00 and 06:00 UTC on 6 September 2010, are displayed in Fig. 7a, b, c and d for PEARP runs. High values of probability are obtained whatever the forecast range (even for the longest forecast range). That is a completely different result with respect to the Var case. On 6 September 2010 at 06:00 UTC, one can see in the PEARP run values of probability higher than 90 %

but slightly misplaced just west of the Ardèche department (Fig. 7a). In contrast to the Var event, these probabilities last and even increase with time in magnitude and also in coverage (Fig. 7b and c). On 7 September 2010 at 00:00 UTC, the area of high precipitation probabilities is largest but is still displaced westward.

Figure 7e and f shows the results for the REF ensemble experiment. Compared to PEARP, the REF ensemble yields better simulations of the precipitation event, shifting the strong probability values more over the flooded area. One can also remark that it better represents precipitation associated with the surface cold front approaching from the west.

Figure 8 shows the 24-h accumulated simulated precipitation amounts for the REF experiment. As was expected for the Gard-Ardèche case, the ensemble performs much better in terms of QPFs than it does for the Var case. Although most of the simulated precipitation amounts are still slightly underestimated, a few members are very close to observations. For instance member 11 predicts near 360 mm in 24 h in very good agreement with observations. The spread of precipitation is quite reduced with respect to the Var case and

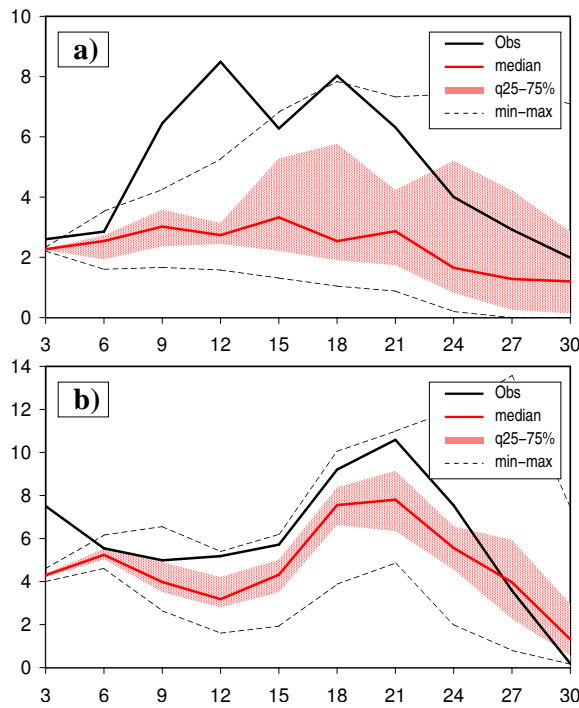


**Fig. 9.** Time series of the 3-h surface precipitation (mm) for REF and for the Var (a) and Gard (b) cases, averaged over the subdomain seen in Figs. 6 and 8, respectively. Interquartile ranges (25 %–75 %), minimum, maximum and medians are shown. Initial times of the forecasts are 00:00 UTC of 15 June 2010 for the Var case and 00:00 UTC of 7 September 2010 for the Gard case, respectively.

the weakest precipitation amounts are obtained for member 3 with 120 mm.

As for the Var case, the last panel of Fig. 8 presents the 24-h ensemble mean accumulated simulated precipitation amounts and the associated normalised spread. The Gard-Ardèche case, unlike to the Var event, is characterised by small normalised spread denoting high predictability. Normalised spread values are mainly below 0.2 over the Ardèche department and are colocalized with the strongest precipitation peak. Higher values of about 0.8 are also found in southern Gard probably in association with some scenarios in the ensemble starting convective activity earlier over the department.

## 5 Discussion

After having evaluated the REF ensemble simulation, we now emphasise the mesoscale ingredients that favoured these long-lasting HPEs and controlled their predictability. For that purpose, the ensemble-mean water vapour fluxes  $\|q_v \mathbf{V}_h\|$ ,

where  $q_v$  is the specific humidity and  $\mathbf{V}_h$  is the horizontal wind at 925 hPa, are shown in Fig. 10.

Afterwards, the methodology of selection is evaluated then refined using statistical predictors arising from analysis of these propitious mesoscale ingredients.

### 5.1 Detailed analysis of favourable mesoscale ingredients

In order to analyse time evolution of rainfall, Fig. 9 shows time series of simulated precipitation with maximum, minimum, median and interquartile range averaged over the sub-domain seen in Fig. 2c for the Var case and Fig. 4c for the Gard-Ardèche case, respectively. The observations (bold solid line) attest the generally high skill of the ensemble median and 75 % quartile for the Gard-Ardèche case (Fig. 9b), on agreement with the small values of normalised spread discussed earlier. These quantities enable to fairly capture the precipitation peak observed near 21:00 UTC on 7 September 2010. For the Var case, the ensemble median fails to reproduce the maximum for rainfall amounts and rainfall amounts are strongly underestimated. Most of ensemble scenarios fail to capture the highest precipitation over the flooded area and these results are consistent with high normalised spread noticed in Sect. 4. Nevertheless, the last quartile (i.e. 75 %) better describe time evolution of precipitation with two peaks shifted later.

An analysis of the favourable mesoscale ingredients helps to better understand the fine-scale simulated rainfall distribution from the REF ensemble. Although the averaged fields are strongly smoothed, Fig. 10a displays, at 12:00 UTC on 15 June 2010 (i.e. just before the period of heaviest rainfall for the Var case), two converging tongues of high values of water vapour flux coming from west and northwest of Sardinia. A maximum of about  $100 \text{ g kg}^{-1} \text{ m s}^{-1}$  is found over the Mediterranean Sea and another stronger one of about  $150 \text{ g kg}^{-1} \text{ m s}^{-1}$  over the Var department. The low-level horizontal winds clearly depict a surface low centered along  $6^\circ \text{ E}$ , strengthening the southeasterly low-level flow and thus advecting warm and moist air masses toward the French southeastern coast. At 00:00 UTC on 16 June 2010, the low moves eastwards while the low-level flow is decreasing, and the favourable environment in terms of moisture flux also shifts over Ligurian Sea. In contrast to the Var case, Fig. 10c shows values of low-level water vapour stronger than  $200 \text{ g kg}^{-1} \text{ m s}^{-1}$ . As a matter of fact, strong forcing prevails at the surface for the Gard-Ardèche case. Indeed, as the cold front moves slowly eastwards, the southerly low-level flow is increased ahead of the front with strong convergence over the Gulf of Lyon, bringing more moisture in to feed deep convection over the region. At 00:00 UTC on 8 September 2010, as the cold front moves further eastwards, the low-level convergence of moisture flux is displaced near the southern Alps (Fig. 10d).

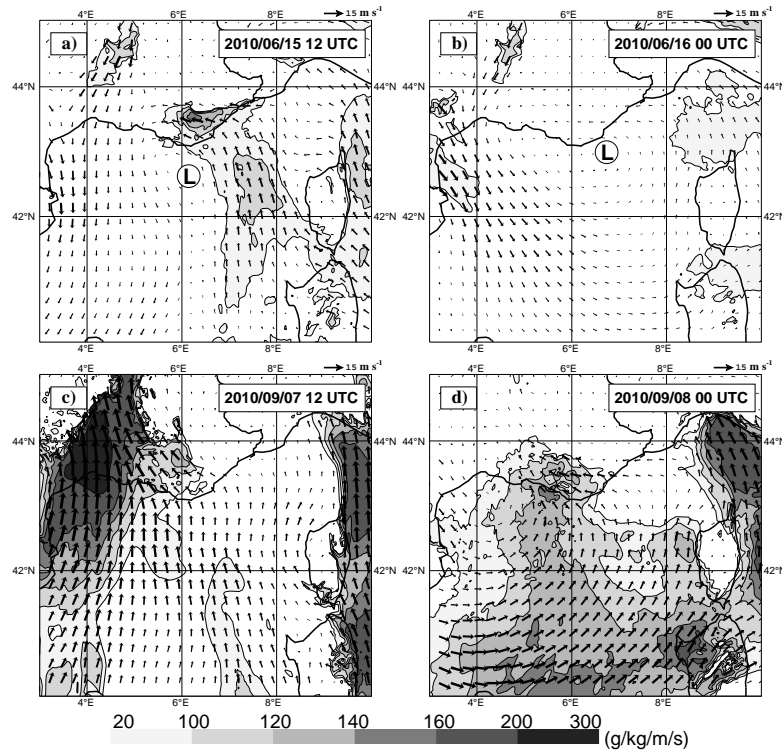


**Fig. 10.** 925-hPa horizontal moisture flux magnitude (shading,  $\text{g kg}^{-1} \text{m s}^{-1}$ ) and wind vector ( $\text{m s}^{-1}$ ) ensemble-mean for the Var case (**a** and **b**) and the Gard-Ardèche case (**c** and **d**, respectively. Ensemble experiments shown are REF in both cases. Initial times of the forecasts are 00:00 UTC of 15 June 2010 for the Var case and 00:00 UTC of 7 September 2010 for the Gard case, respectively.

Since our study considers only uncertainty arising from synoptic scale and LBCs, the variability of high-resolution precipitation forecasts are closely related to predictability of both meteorological forcings previously discussed. In the Var case, the predictability of the surface low is very low (i.e. spread is high), and there are few members able to fairly predict the strong southeasterly low-level flow advecting the supply of moisture to sustain very intense precipitation over the Var department. This result suggests that the Var case is very sensitive to the prescribed LBCs and to their interactions with other mesoscale and convective-scale processes. Indeed, Bresson (2011) revealed that the quasi-stationary convective line over the Var region and over the Mediterranean Sea was driven primarily by a surface low over the Gulf of Lyon inducing a strong convergent low-level flow, and by convective-scale mechanisms, such as a low-level cold pool and the triggering of deep convection by small orography features. In the opposite side, the predictability of the surface cold front is higher in the Gard-Ardèche case and there is a large majority of members depicting large southerly low-level water vapour advection ahead of the surface front. The Gard-Ardèche case appears to have a better predictability even in PEARP and it seems to be an event more controlled

by synoptic-scale conditions propagating through AROME lateral boundaries.

## 5.2 Impact of selected LBCs

In this section we investigate the sensitivity of the high-resolution forecasts to different selections of LBCs from PEARP ensemble.

In a first step, we compare results obtained for sub-ensembles in which LBCs are randomly selected against a method based on a cluster analysis. Figure 11a and b show, for the Var case, time series of 3-h simulated rainfall amounts (same as Fig. 9) and the 24-h ensemble-mean accumulated simulated precipitation (solid lines) superimposed to normalised spread (shading). For the RAND1 experiment, the evolution of the domain-averaged rainfall is slightly improved as the median indicates a peak of precipitation near 15:00 UTC on 15 June 2010. The highest quartile (i.e. 75 %) is still also showing a maximum of precipitation (Fig. 11a). However, this increase in precipitation on average is associated with higher values of normalised spread everywhere over the Var department, and the forecast uncertainty increases in the RAND1 ensemble. For the second set of

**Table 1.** Var case population and RMs for the *CLUST-REF*, *CLUST-MOIST* and *LAG* ensembles: columns 2, 3 and 4, respectively. The clustering time is 00:00 UTC on 15 June 2010. The RMs (in parenthesis) are expressed as MMDD “p”nn, where nn indicates the perturbed element of the ensemble started on day DD. See also text for more details.

Cluster		Cluster population and RM		
number		<i>CLUST-REF</i>	<i>CLUST-MOIST</i>	<i>LAG</i>
cl 1	3 (0615p29)	4 (0615p1)	17 (0615p31)	
cl 2	2 (0615p30)	3 (0615p30)	24 (0615p26)	
cl 3	4 (0615p17)	6 (0615p3)	7 (0614p23)	
cl 4	6 (0615p20)	10 (0615p32)	5 (0614p31)	
cl 5	9 (0615p25)	7 (0615p25)	4 (0614p32)	
cl 6	8 (0615p32)	2 (0615p33)	8 (0614p18)	
cl 7	2 (0615p34)	2 (0615p34)	4 (0614p26)	

randomly selected LBCs (RAND2 ensemble), the time series plot does better to fit observations in terms of interquartile distance mainly during the last 6 h of simulation. Since the forecast variability is already strong in REF for the Var case, both random experiments have very different behaviours due to the random nature of the selection of the LBCs.

As described in Sect. 3, the classification method enables to select 7 RMs out of, either the 35 elements which compose one PEARP run or the 70 that compose two successive PEARP runs. Table 1 reports cluster populations and RMs for each of the three clustering method and for the Var case. It can be noticed that, in *LAG*, the method selects members from both PEARP runs and members with different reference time also mix in some clusters. For instance, the representative member of cluster cl3 is selected from the *LAG* ensemble starting on 14 June (more precisely, the perturbed element p23 is selected within a cluster with 7 elements). *CLUST-REF* and *CLUST-MOIST* ensembles both produce clusters with a comparable number of elements, except for *LAG* in which the two populated clusters are able to gather near 60 % of the total of elements. One reason for such distribution with more clusters with low populations is that the “older” run of PEARP is more confident in its results (more similar members) for the Var case, leading to more variability to be classified in *LAG*. For the Gard case, the *LAG* has fewer clusters with low populations, whereas the two PEARP runs have more comparable variability (column 4 of Table 2).

When *CLUST-REF* is performed, the variability within the LBCs is thus better classified compared to random experiments, and the so-obtained sub-ensemble clearly enables to predict and focus more precipitation over the Var department in average (Fig. 11f). Two areas of strongest values of normalised spread are confined to the southwestern and southeastern part of the Var department.

When relevant meteorological parameters for the convective events of interest (i.e. geopotential height at 500 hPa and horizontal moisture flux at 925 hPa) are considered (*CLUST-*

**Table 2.** Gard case population and RMs for the *CLUST-REF*, *CLUST-MOIST* and *LAG* ensembles: columns 2, 3 and 4, respectively. The clustering time is 00:00 UTC on 7 September 2010. The RMs (in parenthesis) are expressed as MMDD “p”nn, where nn indicates the perturbed element of the ensemble started on day DD. See also text for more details.

Cluster		Cluster population and RM		
number		<i>CLUST-REF</i>	<i>CLUST-MOIST</i>	<i>LAG</i>
cl 1	9 (0907p17)	9 (0907p17)	16 (0907p17)	
cl 2	9 (0907p18)	12 (0907p18)	10 (0906p4)	
cl 3	4 (0907p5)	4 (0907p5)	25 (0907p18)	
cl 4	5 (0907p6)	5 (0907p6)	10 (0906p23)	
cl 5	3 (0907p28)	1 (0907p14)	4 (0906p5)	
cl 6	3 (0907p23)	2 (0907p25)	3 (0906p10)	
cl 7	1 (0907p26)	1 (0907p26)	1 (0906p17)	

*MOIST*), the ensemble-mean is increased in terms of surface precipitation maximum over the flooded area (Fig. 11h). Despite a slight decrease in terms of interquartile distance in time series, *CLUST-MOIST* enables to better regionalise and capture the forecast uncertainty. Indeed, the strong normalised spread simulated mainly over the southeastern portion of the area clearly indicates the possible occurrence of flooding over the region of Draguignan (Fig. 11h). Furthermore, one reason for the reduction in interquartile distance could be that *CLUST-MOIST* leads to more variability but which is spatially more localised at the “high-impact region” due to the selection of more mesoscale parameters in the clustering.

Since it has been shown in Sect. 4 that the Var case is better predicted in the “older” PEARP runs, the cluster analysis is applied on a 70-member, lagged ensemble, joining two consecutive PEARP runs (*LAG* experiment). Times are 12:00 UTC on 14 June 2010 and 00:00 UTC on 15 June 2010, respectively. Figure 11g shows that the lagged-classification leads to improvement in terms of QPF, as the median is closer to observations, but the uncertainty is also increased (i.e. more normalised spread). Time series indicates more clearly the triggering time of the heaviest precipitation than any other clustering experiments. However, for *LAG*, the maximum ensemble-mean rainfall amounts are more spatially extended northwestwards over the Bouches du Rhône department with respect to *CLUST-MOIST*, and the forecast uncertainty strongly increases as the normalised spread also extends spatially. However, a lagged approach can nevertheless provide more useful information regarding the potential meteorological situation.

Figure 12 shows the precipitation probability maps for precipitation exceeding 50 mm/24 h for the three ensembles. The impact of the selection of more relevant mesoscale ingredients is definitely noticeable for the Var case in Fig. 12b. Indeed, the probability is about 85 % over the western region of the Var department for the *CLUST-MOIST* and the

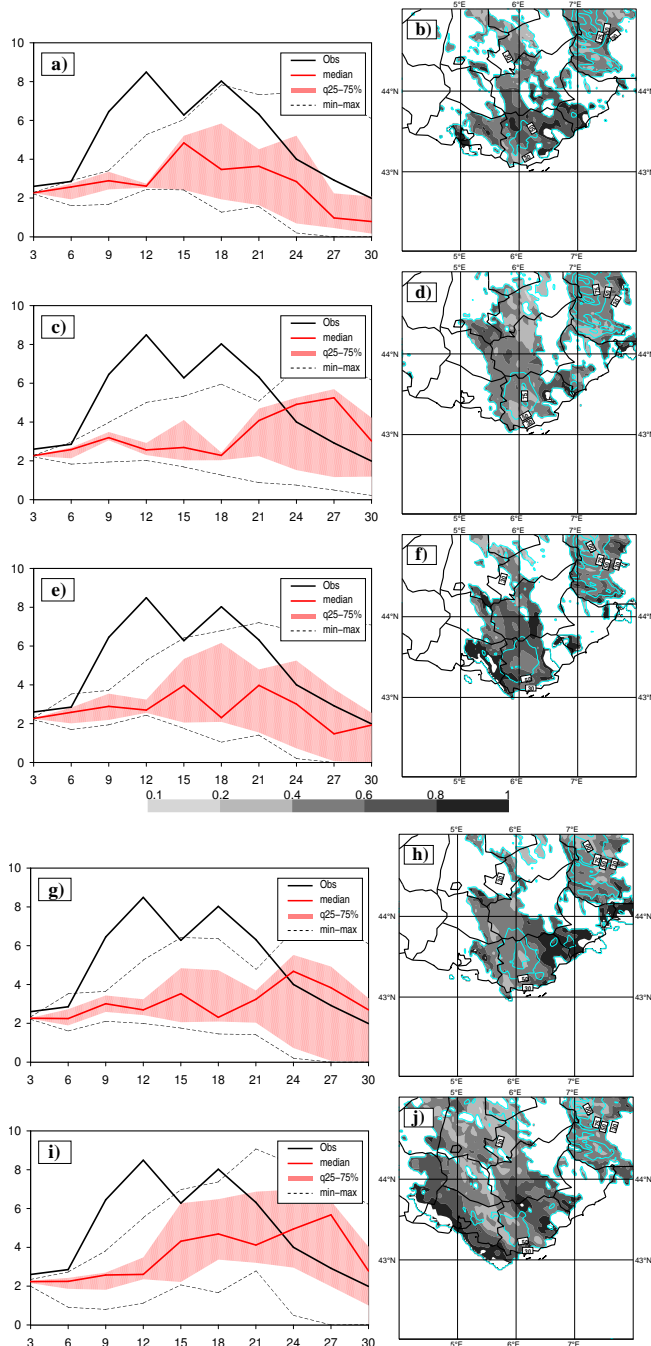


**Fig. 11.** Var case time series of the 3-h surface precipitation averaged over the subdomain seen in Fig. 6 and the 24-h accumulated simulated precipitation ensemble-mean (solid lines) and the normalised spread (shading) for the RAND1 (**a** and **b**), RAND2 (**c** and **d**), CLUST-REF (**e** and **f**), CLUST-MOIST (**g** and **h**), and LAG (**i** and **j**) ensemble experiments. Interquartile ranges (25 %–75 %), minimum, maximum and medians are shown. The accumulation 24-h period starts on 15 June 2010 at 00:00 UTC and ends on 16 June 2010 at 06:00 UTC.

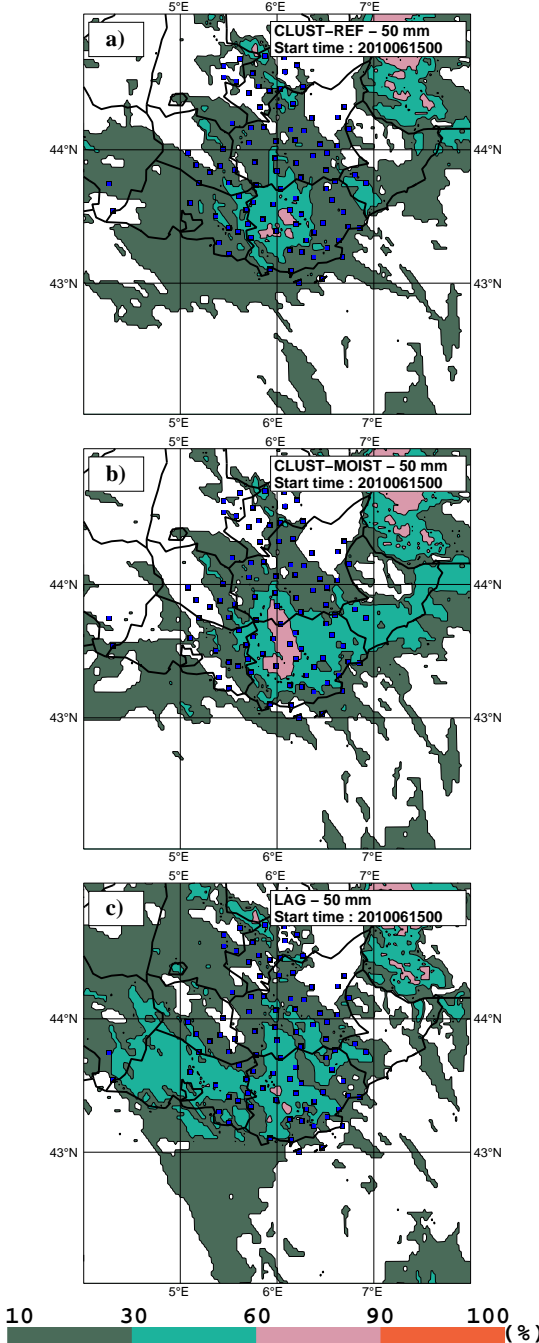


**Fig. 12.** Var case probability map for the 24-h accumulated precipitation (valid at 06:00 UTC on 16 June 2010) exceeding 50 mm and for (a) CLUST-REF, (b) CLUST-MOIST and (d) LAG. The squares are observations (rain-gauges) over the same threshold.

probability values are generally increased everywhere over Var compared to CLUST-REF. As for LAG, probability values are generally higher than CLUST-REF but they are more spatially extended, probably related to more spread in LAG.

The same sensitivity experiments are carried out for the Gard-Ardèche case (Fig. 13). For both RAND1 and RAND2 ensemble experiments, the spatial distributions of normalised spread are close except for a narrow band of high values of spread of about 0.8 oriented southwest-northeast through the Ardèche department in RAND2 (Fig. 13b and d). Both series have virtually the same departure to observations (Fig. 13a and c). Both selections from cluster analysis (CLUST-REF and CLUST-MOIST) indicate a large decrease of the normalised spread and strong values of rainfall amounts over the southwestern part of the department. This implies that both ensembles become more confident as the forecast variability decreases. However, there are still high values of spread west and south of the flooded area associated with some scenarios in the ensemble starting convective activity earlier on 6 September 2010 over the Gard department, and the surface cold front approaching, respectively. When two successive PEARP runs are combined (12:00 UTC on 6 September 2010 and 00:00 UTC on 7 September 2010), the median of the reduced ensemble after the selection is closer to observations and the interquartile distance is fairly increased, again as both PEARP runs have more comparable variability. The spatial distribution of normalised spread is generally the same except for stronger uncertainty northeast of the Ardèche department. In terms of rainfall probability charts, there is much less difference between clustering methods compared to the Var case. The Gard event is well predicted whatever the clustering selection approach (Fig. 14).

It is worth noticing that our C-P ensembles have also to be assessed over longer periods but our results are similar to those obtained by Montani et al. (2003); Marsigli et al. (2005); Montani et al. (2011). They confirm that, although the skill of the most recent ensemble forecasts is better than that of older ensembles and of the whole joined-ensemble, mixing successive global EPS runs provides, especially for some cases with low predictability, higher quality probabilistic forecasts since the joined-ensemble enable to better explore regions of the phase-space of the system otherwise left unexplored by the most recent global ensemble.

## 6 Synthesis and concluding remarks

In this study a methodology of selection of lateral boundary conditions (LBCs) was presented. This approach is dedicated for convection-permitting (C-P) ensemble simulations of heavy precipitation events.

A first reference C-P ensemble was carried out with the AROME model, using the ARPEGE Ensemble Prediction System (PEARP) members as LBCs (REF experiment). In this reference ensemble, the 35 members start from a unique

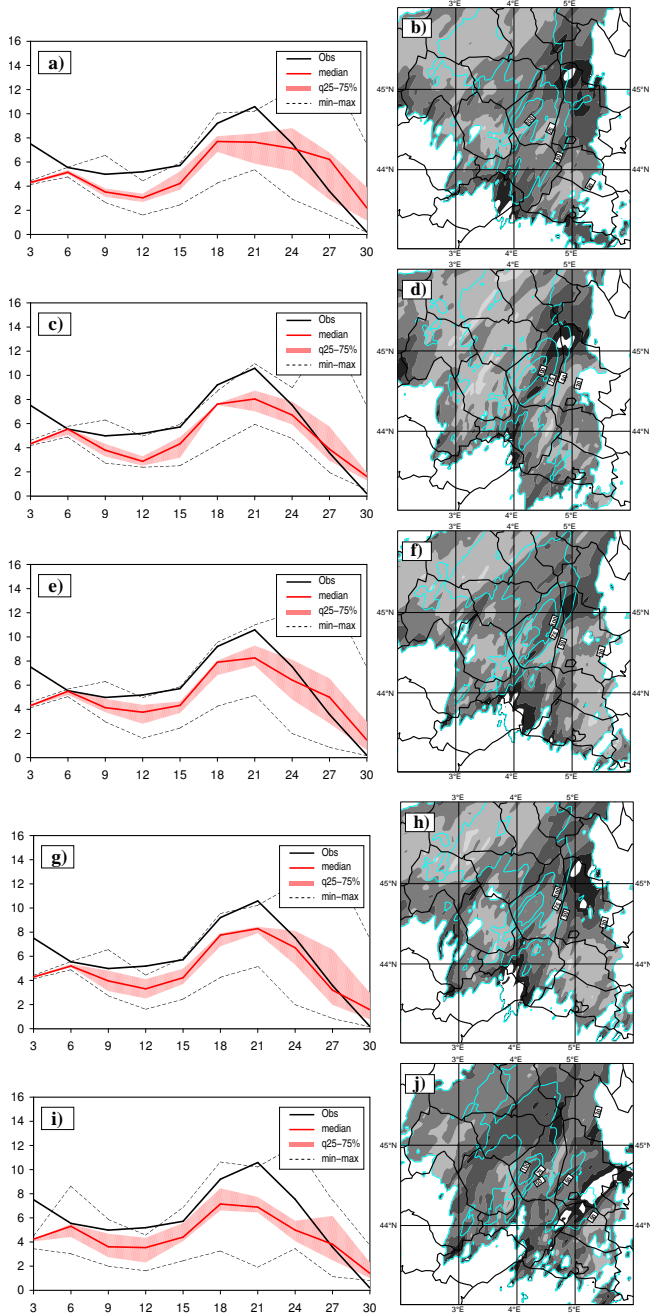


**Fig. 13.** Gard case time series of the 3-h surface precipitation averaged over the subdomain seen in Fig. 8 and the 24-h accumulated simulated precipitation ensemble-mean (solid lines) and the normalised spread (shading) for the *RAND1* (**a** and **b**), *RAND2* (**c** and **d**), *CLUST-REF* (**e** and **f**), *CLUST-MOIST* (**g** and **h**), and *LAG* (**i** and **j**) ensemble experiments. Interquartile ranges (25 %–75 %), minimum, maximum and medians are shown. The accumulation 24-h period starts on 7 September 2010 at 00:00 UTC and ends on 8 September 2010 at 06:00 UTC.

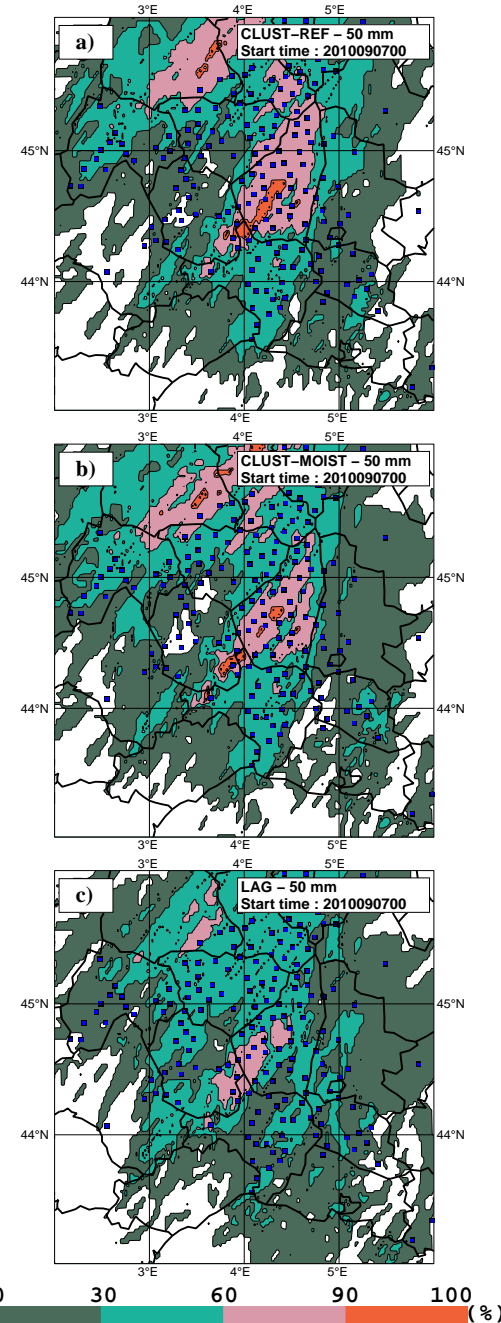


**Fig. 14.** Gard case probability map for the 24-h accumulated precipitation (valid at 06:00 UTC on 8 September 2010) exceeding 50 mm and for: (a) CLUST-REF, (b) CLUST-MOIST and (d) LAG. The squares are observations (rain-gauges) over the same threshold.

initial condition provided by a parallel mesoscale data assimilation performed over the AROME domain in order to get the best initial state as possible. They were also driven by the 35 PEARP members. The REF ensemble was used to assess the predictability of two cases of Mediterranean heavy precipitation events.

A comparison between PEARP and REF was performed. For that purpose, both ensembles were aggregated over boxes of  $0.2 \times 0.2^\circ$ . Predictability was found very different for both case studies. It has been found that the Gard-Ardèche case is more predictable even at PEARP horizontal resolution. Indeed, high values of probability exceeding  $50 \text{ mm day}^{-1}$  of about 90 % were obtained over Ardèche, whatever the time of the PEARP runs. On the other hand, for the Var case, high values of probability were not found at the time closest to the event, but for the longest forecast ranges. Probabilities of about 40 % are located over the northeastern and southwestern part of the Var department on 14 June 2010 at 06:00 UTC, but strongly decreased at 00:00 UTC on 15 June 2010. The predictability of the Var case was highly increased in the C-P ensemble, and the REF ensemble performed better than PEARP. The fine-scale variability of precipitation is closely controlled by the precise location of a quasi-stationary convective line over the Var region and over the Mediterranean Sea. This convective line was driven primarily by a surface low over the Gulf of Lyon inducing a strong convergent low-level flow, and accordingly advecting strong moisture supply from the Mediterranean Sea toward the flooded area.

In the Gard-Ardèche case, the differences between PEARP and REF were less significant. Indeed, in the former case, a surface cold front moved slowly eastwards while increasing the low-level water vapour ahead. These meteorological forcings were already well predictable in PEARP. Nevertheless, thanks to a better description of fine-scale orography in AROME, the REF ensemble succeeded in replacing correctly the precipitation maximum over the flooded-area.

If carrying out such a 35-member size C-P ensemble is easier for research studies, such a running appears less conceivable in an operational framework. A methodology of selection dedicated for C-P ensemble simulations of heavy precipitation events was evaluated. Consequently, the initial size of the reference ensemble is reduced down to 8 members, either randomly selecting 7 LBCs from PEARP members or isolating 7 LBCs from a cluster analysis on PEARP members. The selection based on a cluster analysis of the PEARP members (CLUST-REF) generally better performs against a random selection. The consideration of relevant meteorological parameters for the convective events of interest (i.e. geopotential height at 500 hPa and horizontal moisture flux at 925 hPa) refined the cluster analysis (CLUST-MOIST). It also helped in better capturing the forecast uncertainty variability which is spatially more localised at the “high-impact region” due to the selection of more mesoscale parameters. In LAG, the method selects members from both PEARP runs and members with different reference time also mix in some

clusters. Although there is a strong increase in forecast uncertainty, a lagged approach can provide more useful probabilistic information regarding the potential meteorological situation.

In this study, uncertainty sources arising from LBCs have been taken into consideration. However, it has been also found a strong sensitivity to mesoscale initial conditions in the REF experiment. Indeed, we carried out an additional sensitivity experiment (*ADAP*) not discussed in the present paper, in which each ensemble member used, as mesoscale initial state, one of the PEARP members that is basically interpolated from its native horizontal resolution (of about 15 km over France) toward 2.5 km. LBCs were also provided by the retained PEARP member. The results revealed that the REF ensemble better performed than *ADAP*, especially for the less predictable case (i.e. the Var case). For the Gard-Ardèche case, both REF and *ADAP* were still close since the surface cold front moving slowly eastwards was already well represented in PEARP. A partial conclusion would be that a simple downscaling of global EPS members can be sufficient, in some cases, to sample a large part of the C-P forecast errors.

Nevertheless, the design of a future C-P ensemble will need to combine all the major uncertainty sources and the sampling approach for the AROME mesoscale initial condition uncertainties is a work in progress. An ensemble data assimilation was already evaluated for two Mediterranean heavy precipitation case studies (Vié et al., 2011). Moreover, a stochastic physics scheme (adapted from ECMWF's stochastic perturbation physics tendencies) is currently assessed in the AROME short-range C-P ensemble prediction system (Bouttier et al., 2012). A more systematic evaluation, calculating probabilistic score over longer periods, is needed to validate our results obtained for two heavy precipitation case studies. These scientific issues will be reported in forthcoming publications.

**Acknowledgements.** This work was carried out in the framework of the MEDUP project (grant ANR-07-315 VULN-06-001), funded by the Vulnerabilite Milieux et Climat (VMC) programme of ANR. We gratefully acknowledge the comments made by the anonymous reviewers that helped to significantly improve the quality of the paper.

Edited by: D. Lambert

Reviewed by: two anonymous referees



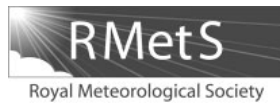
The publication of this article is financed by CNRS-INSU.

## References

- Bénard, P.: On the use of a wider class of linear systems for the design of constant-coefficients semi-implicit time schemes in NWP, *Mon. Weather Rev.*, 132, 1319–1324, 2004.
- Bouttier, F., Vié, B., Nuissier, O., and Raynaud, L.: Impact of stochastic physics in a convection-permitting ensemble, *Mon. Weather Rev.*, doi:10.1175/MWR-D-12-00031.1, 2012.
- Bresson, E.: Mécanismes de formation des systèmes convectifs quasi-stationnaires en Méditerranée nord-occidentale, Application au cas du 15 Juin 2010 sur le Var, Ph.D. thesis, Université Toulouse III Paul Sabatier, 2011.
- Bresson, R., Ricard, D., and Ducrocq, V.: Idealized mesoscale numerical study of Mediterranean heavy precipitating convective systems, *Meteor. Atmos. Phys.*, 103, 45–56, 2009.
- Bubnova, R., Hello, G., Bénard, P., and Geleyn, J.-F.: Integration of the fully elastic equations cast in the hydrostatic pressure terrain-following coordinate in the framework of the ARPEGE/Aladin NWP system, *Mon. Weather Rev.*, 123, 515–535, 1995.
- Caniaux, G., Redelsperger, J.-L., and Lafore, J.-P.: A numerical study of the stratiform region of a fast-moving squall line. 1. general description and water and heat budgets, *J. Atmos. Sci.*, 51, 2046–2074, 1994.
- Chancibault, K., Anquetin, S., Ducrocq, V., and Saulnier, G.-M.: Hydrological evaluation of high-resolution precipitation forecasts of the Gard flash-flood event (8–9 September 2002), *Q. J. Roy. Meteor. Soc.*, 132, 1091–1117, 2006.
- Cuxart, J., Bougeault, P., and Redelsperger, J.-L.: A turbulence scheme allowing for mesoscale and large-eddy simulations, *Q. J. Roy. Meteorol. Soc.*, 126, 1–30, 2000.
- Ducrocq, V., Nuissier, O., Ricard, D., Lebeaupin, C., and Thouvenin, T.: A numerical study of three catastrophic precipitating events over southern France, II: Mesoscale triggering and stationarity factors, *Q. J. Roy. Meteor. Soc.*, 134, 131–145, 2008.
- Federico, S., Avolio, E., Bellecci, C., Lavagnini, A., and Walko, R. L.: Predictability of intense rain storms in the Central Mediterranean basin: sensitivity to upper-level forcing, *Adv. Geosci.*, 12, 5–18, doi:10.5194/adgeo-12-5-2007, 2007.
- Fritsch, J. and Carbone, R.: Improving quantitative precipitation forecasts in the warm season: a USWRP research and development strategy., *B. Am. Meteor. Soc.*, 85, 955–965, 2004.
- Gebhardt, C., Theis, S., Paulat, M., and Ben Bouallègue, Z.: Uncertainties in COSMO-DE precipitation forecasts introduced by model perturbations and variation of lateral boundaries, *Atmos. Res.*, 100, 168–177, 2011.
- Grimit, E. and Mass, C.: Initial results of a mesoscale short-range ensemble forecasting system over the Pacific North-West, *Weather Forecast.*, 17, 192–205, 2002.
- Hohenegger, C. and Schär, C.: Predictability and error growth dynamics in cloud-resolving models, *J. Atmos. Sci.*, 64, 4467–

- 4478, 2007.
- Hohenegger, C., Lüthi, D., and Schär, C.: Predictability mysteries in cloud-resolving models, *Mon. Weather Rev.*, 134, 2095–2107, 2006.
- Kong, F., Xue, M., Drogemeier, K., Bright, D., Coniglio, M., Thomas, K., Wang, Y., Weber, D., Kain, J., Weiss, S., and Du, J.: Preliminary analysis on the real-time storm-scale ensemble forecasts produced as part of the NOAA hazardous weather testbed 2007 spring experiment, in: 22nd Conf. on Weather Analysis and Forecasting/18th Conf. on Numerical Weather Prediction, Amer. Meteor. Soc., vol. 3B.2, available at: [http://ams.confex.com/ams/22WAF18NWP/techprogram/paper\\_124667%.htm](http://ams.confex.com/ams/22WAF18NWP/techprogram/paper_124667%.htm), 2007.
- Lafore, J. P., Stein, J., Asencio, N., Bougeault, P., Ducrocq, V., Duron, J., Fischer, C., Héreil, P., Mascart, P., Masson, V., Pinty, J. P., Redelsperger, J. L., Richard, E., and Vilà-Guerau de Arellano, J.: The Meso-NH Atmospheric Simulation System. Part I: adiabatic formulation and control simulations, *Ann. Geophys.*, 16, 90–109, doi:10.1007/s00585-997-0090-6, 1998.
- Marsigli, C., Montani, A., Nerozzi, F., Paccagnella, T., Tibaldi, S., Molteni, F., and Buizza, R.: A strategy for high resolution ensemble prediction, II: Limited-area experiments in four Alpine flood events, *Q. J. Roy. Meteor. Soc.*, 127, 2095–2115, 2001.
- Marsigli, C., Bocanera, F., Montani, A., and Paccagnella, T.: The COSMO-LEPS mesoscale ensemble system: validation of the methodology and verification, *Nonlin. Processes Geophys.*, 12, 527–536, doi:10.5194/npg-12-527-2005, 2005.
- Mass, C., Ovens, D., Westrick, K., and Colle, B.: Does increasing horizontal resolution produce more skillful forecasts?, *B. Am. Meteor. Soc.*, 83, 407–430, 2002.
- Molteni, F. and Palmer, T.: Predictability and finite time instability of the northern winter circulation, *Q. J. Roy. Meteor. Soc.*, 119, 269–298, 1993.
- Molteni, F., Buizza, F., Palmer, T., and T., and Petroliagis, T.: The ECMWF ensemble prediction system: Methodology and validation, *Q. J. Roy. Meteor. Soc.*, 122, 73–119, 1996.
- Molteni, F., Buizza, R., Marsigli, C., Montani, A., Nerozzi, F., and Paccagnella, T.: A strategy for high resolution ensemble prediction. I: Definition of representative numbers and global-model experiments, *Q. J. Roy. Meteor. Soc.*, 127, 2069–2094, 2001.
- Montani, A., Marsigli, C., Nerozzi, F., Paccagnella, T., Tibaldi, S., and Buizza, R.: The Sovrato flood in Southern Italy: performance of global and limited-area ensemble forecasts, *Nonlin. Processes Geophys.*, 10, 261–274, doi:10.5194/npg-10-261-2003, 2003.
- Montani, A., Cesari, D., Marsigli, C., and Paccagnella, T.: Seven years of activity in the field of mesoscale ensemble forecasting by the COSMO-LEPS system: main achievements and open challenges, *Tellus A*, 63, 605–624, 2011.
- Nuissier, O., Ducrocq, V., Ricard, D., Lebeaupin, C., and Anquetin, S.: A numerical study of three catastrophic precipitating events over southern France, I: Numerical framework and synoptic ingredients, *Q. J. Roy. Meteor. Soc.*, 134, 111–130, 2008.
- Nuissier, O., Joly, B., Joly, A., Ducrocq, V., and Arbogast, P.: A statistical downscaling to identify the large-scale circulation patterns associated with heavy precipitation events over southern France, *Q. J. Roy. Meteor. Soc.*, 137, 1812–1827, 2011.
- Nutter, P., Stensrud, D., and Xue, M.: Effects of coarsely resolved and temporally interpolated lateral boundary conditions on the dispersion of limited-area ensemble forecasts, *Mon. Weather Rev.*, 132, 2358–2377, 2004.
- Pergaud, J., Masson, V., and Malardel, S.: A parameterization of dry thermals and shallow cumuli for mesoscale numerical weather prediction, *Bound.-Lay. Meteorol.*, 132, 83–106, 2009.
- Richard, E., Cosma, S., Tabary, P., Pinty, J.-P., and Hagen, M.: High-resolution numerical simulations of the convective system observed in the Lago Maggiore area on 17 September 1999 (MAP IOP 2a), *Q. J. Roy. Meteor. Soc.*, 129, 543–564, 2003.
- Seity, Y., Brousseau, P., Malardel, S., Hello, G., Bénard, P., Bouttier, F., Lac, C., and Masson, V.: The AROME-France convective scale operational model, *Mon. Weather Rev.*, 139, 976–991, 2011.
- Stein, J., Richard, E., Lafore, J.-P., Pinty, J.-P., Asencio, N., and Cosma, S.: High-resolution non-hydrostatic simulations of flash-flood episodes with grid-nesting and ice phase, *Meteor. Atmos. Phys.*, 72, 203–221, 2000.
- Stensrud, D., Bao, J., and Warner, T.: Using initial conditions and model physics in short-range ensemble simulations of mesoscale convective systems, *Mon. Weather Rev.*, 128, 2077–2107, 2000.
- Toth, Z. and Kalnay, E.: Ensemble forecasting at NCEP and the breeding method, *Mon. Weather Rev.*, 125, 3297–3319, 1997.
- Vié, B., Nuissier, O., and Ducrocq, V.: Cloud-resolving ensemble simulations of mediterranean heavy precipitating events: uncertainty on initial conditions and lateral boundary conditions, *Mon. Weather Rev.*, 139, 403–423, 2011.
- Vincendon, B., Ducrocq, V., Saulnier, G., Bouilloud, L., Chancibault, K., Habets, F., and Noilhan, J.: Benefit of coupling the ISBA land surface model with a TOPMODEL hydrological model dedicated to Mediterranean flash floods, *J. Hydrol.*, 11, 1529–1544, 2010.
- Walser, A., Lüthi, D., and Schär, C.: Predictability of precipitation in a cloud-resolving model, *Mon. Weather Rev.*, 132, 560–577, 2004.
- Zappa, M., Beven, K., Bruen, M., Cofino, A., Kok, K., Martin, E., Nurmi, P., Orfila, B., Roulin, E., Schroter, K., Seed, A., Szturc, J., Vehvilainen, B., German, U., and Rossa, A.: Propagation of uncertainty from observing systems and NWP into hydrological models: COST-731 working group 2, *Atmos. Sci. Lett.*, 11, 83–91, 2010.
- Zhang, F., Meng, Z., and Aksoy, A.: Tests of an ensemble Kalman filter for mesoscale and regional-scale data assimilation, Part I: perfect model experiments, *Mon. Weather Rev.*, 134, 722–736, 2006.

## 1.2. PUBLICATIONS MAJEURES POUR LA SOUTENANCE DE L'HABILITATION À DIRIGER DES RECHERCHE



## Idealized numerical simulations of quasi-stationary convective systems over the Northwestern Mediterranean complex terrain

E. Bresson,<sup>a\*</sup> V. Ducrocq,<sup>a</sup> O. Nuissier,<sup>a</sup> D. Ricard<sup>a</sup> and C. de Saint-Aubin<sup>b</sup>

<sup>a</sup>CNRM/GMME, Météo-France, Toulouse, France

<sup>b</sup>SCHAPI, Toulouse, France

\*Correspondence to: E. Bresson, CNRM/GMME/MICADO, 42 av. Coriolis, 31057 Toulouse Cedex, France.

E-mail: emilie.bresson@cnrm.meteo.fr

Northwestern Mediterranean coastal regions are frequently affected by torrential rainfall associated with quasi-stationary mesoscale convective systems (MCSs). The present work examines how the characteristics of a conditionally unstable flow impinging on the coastal complex terrain of the Northwestern Mediterranean can affect the location and intensity of quasi-stationary MCSs. The study is based on idealized simulations, but including the major ingredients of Northwestern Mediterranean heavy precipitation events: a moist conditionally unstable marine flow of about 100 km width facing the true terrain, composed of the Massif Central surrounded by the Alps and the Pyrenees.

We find that MCSs are located upstream of the mountain range with a slow flow, whereas with a rapid flow the heaviest precipitation is over the Massif Central slopes. In a similar way, when the lateral environment is drier the heaviest precipitation is located upstream whereas a humid environment favours precipitation over the slopes. The dominant lifting mechanism is strongly related to the location of the system: (1) direct orographic triggering for systems over mountain slopes and (2) cold-pool triggering for upstream systems. In addition, the neighbouring mountains interplay through deflection of the flow and induced low-level convergence favoured by slow or dry lateral environments and through cold-pool blocking within valleys.

Copyright © 2012 Royal Meteorological Society

*Key Words:* deep convection; heavy precipitation; mesoscale processes

*Received 11 October 2011; Revised 31 January 2012; Accepted 1 February 2012; Published online in Wiley Online Library 21 March 2012*

*Citation:* Bresson E, Ducrocq V, Nuissier O, Ricard D, de Saint-Aubin C. 2012. Idealized numerical simulations of quasi-stationary convective systems over the Northwestern Mediterranean complex terrain. *Q. J. R. Meteorol. Soc.* 138: 1751–1763. DOI:10.1002/qj.1911

### 1. Introduction

Most of the Mediterranean countries face heavy precipitating events (HPEs), especially during autumn. More than 100 mm of precipitation in under 6 hours is not uncommon in these regions. These torrential rainfalls over the small to medium watersheds of the Mediterranean region often lead to flash floods, resulting in damage and sometimes human losses. These HPEs most of the time involve back-building of quasi-stationary mesoscale convective systems (MCSs) with a continuous convective cell renewal at the same location (Bluestein and Jain, 1985). Usually, the heaviest precipitation

is located along the mountain range foothills facing the moist low-level sea winds. For the French Mediterranean region, a typical location is the Massif Central foothills (see figure 2 of Nuissier *et al.*, 2008). However, in some cases the quasi-stationary MCS anchors further upstream, over the plains or even over the sea. The very devastating HPE of 8–9 September 2002 (Delrieu *et al.*, 2005) was such a case, with the maximum of precipitation located over the Gard plain. Despite being over the plains, such a precipitating system can induce large rainfall amounts, as high as about 700 mm in 24 hours for the 8–9 September 2002 HPE.

The Mediterranean Sea, still warm during autumn, is a major source of moistening and heating of the marine boundary layer through air-sea sensible and latent heat fluxes (Duffourg and Ducrocq, 2011). In addition, the southerly to easterly low-level sea winds that prevail during HPEs transport this moist and conditionally unstable air toward the coast (Ricard *et al.*, 2011). Such low-level conditions are favoured by typical synoptic patterns. Nuissier *et al.* (2011) found that the synoptic-scale pattern propitious to HPEs over the French Mediterranean region consist of an upper-level trough located over the west of France and an upper-level ridge over central Europe. Nuissier *et al.* (2008) underlined the slow evolution of this synoptic pattern, which is an essential condition to maintain favourable low-level mesoscale conditions for a long enough time.

When this conditionally unstable low-level flow impinges on some of the mountain range foothills that border the Western Mediterranean Sea, deep convective precipitating cells can be triggered and renewed at the same location, as long as the same low-level conditions persist. Orographic lifting has been largely proposed in past studies as a mechanism for triggering heavy precipitation events over the western Mediterranean (e.g. Smith, 1979; Houze, 1993; Lin, 1993; Buzzi *et al.*, 1998; Buzzi and Foschini, 2000; Lin *et al.*, 2001; Rotunno and Ferretti, 2001; Pradier *et al.*, 2002; Bousquet and Smull, 2003; Georgis *et al.*, 2003 among others). Whereas precipitation formation induced by uplift of a stably stratified flow over a mountain ridge has been thoroughly investigated in idealized numerical frameworks, few studies have been devoted to the more challenging issue of a conditionally unstable flow impinging on a mountain range. Chu and Lin (2000) and Chen and Lin (2005) performed idealized simulations for a conditionally unstable flow over a two-dimensional mountain. Chu and Lin (2000) identified three precipitation regimes: (1) the convective system associated with a density current propagates upstream; (2) the convective system is stationary over the mountain peak, upslope or lee slope; (3) the convective or mixed convective-stratiform precipitation system over the mountain coexists with a downstream-propagating convective system. The study of Chen and Lin (2005, CL05 hereafter) added a fourth precipitation regime flow with an orographic stratiform precipitation system over the mountain. For a given Convective Available Potential Energy (CAPE), the flow regime increases when the Froude number (or wind speed) increases. Conversely, for a given Froude number the flow regime decreases when the CAPE increases. This can be interpreted in terms of competition between the forcing associated with the flow and the forcing associated with the cold outflow generated by evaporation of falling precipitation. However, as recognized by the authors, the relationship between the cold outflow forcing and the CAPE is not straightforward. Moreover, Miglietta and Rotunno (2009, MR09 hereafter) question the validity of the Froude number as a parameter controlling the precipitation regimes. Their simulations performed with different wind speeds or different mountain heights but the same Froude number lead to different precipitation regimes. The prediction of the location of the heavy precipitation is much more complex than reducing it in a two adimensional number regime diagram. It is influenced by other factors, such as the height of the condensation level, the slope of the mountain and the time for which a convective cell travels

toward the mountain peak. The cold-pool propagation and its facing against the upstream low-level flow also influence the location of heavy precipitation. A balance between both of these contributions leads to a stationary cold pool and therefore to an upstream stationary convective system (Miglietta and Rotunno, 2010).

These studies have considered a horizontally uniform wind over a single 2D mountain ridge within a 2D (Chu and Lin, 2000; CL05) or 3D (MR09) numerical simulation framework. This simple framework fails to represent some other key topographic characteristics of the Northwestern Mediterranean area. The neighbouring mountain ranges – Alps and Pyrenees for a low-level jet facing the Massif Central – could bring additional forcing such as low-level convergence induced by the deflection of the flow around them or participate in the blocking of the cold pool in the Rhône valley (Ducrocq *et al.*, 2008). The Mediterranean Sea, through its moisture and heat exchanges with the atmospheric boundary layer, also modulates the thermodynamic characteristics of the impinging low-level flow (Lebeaupin *et al.*, 2006). Bresson *et al.* (2009, BRD09 hereafter) performed idealized experiments in which the real topography of the region is kept to investigate the behaviour of a conditionally unstable low-level marine flow facing the Massif Central. In contrast to the CL05 or MR09 studies, the BRD09 numerical framework allowed us to simulate upstream stationary convective systems, as observed in that region. As in the previous studies, BRD09 found that larger winds shift the stationary convective system toward the mountain upslope. The influence of some other factors, such as the moisture and CAPE, was also examined. The aim of this present study is to explore further the behaviour of a conditionally unstable flow over the complex northwestern Mediterranean topography by taking a more systematic approach than BRD09 in order to enlarge their results. First, a larger range of wind speed and moisture content will be explored. Also, the impact of the different mountain ranges will be studied to understand better their role in precipitation formation and sustenance.

This article is organized as follows: Section 2 describes the experimental design, the results of the control and sensitivity simulations are presented in section 3 and then discussed in section 4 and concluding remarks are given in section 5.

## 2. Experiment design

### 2.1. Model set-up

The numerical simulations are carried out with a three-dimensional version of the French Meso-NH non-hydrostatic mesoscale numerical model (Lafore *et al.*, 1998). Meso-NH has already shown its capability to simulate HPEs in either a real or idealized framework (Ricard, 2005; Nuissier *et al.*, 2008; Ducrocq *et al.*, 2008; BRD09). For this study, the domain is centred over the southeastern regions of France and has a horizontal grid spacing of about 2.4 km (Figure 1). It extends further south than in BRD09 simulations in order better to represent convective cells triggering over the sea. Moreover, islands are removed and replaced by sea points to focus on the main mountain range effects. The lateral boundary conditions do not evolve with time and are identical to initial conditions during the entire simulation. An open wave radiation condition (Carpenter,

## 1.2. PUBLICATIONS MAJEURES POUR LA SOUTENANCE DE L'HABILITATION À DIRIGER DES RECHERCHE

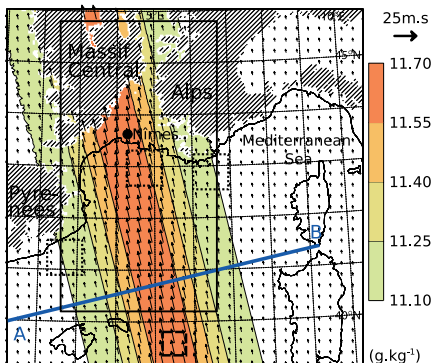


**Figure 1.** Initial conditions for the CTRL experiment in terms of water-vapour mixing ratio (coloured areas) and horizontal wind (arrows) at 500 m ASL. Orography higher than 500 m ASL is hatched. Boxes with solid, dotted and dashed lines are used for the time series seen in Figure 3, the calculation of moist Froude number shown in Table 2 and the computation of spatial average diagnostics shown in Table 3. This figure is available in colour online at [wileyonlinelibrary.com/journal/qj](http://wileyonlinelibrary.com/journal/qj)

1982) combined with a five-grid-point relaxation flow scheme (Davies, 1976) are applied at the boundaries.

The Meso-NH version used here includes a bulk microphysical scheme (Canaux *et al.*, 1997; Pinty and Jabouille, 1998) governing the equations of the six water species: water vapour, cloud water, rain water, primary ice, snow aggregates and graupel. The turbulence parametrization models the three-dimensional turbulent fluxes based on a 1.5-order closure (Cuxart *et al.*, 2000) and a mixing length following the method of Bougeault and Lacarrère (1989). The radiation parametrization is based on the Rapid Radiative Transfer Model (RRTM) of the European Centre for Medium-Range Weather Forecasts (Mlawer *et al.*, 1997). The solar hour is kept constant and fixed to 1600 UTC to remove the effect of the diurnal cycle in our simulations. A subgrid condensation scheme is activated, but deep convection is explicitly resolved (no deep convection parametrization).

### 2.2. Initial conditions

Since we are interested in the Cévennes area, our initial conditions are designed to represent a 100 km wide moist and conditionally unstable jet impinging on the southeastern part of the Massif Central. A vertically uniform southerly to southeasterly wind almost perpendicular to the main Massif Central ridge is considered (Figure 1). The wind speed is decreased from  $U_0$  at the central southeasterly-oriented axis to  $U_1$  at the boundaries according to a Gaussian shape (Figure 2(a)). This shape is quite different from that used in BRD09 (i.e. linear profiles as a function of height). Temperature and humidity conditions along the central southeasterly-oriented axis are derived from the sounding observed at Nîmes on 8 September 2002 at 1200 UTC (see figure 1(a) of BRD09) during the extreme HPE over Gard. This sounding is near saturation at low levels and conditionally unstable ( $\text{CAPE} = 400 \text{ J kg}^{-1}$ ). As for wind, water vapour is exponentially decreased from  $r_0(z)$ , given by the Nîmes sounding, to  $\alpha r_0(z)$  at the boundaries to focus moisture within the jet (Figure 2(b)). Also, for water vapour there are differences between the

present horizontal moisture distribution and that used in BRD09. The temperature is taken to be horizontally uniform. The sea-surface temperature is set to Levitus (1982)'s climatological value for the September month. For the control (CTRL) simulation  $U_0 = 20 \text{ m s}^{-1}$ ,  $U_1 = 5 \text{ m s}^{-1}$  and  $\alpha = 0.95$  (Table 1).

To study the sensitivity to the wind speed and the moisture content of the flow, two sets of simulations are also carried out. For the first set, the wind speed  $U_0$  is varied from  $10 \text{ m s}^{-1}$  to  $40 \text{ m s}^{-1}$  (Table 1; Figure 2(a)). These simulations are hereafter denoted WXX, XX being the value of  $U_0$ . Then, for experiments Q85, Q90, Q100, the parameter  $\alpha$  is set to 0.85, 0.9 and 1, respectively (Table 1; Figure 2(b)). The central value  $r_0(z)$  is kept, so that the differences between the initial states of the experiments increase with distance to the central axis. They are designed mainly to study the influence of the moisture content of the flow facing the neighbouring mountain ranges (Alps, Pyrenees). Another experiment is dedicated to studying the influence of the moisture content within the low-level jet. The C85 experiment is similar to Q85 at the boundaries but lowered by about a tenth within the low-level jet, as the central values of  $r_0(z)$  are scaled by 0.85/0.95 in order to keep the rate of mixing ratio between the central axis and the boundaries to 0.95 as in the CTRL experiment (Table 1; Figure 2(b)). Finally, the last set of simulations is designed to study the influence of the mountain ranges by removing, one by one, the different mountain ranges (Table 1).

## 3. Results

### 3.1. Control simulation (CTRL)

The control simulation, as well as all the other idealized experiments presented in this study, succeeds in reproducing a heavy precipitating MCS, reaching a quasi-stationary stage after a transient phase of a few hours (see Figure 3).

Hereafter, the study focuses on the quasi-stationary phase only. The precipitating system is organized in a 400 km long south–north convective line, extending from the Mediterranean Sea to the Massif Central foothills (Figure 4). The heaviest cumulative precipitation, more than 100 mm in 24 hours, spreads over quite a large area ( $20 \times 10^3 \text{ km}^2$ ). The deep convective cells within the MCS are preferentially located along the eastern edge of the system facing the south–southeasterly flow. The maximum of accumulated precipitation is located over the plains, reaching about 420 mm in 24 hours. The convective system is associated with a low-level cold pool delineated in Figure 4 by the 294 K virtual potential temperature isoline. The virtual potential temperature drops down to 291 K inside the cold pool. The surface winds, after having converged over the sea, rush between the Pyrenees and the Massif Central and deflect over the Alps. The cold-pool spreading is blocked between the Massif Central and Alps foothills (Figure 4).

### 3.2. Sensitivity to the meteorological environment

#### 3.2.1. Sensitivity to the wind speed

Figure 5 summarizes the effect of a more or less intense wind based on the W10 and W40 experiments. With a slower flow than in the CTRL experiment, the precipitating system is located over the Sea (Figure 5(a)), whereas with

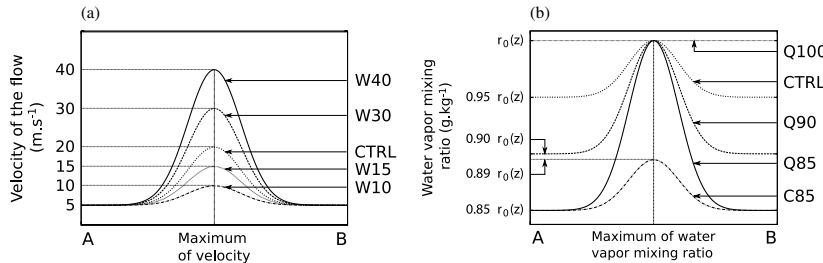


**Figure 2.** Horizontal profiles along the A–B vertical cross-section shown in Figure 1: (a) wind speed and (b) water-vapour mixing ratio for the numerical experiments described in Table 1.

Table 1. Characteristics of the numerical experiments. See text for parameter description.

Experiments	$U_0$ (m s <sup>-1</sup> )	Central axis moisture value	$\alpha$	Model terrain
CTRL	20	$r_0(z)$	0.95	real
W10, W15, W30, W40	10, 15, 30, 40	$r_0(z)$	0.95	real
Q85, Q90, Q100	20	$r_0(z)$	0.85, 0.90, 1	real
C85	20	<b>0.89</b> $r_0(z)$	<b>0.85</b>	real
ALPS, PYREN, MC	20	$r_0(z)$	0.95	<i>without</i> Alps, Pyrenees, Massif Central

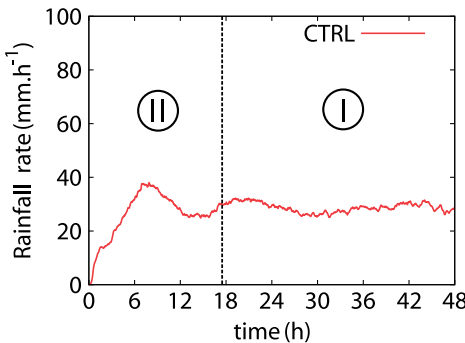


**Figure 3.** Time series of surface precipitation rates ( $\text{mm h}^{-1}$ ) for the CTRL simulation averaged over the domain shown in Figure 1. (I) and (II) stand for the transient and the quasi-stationary phases, respectively. This figure is available in colour online at [wileyonlinelibrary.com/journal/qj](http://wileyonlinelibrary.com/journal/qj)

a more rapid flow the system anchors further downstream with a maximum of precipitation located over the Massif Central slopes (Figure 5(b)). With a more rapid flow, the MCS is more developed and the maximum of surface precipitation is much more intense. The cold pool beneath the convective system vanishes with a more intense flow. In contrast, with a slower flow the precipitating system is less spread and the surface precipitation maximum weaker. The system also shifts to a southwest–northeast line orientation.

In order to quantify further the intensity of the precipitating system in the different experiments, the size of the region affected by surface precipitation larger than 100 mm between 24 h and 48 h of simulation, as well as the corresponding volume of precipitation received by this area, is presented in Figure 6(a) and (b). Figure 6(c) shows the size of the cold pool in the different experiments, defined as the region where the virtual potential temperature at 36 m above ground level (AGL) is colder than 294 K. The

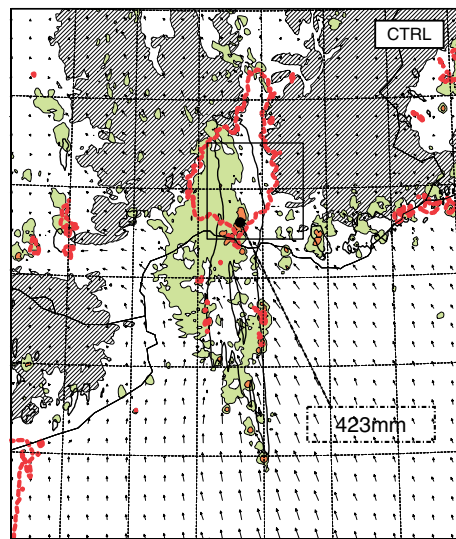


**Figure 4.** Total hydrometeor content at 10 km (shaded areas, coloured in the online article), 10 m horizontal wind (arrows) and 294 K contour line for the virtual potential temperature at 36 m AGL (dashed line, red in the online article) after 24 hours for the CTRL simulation, together with 100 mm contour line of the 24 h cumulative surface rainfall between 24 and 48 hours of simulation (solid black line), where the location and value of the maximum are indicated by the black bullet and dashed frame. Orography higher than 500 m ASL is hatched; the budget domain used for Figure 14 is drawn in a solid-line box. This figure is available in colour online at [wileyonlinelibrary.com/journal/qj](http://wileyonlinelibrary.com/journal/qj)

area affected by precipitation above 100 mm in 24 hours increases with the speed of the environmental wind. The volume of precipitation received by the corresponding areas clearly increases with the flow speed, from 1.5 km<sup>3</sup> for W10 to about 6 km<sup>3</sup> for W40. The spread of the cold pool is not so directly correlated with the flow speed, although no cold pool

## 1.2. PUBLICATIONS MAJEURES POUR LA SOUTENANCE DE L'HABILITATION À DIRIGER DES RECHERCHE

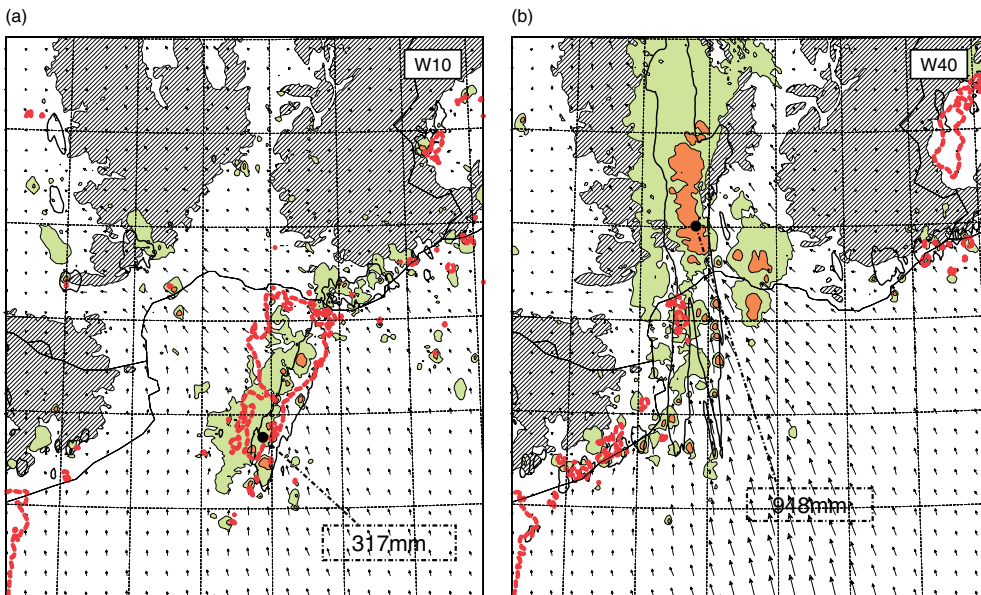


**Figure 5.** As Figure 4, but for (a) W10 and (b) W40 experiments. This figure is available in colour online at [wileyonlinelibrary.com/journal/qj](http://wileyonlinelibrary.com/journal/qj)

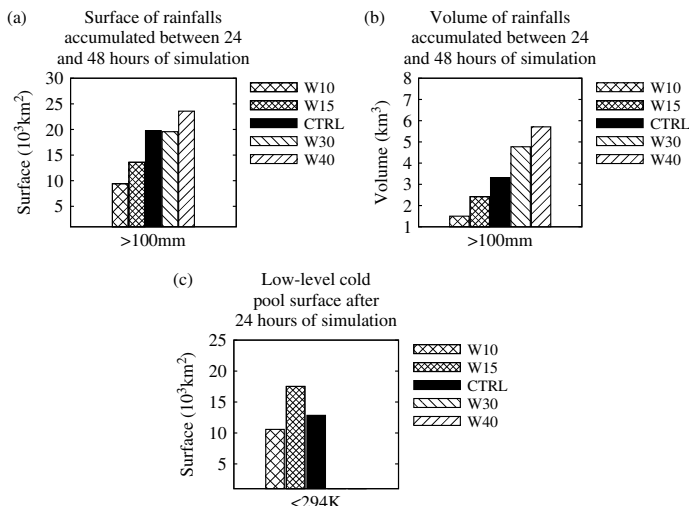


**Figure 6.** (a) Size of the region affected by 24 h surface rainfall above 100 mm (accumulated between 24 and 48 hours of simulation) and (b) volume of precipitation accumulated between 24 and 48 hours of simulation and above 100 mm. Panel (c) represents the size of the region where the virtual potential temperature at 36 m AGL is colder than 294 K after 24 hours of simulation for W10, W15, CTRL, W30 and W40 experiments. The quantities are calculated over the solid-line box shown in Figure 1.

is detected for wind speed  $U_0$  above  $30 \text{ m s}^{-1}$  (Figure 6(c)). The largest and most intense cold pool is obtained for moderate winds ( $U_0 = 15 \text{ m s}^{-1}$ ). It is worth mentioning that this result occurs as a kind of balance between the propagation of the cold pool and the environmental flow advection was obtained. This point will be discussed in section 4.3.

### 3.2.2. Sensitivity to moisture

When the lateral environment is drier than the CTRL experiment (experiments Q85 and Q90), the precipitating

system anchors further upstream, with the maximum of precipitation located over the sea (Figure 7(a)). The precipitating system is less spread when the lateral moisture is weaker (Figure 8(a)), but rainfall is more intense (Figure 8(b)). The cold pool is also larger (Figure 8(c)), extending further to the south (Figure 7(a)).

The Q100 experiment is initialized and forced with a uniform horizontal distribution of humidity given by the central axis profile. The lateral environment in Q100 is thus more humid than the CTRL one. The Q100 experiment produces a quasi-stationary MCS with maximum of precipitation over the slopes of the Massif

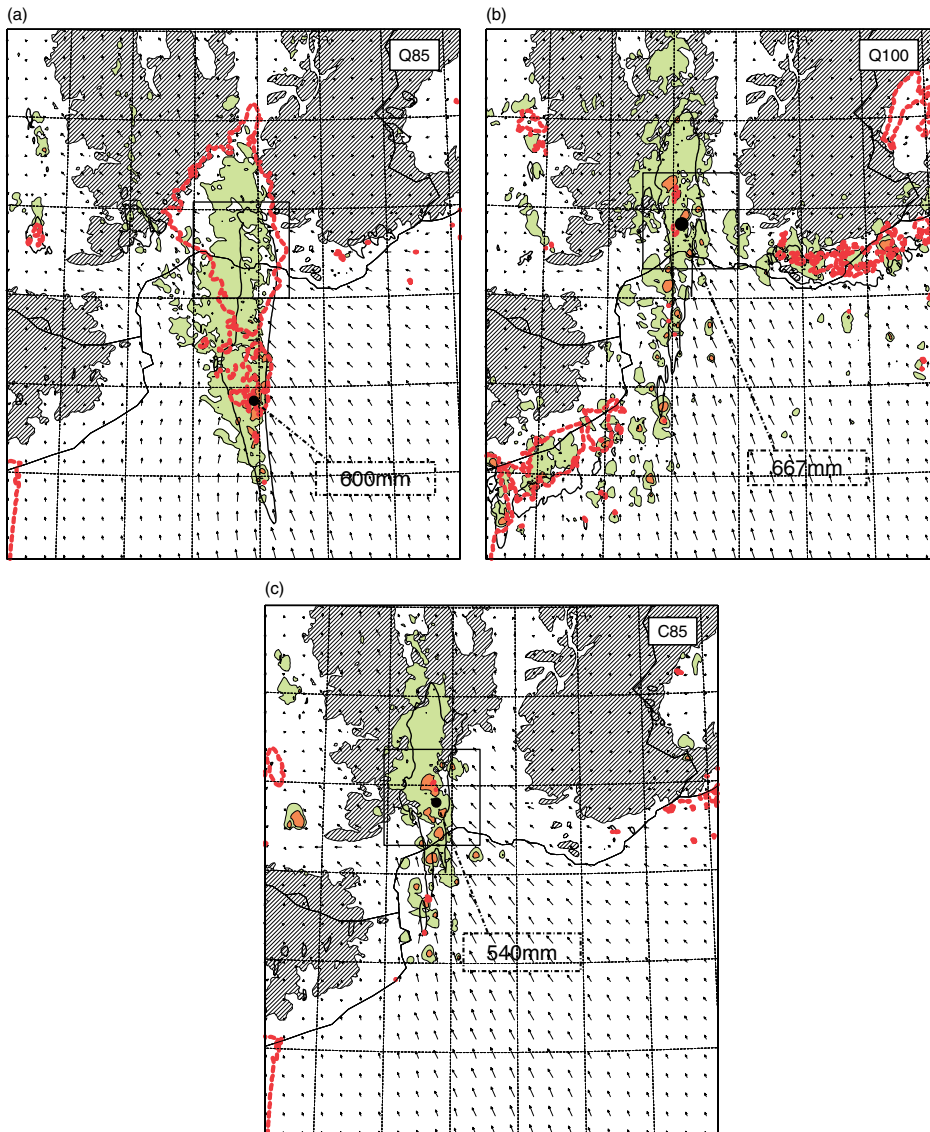


Figure 7. As Figure 4, but for (a) Q85, (b) Q100 and (d) C85 experiments. This figure is available in colour online at [wileyonlinelibrary.com/journal/qj](http://wileyonlinelibrary.com/journal/qj)

Central (Figure 7(b)) and without a significant cooling beneath the precipitating system (Figure 8(c)). The system shape, quite different from that of Q85, Q90 or CTRL, is less extended, mainly settled over the relief and the plains, and consists of different separated convective cells. Widespread weak precipitation is also simulated along the Alps and Spanish coasts. The size of the surface of the precipitation region and the associated volume of precipitation are weaker than the CTRL ones (Figure 8).

For the C85 experiment, the central profile values of mixing ratio are reduced by about 10% and a lateral drying is also applied to reach the lateral values of Q85 (Figure 2). It is thus a dry offset of the horizontal humidity distribution used for CTRL. With respect to CTRL and Q85, the MCS produced by C85 is less spread and the maximum of precipitation is located over the Massif Central

slopes (Figure 7(c)). No cooling area is detected beneath the system during the quasi-stationary phase (Figure 8(c)). The surface affected by heavy rainfall and the precipitation volume are about half the CTRL ones (Figure 8(a) and (b)), although the maximum of precipitation is higher by about 110 mm.

### 3.2.3. Synthesis

Figure 9 presents a synthesis of the location of the maximum of precipitation with respect to the environmental flow characteristics. The heaviest precipitation is located upstream of the mountain range with a slow flow whereas with a rapid flow the heaviest precipitation is over the Massif Central slopes. In a similar way, when the

## 1.2. PUBLICATIONS MAJEURES POUR LA SOUTENANCE DE L'HABILITATION À DIRIGER DES RECHERCHE

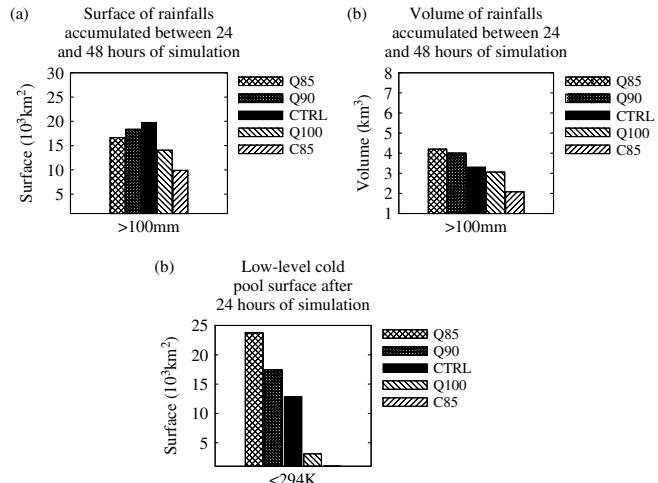


Figure 8. As Figure 6, but for Q85, Q90, CTRL, Q100 and C85 experiments.

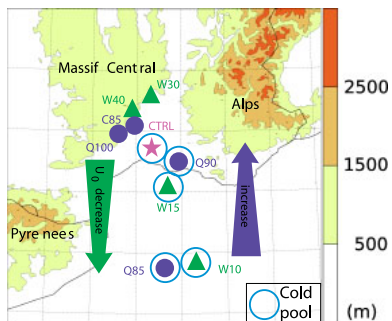


Figure 9. Location of the maximum of 24 h surface rainfall totals for the CTRL experiment (star), the wind sensitivity experiments (triangles) and the humidity sensitivity experiments (dots). Circles indicate the occurrence of a stationary cold pool in the simulation. The left arrow (green in the online article) and right arrow (purple in the online article) indicate respectively the decrease of  $U_0$  and increase of  $\alpha$ . This figure is available in colour online at [wileyonlinelibrary.com/journal/qj](http://wileyonlinelibrary.com/journal/qj)

lateral environment is drier the heaviest precipitation is located upstream whereas a humid environment favours precipitation over the slopes. The cold pool is more developed when the environment is slower or drier, whereas no significant low-level cooling is obtained for a rapid or moist environment. Similarities with some precipitation regimes found in previous idealized numerical studies are obtained: (1) a quasi-stationary convective system over the upstream side of the ridge with no cold pool is present with large values of wind speed in CL05 and MR09; (2) the maximum of precipitation located upstream of the mountain range associated with a cold pool is obtained for a moderate wind-speed environment in MR10 for low CAPE.

## 4. Discussion

The previous studies, based on purely idealized simulations, have identified several mechanisms that explain the location and intensity of the precipitation within a conditionally unstable flow impinging on a mountain ridge. The extent to which the conclusions of these studies apply to our more

real-world idealized simulations is the question addressed in this section.

### 4.1. Effects of orography

The intensity of the direct orographic lifting of the Massif Central is proportional to the speed of the impinging flow. The higher precipitation rate in W40 than in W30 is thus consistent with more intense orographic lifting. For the other experiments with slower environmental winds, the relationship between the precipitation rate and the intensity of the direct orographic lifting is less obvious, as the maximum rainfall is located upstream of the mountain range. In order to highlight the role of the Massif Central, it has been removed in the MC experiment. Other parameters are identical to the CTRL ones. The maximum of precipitation is found at almost the same location in MC as in CTRL (Figure 10(a); compare this with Figure 4). Thus, direct orographic lifting is not the main triggering mechanism in moderate to slow wind regimes. The rainfall totals are, however, significantly weaker than the CTRL ones and thus the Massif Central contributes to enhancement of the precipitation totals.

The role of the Alps and Pyrenees is highlighted with the experiments ALPS and PYREN, which remove the Alps and the Pyrenees, respectively. The results of the PYREN experiment are very close to the CTRL ones for the main quasi-stationary system (Figure 10(b)). The main role of the Pyrenees is to prevent the formation of convective cells over the southern part of Massif Central. Without the Alps, the maximum of precipitation is located at the same place as in CTRL (Figure 10(c)) but the volume of rainfall is reduced by about a factor of 2 (Figure 11(b)). One common characteristic between ALPS and MC is that the cold pool spreads over a larger surface (Figure 11(c)) but its depth is smaller. The Alps or/and the Massif Central thus have a role in blocking the cold pool against the mountains.

The ALPS and to a lesser extent the PYREN experiments also point out the role of the highest and neighbouring mountain ranges (Alps and Pyrenees) in deflecting low-level southeasterly winds. To illustrate this, Lagrangian parcels

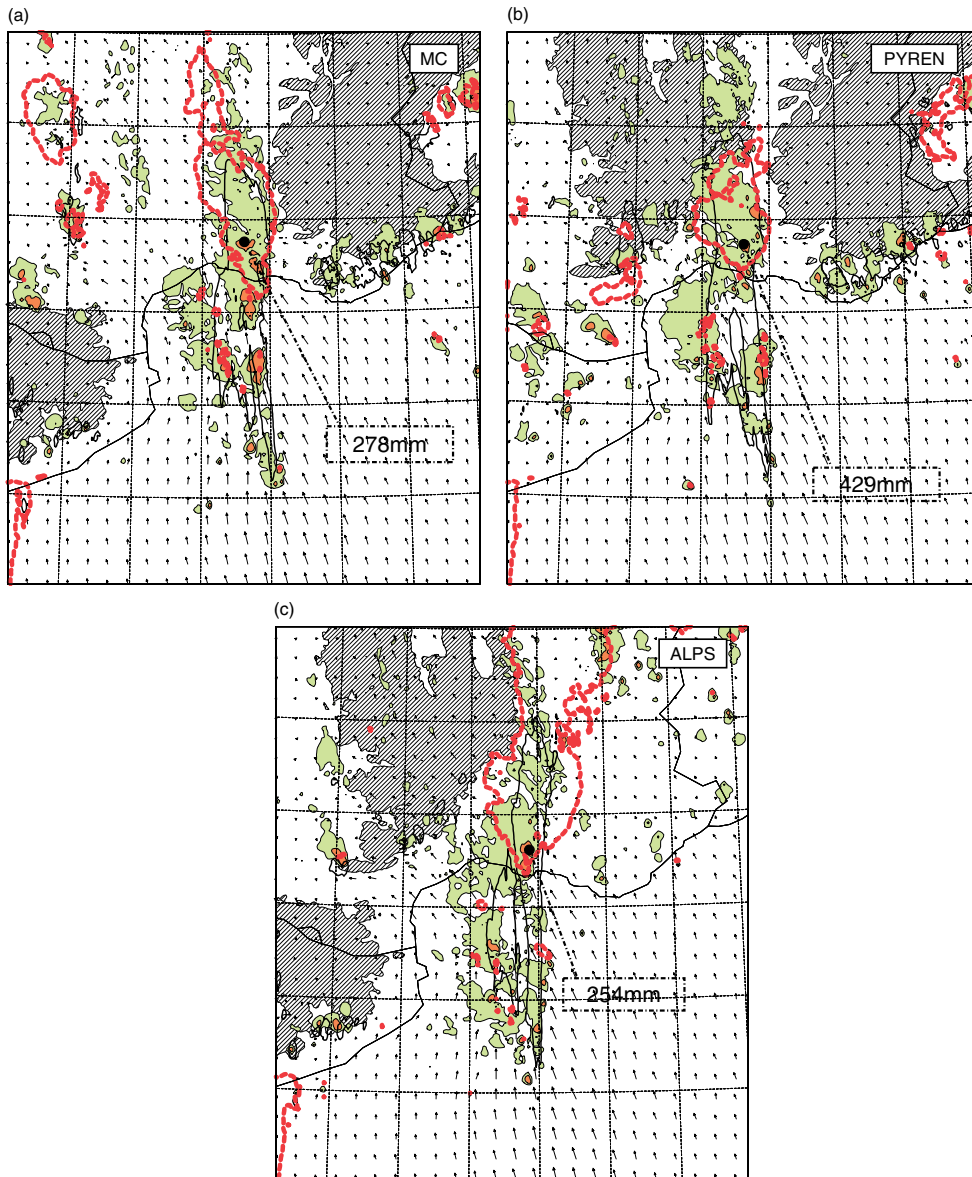


Figure 10. As Figure 4, but for (a) MC, (b) PYREN and (c) ALPS experiments. This figure is available in colour online at [wileyonlinelibrary.com/journal/qj](http://wileyonlinelibrary.com/journal/qj)

have been launched from four juxtaposed 90 km width and 500 m depth near-surface boxes in the CTRL and ALPS simulations and have been followed over 9 hours (Schär and Wernli, 1993; Gheusi and Stein, 2002; Figure 12). In the ALPS experiment the plumes of Lagrangian parcels have a straight path. Note that the parcels from the eastern boxes have a shorter path, as the winds decrease from the central axis to the eastern side of the domain. For the CTRL experiment, the plumes from these eastern boxes deviate to the west along their path and thus show evidence of deflection of the flow by the Alps and the resulting low-level convergence. The potential of a moist flow to go over a mountain or around can be characterized through the moist

Froude number  $Fr_w$  (Chen and Lin, 2005), defined as

$$Fr_w = \frac{\int_0^{h_m} U(z) dz}{h_m \int_0^{h_m} N_v(z) dz}, \quad (1)$$

with  $U$  the wind speed,  $h_m$  the characteristic height of the mountain and  $N_v$  the Brunt–Väisälä frequency for moist air.

When  $Fr_w < 1$ , the ‘flow around’ regime is favoured, whereas flow over the mountain range is favoured when  $Fr_w > 1$ . The moist Froude number was computed over boxes (drawn as dotted lines in Figure 1) upstream of the three mountain ranges: Alps, Massif Central and Pyrenees, respectively. The characteristic heights used for Massif Central, Pyrenees and Alps are 1200, 1800 and 3000 m,

## 1.2. PUBLICATIONS MAJEURES POUR LA SOUTENANCE DE L'HABILITATION À DIRIGER DES RECHERCHE

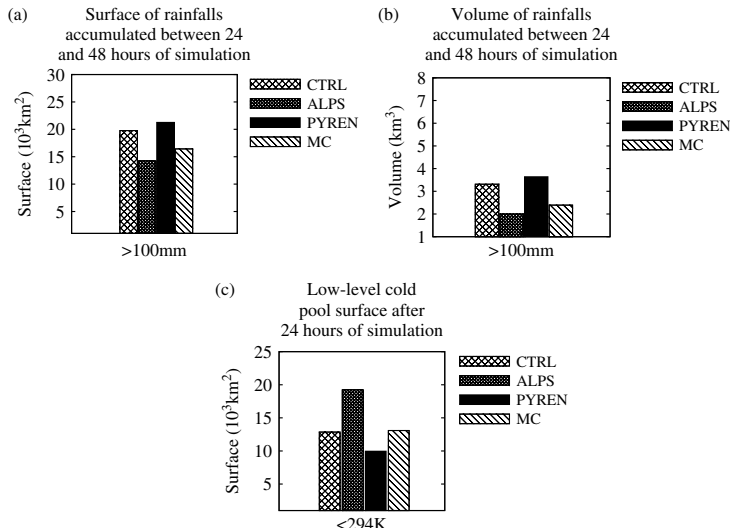


Figure 11. As Figure 6, but for CTRL, ALPS, PYREN and MC experiments.

Table 2. Moist Froude number for the characteristic height of each relief (1200 m for Massif Central, 1800 m for the Pyrenees and 3000 m for the Alps) averaged over the dotted-line boxes shown in Figure 1, after 3 h.

Simulations	CTRL	W10	W15	W30	W40	Q85	Q90	Q100	C85
Massif Central	1.60	0.86	1.21	2.31	3.03	1.65	1.62	1.59	1.70
Pyrenees	0.33	0.30	0.31	0.37	0.40	0.26	0.29	0.40	0.26
Alps	0.17	0.15	0.16	0.18	0.20	0.14	0.15	0.19	0.12

respectively. The averaged values of  $Fr_w$  over the boxes are listed in Table 2 for all simulations. Upstream of the Alps,  $Fr_w$  is smaller than 1 for all simulations, suggesting deflection of the low-level flow around Alps in all the experiments. As expected,  $Fr_w$  values are smaller when the upstream flow is slower or drier. This results in more deflection and thus low-level convergence of the flow as illustrated by the plumes of parcels for the Q85 simulation (Figure 12).

The Froude number of the flow facing the Massif Central is larger than 1 for most of the simulations and always larger than the values for the Alps and Pyrenees, due to a smaller mountain height and larger winds and humidity in the central part of the flow facing the Massif Central. Flow over Massif Central is thus favoured in all simulations except for the W10 simulation.

### 4.2. Low-level cold pool

Besides the direct orographic forcing and the deflection-induced low-level convergence, the low-level cold pool is another lifting mechanism that operates in the simulations. The cold pool forces the low-level air parcels at its leading edge up to their level of free convection. In order to illustrate this mechanism, 6 h backward trajectories for parcels selected at 9 km altitude in the convective part of the system have been performed (Schär and Wernli, 1993; Gheusi and Stein, 2002). These backward trajectories indicate the past evolution of a selected particle. Figure 13 shows such a trajectory for the Q85 experiment, which is the experiment with the largest cold pool. Six hours prior, the parcel was within the very low layer on the southeastern

side of the domain. The parcel was transported at the same level by the environmental southeasterly winds until it encountered the leading edge of the cold pool, where it was lifted up to 9 km in under 30 minutes.

This cold pool is due to rainfall evaporation in the subsaturated layer beneath the convective system. In-line budgets have been performed within the simulated convective systems to quantify the rainfall evaporation and its impact on the cold-pool strength. Rain evaporation and thus cooling are maximum around 1.5 km altitude (Figure 14(a)). The maximum cooling rate is obtained for the Q85 experiment, in agreement with the coldest and largest cold pool obtained for this simulation. As Q100 is less subsaturated than the Q85, Q90 and CTRL experiments, the cooling rate is significantly weaker in Q100, in agreement with a less developed cold pool. For the C85 experiment, although the environment is more subsaturated than the CTRL one, the cooling rate is weaker (Figure 14). This can be explained by less convective activity and thus less rainfall to evaporate (Figure 7(c)).

### 4.3. Parameter study

Even though in all simulations a stationary convective system is obtained, the dominant lifting mechanism is different from one simulation to another. The dominant lifting mechanism is strongly related to the location of the system (over/upstream of the mountain). In the 2D idealized simulations of MR09, the location of the cells was explained by the ratio between the advective time-scale  $\tau_a = a/U$  (with  $a$  the width of the mountain ridge) to the time-scale

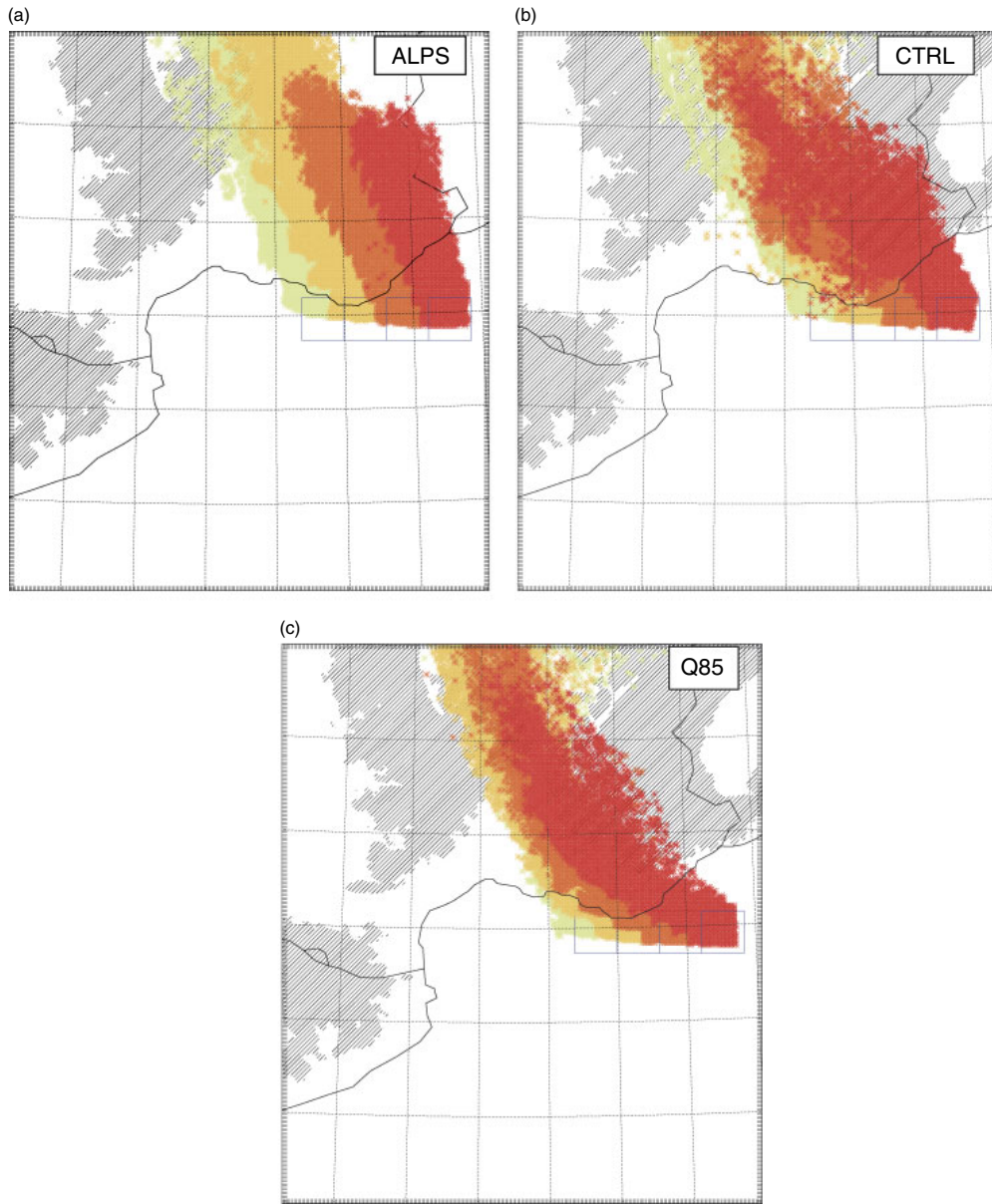


**Figure 12.** Time series (9 h duration) of plumes of Lagrangian parcels originally in boxes of 90 km width at 18 h for (a) ALPS, (b) CTRL and (c) Q85 experiments. Orography above 500 m is hatched. This figure is available in colour online at [wileyonlinelibrary.com/journal/qj](http://wileyonlinelibrary.com/journal/qj)

representative of the convective cell  $\tau_c = h_t/\text{CAPE}^{1/2}$  (with  $h_t$  the tropopause height). The intensity of the rainfall was related to  $\tau_a/\tau_c$ ,  $h_m/\text{LFC}$  (triggering needed) and  $Uh_m/a$  (orographic forcing). These parameters have been estimated in our study for upstream conditions. The central part of the low-level flow is considered as upstream conditions (dashed box in Figure 1). Table 3 lists the values of several parameters characterizing the upstream conditions: the level of free convection (LFC), CAPE, Downdraft Convective Available Potential Energy (DCAPE),  $\text{CAPE}^{1/2}/U$ ,  $D\text{CAPE}^{1/2}/U$  and  $N_v\text{LFC}/U$ .  $\text{CAPE}^{1/2}/U$  is proportional to  $\tau_a/\tau_c$ , as  $a$  and  $h_t$  do not vary in our simulations. The location of the

precipitating systems seems, on the whole, correlated to  $\tau_a/\tau_c$  as proposed by MR09 (Table 3). The convective system is located upstream of the mountain slope for larger values of the ratio (W10, W15, CTRL, Q90) and over the mountain slopes for smaller values of the ratio (W40, C85, W30). With large values of  $U$  (W30, W40), there is not enough time for development of convective updraughts and for downward transport of parcels to cool significantly before they reach the mountain range. No cold pool is thus present. In addition, deflection by the Alps is not favoured with large wind values. Direct orographic forcing is thus the dominant lifting mechanism. It is worth

## 1.2. PUBLICATIONS MAJEURES POUR LA SOUTENANCE DE L'HABILITATION À DIRIGER DES RECHERCHE

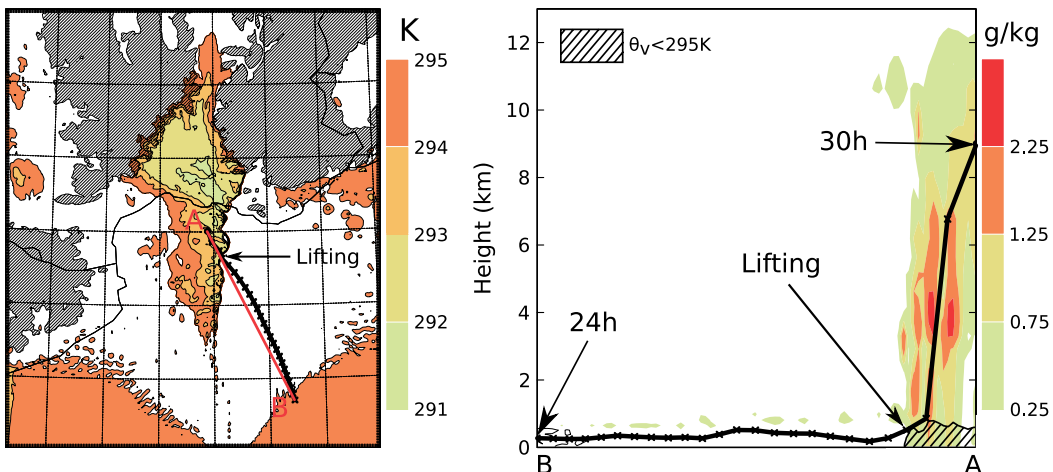


**Figure 13.** Panel (a) depicts the 6 h backward trajectory of a parcel at 9 km in the convective part after 30 h of simulation, superimposed on virtual potential temperature at 36 m AGL. Panel (b) depicts its projection along the vertical cross-section A–B superimposed on the total hydrometeor content (shaded areas, coloured in the online article) and  $\theta_v < 294$  K. Orography above 500 m is shown hatched in (a). This figure is available in colour online at [wileyonlinelibrary.com/journal/qj](http://wileyonlinelibrary.com/journal/qj)

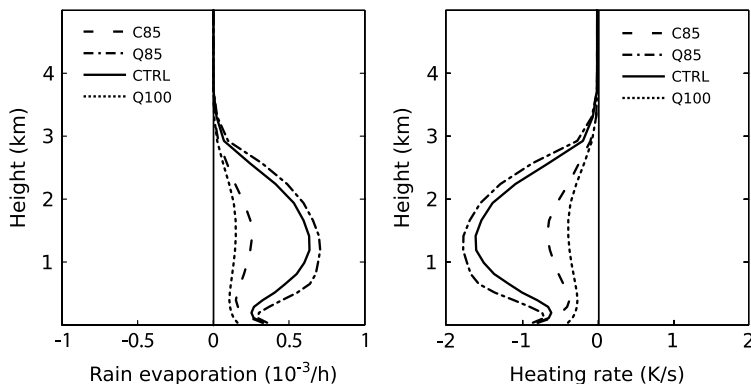


**Figure 14.** Rainfall evaporation contribution to (a) the water-vapour budget and (b) the temperature budget of C85, Q85, CTRL and Q100 experiments, respectively, computed for the boxes shown in Figures 7(c), 7(a), 4 and 7(b), after 24 h.

mentioning that the CAPE value increases with wind speed in our experiments, even though the same thermodynamic conditions are applied at lateral boundaries. This results from the increase with wind of latent heat and sensible heat surface fluxes along the low-level parcel paths over the sea domain that further destabilize the near-upstream conditions. With low to moderate values of  $U$  (W10, W15, CTRL), there is more time for convective cells to develop and for the cold pool to form by evaporation of rain from precipitating convective cells. The main mechanism for continuous cell development is thus the lifting at the leading edge of the cold pool.

For the C85 experiment, the uplift required to trigger convection is more important than for the other experiments, as the LFC value for C85 is the highest. Enough orographic lifting is thus needed to trigger convection. In addition, as CAPE is weaker, convective updraughts are also weaker and convective cells take more time to develop with respect to the advective time. However, for the other experiments varying the humidity (Q85, Q90, CTRL, Q100), location and intensity of the convective systems are

not simply linked to  $\tau_a/\tau_c$ ,  $h_m/LFC$  (triggering needed) or  $Uh_m/a$  (orographic forcing) as proposed initially in MR09. These experiments indeed have almost the same values of these parameters, but different locations of the heaviest precipitation. Noting that quasi-stationary cold-pool and convective systems are obtained when the density current and the environmental flow approximately counterbalance each other, MR10 suggested that two other non-dimensional parameters have to be considered, especially with a lower CAPE environment:  $DCAPE^{1/2}/U$ , which represents a measure of the propagation of the cold pool with respect to the environment flow advection, and  $N_vLFC/U$ , a measure of the flow deceleration induced by the cold pool; MR10 found that for low CAPE these two parameters have a specific value in simulations where the density current and the environmental flow approximately counterbalance each other. However, in our simulations the same location of the convective system and strength of the cold pool are obtained with very different values of  $DCAPE^{1/2}/U$  and conversely a different location of the convective system and strength of the cold pool are obtained with the same

Table 3. Level of free convection (LFC), Convective Available Potential Energy (CAPE), Downdraft Convective Available Potential Energy (DCAPE),  $\text{CAPE}^{1/2}/U$ ,  $\text{DCAPE}^{1/2}/U$  and  $N_v \text{LFC}/U$  for the upwind profile averaged over the dashed-line domain shown in Figure 1, after 24 hours of simulation.

Simulations	CTRL	W10	W15	W30	W40	Q85	Q90	Q100	C85
LFC (hPa)	980	980	980	980	980	979	980	980	967
CAPE ( $\text{J kg}^{-1}$ )	752	640	698	875	976	765	774	740	358
DCAPE ( $\text{J kg}^{-1}$ )	219	228	221	220	206	212	215	234	245
$\text{CAPE}^{1/2}/U$	1.38	2.53	1.76	0.96	0.75	1.36	1.36	1.36	0.87
$\text{DCAPE}^{1/2}/U$	0.74	1.51	0.99	0.49	0.36	0.73	0.73	0.77	0.78
$N_v \text{LFC}/U$	0.22	0.53	0.33	0.12	0.08	0.22	0.22	0.23	0.22

value of  $\text{DCAPE}^{1/2}/U$  and  $N_v \text{LFC}/U$  (Q85, Q90, CTRL). In addition, simulations with more intense cold pools do not necessarily have the largest DCAPE and thus the largest ratio  $\text{DCAPE}^{1/2}/U$ . These results confirm that it is not possible to determine from only the five adimensional parameters proposed by MR10 the location and intensity of the convective system in our more complex idealized environment. These differences between MR09/MR10 and our study can arise from different upstream soundings. The low-level convergence induced by the neighbouring mountain ranges is missing in the MR09/MR10 idealized framework. In addition, MR09/MR10 used a uniform horizontal environment, whereas this is not the case in our simulations. It is thus more difficult to define a single value for each adimensional parameter characterizing the simulations. For instance, we also calculated these parameters (not shown) in the dotted boxes upstream of the Alps and Pyrenees seen in Figure 1. The parameter values for these boxes are quite different from those over the central axis. For instance, for the CTRL experiment, CAPE and DCAPE are larger by more than  $150 \text{ J kg}^{-1}$  for the Alps box, whereas LFC is slightly higher. Nevertheless, similar values of  $\text{DCAPE}^{1/2}/U$  and  $N_v \text{LFC}/U$  are still found for experiments having different location and strength of the cold pool (Q85, Q90, CTRL).

## 5. Conclusion

The present study examines the interaction of a moist conditionally unstable flow with the Northwestern Mediterranean complex terrain, based on idealized simulations. Sensitivity experiments were carried out to study the influence of the characteristics of the impinging flow. Two different locations and characteristics of the quasi-stationary mesoscale convective system were obtained: (1) the heaviest precipitation over the Massif Central slopes and (2) a quasi-stationary convective system associated with a cold pool located upstream of the mountain range. The system over the mountain-slope regime is obtained with rapid flow facing the Massif Central or a moist environment. Slower flow or a drier lateral environment favour systems over the plain or the Mediterranean Sea.

The dominant mechanisms underlying these two types of MCS regime are (1) direct orographic triggering for systems over the Massif Central and (2) cold-pool triggering for upstream systems. In addition, the neighbouring mountains interplay through the deflection of the flow and low-level convergence enhancement favoured by a slow or dry lateral environment. They also contribute to cold-pool blocking within a valley. Our more ‘real-world’ idealized simulations allow us to highlight such contributions with respect to past highly idealized experiments. Both true terrain and

non-uniform flow are mandatory. It is therefore difficult to summarize the relationship between the flow characteristics and the location and intensity of the precipitating system by a few adimensional numbers.

This present study focused only on some characteristics of the low-level flow impinging on the Cévennes region (southeastern part of the Massif Central). To enlarge these results, it would be interesting to consider other factors controlling the location and intensity of heavy precipitation over this area by performing additional sensitivity experiments. For instance, a sheared flow (with vertical wind shear in both speed and direction instead of a vertically uniform wind) could be introduced as an initial condition. Indeed, it is recognized that rotation of winds with altitude can favour the decoupling of inflow/updraughts and precipitation/downdraughts and therefore the maintenance of convective systems. Furthermore, the sensitivity to the position and direction of the low-level jet with respect to the Massif Central could be studied by slightly veering or shifting the maximum wind and humidity axis northeastwards or southwestwards (i.e. turned around or uncentred with respect to the Cévennes region). These results will be examined and discussed in forthcoming articles.

Despite a simplified low-level flow, this study suggests that a good description of the mesoscale characteristics of the impinging flow over the Northwestern Mediterranean region is key for accurate prediction of the location of quasi-stationary precipitating systems. It is one goal of the Hydrological cycle in the Mediterranean EXperiment (HyMeX, <http://www.hymex.org>) field campaign in autumn 2012, which will be dedicated to the study of heavy precipitation in the Northwestern Mediterranean. The present study guides the design of the research instrument deployment plan within HyMeX.

## Acknowledgements

This work has been sponsored by the MISTRALS/HyMeX programme. The authors thank the Meso-NH support team for its help in using the Meso-NH model. The authors are grateful to the reviewers for their pertaining remarks and careful reading.

## References

- Bluestein HB, Jain MH. 1985. Formation of mesoscale lines of precipitation: severe squall lines in Oklahoma during the spring. *J. Atmos. Sci.* **42**: 1711–1732.
- Bougeault P, Lacarrère P. 1989. Parameterization of orography-induced turbulence in a meso-beta scale model. *Mon. Weather Rev.* **117**: 1870–1888.
- Bousquet O, Smull B. 2003. Observations and impacts of upstream blocking during a widespread orographic precipitating event. *Q. J. R. Meteorol. Soc.* **129**: 391–409.

## 1.2. PUBLICATIONS MAJEURES POUR LA SOUTENANCE DE L'HABILITATION À DIRIGER DES RECHERCHES

- Bresson R, Ricard D, Ducrocq V. 2009. Idealized mesoscale numerical study of Mediterranean heavy precipitating convective systems. *Meteorol. Atmos. Phys.* **103**: 45–55.
- Buzzi A, Foschini L. 2000. Mesoscale meteorological features associated with heavy precipitation in the southern Alpine region. *Meteorol. Atmos. Phys.* **72**: 131–146.
- Buzzi A, Tartaglione N, Malguzzi P. 1998. Numerical simulations of the 1994 Piemont flood: Role of the orography and moist processes. *Mon. Weather Rev.* **126**: 2369–2383.
- Caniaux G, Redelsperger J, Lafore J. 1997. A numerical study of stratiform region of a fast-moving squall line. Part I: General description and water and heat budgets. *J. Atmos. Sci.* **51**: 2046–2074.
- Carpenter K. 1982. Note on the paper: Radiational condition for the lateral boundaries of limited-area numerical models by MJ Miller and AJ Thorpe. *Q. J. R. Meteorol. Soc.* **108**: 717–719.
- Chen C, Lin Y. 2005. Orographic effects on a conditionally unstable flow over an idealized three-dimensional mesoscale mountain. *Meteorol. Atmos. Phys.* **88**: 1–21.
- Chu C, Lin Y. 2000. Effects of orography on the generation and propagation of mesoscale convective systems in a two-dimensional unsteady flow. *J. Atmos. Sci.* **57**: 3817–3837.
- Cuxart J, Bougeault P, Redelsperger JL. 2000. A turbulence scheme allowing for mesoscale and large-eddy simulations. *Q. J. R. Meteorol. Soc.* **126**: 1–30.
- Davies H. 1976. A lateral boundary formulation for multi-level prediction models. *Q. J. R. Meteorol. Soc.* **102**: 405–418.
- Delrieu G, Nicol J, Yates E, Kirstetter P, Creutin J, Anquetin S, Obled C, Saulnier G, Ducrocq V, Gaume E, Payrastre O, Andrieu H, Ayral P, Bouvier C, Neppel L, Livet M, Lang M, Parent-du-Châtelet J, Walpersdorf A, Wobrock W. 2005. The catastrophic flash-flood event of 8–9 September 2002 in the Gard region, France: A first case study for the Cévennes–Vivarais Mediterranean Hydrometeorological Observatory. *J. Hydrometeorol.* **6**: 34–52.
- Ducrocq V, Nuissier O, Ricard D, Lebeaupin C, Thouvenin T. 2008. A numerical study of three catastrophic precipitating events over southern France. II: Mesoscale triggering and stationarity factors. *Q. J. R. Meteorol. Soc.* **134**: 131–145.
- Duffour F, Ducrocq V. 2011. Origin of the moisture feeding the heavy precipitating systems over southeastern France. *Nat. Hazards Earth Syst. Sci.* **11**: 1163–1178.
- Georgis J, Roux F, Chong M, Pradier S. 2003. Triple-Doppler radar analysis of the heavy rain event observed in the Lago Maggiore region during MAP IOP2b. *Q. J. R. Meteorol. Soc.* **129**: 495–522.
- Gheusi F, Stein J. 2002. Lagrangian description of airflows using Eulerian passive tracers. *Q. J. R. Meteorol. Soc.* **128**: 337–360.
- Houze RJ. 1993. *Cloud Dynamics, International Geophysics Vol. 53*. Academic Press: New York, NY.
- Lafore J, Stein J, Asencio N, Bougeault P, Ducrocq V, Duron J, Fisher C, Hereril P, Mascart P, Pinty J, Redelsperger J, Richard E, Vila-Guerau de Arellano J. 1998. The Meso-NH atmospheric simulation system. Part I: Adiabatic formulation and control simulations. *Ann. Geophys.* **16**: 90–109.
- Lebeaupin C, Ducrocq V, Giordani H. 2006. Sensitivity of torrential rain events to the sea surface temperature based on high resolution numerical forecasts. *J. Geophys. Res.* **111**: 1–19.
- Levitus S. 1982. ‘Climatological Atlas of the World Ocean’, Technical Report 13, NOAA Professional Paper. NOAA/ERL/GFDL: Princeton, NJ.
- Lin Y. 1993. Orographic effects on airflow and mesoscale weather systems over Taiwan. *Terr. Atmos. Ocean* **4**: 381–420.
- Lin Y, Chiao S, Wang T, Kaplan M, Weglarz R. 2001. Some common ingredients for heavy orographic rainfall. *Weather and Forecasting* **16**: 633–660.
- Miglietta M, Rotunno R. 2009. Numerical simulations of conditionally unstable flows over a mountain ridge. *J. Atmos. Sci.* **66**: 1865–1885.
- Miglietta M, Rotunno R. 2010. Numerical simulations of low-CAPE flows over a mountain ridge. *J. Atmos. Sci.* **67**: 2391–2401.
- Mlawer E, Taubman S, Brown P, Iacono M, Clough S. 1997. Radiative transfer for inhomogeneous atmospheres: RRTM, a validated correlated-k model for long-wave. *J. Geophys. Res.* **102D**: 16663–16682.
- Nuissier O, Ducrocq V, Ricard D, Lebeaupin C, Anquetin S. 2008. A numerical study of three catastrophic precipitating events over southern France. I: Numerical framework and synoptic ingredients. *Q. J. R. Meteorol. Soc.* **134**: 111–130.
- Nuissier O, Joly B, Joly A, Ducrocq V, Arbogast P. 2011. A statistical downscaling to identify the large-scale circulation patterns associated with heavy precipitation events over southern France. *Q. J. R. Meteorol. Soc.* **137**: 1812–1827, DOI:10.1002/qj.866.
- Pinty J, Jabouille P. 1998. ‘A mixed-phased cloud parametrization for use in a mesoscale non-hydrostatic model: Simulations of a squall line and orographic precipitation’. In *Preprints, Conference on Cloud Physics, Everett, WA*. Amer. Meteorol. Soc: Boston, MA; pp 217–220.
- Pradier S, Chong M, Roux F. 2002. Radar observations and numerical modelling of a precipitating line during MAP IOP5. *Mon. Weather Rev.* **130**: 2533–2553.
- Ricard D. 2005. Modélisation à haute résolution des pluies intenses dans les Cévennes: le système convectif des 13 et 14 octobre 1995. *La Météorologie* **42**: 28–38.
- Ricard D, Ducrocq V, Auger L. 2011. A climatology of mesoscale environment associated with heavy precipitating events over a Northwestern Mediterranean area. *J. Appl. Meteorol. Clim.* DOI: 10.1175/JAMC-D-11-017.1.
- Rotunno R, Ferretti R. 2001. Mechanisms of intense Alpine rainfall. *J. Atmos. Sci.* **58**: 1732–1749.
- Schär C, Wernli H. 1993. Structure and evolution of an isolated semi-geostrophic cyclone. *Q. J. R. Meteorol. Soc.* **119**: 57–90.
- Smith R. 1979. The influence of mountains on the atmosphere. *Adv. Geophys.* **21**: 87–230.



# Hydro-meteorological evaluation of a convection-permitting ensemble prediction system for Mediterranean heavy precipitating events

B. Vié<sup>1</sup>, G. Molinie<sup>2</sup>, O. Nuissier<sup>1</sup>, B. Vincendon<sup>1</sup>, V. Ducrocq<sup>1</sup>, F. Bouttier<sup>1</sup>, and E. Richard<sup>3</sup>

<sup>1</sup>Groupe d'étude de l'atmosphère météorologique (GAME) – URA1357, Météo-France/CNRS, Toulouse, France

<sup>2</sup>LTHE, Laboratoire d'études des transferts en hydrologie et environnement – (CNRS, UJF, IRD, INPG), Grenoble, France

<sup>3</sup>Laboratoire d'Aérologie, CNRS et Université de Toulouse, Toulouse, France

Correspondence to: B. Vié (benoit.vie@meteo.fr)

Received: 28 February 2012 – Revised: 26 June 2012 – Accepted: 6 July 2012 – Published: 21 August 2012

**Abstract.** An assessment of the performance of different convection-permitting ensemble prediction systems (EPSs) is performed, with a focus on Heavy Precipitating Events (HPEs). The convective-scale EPS configuration includes perturbations of lateral boundary conditions (LBCs) by using a global ensemble to provide LBCs, initial conditions (ICs) through an ensemble data assimilation technique and perturbations of microphysical parameterisations to account for part of model errors. A probabilistic evaluation is conducted over an 18-day period. A clear improvement is found when uncertainties on LBCs and ICs are considered together, but the chosen microphysical perturbations have no significant impact on probabilistic scores.

Innovative evaluation processes for three HPE case studies are implemented. First, maxima diagrams provide a multi-scale analysis of intense rainfall. Second, an hydrological evaluation is performed through the computation of discharge forecasts using hourly ensemble precipitation forecasts as an input. All ensembles behave similarly, but differences are found highlighting the impact of microphysical perturbations on HPEs forecasts, especially for cases involving complex small-scale processes.

## 1 Introduction

The north-western Mediterranean basin is frequently hit by Heavy Precipitating Events (HPEs), mainly during the fall. The mesoscale convective systems associated with these HPEs typically produce over 200 mm in 6–24 h. Such in-

tense rainfall events occurring over the small and steep Mediterranean hydrological catchments can trigger catastrophic flash-floods, threatening both people and property. The most dramatic of these events have been extensively studied (see Buzzi et al., 1998; Nuissier et al., 2008; Ducrocq et al., 2008, among others). It was shown that their predictability is strongly affected by the complex interactions of different small scale processes, such as convective instability or microphysical processes.

Thus, although Convection-Permitting Models (CPMs) simulate realistic precipitating systems, forecasting those systems precisely remains a great challenge, and still the hydrological runoff forecasts for such small catchments are very sensitive to both the rainfall maximum intensity and location. It is, therefore, essential to evaluate the uncertainty of convective-scale forecasts.

Ensemble prediction is now a well-known tool for quantifying uncertainties of weather forecasts. While global, medium-range Ensemble Prediction Systems (EPSs) are operational since the 1990s to assess the predictability of large-scale atmospheric flows, the design of convection-permitting EPSs adapted to the evaluation of the predictability of local, high-impact weather is still at an early stage. The different sensitivity to Initial Conditions (ICs), the faster growth of convective-scale perturbations due to the more nonlinear physical parameterisations, the need to account for the uncertainty of the Lateral Boundary Conditions (LBCs), as well as the much higher computing time required by CPMs make it difficult to adapt the methods used to generate global EPSs.

Thus, the design of a convection-permitting EPS remains an open question.

Recent studies on convection-permitting EPSs have explored various techniques to generate ensembles. Hohenegger et al. (2008) compared different downscaling procedures to generate both ICs and LBCs for their convection-permitting EPSs and found that the added value of the CPM forecasts varied with the synoptic-scale conditions. For their model set-up, the impact of uncertainty on LBCs became predominant after 12 h. Hohenegger and Schär (2007a) focused on the impact of differences in the initial conditions and compared a shifted initialisation technique to perturbations in the initial temperature field. They showed that all methods had a similar impact and identified the same region of lower predictability. Gebhardt et al. (2011) designed three ensembles to sample the uncertainties on LBCs and model physics, separately at first, and then together. They found that physics perturbations are dominant over the first 4 to 6 h of simulation. The LBCs have generally more impact on the convection-permitting ensemble spread after 6 h, although in some cases physics perturbations have a strong impact on longer forecast ranges as well. They also concluded that sampling both sources of uncertainty together increased the ensemble quality. Fresnay et al. (2012) studied the sensitivity of a CPM to the auto-conversion, accretion and evaporation tendencies, for a Mediterranean HPE. Perturbations of these microphysical tendencies mostly impacted rainfall intensity, but sometimes displaced the precipitating systems as well. Clark et al. (2009, 2010), using data from the 2007 NOAA Hazardous Weather Testbed Spring Experiment, discussed the factors influencing the growth of ensemble spread and highlighted the value of convection-permitting ensemble forecasts compared to regional EPSs, despite the lower number of members.

Vié et al. (2011) assessed the relative impact on CPM forecasts of uncertainties associated with convective-scale ICs and synoptic-scale LBCs. Comparing distinct ensembles over both a 1-month period and case studies of HPEs, they showed that the impact of these two sources of uncertainty were different. Initial perturbations mostly impact short forecast ranges, while uncertainty coming from the LBCs rapidly becomes predominant (after 12 h in their experiment set-up) and accounts for most of the ensemble spread. However, even if initial perturbations have generally little impact beyond 12 h, they remain important for some of the HPE case-studies. Both ensembles had satisfying probabilistic scores, but suffered from a strong lack of spread, especially for low-level parameters, known to strongly influence Mediterranean HPEs.

The present work assesses the benefit of accounting for these two sources of uncertainty in a single convection-permitting EPS, both in terms of ensemble spread and probabilistic scores. In an effort to sample model errors, a convection-permitting ensemble including perturbations of the microphysics scheme is also evaluated.

**Table 1.** Characteristics of the different ensemble experiments.

Experiment name	LBCs	Data assimilation	Microphysical perturbations
E1	PEARP EPS	Unperturbed obs.	No
E2	ARPEGE deterministic fc.	Perturbed obs.	No
E3	PEARP EPS	Perturbed obs.	No
E4	PEARP EPS	Perturbed obs.	Yes

Designing and comparing convection-permitting EPSs for rare, high-impact events also raises the question of probabilistic forecast verification and evaluation. In addition to the common probabilistic evaluation using ensemble scores such as rank histograms and Relative Operating Characteristics (ROC) curves, an innovative evaluation is performed over three case studies of Mediterranean HPEs. The computation of maxima diagrams provides a multi-scale assessment of simulated and observed rainfall, as in Ceresetti et al. (2012), in relation with the structure of the precipitating systems. Precipitation forecasts are also used as input for hydrological ensemble runoff forecasts, to assess the value of our ensembles for flash-flood forecasting.

This paper is structured as follows. In Sect. 2, the forecasting system is detailed. Section 3 presents the results of the probabilistic evaluation of the ensemble forecasts over an 18-day period. The evaluation of the ensembles for the three case studies is performed in Sect. 4, using both maxima diagrams and hydrological discharge forecasts. Conclusions are drawn in the last section.

## 2 Methodology

### 2.1 The convection-permitting model AROME

The operational CPM Application of Research to Operations at MEscale (AROME) from Météo-France was used in this study. The AROME forecasting system is extensively described in Seity et al. (2010). It is based on adiabatic, non-hydrostatic equations from the limited-area ALADIN model. An horizontal grid-spacing of 2.5 km and 41 vertical levels are used. AROME uses physical parameterisations from the research model Meso-NH (Lafore et al., 1998), including a bulk, one-moment microphysics scheme following Caniaux et al. (1994) which represents six water species. An eddy diffusivity Kain-Fritsch (EDKF) scheme (Pergaud et al., 2009) is used for shallow convection parameterisation, and the turbulent scheme follows Cuxart et al. (2000).

AROME has its own 3D-VAR data assimilation scheme, with background and observation statistics adapted to its fine resolution (Yan et al., 2009; Boniface et al., 2009). Ground-based observations, as well as satellite data and doppler radial winds from the weather radar network are assimilated.

**Table 2.** Multiplying factors applied to the auto-conversion, accretion and evaporation tendencies, for each member of the E4 ensemble.

Ens. member	0	1	2	3	4	5	6	7	8	9	10
Autoconversion	1	0.75	0.75	0.75	0.75	1.25	1.25	1.25	1.25	1	1
Accretion	1	0.75	0.75	1.25	1.25	0.75	0.75	1.25	1.25	1	1
Evaporation	1	0.75	1.25	0.75	1.25	0.75	1.25	0.75	1.25	0.5	1.5

**Table 3.** Brier Skill Score computed for different precipitation thresholds for the E1, E2 and E3 ensembles. The reference is the deterministic AROME forecast. Bold numbers for each threshold show the best performing ensemble.

threshold (mm)	0.5	2	5	10	20	30	40	50	75	100
E1	0.33	0.29	0.27	<b>0.26</b>	<b>0.33</b>	0.35	0.36	0.27	0.29	0.26
E2	0.29	0.28	0.27	0.22	0.23	0.26	0.26	0.23	0.31	0.31
E3	<b>0.35</b>	<b>0.31</b>	<b>0.29</b>	<b>0.26</b>	<b>0.33</b>	<b>0.38</b>	<b>0.38</b>	<b>0.29</b>	<b>0.34</b>	<b>0.33</b>

## 2.2 The ensemble forecasts

Clark et al. (2011) showed that most of the probabilistic quantitative precipitation forecast skill for a convection permitting ensemble is obtained with around 10 members for forecast lead times up to 30 h. All the ensembles described below are composed of 11 parallel AROME data assimilation cycles, with a 3-hourly data analysis frequency. One 24-h forecast is issued each day at 12:00 UTC. Two ensembles sample the uncertainty separately on LBCs and convective-scale ICs. Another ensemble combines the representation of both uncertainty sources, the last one also accounts for part of model uncertainty as well as through the perturbation of microphysical tendencies. Table 1 summarises the characteristics of these four ensembles.

The E1 ensemble (named AROME-PEARP2 in Vié et al., 2011) samples the uncertainty coming from the imperfect LBCs by driving the 11 AROME data assimilation cycles and forecasts with the members of the Météo-France global, short-range EPS, called Prévision d'Ensemble ARPEGE (PEARP). The PEARP members are first down-scaled using the regional model ALADIN to prevent a large gap in resolution. The E2 ensemble (named AROME-PERTOBS in Vié et al., 2011) assesses the impact of uncertainty on convective-scale ICs through an ensemble data assimilation technique, as in Berre et al. (2006) and Houtekamer et al. (1996). The analysis error is sampled by the cycled assimilation of randomly perturbed observations (every 3 h), creating different ICs for each of the 11 E2 forecasts. Each member has LBCs provided by the operational, deterministic ALADIN forecast.

The E3 ensemble combines the two methods to generate an ensemble accounting for both uncertainty on the LBCs and the ICs at convective scale. Each of the 11 members of E3 uses randomly perturbed observations in its data assimilation cycle, as in E2, and uses LBCs provided by one member of the PEARP ensemble as in E1. Figure 1 describes the numerical set-up for the E3 ensemble. The 24-h forecasts issued

daily at 12:00 UTC, and the preceding assimilation cycles, are drawn in black. Running assimilation cycles are shown in light grey.

Based on the E3 ensemble, E4 in addition accounts for model errors in its representation of forecast uncertainty. Perturbations of the warm rain microphysical parameterisation, as in Fresnay et al. (2012), are introduced during the data assimilation and forecasts. Auto-conversion of cloud droplets into raindrops, accretion of cloud droplets by raindrops and rain evaporation processes are perturbed by applying a multiplying factor to each tendency. This factor is constant in both space and time, that is, for one given member of the ensemble, the multiplying factor is the same at each grid point and throughout the whole data assimilation and forecast period. The perturbations selected for each member ranged from 0.5 to 1.5 (Table 2).

An ensemble, E5, has been specifically designed to study the impact of microphysical parameterisation perturbations alone, using a single set of initial and lateral boundary conditions for all members.

## 3 Statistical evaluation

The ensembles are evaluated over the same period used in Vié et al. (2011), which corresponds to 18 consecutive days, from 15 October 2008 to 1 November 2008 inclusive. This period includes days with different atmospheric conditions. Precipitation and lightning observations (not shown) indicate that convective activity occurred on 20–24 October 2008 and from 30 October to 1 November 2008. The statistical evaluation of our ensembles was carried out for 24-h accumulated precipitation, surface and low-level parameters. Definition of the scores used in this study can be found in Vié et al. (2011).

Rank histograms are a measure of ensemble spread. An ensemble with an adequate spread would produce a flat histogram, a U-shaped histogram highlights a lack of spread in the ensemble forecast. Figure 3 shows rank histograms

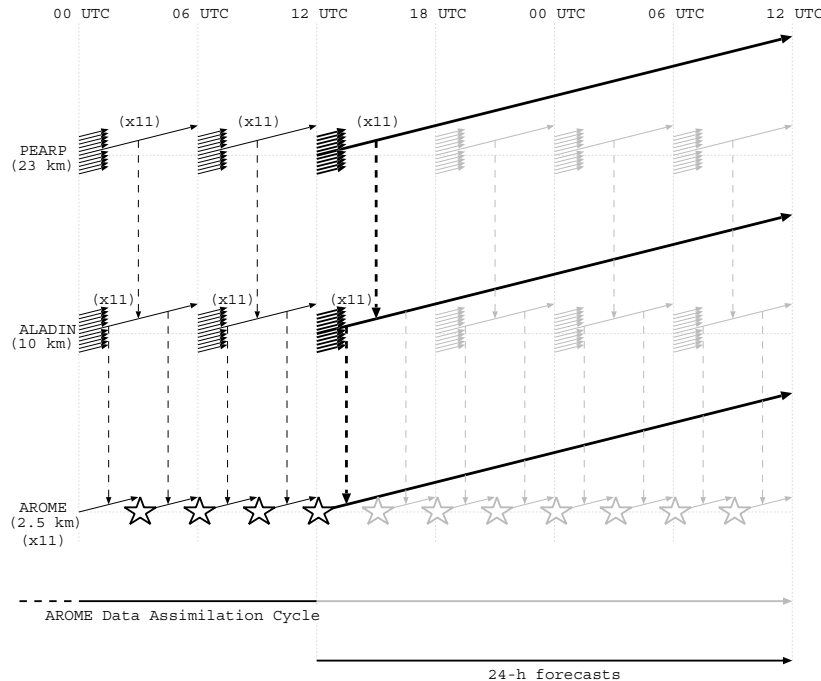


**Fig. 1.** The E3 ensemble experiment. Each nested model run is schematised along one row. Each plain (thick) arrow indicates the behavior of the eleven ensemble members (x11) short (long) runs. Their coupling along time is figured by the vertical dashed arrows. Each PEARP member provides LBCs to one ALADIN downscaling forecast, itself providing LBCs to one AROME data assimilation cycle with data analysis using randomly perturbed observations (stars) every 3 h. Each day, 24-h AROME forecasts are run at 12:00 UTC. The continuing assimilation cycles after 12:00 UTC are shown in light grey.

for the three ensembles E1, E2 and E3, computed for wind speed at 925 hPa, against the operational AROME analysis, for forecast ranges of 3, 6, 12 and 24 h. Although the E3 ensemble is still under-dispersive at all forecast ranges, the combined use of the ensemble data assimilation technique and different coupling conditions for each member clearly yields a better spread than each method used separately. It is especially interesting that the improvement is larger for intermediate forecast ranges (6 to 12 h), when the impact of initial spread is already largely reduced and the use of different LBCs begins to produce significant spread.

Brier Skill Scores (BSS) computed for different thresholds of 24-h accumulated precipitation, using the operational deterministic AROME forecast as reference, are shown in Table 3. A perfect forecast has  $BSS = 1$ . Positive BSSs for all three ensembles and every threshold highlight the added value of a probabilistic forecast compared to a single deterministic forecast. The E3 ensemble has better scores than any of the other two ensembles for each precipitation threshold (equal to E1 for 10 and 20 mm), which again shows the benefit of sampling both sources of uncertainty simultaneously.

Relative Operating Characteristics (ROC) and reliability diagrams (computed for precipitation intervals of  $0 < 0.5 <$

$2 < 5 < 10 < 20 < 50 < +\infty$ , and wind intervals of  $0 < 1 < 2 < 4 < 6 < 8 < 10 < +\infty$ ) are shown in Fig. 4 for 24-h accumulated precipitation and 10-m wind speed, computed against ground-based observations (hourly rainfall amounts provided by automated raingauges, 10-m wind speeds measured by automated land-surface stations). ROC curves for E1 and E3 are very close, both for wind speed and precipitation. Both ensembles, thus, have a similar resolution. However, reliability diagrams, especially for precipitation (Fig. 4c), show that the E3 ensemble has a better reliability.

Figure 4 also shows that the addition of microphysical tendencies perturbations in the E4 ensemble has very little impact on the probabilistic scores. This is confirmed by rank histograms shown in Fig. 5 among other scores and parameters computed for this ensemble (not shown). The microphysical perturbations applied in the E4 ensemble focus only on warm microphysical processes. Thus, one can expect an impact of these perturbations for precipitating days, much less for days with no rain. For this reason, no significant effect was found on probabilistic scores applied to the whole period.

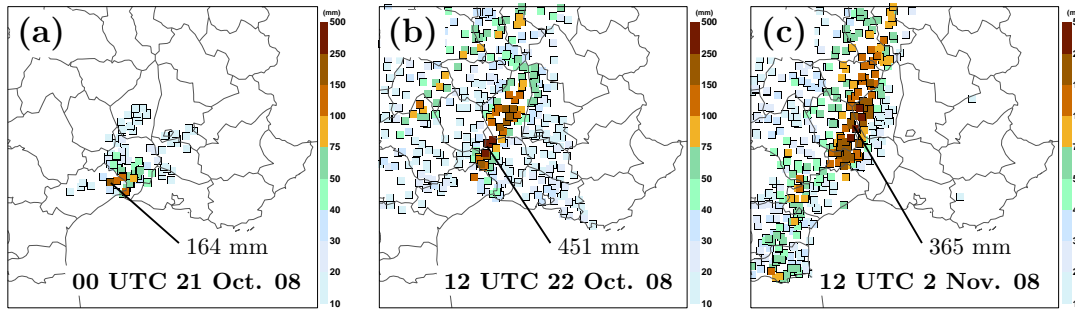


**Fig. 2.** Observed 24-h accumulated precipitation (mm) at (a) 00:00 UTC 21 October 2008, (b) 12:00 UTC 22 October 2008 and (c) 12:00 UTC 2 November 2008.

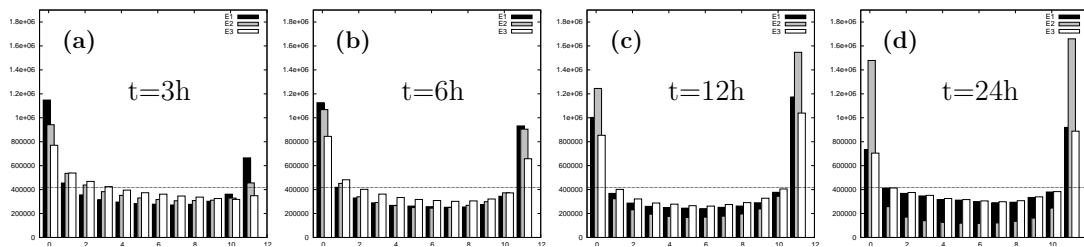


**Fig. 3.** Rank histograms for the 925-hPa wind speed from 15 October 2008 to 1 November 2008 at a forecast range of (a) 3, (b) 6, (c) 12 and (d) 24 h. E1 (black), E2 (gray) and E3 (white).

#### 4 Heavy Precipitating Events case studies

During this 18-day period, three HPEs occurred on 20, 21–22 October and 1–2 November 2008, as evidenced by the 24-h accumulated precipitation observations for these events (Fig. 2).

On 20 October 2008 (Case 1), a quasi-stationary MCS formed over the plain upstream of the Massif Central foothills, between 13:00 UTC and 17:00 UTC. Synoptic scale conditions showed only a weak baroclinic activity and the MCS was driven mainly by mesoscale mechanisms involving interaction with a low-level cold pool. Due to the convective activity beginning around 06:00 UTC, 24-h ensemble forecasts were issued at 00:00 UTC for this case, to simulate the whole event.

On 21–22 October 2008 (Case 2), localised convective cells formed between 10:00 UTC and 16:00 UTC over the Massif Central, ahead of a cold front moving south-eastward. Then, convective activity decreased with the cold front approaching south-eastern France, to evolve into an organised convective line from 21:00 UTC. The convective system merged with the cold front and intensified until 06:00 UTC, then the system decayed and moved south-eastward over the sea. This system produced 450 mm of precipitation in 24 h locally.

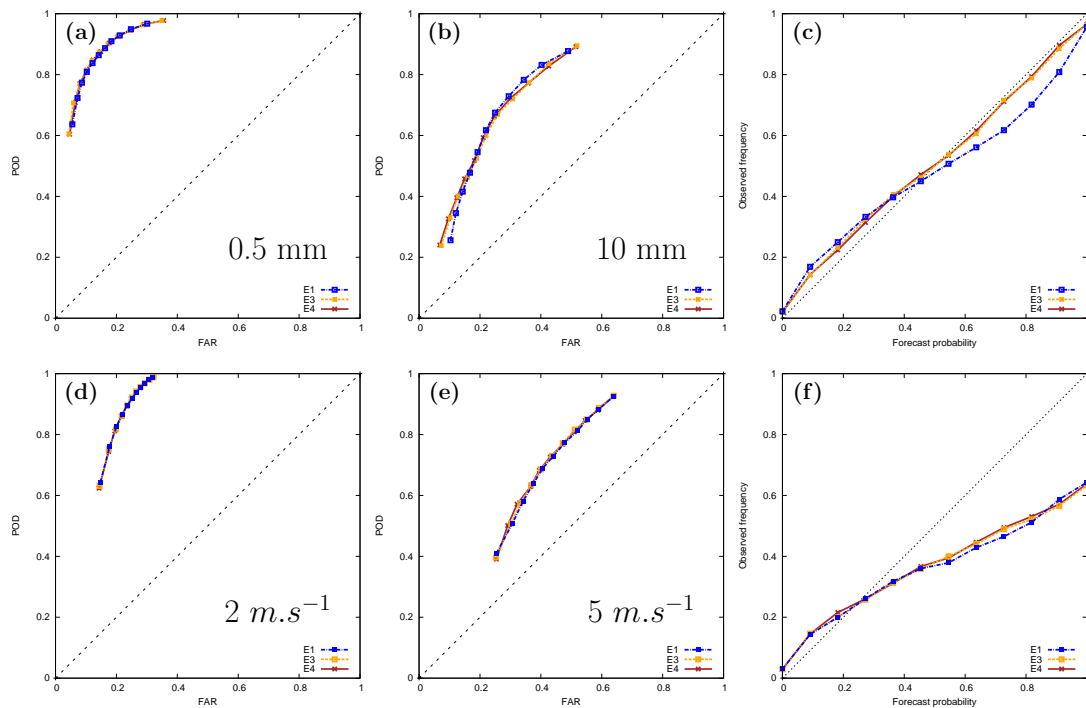
On 1–2 November 2008 (Case 3), convection formed in connection with a large trough over western France. A very

strong low-level jet, bringing moist, unstable air, was lifted by the Massif Central. An upper-level low, at the west of the region, induced a strong divergent flow over south-eastern France. Rainfall amounts up to 365 mm in 24 h were observed.

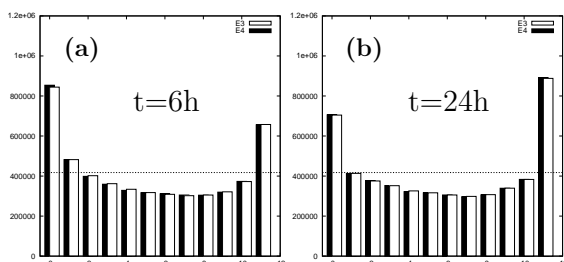
##### 4.1 Ensemble precipitation forecasts

Figure 6a–c shows the ensemble average and spread of 24-h accumulated precipitation forecasts for Case 3, for the E1, E3 and E4 ensembles, respectively. There are only minor differences between the three ensembles. Since this case is largely driven by the synoptic-scale forcing, it was expected that members using the same LBCs would behave similarly, and perturbations of initial conditions or physics parameterisations have little impact. For some members, the difference between E1 and E3 is slightly greater than between E3 and E4. For instance, for member 4 (Fig. 6d–f), E3 and E4 have similar maximum precipitation accumulation, a little higher than in E1, and both produced a secondary precipitation line south-east of the main precipitation area.

Case 2 involves both mesoscale processes and interactions with synoptic-scale conditions. Figure 7 shows ensemble averages of 24-h accumulated precipitation (a–c) and individual forecasts from members 8 and 9 (d–i). There are more significant differences between ensembles for this case, showing the greater impact of perturbations on initial



**Fig. 4.** ROC curves for precipitation thresholds of (a) 0.5 and (b) 10 mm and for 10-m wind speed thresholds of (d) 2 and (e)  $5 m.s^{-1}$ . Reliability diagrams for (c) precipitation and (f) 10-m wind speed.



**Fig. 5.** Same as Fig. 3 for E3 (white) and E4 (black), at forecast ranges of (a) 6 and (b) 24 h.

conditions than for Case 3. E1 produces higher rainfall totals, as shown by the ensemble mean, as well as forecasts from members 8 and 9. For all ensembles, the ensemble spread reaches similar values and is colocated with maximum rainfall amounts, but E3 and E4 have a slightly more extended 20 mm spread region. Differences between the E3 and E4 ensembles remain small, and are especially much smaller than between E1 and E3 (see for instance members 8 and 9, Fig. 7d-i). Perturbations of the microphysical parameterisations again bring little improvement to these probabilistic forecasts.

The quasi-stationary MCS on 20 October 2008 (Case 1) is mainly driven by mesoscale processes. It is, therefore, expected that the impact of initial conditions and microphysical perturbations will be larger than for the previous two cases. Ensemble averages of 24-h accumulated precipitation (Fig. 8a-c) show higher rainfall amounts for E1. For all ensembles, the ensemble spread highlights that the uncertainty is larger on the south-eastern side of the precipitating system. Members from different ensembles show greater differences than in the previous cases, highlighting the more important impact of perturbations of ICs and microphysical parameterisations. However, the impact of microphysical perturbations still seems smaller, for instance in members 5 and 8 (respectively, in Fig. 8d-f and g-i).

Overall, combining different LBCs and perturbations to the observations in the mesoscale data assimilation produces significant differences. As Vié et al. (2011) found, the impact of the addition of initial conditions perturbations in the E3 ensemble depends on the atmospheric conditions, and is larger for days with a weaker synoptic-scale circulation. The perturbation of microphysical parameterisations has a much smaller impact, noticeable only for Case 1 when the system is mainly driven by a rain evaporation induced cold-pool. To further assess the impact of microphysical perturbations, an E5 ensemble forecast is issued for Case 1. Unique initial and

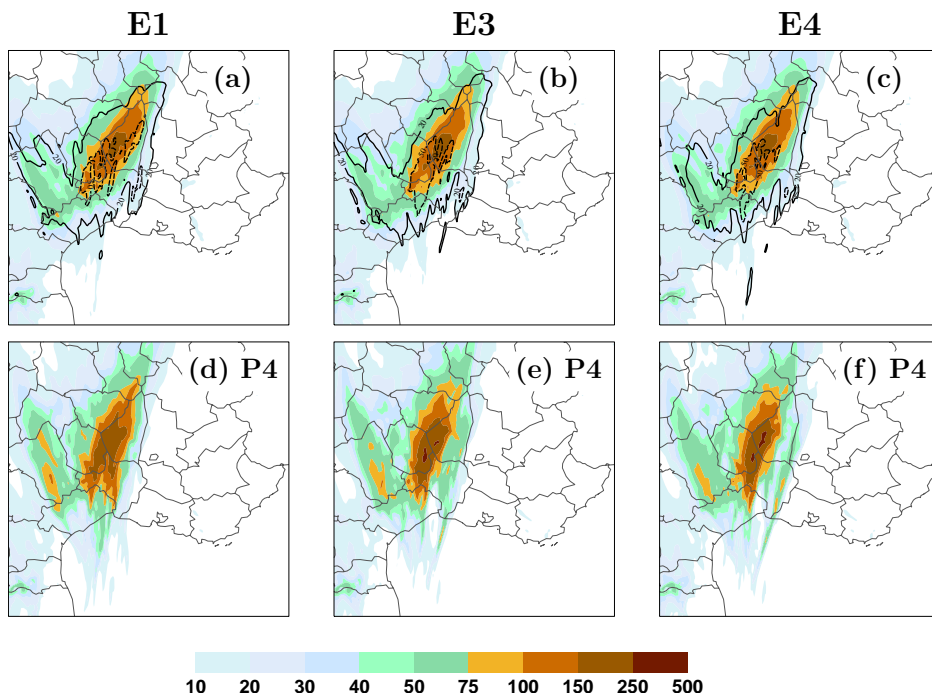


**Fig. 6.** 24-h accumulated precipitation forecasts (mm) for Case 3, at 12:00 UTC 2 November 2008. (a–c) Ensemble mean (colour shading) and standard deviation (solid contour: 20 mm, dashed contour: 50 mm), and (d–f) precipitation forecast by member 4, from the E1 (left), E3 (centre) and E4 (right) ensembles.

lateral boundary conditions for all members come from the member 8 of the E3 ensemble. The 24-h accumulated precipitation produced by the E3 member 8 is shown in Fig. 8h. These initial and lateral boundary conditions were chosen because the issued forecast simulated an intense system southward over the plains.

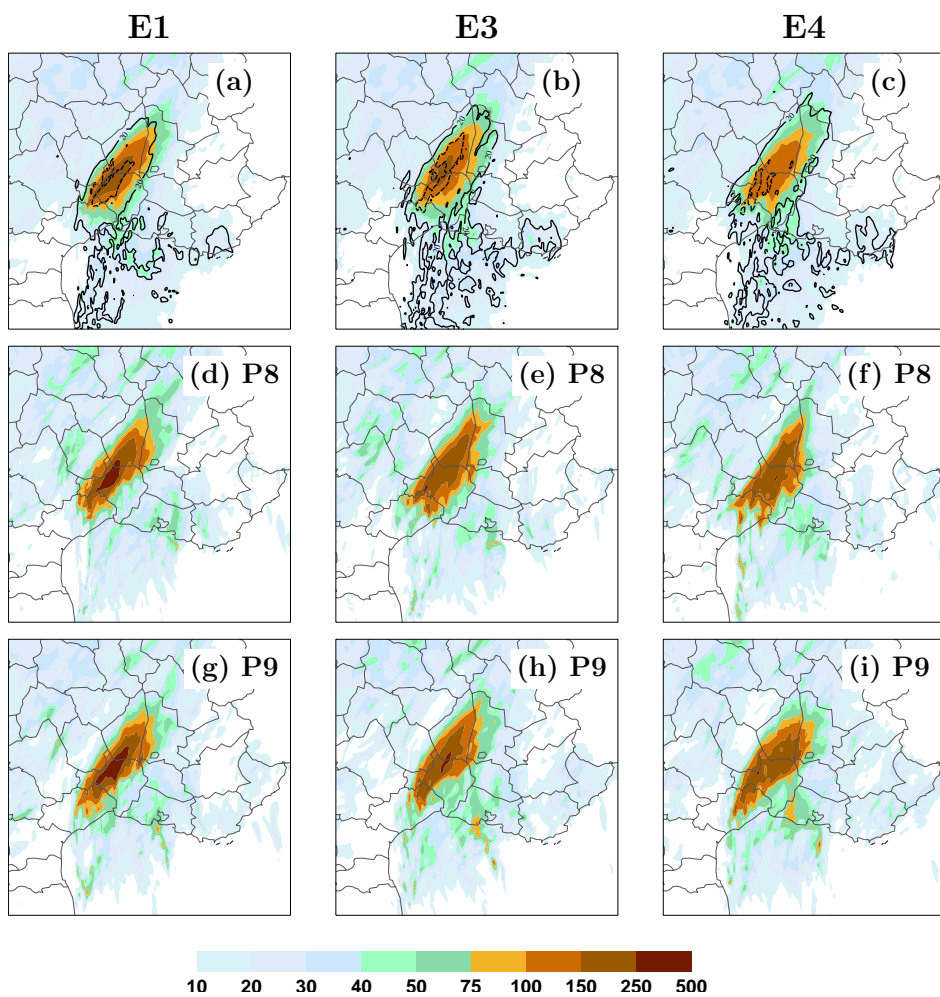
This case involved interactions between the moist, unstable low-level jet and a low-level cold pool, pushing the convective system southward. The microphysical perturbations are expected to have the most impact on this kind of simulation where mesoscale processes are important. In this case, one could expect the rain microphysical perturbations to impact the evaporative cooling and, therefore, affect both rainfall intensity and position. Figure 9 shows 24-h accumulated precipitation forecasts from the 11 E5 ensemble members, as well as the ensemble mean and standard deviation in panel (l). It shows moderate differences on the intensity and spatial structure of rainfall, as well as on the position of the precipitating systems. The ensemble spread is clearly located on the south-eastern side of the precipitating system, showing that the microphysical perturbations have more impact on the triggering of convective cells.

Figure 10 shows, for all ensembles, the virtual potential temperature ensemble spread, as well as the 292 K contour of the ensemble average of the virtual potential temperature,

at 15:00 UTC 20 October 2008. Microphysical perturbations in the E5 ensemble indeed have an impact at the edge of the low-level cold air region, where the new convective cells are triggered. However, even in this case where mesoscale processes play an important role, the impact of microphysical perturbations is weaker than that of lateral boundary conditions and even more initial conditions. In this case, the cold air pool which helps the triggering of convection over the plains is present in initial conditions (at 00:00 UTC 20 October 2008, not shown).

#### 4.2 Scale-dependent analysis of heavy rainfall

Ramos et al. (2005) introduced severity diagrams, a scale-dependent analysis of extreme rainfall events based on their return period. In order to avoid extrapolating rainfall intensities by means of probability density functions of extreme values, we perform here an assessment of maximum rainfall intensities, through maximum intensity diagrams similarly to Ceresetti et al. (2012). Therefore, rainfall intensities of the studied events are accumulated by means of moving average operations over all the possible combinations of the discrete temporal and spatial scales.



**Fig. 7.** Same as Fig. 6, for Case 2 at 12:00 UTC 22 October 2008, for members 8 (d–f) and 9 (g–i).

The shape of maxima diagrams gives information about the characteristics of the observed or simulated precipitating system.

Figure 11a–c shows the maximum observed rainfall intensities during the three HPEs for a range of spatial and temporal scales. Case 1 yields the lowest intensities, with a maximum around  $55 \text{ mm h}^{-1}$  for small spatial and temporal accumulation scales, while Cases 2 and 3 reach over  $70 \text{ mm h}^{-1}$ .

The maximum diagrams also allow a scale-dependent comparison and give information about the characteristics of the observed or simulated precipitating system. For Case 1, rainfall intensities remain high for accumulation over large areas for very short integration duration (one to two hours), but decrease very rapidly with a growing accumulation time. For the other two cases, rainfall intensities for accumulation durations longer than 3 h remain more important, and the di-

agrams display a more symmetric decrease in intensity with increasing spatial or temporal scales. Berne et al. (2009) have depicted the rain-cell structures highlighting the advection role. The symmetric figures for Cases 2 and 3 show the stationarity of the convective systems, while Case 1 shows some advection.

Figure 12 shows, for each ensemble and each case, the normalised difference between the average forecast maximum intensity and the observed maximum intensity (defined as  $\frac{\text{mean}(\max[\text{sim}]) - \max[\text{obs}]}{\max[\text{obs}]}$ ). These diagrams show no differences between the E1, E3 and E4 ensembles. The structure and behaviour of precipitating cells and systems are, therefore, not significantly changed by the different perturbations.

For Case 1, Fig. 12a–c shows that the maximum intensities simulated for scales between 30 and 80 km, and accumulation durations of 1 to 3 h, are underestimated by around

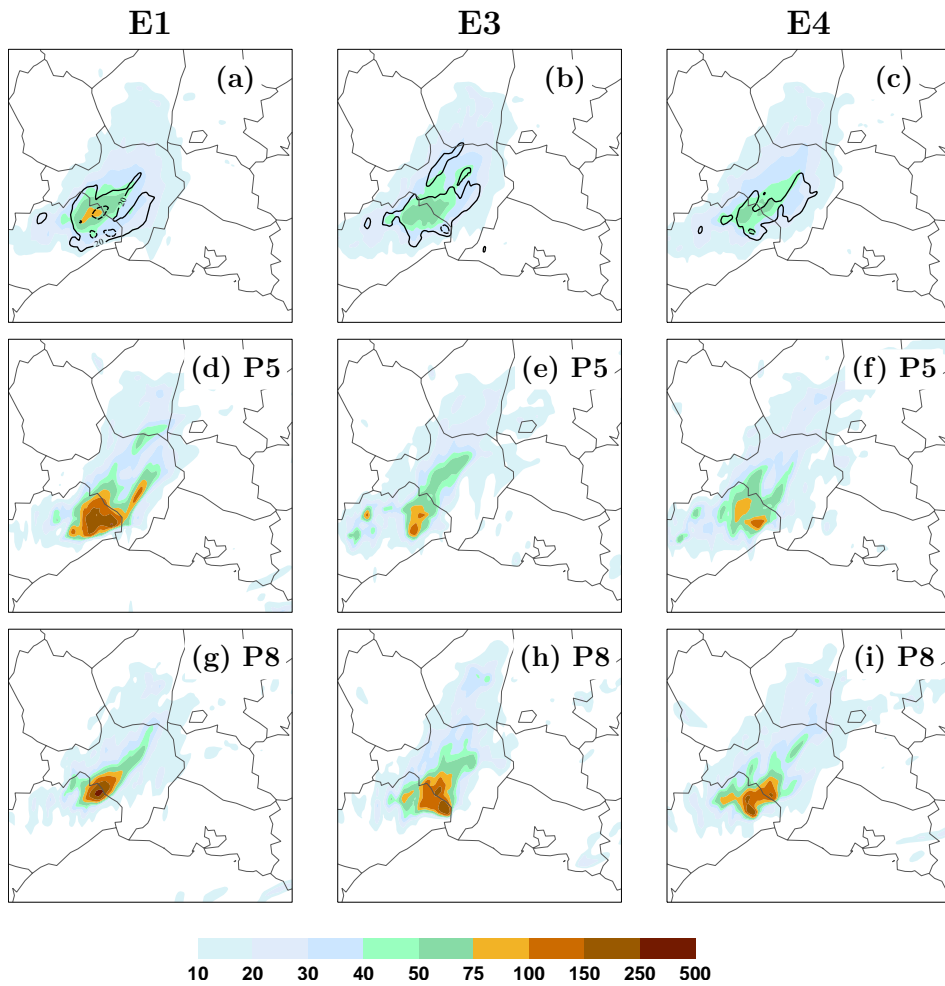


**Fig. 8.** Same as Fig. 6, for Case 1 at 00:00 UTC 21 October 2008, for members 5 (d–f) and 8 (g–i).

50 %. For smaller spatial scales, the simulated maxima are close to the observed ones. This indicates that the convective cells simulated for this case have a correct intensity, but they did not organise into a convective system as large as was observed. Simulations for Case 1 also exhibit an overestimation of maximum intensities for larger spatial and temporal scales (50 km, 18 h). This may be caused by disorganised convective cells producing precipitation in a larger region than was observed, and the simulations producing too much light rain. This is consistent with time series of average precipitation, which show that the peak of precipitation is underestimated, but precipitation is overestimated before and after the peak (see Vié et al., 2011, their Fig. 13b).

The ensembles perform better for Case 2 (Fig. 12d–f), with only an underestimation of about 30 % for spatial scales under 30 km and an overestimation for spatial scales around

50 km. Ensemble forecasts for Case 3 (Fig. 12g–i) produce a more symmetric maxima diagram, with an underestimation of maximum intensities for small spatial and temporal scales and a strong overestimation of intensities for large scales. This shows that the intensity of convective cells is only slightly underestimated, but the simulated precipitating system has a wider extension than the observed one. In both cases, the simulated precipitating region is more extended than in the observations and covers most of the Cévennes. This may indicate that the orographic forcing is too strong in the numerical model.

#### 4.3 Hydrological ensemble discharge forecasts

An evaluation of the AROME ensembles performance for flash-flood forecasting was performed through the computation of hydrological ensemble discharge forecasts using the

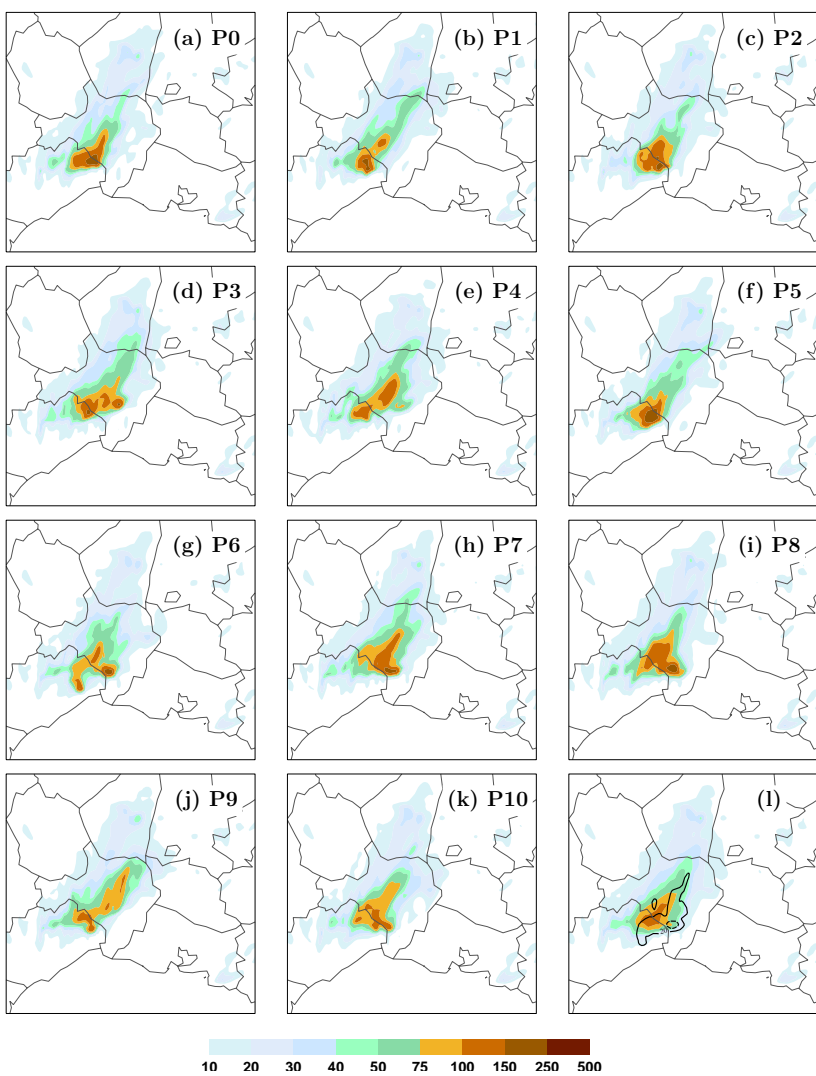


**Fig. 9.** 24-h accumulated precipitation forecasts (mm) for Case 1, at 00:00 UTC 21 October 2008, from each member of the E5 ensemble. Panel (l) shows the ensemble mean (colour shading) and 20 mm (solid) and 50 mm (dashed) standard deviation contours.

ISBA-TOPMODEL coupled system. This system is a full coupling between the land surface model ISBA, which manages soil water budget on soil columns, and TOPMODEL which takes care of the lateral redistribution of soil moisture based on the topography. This coupled system is run in forecasting mode, using hourly precipitation data (as well as other surface parameters, such as humidity and temperature) from the AROME ensemble members to produce runoff forecasts. Initial conditions are prepared by a 48-h run before the event, started from a larger scale soil analysis (for soil moisture and temperature) and driven by the observed precipita-

tion data during these 48 h. For more details on this forecasting chain, refer to Vincendon et al. (2011) (their Sect. 2.1).

Discharge forecasts were performed for three catchments of the Cévennes-Vivarais region, at Vallon Pont d'Arc for the Ardèche river, at Bagnols-sur-Cèze for the Cèze river and at Boucoiran for the Gardons river (Fig. 1 of Vincendon et al., 2011). Since the precipitating system on 20 October 2008 (Case 1) produced rainfall over the plains south of these three catchments, no hydrological forecasts are performed for this case. Ensemble discharge forecasts were computed for Cases 2 and 3, on 21–22 October and 1–2 November 2008, for the E1, E3 and E4 ensembles.

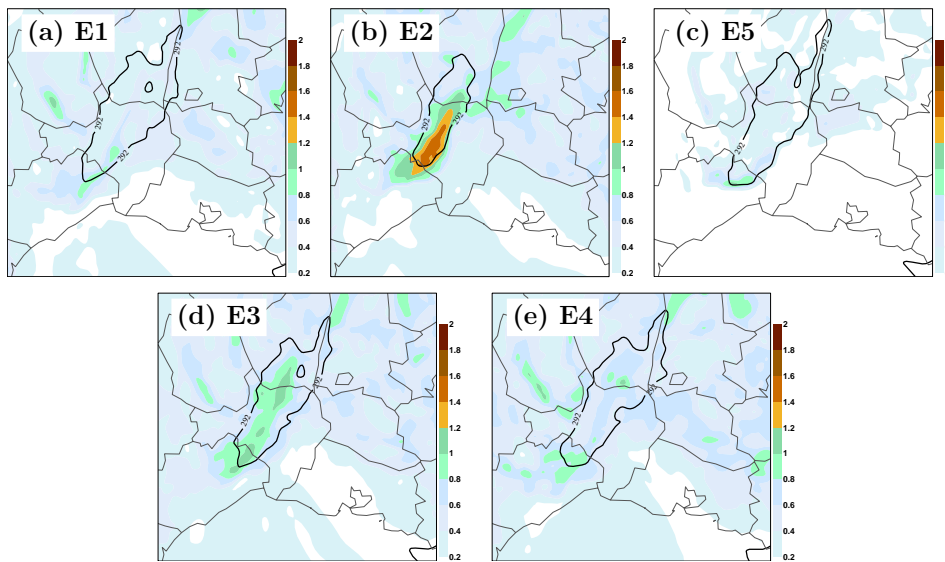


**Fig. 10.** Virtual potential temperature, ensemble spread (colour shading) and 292 K contour of the ensemble mean (black), at 15:00 UTC 20 October 2008, for (a) E1, (b) E2, (c) E5, (d) E3 and (e) E4.

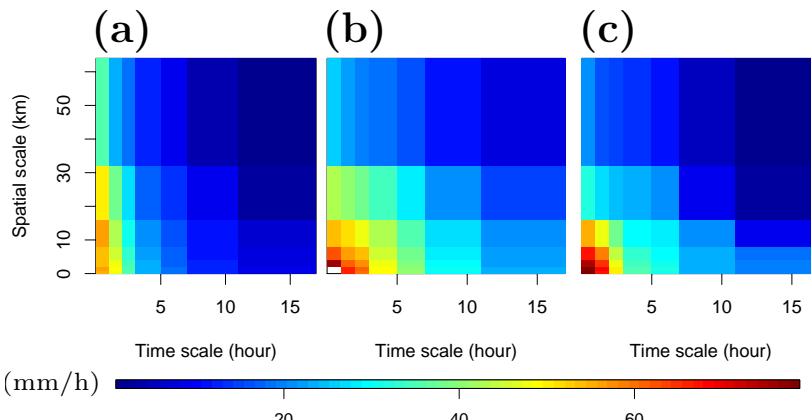
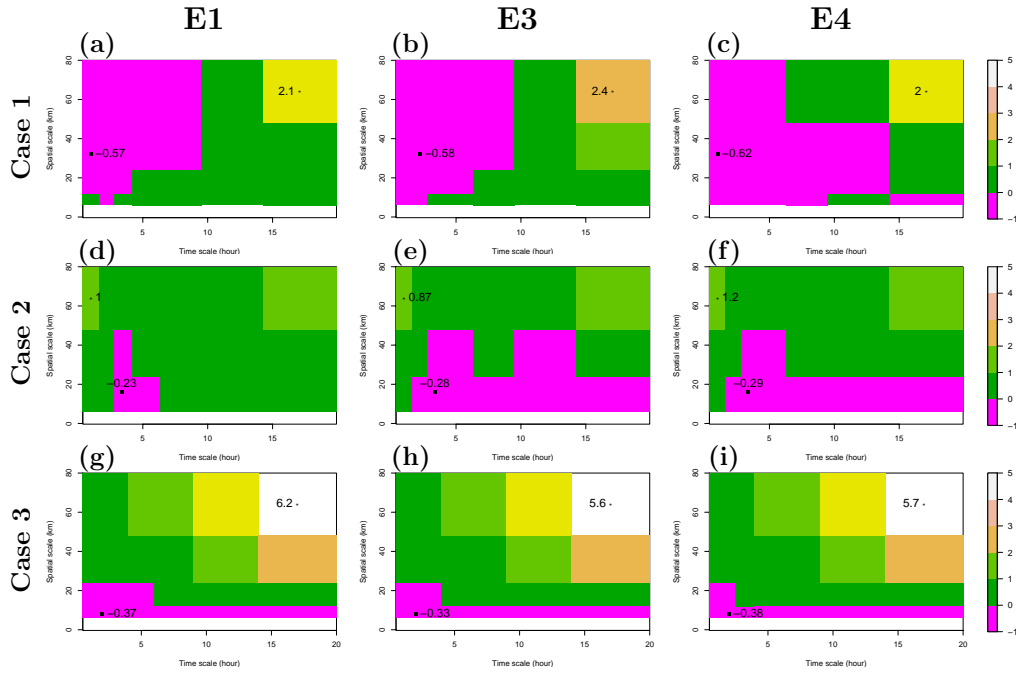


**Fig. 11.** Maxima diagrams: maximum observed rainfall intensities ( $\text{mm h}^{-1}$ ) as a function of accumulation duration and area, for (a) Case 1, (b) Case 2 and (c) Case 3.

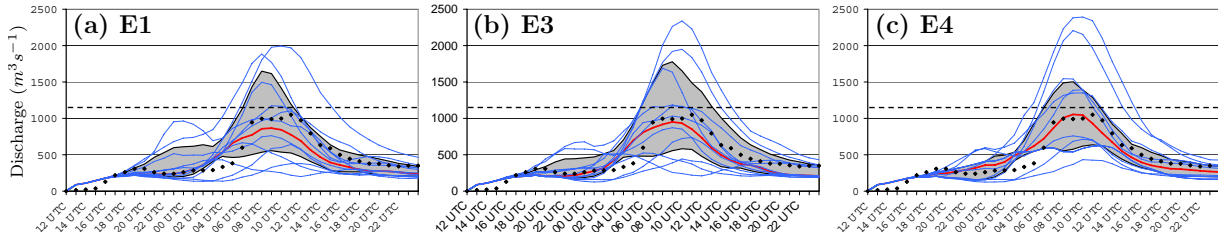
Discharge simulations for Case 3 do not show significant differences between the three ensembles. Forecasts for the Gardons river for each ensemble are shown in Fig. 13. As detailed in the previous section, most of the uncertainty on this case emerges from the synoptic-scale conditions. LBCs have a dominant impact on the AROME forecasts, so that the three ensembles produced similar precipitation forecasts, and the hydrological forecasts behave similarly as well.

Figure 14 shows discharge forecasts for the E1, E3 and E4 ensembles for the Ardèche, Cèze and Gardons rivers for Case 2. As previously stated, the E1 ensemble produced

higher rainfall totals than E3 and E4, which explains that hydrological forecasts driven by the E1 ensemble members simulated stronger discharges. This is especially clear for the Cèze (Fig. 14d–f) and Gardons (Fig. 14g–i) rivers. Differences exist between E3 and E4, although they are again weaker than differences between E1 and E3. Discharge forecasts from both ensembles are close for the Ardèche river (the northernmost catchment). For the Cèze river, and even more for the Gardons (the southernmost catchment), the E3 ensemble members produced a shifted discharge peak either too early or too late at 12:00 UTC and 20:00 UTC



**Fig. 12.** Normalised anomalies of average forecast maximum intensity relative to the observed maximum intensity, for (a–c) Case 1, (d–f) Case 2 and (g–i) Case 3, and for the (a,d,g) E1, (b,e,h) E3 and (c,f,i) E4 ensembles. Extreme values are plotted on each diagram.



**Fig. 13.** Observed and forecast hydrological discharge for the Gardons river for Case 3, from 12:00 UTC 1 November 2008 to 00:00 UTC 3 November 2008, for the (a) E1, (b) E3 and (c) E4 ensembles. Hourly observed discharge is plotted as black diamonds, blue lines stand for each ensemble member, the ensemble median is shown in red. The grey shading represents the interquartile range. Dashed lines represent the discharge for a reference flood on each watershed.

22 October 2008 at Bagnols-sur-Cèze (Fig. 14e) and at 02:00 UTC and 12:00 UTC 22 October 2008 at Boucoiran (Fig. 14h). The E4 ensemble produces a single peak, around 16:00 UTC 22 October 2008 at Bagnols-sur-Cèze (Fig. 14f), and 10:00 UTC 22 October 2008 at Boucoiran (Fig. 14i). These differences affect more the southernmost catchment, which is where the convective system is regenerated, that is, where new convective cells are created. This could be explained by the role of the microphysical parameterisation during the triggering of convection, or their impact on

mesoscale mechanisms, such as the development of a cold pool, as discussed in Sect. 4.1.

## 5 Conclusion

Previous research on convection permitting ensemble forecasts by Vié et al. (2011) assessed the impact of uncertainties separately on initial conditions and lateral boundary conditions. The present study focused on the combination of both uncertainty sources in a single ensemble, and on the assessment of part of model errors through the addition of

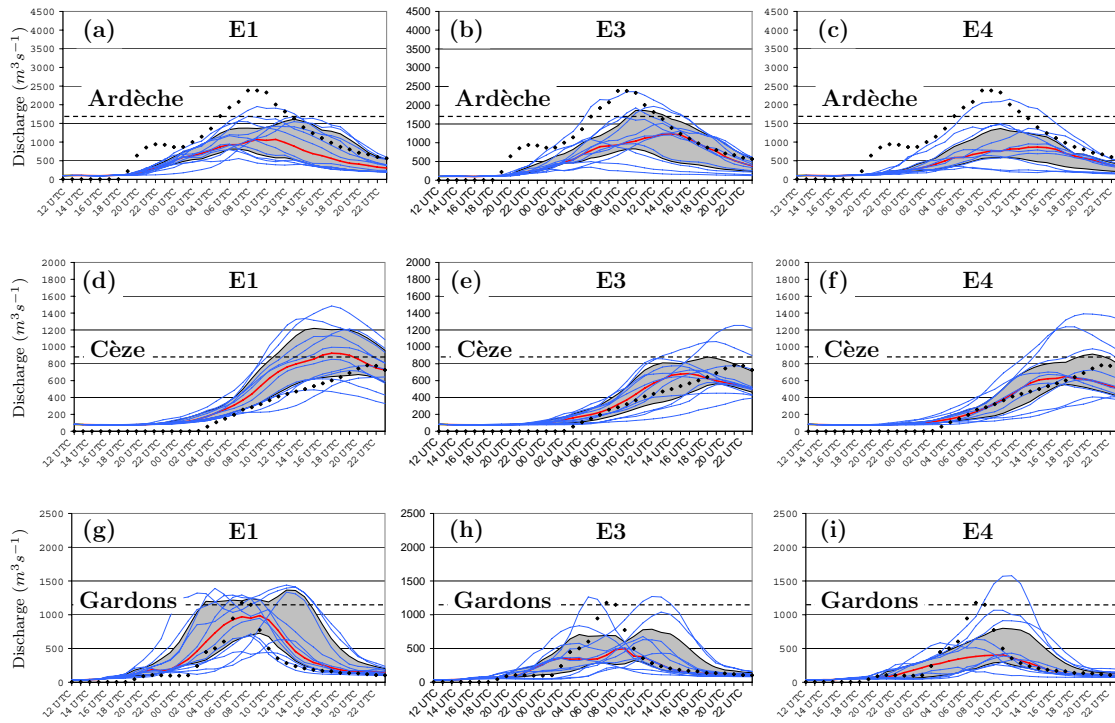


**Fig. 14.** Same as Fig. 13, for (a–c) the Ardèche, (d–f) the Cèze and (g–i) the Gardons rivers, for Case 2, from 12:00 UTC 21 October 2008 to 00:00 UTC 23 October 2008, for the (a,d,g) E1, (b,e,h) E3 and (c,f,i) E4 ensembles.

microphysical perturbations. Following Fresnay et al. (2012), and focusing on HPEs, perturbations were applied to the auto-conversion, accretion and evaporation tendencies.

The ensembles were evaluated using probabilistic scores on an 18-day period, including three HPE case studies. For the three case studies, an innovative evaluation process was set up. Rainfall forecasts were evaluated in a scale-independent framework using maxima diagrams Ceresetti et al. (2012). Furthermore, an hydrological evaluation was conducted through ensemble discharge forecasts for typical Mediterranean coastal watersheds, as in Vincendon et al. (2011).

The statistical evaluation showed the benefit of accounting for both uncertainties on initial and lateral boundary conditions in the E3 ensemble. Probabilistic scores are either as good as, or better than any of the E1 and E2 ensembles taken separately. Moreover, a significant gain in ensemble spread has been found, especially for intermediate forecast ranges, when the E1 and E2 ensembles performed the worst. The statistical evaluation of the E4 ensemble showed no improvement over the E3 ensemble. An impact of the perturbation of the microphysical parameterisation was found for the HPE case studies. This impact is more important when the convective system involves complex mesoscale processes, such as a low-level cold pool on 20 October 2008, than for systems

having stronger interactions with the synoptic-scale circulation (on 21–22 October and 1–2 November 2008). However, even for the HPE on 20 October 2008, these perturbations had a weaker impact than perturbations of either initial or lateral boundary conditions.

The hydro-meteorological evaluation of our ensembles on the three case studies confirms that the E1, E3 and E4 ensembles behave quite similarly. Maxima diagrams show that the perturbations used in the ensembles have no noticeable impact on the characteristics of the simulated precipitating systems. For Case 1, they confirm that the peak of precipitation is underestimated, and indicate that simulated convective cells do not organise into a well-formed convective system. For Cases 2 and 3, the forecast convective cells are slightly weaker than observed, but the precipitating system has a wider extension over the Cévennes mountains.

The hydrological discharge forecasts for HPEs on 21–22 October and 1–2 November 2008 also show small differences between ensembles. Differences are more important on 21–22 October 2008, especially for the southernmost watershed. This shows that, despite having little noticeable impact on the 24-h accumulated precipitation forecasts, the microphysical perturbations can affect the convective system initiation and development, at scales that are relevant for flash-flood forecasts. The impact of microphysical perturbations

seems located at the southern end of the precipitating system, where the convection is continuously regenerated by the triggering of new cells.

Overall, the three chosen microphysical perturbations, focusing on precipitation, have no impact on probabilistic scores. They may affect ensemble forecasts of heavy precipitating events, although not as much as initial or lateral boundary conditions. Another approach to sample the model error in ensemble forecasts is detailed in Bouttier et al. (2012). They use the ECMWF stochastic perturbation of physics tendencies (SPPT) scheme, adapted to convective-scale forecasts. They found an improvement in probabilistic scores as well as on case studies, even on low-level fields despite the lack of surface perturbations. To specifically enhance the spread at lower levels, it is planned to investigate perturbations of surface fields and surface-atmosphere fluxes. Further research also focuses on different parameterisations, such as the turbulence one. These scientific issues will be addressed in forthcoming studies.

**Acknowledgements.** This work was carried out in the framework of the MEDUP project (grant ANR-07-315 VULN-06-001), funded by the Vulnerabilité Milieux et Climat (VMC) programme of ANR. The authors thank the two reviewers for their comments and suggestions.

Edited by: P. Drobinski

Reviewed by: R. Rotunno and another anonymous referee



The publication of this article is financed by CNRS-INSU.

## References

- Berne, A., Delrieu, G., and Boudevillain, B.: Variability of the spatial structure of intense Mediterranean precipitation, *Adv. Water Resour.*, 32, 1031–1042, 2009.
- Berre, L., Stefanescu, S. E., and Belo Pereira, M.: The representation of the analysis effect in three error simulation techniques, *Tellus A*, 58, 196–209, 2006.
- Boniface, K., Ducrocq, V., Jaubert, G., Yan, X., Brousseau, P., Masson, F., Champollion, C., Chéry, J., and Doerflinger, E.: Impact of high-resolution data assimilation of GPS zenith delay on Mediterranean heavy rainfall forecasting, *Ann. Geophys.*, 27, 2739–2753, doi:10.5194/angeo-27-2739-2009, 2009.
- Bouttier, F., Vié, B., Nuissier, O., and Raynaud, L.: Impact of stochastic physics in a convection-permitting ensemble, *Mon. Wea. Rev.*, accepted, doi:10.1175/MWR-D-12-00031.1, 2012.
- Buzzi, A., Tartaglione, N., and Malguzzi, P.: Numerical simulations of the 1994 Piedmont flood: Role of orography and moist processes, *Mon. Wea. Rev.*, 126, 2369–2383, 1998.
- Caniaux, G., Redelsperger, J., and Lafore, J. P.: A Numerical Study of the Stratiform Region of a Fast-Moving Squall Line. 1. General Description and Water and Heat Budgets, *J. Atmos. Sci.*, 51, 2046–2074, 1994.
- Ceretti, D., Anquetin, S., Molinié, G., Leblois, E., and Creutin, J.-D.: Multiscale Evaluation of Extreme Rainfall Event Predictions Using Severity Diagrams, *Wea. Forecasting*, 27, 174–188, 2012.
- Clark, A. J., Gallus Jr., W. A., Xue, M., and Kong, F.: A Comparison of Precipitation Forecast Skill between Small Convection-Allowing and Large Convection-Parameterizing Ensembles, *Wea. Forecasting*, 24, 1121–1140, 2009.
- Clark, A. J., Gallus Jr., W. A., Xue, M., and Kong, F.: Growth of spread in convection-allowing and convection-parameterizing ensembles, *Wea. Forecasting*, 25, 594–612, 2010.
- Clark, A. J., Kain, J. S., Stensrud, D. J., Xue, M., Kong, F., Coniglio, M. C., Thomas, K. W., Wang, Y., Brewster, K., Gao, J., Wang, X., Weiss, S. J., and Du, J.: Probabilistic Precipitation Forecast Skill as a Function of Ensemble Size and Spatial Scale in a Convection-Allowing Ensemble, *Mon. Wea. Rev.*, 139, 1410–1418, 2011.
- Cuxart, J., Bougeault, P., and Redelsperger, J.: A turbulence scheme allowing for mesoscale and large-eddy simulations, *Quart. J. Roy. Meteor. Soc.*, 126, 1–30, 2000.
- Ducrocq, V., Nuissier, O., Ricard, D., Lebeaupin, C., and Thouvenin, T.: A numerical study of three catastrophic precipitating events over southern France. II: Mesoscale triggering and stationarity factors, *Quart. J. Roy. Meteor. Soc.*, 134, 131–145, 2008.
- Fresnay, S., Hally, A., Garnaud, C., Richard, E., and Lambert, D.: Heavy precipitation events in the Mediterranean: Sensitivity to cloud physics parameterisation uncertainties, *Nat. Hazards Earth Syst. Sci.*, in press, 2012.
- Gebhardt, C., Theis, S. E., Paulat, M., and Ben Bouallègue, Z.: Uncertainties in COSMO-DE precipitation forecasts introduced by model perturbations and variation of lateral boundaries, *Atmos. Res.*, 100, 168–177, 2011.
- Hohenegger, C. and Schär, C.: Predictability and error growth dynamics in cloud-resolving models, *J. Atmos. Sci.*, 64, 4467–4478, 2007a.
- Hohenegger, C., Walser, A., Langhans, W., and Schär, C.: Cloud-resolving ensemble simulations of the August 2005 Alpine flood, *Quart. J. Roy. Meteor. Soc.*, 134, 889–904, 2008.
- Houtekamer, P. L., Lefavre, L., Derome, J., Ritchie, J., and Mitchell, H. L.: A system simulation approach to ensemble prediction, *Mon. Wea. Rev.*, 124, 1225–1242, 1996.
- Lafore, J., Stein, J., Asencio, N., Bougeault, P., Ducrocq, V., Duron, J., Fischer, C., Hereil, P., Mascart, P., Masson, V., Pinty, J., Redelsperger, J., Richard, E., and de Arellano, J.: The Meso-NH atmospheric simulation system. Part I: Adiabatic formulation and control simulations, *Ann. Geophys.*, 16, 90–109, 1998, <http://www.ann-geophys.net/16/90/1998/>.
- Nuissier, O., Ducrocq, V., Ricard, D., Lebeaupin, C., and Anquetin, S.: A numerical study of three catastrophic precipitating events over southern France. I: Numerical framework and synoptic ingredients, *Quart. J. Roy. Meteor. Soc.*, 134, 111–130, 2008.
- Pergaud, J., Masson, V., and Malardel, S.: A parameterization of dry thermals and shallow cumuli for mesoscale numerical weather prediction, *Bound.-Layer Meteor.*, 132, 83–106, 2009.
- Ramos, M. H., Creutin, J.-D., and Leblois, E.: Visualization of storm severity, *J. Hydrol.*, 315, 295–307, 2005.

Seity, Y., Brousseau, P., Malardel, S., Hello, G., Bénard, P., Bouttier, F., Lac, C., and Masson, V.: The AROME-France Convective-Scale Operational Model, *Mon. Wea. Rev.*, 139, 976–991, 2010.

Vincendon, B., Ducrocq, V., Nuissier, O., and Vié, B.: Flash-flood ensemble forecasts based on convective-scale NWP, *Nat. Hazards Earth Syst. Sci.*, 11, 1529–1544, 2011,  
<http://www.nat-hazards-earth-syst-sci.net/11/1529/2011/>.

Vié, B., Nuissier, O., and Ducrocq, V.: Cloud-resolving ensemble simulations of Mediterranean heavy precipitating events: uncertainty on initial conditions and lateral boundary conditions, *Mon. Wea. Rev.*, 139, 403–423, 2011.

Yan, X., Ducrocq, V., Jaubert, G., Brousseau, P., Poli, P., Champlion, C., Flamant, C., and Boniface, K.: The benefit of GPS zenith delay assimilation to high-resolution quantitative precipitation forecasts: a case-study from COPS IOP 9, *Quart. J. Roy. Meteor. Soc.*, 135, 1788–1800, 2009.

## 1.3 Activités

### 1.3.1 Encadrement de chercheurs ayant permis l'obtention d'un diplôme

- Julien PICART (2008) : "Propagation des incertitudes d'échelle synoptique dans la prévision à haute résolution des épisodes de pluies intenses sur le Sud-Est de la France". Stage de Master 2 Spécialité Recherche Océan Atmosphère et Surfaces Continentales soutenu le 19 juin 2008. Encadrement : O. NUISSIER et M. PLU.
- Benoît VIE (2009) : "Impact des incertitudes sur les conditions initiales d'échelle synoptique et à méso-échelle et les conditions aux limites dans la prévision à haute résolution des épisodes de pluie intense en Méditerranée". Stage de Master 2 Spécialité Recherche Océan Atmosphère et Surfaces Continentales soutenu le 16 juin 2009. Encadrement : O. NUISSIER.
- Nicolas CANAL (2011) : "Utilisation des images satellites pour la vérification des modèles AROME\_WMED et AROME\_NWMED ; apport de l'approche ensembliste". Stage de Master 2 Spécialité Recherche Océan Atmosphère et Surfaces Continentales soutenu le 16 juin 2011. Encadrement : M. NURET et O. NUISSIER.
- Emilie BRESSON (2011) : "Mécanismes de formation des systèmes convectifs quasi-stationnaires en Méditerranée nord-occidentale : Application au cas du 15 Juin 2010 sur le Var". Thèse de 3ème cycle Université Paul Sabatier – Toulouse III, formation doctorale Sciences de l'Univers, de l'Environnement et de l'Espace (soutenue le 13 décembre 2011). Encadrement : V. DUCROCQ et O. NUISSIER.
- Benoît VIE (2012) : "Méthodes de prévisions d'ensemble pour l'étude de la prévisibilité à l'échelle convective des épisodes de pluie intense en Méditerranée". Thèse de 3ème cycle Université Paris-Est, formation doctorale Ville et Environnement (soutenue le 29 novembre 2012). Encadrement : O. NUISSIER et V. DUCROCQ.
- Mylène CIVIATE (2013) : "Mécanismes de génération de pluie intense en Méditerranée : analyse de simulations numériques à fine échelle d'un cas d'étude de la campagne expérimentale HyMeX". Stage d'approfondissement 3<sup>eme</sup> année de l'Ecole Nationale de la Météorologie, soutenu le 26 juin 2013. Encadrement : O. NUISSIER.
- Ulrick MEDDA (2014) : "Etude numérique des processus à l'échelle convective impliqués dans les événements de pluie intense méditerranéens". Stage de Master 2 Spécialité Recherche Océan Atmosphère et Surfaces Continentales soutenu le 17 juin 2014. Encadrement : Olivier NUISSIER, Fanny DUFFOURG et Christine LAC.
- Maxime MARTINET : "Etude de l'initiation et de l'organisation des systèmes fortement précipitants méditerranéens dans le cadre de la SOP1 HyMeX". Thèse de 3ème cycle Université Paul Sabatier – Toulouse III, formation doctorale Sciences de l'Univers, de l'Environnement et de l'Espace (soutenance prévue automne 2017). Encadrement : O. NUISSIER et F. DUFFOURG.

### 1.3.2 Implication dans des projets nationaux et internationaux

- FLOODsite FP6 : Integrated Flood Risk Analysis and Management Methodologies. Analyse de 3 situations de pluie intense sur le Sud-Est de la France à partir de simulations numériques.
- CYPRIM : Cyclogenèses et précipitations intenses en Méditerranée. Mise en oeuvre de méthodes de descente d'échelle et de détection d'environnements synoptiques favorables aux précipitations intenses pour estimer l'impact du changement climatique.

- MEDUP : MEditerranean Uncertainty Propagation. Mise en oeuvre de méthodes d'ensemble avec le modèle AROME pour quantifier la prévisibilité des épisodes fortement précipitants Méditerranéens.
- HyMeX : HYdrological cycle in Mediterranean EXperiment. Mise en oeuvre d'un démonstrateur de prévision d'ensemble avec le modèle AROME. Participation aux vols avions (Falcon 20) lors de la 1<sup>re</sup> période d'observation spéciale à l'automne 2012.
- MUSIC : Multiscale process studies of intense convective precipitation events in Mediterranean. Analyse des processus impliqués dans la génération des pluies intenses à partir de simulations aux échelles sub-kilométriques.

### 1.3.3 Autres activités

- Relectures d'articles dans des revues scientifiques : Quarterly Journal of the Royal Meteorology Society et Atmospheric Research.
- Membre du Conseil de Laboratoire depuis 2007.
- Co-coordination de la tâche prévision d'ensemble hydrométéorologique dans HyMeX depuis 2010.

## 1.4 Publications

### 1.4.1 Publications dans des revues à comité de lecture

1. Beaulant A.-L., Joly. B, **Nuissier O.**, Somot S, Ducrocq V., Joly A., Sevault F., Déqué M. and Ricard D., 2011 : Statistico-dynamical downscaling for Mediterranean heavy precipitation. *Q.J.R. Meteorol. Soc.*, DOI : 10.1002/qj.796.
2. B. Boudevillain, S. Argence, C. Claud, V. Ducrocq, B. Joly, A. Joly, D. Lambert, **O. Nuissier**, M. Plu, D. Ricard, Ph. Arbogast, A. Berne, J.-P. Chaboureau, B. Chapon, F. Crépin, G. Delrieu, E. Doerflinger, B. Funatsu, P.-E. Kirtstetter, F. Masson, K. Maynard, E. Richard, E. Sanchez, L. Terray et A. Walpersdorf (2009) : Cyclogenèses et précipitations intenses en région méditerranéenne : origine et caractéristiques, La Météorologie. N°66 août 2009, p 18-28.
3. Bouttier, F., B. Vié, **O. Nuissier**, L. Raynaud, 2012 : Impact of Stochastic Physics in a Convection-Permitting Ensemble. *Mon. Wea. Rev.*, 140, 3706–3721.
4. Bouttier, F., Raynaud, L., **Nuissier, O.** and Ménétrier, B., 2015 : Sensitivity of the AROME ensemble to initial and surface perturbations during HyMeX. *Q.J.R. Meteorol. Soc.*. doi : 10.1002/qj.2622.
5. Bresson, E., Ducrocq, V., **Nuissier, O.**, Ricard, D. and de Saint-Aubin, C. (2012), Idealized numerical simulations of quasi-stationary convective systems over the Northwestern Mediterranean complex terrain. *Q.J.R. Meteorol. Soc.*, 138 : 1751–1763. doi : 10.1002/qj.1911
6. Chaboureau, J.-P., **Nuissier, O.**, and Claud, C. : Verification of ensemble forecasts of Mediterranean high-impact weather events against satellite observations, *Nat. Hazards Earth Syst. Sci.*, 12, 2449-2462, doi :10.5194/nhess-12-2449-2012, 2012.
7. Ducrocq, V., **Nuissier O.**, Ricard D., Lebeaupin C. and Thouvenin T., 2008 : A numerical study of three catastrophic precipitating events over southern France. II : Mesoscale triggering and stationarity factors. *Q.J.R. Meteorol. Soc.*, 134 : 131-145.

8. Duffourg, F., Nuissier, O., Ducrocq, V., Flamant, C., Chazette, P., Delanoe, J., Doerenbecher, A., Fourrié, N., Di Girolamo, P., Lac, C., Legain, D., Martinet, M., Saïd, F., Bock, O., 2015 : Offshore deep convection initiation and maintenance during HyMeX IOP 16a heavy precipitation event. *Q. J. R. Meteorol. Soc.* DOI : 10.1002/qj.2725
9. Fourrié, N., Bresson, É., Nuret, M., Jany, C., Brousseau, P., Doerenbecher, A., Kreitz, M., Nuissier, O., Sevault, E., Bénichou, H., Amodei, M., and Pouponneau, F. : AROME-WMED, a real-time mesoscale model designed for the HyMeX special observation periods, *Geosci. Model Dev.*, 8, 1919-1941, doi :10.5194/gmd-8-1919-2015, 2015.
10. Hally, A., Caumont, O., Garrote, L., Richard, E., Weerts, A., Delogu, F., Fiori, E., Rebora, N., Parodi, A., Mihalović, A., Ivković, M., Dekić, L., van Verseveld, W., Nuissier, O., Ducrocq, V., D'Agostino, D., Galizia, A., Danovaro, E., and Clematis, A., 2015 : Hydro-meteorological multi-model ensemble simulations of the 4 November 2011 flash flood event in Genoa, Italy, in the framework of the DRIHM project, *Nat. Hazards Earth Syst. Sci.*, 15, 537-555, doi :10.5194/nhess-15-537-2015, 2015.
11. Martin, E., V. Ducrocq, A. Joly, B. Joly, O. Nuissier, P. Quintana-Seguí, D. Ricard, F. Sevault, S. Somot and P. Drobinski, 2007 : La Méditerranée, région témoin : de Cyprim à Hymex. *La Houille Blanche*, 6, 90-96.
12. Nuissier, O., Rogers R. F. and Roux F., 2005 : A numerical simulation of Hurricane Bret on 22-23 August 1999 initialized with airborne Doppler radar and dropsonde data". *Q.J.R. Meteorol. Soc.*, 131, 155-194.
13. Nuissier, O., Ducrocq V., Ricard D., Lebeaupin C. and Anquetin S., 2008 : A numerical study of three catastrophic precipitating events over southern France. I : Numerical framework and synoptic ingredients. *Q.J.R. Meteorol. Soc.*, 134, 111-130.
14. Nuissier, O., Joly B., Joly A., Ducrocq V. and Arbogast P., 2011 : A statistical downscaling to identify the large-scale circulation patterns associated with heavy precipitation events over southern France. *Q.J.R. Meteorol. Soc.*, DOI : 10.1002/qj.866.
15. Nuissier, O., Joly, B., Vié, B., and Ducrocq, V. : Uncertainty of lateral boundary conditions in a convection-permitting ensemble : a strategy of selection for Mediterranean heavy precipitation events, *Nat. Hazards Earth Syst. Sci.*, 12, 2993-3011, doi :10.5194/nhess-12-2993-2012, 2012.
16. Nuissier, O., Marsigli, C., Vincendon, B., Hally, A., Bouttier, F., Montani, A., and Pacagnella, T., 2015 : Evaluation of two convection-permitting ensembles systems in the HyMeX Special Observation Period (SOP1) framework. *Q. J. R. Meteorol. Soc.* (in revision).
17. D. Ricard, A.-L. Beaulant, J. Boe, M. Déqué, V. Ducrocq, A. Joly, B. Joly, E. Martin, O. Nuissier, P. Quintana Segu, A. Ribes, F. Sevault et S. Somot (2009) : Impact du changement climatique sur les événements de pluie intense du bassin méditerranéen, *La Météorologie.*, N°67 novembre 2009, p 19-30.
18. Roux, F., Chane-Ming F., Lasserre-Bigorry A. and Nuissier O., 2004 : Structure and evolution of intense tropical cyclone Dina near la Reunion on 22 January 2002 : GB-EVTD analysis of single Doppler radar observations. *J. Atmos. Oceanic. Technol.*, 21, 1501-1518.
19. Thévenot, O., Bouin, M.-N., Ducrocq, V., Lebeaupin Brossier, C., Nuissier, O., Pianezze, J. and Duffourg, F. (2015), Influence of the sea state on Mediterranean heavy precipitation : a case-study from HyMeX SOP1. *Q.J.R. Meteorol. Soc.*. doi : 10.1002/qj.2660.

20. Vié, B., **Nuissier O.** and Ducrocq V., 2011 : Cloud-resolving ensemble simulations of Mediterranean heavy precipitating events : uncertainty on initial conditions and lateral boundary conditions. *Mon. Wea. Rev.*, 139, 403-423.
21. Vié, B., Molinié, G., **Nuissier, O.**, Vincendon, B., Ducrocq, V., Bouttier, F., and Richard, E. : Hydro-meteorological evaluation of a convection-permitting ensemble prediction system for Mediterranean heavy precipitating events, *Nat. Hazards Earth Syst. Sci.*, 12, 2631-2645, doi :10.5194/nhess-12-2631-2012, 2012.
22. Vincendon, B., Ducrocq, V., **Nuissier, O.**, and Vié, B. : Perturbation of convection-permitting NWP forecasts for flash-flood ensemble forecasting, *Nat. Hazards Earth Syst. Sci.*, 11, 1529-1544, doi :10.5194/nhess-11-1529-2011, 2011.
23. Wiedner, M., C. Prigent, J. R. Pardo, **O. Nuissier**, J.-P. Chaboureau, J.-P. Pinty and P. Mascart, 2004 : « Modeling of passive microwave responses in convective situations using outputs from mesoscale models : comparison with TRMM/TMI satellite observations. *J. Geophys. Res.*, 109, D06214, doi :10.1029/2003JD004280

#### 1.4.2 Communications lors de congrès, conférences, séminaires, etc

- Caumont, O., A. Hally, L. Garrote, É. Richard, A. Weerts, F. Delogu, E. Fiori, N. Rebora, A. Parodi, A. Mihalović, M. Ivković, L. Dekić, W. van Verseveld, **O. Nuissier**, V. Ducrocq, D. D'Agostino, A. Galizia, E. Danovaro, A. Clematis, 2015 : Multi-model ensemble hydrometeorological simulations of the 2011 and 2014 flash floods in Genoa, Italy : a comparison study in the framework of the DRIHM project. 9th Mediterranean-HyMeX workshop, 2015, Mykonos, Greece.
- Fosser, G., R. Roehrig, **O. Nuissier**, C. Dubois and S. Somot, 2015 : Sensitivity of the representation of Heavy Precipitation Events over the western Mediterranean region to the new physical parameterizations in the Regional Climate Model ALADIN. 9th Mediterranean-HyMeX workshop, 2015, Mykonos, Greece.
- Keil, C., M. Westphal, C. Marsigli, **O. Nuissier**, 2015 : Predictability of high impact weather events in the Mediterranean. 9th Mediterranean-HyMeX workshop, 2015, Mykonos, Greece.
- Martinet, M., **O. Nuissier**, F. Duffourg and V. Ducrocq, 2015 : Offshore deep convection initiation and maintenance during HyMeX IOP16a heavy precipitation event. 9th Mediterranean-HyMeX workshop, 2015, Mykonos, Greece.
- Roehrig, R., G. Fosser, **O. Nuissier**, F. Duffourg, I. Beau and S. Somot, 2015 : Improving convection parameterization in the context of Mediterranean heavy precipitating events over land. 9th Mediterranean-HyMeX workshop, 2015, Mykonos, Greece.
- Duffourg, F. and **Nuissier, O.**, 2014 : Fine-scale analysis of the physical processes involved in IOP13 convection. 8th Mediterranean-HyMeX workshop, 2014, La Valetta, Malta.
- Fosser, G., Roehrig, R., **Nuissier, O.**, Dubois, C. and Somot, S., 2014 : Representation of Heavy Precipitation Events over the Western Mediterranean region in regional climate models. 8th Mediterranean-HyMeX workshop, 2014, La Valetta, Malta.
- Hally, A., O. Caumont, **O. Nuissier**, V. Ducrocq, É. Richard, J. Escobar, A. Parodi, N. Rebora, E. Fiori, F. Delogu, F. Pintus, A. Clematis, D. D'Agostino, A. Galizia, A. Quarati, E. Danovaro, L. Garrote, M. C. Llasat, Q. Harpham, H. R. A. Jagers, A. Weerts, A. Taferner, C. Forster, V. Dimitrijević, L. Dekić, A. Mihalović, M. Ivković, R. Hooper, 2014 : Multi-model ensemble hydrometeorological modelling of the 4 November 2011 Genoa, Italy flash flood in the framework of the DRIHM project. 8th Mediterranean-HyMeX workshop, 2014, La Valetta, Malta.

- **Nuissier, O.**, Hally, A., Vincendon, B., Marsigli, C., Montani, A. and Paccagnella, T., 2014 : Ensemble forecasting activities during SOP1 : a comparison between convection-permitting ensemble systems. 8th Mediterranean-HyMeX workshop, 2014, La Valetta, Malta.
- Thévenot, O., Bouin, M.-N., Ducrocq, V., Lebeaupin-Brossier, C., **Nuissier, O.** and Dufourg, F., 2014 : Sensitivity study of an Heavy Precipitating Event to the sea state using convection-permitting model simulations.
- Chabot, E., **Nuissier, O.** and Bouttier, F., 2013 : Contribution of a convection-permitting ensemble prediction system in a decision process : a subjective study of AROME-NWMED EPS during SOP1. 7th Mediterranean-HyMeX workshop, 2013, Cassis, France.
- Civiate, M., F. Duffourg and **Nuissier O.**, 2013 : A numerical study of the heavy precipitation event on October 26 2012 (IOP16a) in the Var region (South-East of France). 7th Mediterranean-HyMeX workshop, 2013, Cassis, France.
- **Nuissier O.**, 2013 : Characteristics of heavy rainfall during late summer and autumn 2012 (SOP1). HyMeX SOPs' Debriefing Workshop, 2013, Toulouse, France.
- **Nuissier, O.**, Marsigli, C., Bouttier, F., Montani, A. and Paccagnella, T., 2013 : Ensemble forecasting activities during HyMeX SOP1 : a comparison between convection-permitting ensemble systems. 7th Mediterranean-HyMeX workshop, 2013, Cassis, France.
- Vincendon, B., **Nuissier, O.**, Caumont, O. and Ducrocq, V., 2013 : Real-time hydrometeorological ensemble forecasting during the HyMeX SOP1 : evalutation of two-hourly discharge ensembles. 7th Mediterranean-HyMeX workshop, 2013, Cassis, France.
- Bresson E., Ducrocq V., Duffourg F. , **Nuissier O.** and Nuret M., 2012 : Triggering and support mechanisms of the catastrophic heavy rainfall over the Var region (June 2010). 6th Mediterranean-HyMeX workshop, 2012, Primosten, Croatia.
- Chaboureau J-P, Alhammoud B, Funatsu B. , Lebeaupin-Brossier C., Claud C, **Nuissier O.**, Beranger K., Drobinski P., 2012 : Verification of model prediction of cloud cover and rain by satellite observation. 6th Mediterranean-HyMeX workshop, 2012, Primosten, Croatia.
- **Nuissier O.**, Vié B and Vincendon B., 2012 : A dedicated hydrometeorological ensemble prediction chain for flash-floods during the HYMEX NW\_MED SOP. 6th Mediterranean-HyMeX workshop, 2012, Primosten, Croatia.
- Bousquet O., J. Beck, M. Nuret, E Bresson, **O. Nuissier** and V. Ducrocq, 2011 : Observation and Numerical Modeling of an Exceptionally Intense Orographic Precipitation Event in Southern France. 14th Conference on Mesoscale Processes, 1–4 August 2011, Los Angeles, California, USA.
- Bresson E., V. Ducrocq, **O. Nuissier** and M. Nuret, 2011 : The catastrophic heavy precipitation event on June 15, 2010 in the Var region (south-east of France). 5th Mediterranean-HyMeX workshop, 2011, Sant Lluís, Spain.
- Nuret M., P. Brousseau, O. Caumont, N. Fourrié, **O. Nuissier** : Mesoscale simulation of two Heavy Precipitating Events with AROME\_WMED : the Var (June 2010) and Gard-Ardèche (September 2010) cases studies. 5th Mediterranean-HyMeX workshop, 2011, Sant Lluís, Spain.
- Vié B., **O. Nuissier** and V. Ducrocq, 2011 : A convection-permitting ensemble prediction system to study the predictability of Mediterranean Heavy Precipitating Events. 5th Mediterranean-HyMeX workshop, 2011, Sant Lluís, Spain.
- Vié, B., **Nuissier, O.** and Ducrocq, V., 2011 : A convection-permitting Ensemble Prediction System to study the predictability of Mediterranean Heavy Precipitating Events, 14th AMS Conf. on Mesoscale Processes, 1-4 August 2011, Los Angeles, California, USA.

- Vincendon B., V. Ducrocq, **O. Nuissier** and B. Vié, 2011 : Hydrometeorological ensemble forecasting of mediterranean flash-flood events. 5th Mediterranean-HyMeX workshop, 2011, Sant Lluís, Spain.
- **Nuissier O.**, 2010 : Convective-scale and short-range predictability of high-impact weather events, ECMWF Seminar on Predictability in the European and Atlantic regions, seminar proceedings, pp 137-146, 6-9 Sept. 2010, Reading, UK.
- **Nuissier O.** and M. Nuret M., 2010 : High-resolution forecasts of a Mediterranean cyclogenesis case study on 17-19 February 2010 : deterministic and ensemble strategies. 4th atelier HyMeX, Bologna, Italy, 2010.
- Vié B., **O. Nuissier**, V. Ducrocq, 2010 : Cloud-resolving ensemble simulations of Mediterranean Heavy Precipitating Events : Uncertainty on meso-scale initial conditions vs. uncertainty on lateral boundary conditions. 4th atelier HyMeX, Bologna, Italy, 2010.
- **Nuissier O.**, B. Vié and V. Ducrocq, 2009 : Ensemble methods for evaluating the convective-scale predictability of Mediterranean Precipitation Events, Proc. Third THORPEX International Science Symposium (TTISS), 14-18 sept. 2009, Monterrey, California, USA.
- Vié B., **O. Nuissier** and V. Ducrocq, 2009 : Ensemble methods for evaluating the convective-scale predictability of Mediterranean Precipitation Events. 9th EMS Annual Meeting, 28 sept. – 2 oct. 2009, Toulouse, France.
- Joly, B., **O. Nuissier**, A.-L. Beaulant, V. Ducrocq, A. Joly, S. Somot, F. Sevault, M. Déqué, 2008 : Statistical downscaling of large scale environments for high precipitating events over southeastern France in a regional coupled model climate scenario. 2nd atelier HyMeX, 2-4 juin 2008, Palaiseau, France.
- **Nuissier, O.**, J. Picart, M. Plu, V. Ducrocq, 2008 : Predictability of high-resolution forecasts of heavy precipitating events in the Mediterranean. 2nd atelier HyMeX, 2-4 juin 2008, Palaiseau, France.
- Joly, B., **O. Nuissier**, Somot, S., Ducrocq, V., Joly, A., 2007 : Statistical downscaling of southern France High Precipitating Events synoptic forcing conditions over precipitation patterns in a future climate, 7th EMS Annual Meeting, 1-5 Octobre 2007, San Lorenzo de El Escorial, Espagne.
- Joly, B., **O. Nuissier**, Somot, S., Ducrocq, V., Joly, A., 2007 : Statistical downscaling of synoptic environments for high precipitation events over southern France : an objective method of selection, 9th Plinius Conference on Mediterranean Storms, 10-13 Septembre 2007, Varenna, Italy.
- Joly, B., **O. Nuissier**, V. Ducrocq, A. Joly, 2007 : Mediterranean synoptic scale ingredients involved in Heavy Precipitating Events triggering over Southern France : a clustering approach. 1er atelier HyMeX, 9-11 janvier 2007, Toulouse, France.
- Martin, E., V. Ducrocq, A. Joly, B. Joly, **O. Nuissier**, P. Quintana-Segui, D. Ricard, F. Sevault, S. Somot, P. Drobinski, 2007 : La Méditerranée, région témoin : de CYPRIM à HyMeX, La Houille blanche, 6, 90-95.
- **Nuissier, O.**, V. Ducrocq, D. Ricard, 2007 : Triggering and stationarity factors for Heavy Precipitating Events over Southern France, 1er atelier HyMeX, 9-11 janvier 2007, Toulouse, France.
- **Nuissier, O.**, Joly, B., Somot, S., Ducrocq, V., Joly, A., 2007 : Heavy Precipitating Events (HPEs) over Southern France in a climate change scenario : a dynamical downscaling approach, 9th Plinius Conference on Mediterranean Storms, 10-13 Septembre 2007, Varenna, Italy.
- Ricard, D., V. Ducrocq, G. Jaubert, **O. Nuissier**, R. Bresson, 2007 : Variability of high-resolution simulations of Mediterranean heavy precipitation events, 9ème Conférence

- Internationale sur les Précipitations, Marne-La-Vallée, novembre 2007.
- Ducrocq, V., C. Lebeaupin, **O. Nuissier**, D. Ricard, H. Giordani, 2005 : High-resolution Non-hydrostatic Numerical Weather Prediction of Mediterranean torrential rain events, WSN05, 5-9 septembre 2005, Toulouse.
  - **Nuissier, O.**, V. Ducrocq, D. Ricard, 2005 : Numerical study of three torrential rain events over the Western Mediterranean region (Southern France), 7th Plinius Conference, 5-7 October 2005, Rethymnon, Crète, Grèce.
  - **Nuissier, O.**, Ducrocq, V. and Anquetin, S., 2005 : A numerical study of 3 typical flash-flood events : stationarity aspects. FLOODsite workshop on flash-flood events, Grenoble (France), 21-22 septembre 2005.
  - **Nuissier, O.**, Ducrocq, V. and Ricard, D., 2005 : Numerical study of three torrential rain events over the Western Mediterranean region (Southern France). 5èmes journées d'étude de l'OHM-CV, Grenoble (France), 17-18 novembre 2005.
  - **Nuissier, O.**, et F. Roux, 2003 : Utilisation de données de radars météorologiques Doppler pour l'initialisation du modèle Méso-NH : application au cas de cyclones tropicaux. 2nde Réunion des Utilisateurs du modèle Méso-NH, Toulouse, 3-4 Février 2003.
  - Burlaud, C., **O. Nuissier**, N. Viltard et F. Roux, 2002 : Simulations numériques et observations en radiométrie micro-ondes du cyclone tropical Bret (août 1999). Comptes-rendus des Ateliers Expérimentation- Instrumentation, Météo France, Toulouse, 29-30 Janvier 2002, 7p.
  - Burlaud, C., N. Viltard, O. Nuissier et F. Roux, 2002 : Numerical simulation and observations in passive microwave radiometry of the tropical Hurricane Bret (August 1999). Proceedings of the "25th Conference on Hurricanes and Tropical Meteorology", Amer. Meteor. Soc., San Diego, Ca., USA, 29 April – 3 May 2002., 412-413.
  - **Nuissier, O.**, et F. Roux, 2002 : Simulation du cyclone tropical Bret (1999) avec le modèle Méso-NH. Atelier de Modélisation de l'Atmosphère, Météo France, Toulouse, 17-19 Décembre 2002.
  - **Nuissier, O.**, R. F. Rogers et F. Roux, 2002 : An initialization technique using airborne Doppler radar observations for numerical simulations of Hurricane Bret (21-23 August 1999). Proceedings of the « 25th Conference on Hurricanes and Tropical Meteorology », Amer. Meteor. Soc., San Diego, Ca., USA, 29 April – 3 May 2002., 403-404.
  - F. Roux, F. Chane-Ming, A. Lasserre-Bigorry et **O. Nuissier**, 2002 : Doppler radar observations of tropical cyclone Dina. Proceeding of the « 2nd European Conference on Radar Meteorology, Delft (Pays-Bas), 18-21 Novembre 2002, 6p.
  - **Nuissier, O.**, 2001 : Utilisation de données de radars météorologiques Doppler et de dropsondes pour la simulation numérique de cyclones tropicaux : application au cas de l'ouragan Bret le 21-23 août 1999. Séminaires du laboratoire de Physique de l'Atmosphère Tropicale (Université des Antilles et de la Guyane), Pointe-à-Pitre, 20 Septembre 2001.
  - **Nuissier, O.**, 2001 : Utilisation de données de radars météorologiques Doppler et de dropsondes pour la simulation numérique de cyclones tropicaux : application au cas de l'ouragan Bret le 21-23 août 1999. Séminaires du laboratoire d'Aérologie, Toulouse, 18 Octobre 2001.
  - **Nuissier, O.**, F. Roux et N. Viltard, 2001 : Numerical simulations of Hurricane Bret (21-23 August 1999) observed by TRMM. XXVI General Assembly of the European Geophysical Society, Nice, 25-30 Mars 2001.
  - **Nuissier, O.**, F. Roux et N. Viltard, 2001 : Numerical simulations of Hurricane Bret (21-23 August 1999) observed by TRMM. Proceedings of the « Ninth Conference on Mesoscale

- Processes », Amer. Meteor. Soc., Fort Lauderdale, Fl., USA, 30 Juillet – 2 Août 2001, 211-215.
- **Nuissier, O.**, et F. Roux, 2001 : Utilisation de données de radars météorologiques Doppler pour la simulation de cyclones tropicaux. 1ère Réunion des Utilisateurs du modèle Méso-NH, Toulouse, 8-9 Février 2001.
  - **Nuissier, O.**, et F. Roux, 2000 : Utilisation de données de radars météorologiques Doppler pour la simulation de cyclones tropicaux. Comptes-rendus des Ateliers de Modélisation de l'Atmosphère, Météo France, Toulouse, 29 Nov.- 1 Déc. 2000, 97-100.
  - **Nuissier, O.**, F. Roux et C. Claud, 2000 : Numerical simulations of tropical cyclones and polar lows. XXV General Assembly of the European Geophysical Society, Nice, 25-29 Avril 2000.

## **Chapitre 2**

# **Synthèse des travaux de recherche**

### **2.1 Introduction**

Tremblements de terre, éruptions volcaniques, tornades, raz-de-marée, cyclones tropicaux, inondations... La société des Hommes est toujours désemparée face aux éléments naturels qui se déchaînent. Le mieux que l'on puisse faire pour atténuer les conséquences de tels cataclysmes, c'est d'essayer de les prévoir, au mieux de s'en protéger et réduire ainsi leurs effets. Mais la tâche n'est pas si simple car le système Terre demeure très complexe. Les scientifiques doivent s'attacher à décrire et comprendre en détail chacun des éléments et rouages qui forment cette immense machinerie et qui s'influencent mutuellement en une cascade de causes à effets et de rétroactions.

Parmi tous ces évènements naturels cataclysmiques, les cyclones sont une spécificité des régions tropicales qu'ils dévastent régulièrement. Ce sont des phénomènes conditionnés par les interactions entre l'océan et l'atmosphère, dans les zones les plus chaudes et les plus humides de la planète. Lorsque certaines conditions dynamiques et thermodynamiques sont réunies, de simples nuages d'orages peuvent s'assembler, s'intensifier et dégénérer en de gigantesques tourbillons martelant, écrasant et soufflant tout sur leur passage. Les précipitations qui accompagnent ces phénomènes sont d'une rare intensité. En quelques jours ils peuvent déverser autant de pluies qu'il en tombe en 2 ans sur la région parisienne. Un cyclone tropical d'intensité moyenne produit une énergie équivalente à plusieurs centaines de centrales nucléaires à pleine puissance générant des vents dont la vitesse peut excéder les 250 km/h.

Malgré tout, les cyclones tropicaux ne sont pas exclusivement meurtriers et destructeurs. Lorsqu'ils évoluent loin de toute terre habitée, ils retrouvent leur fonction première de soufflage de sûreté des océans et contribuent à une redistribution énergétique efficace entre les zones surchauffées du globe et les régions plus froides. L'Homme reste actuellement impuissant à combattre ces monstres naturels qui meurent d'eux-mêmes en pénétrant sur les continents ou en s'aventurant au-dessus d'eaux plus froides. Seules la prévision et la prévention peuvent atténuer leurs effets dévastateurs. Devant les conséquences négatives des cyclones, nous comprenons aisément pourquoi "bien observer, comprendre, prévoir et en dernier ressort alerter" constituent la seule issue possible afin de mettre l'ensemble de la population à l'abri et préserver ainsi les vies humaines.

Aux latitudes tempérées les systèmes précipitants orageux dans nos régions métropolitaines, en raison des phénomènes météorologiques qui les accompagnent (précipitations intenses, foudre, chutes de grêle, fortes rafales de vent), représentent également une sérieuse menace pour la sécurité des biens et des personnes. Les régions méditerranéennes notamment

sont régulièrement touchées par des épisodes de pluie intense durant la période automnale. Ces événements météorologiques méditerranéens à fort impact ont bien souvent comme origine des systèmes convectifs de méso-échelle pouvant rester quasi-stationnaires sur une même zone pendant plusieurs heures. Des volumes de précipitations exceptionnels, tombant dans un intervalle de temps très court au-dessus de régions à relief pentu et encaissé, conduisent bien-souvent à des crues éclair et des inondations. On peut citer par exemple la vingtaine de victimes par noyade et foudroyement recensée lors des inondations catastrophiques sur le Gard en septembre 2002. Plus de 600 mm avaient été alors enregistrés près d'Alès. Le coût des dégâts et dommages a été estimé à plus de 1,5 milliards d'Euros. Plus récemment, les inondations qui ont frappé le Var en juin 2010 avaient pour origine des précipitations exceptionnelles (397 mm de cumul de précipitations en cinq heures sur le pluviographe des Arcs). Elles sont intervenues, soit par ruissellement, soit par débordement des cours d'eau et ont essentiellement affecté la région de Draguignan et la vallée de l'Argens. Cette crue, qualifiée de centennale, a coûté la vie à 23 personnes et les dégâts matériels ont été estimés à plus de 200 millions d'Euros.

Plusieurs facteurs rendent la région méditerranéenne propice au développement de la convection profonde : on a tout d'abord une température de surface de la mer relativement élevée en fin d'été - début d'automne, ce qui fait de la Méditerranée un réservoir de chaleur et d'énergie ; ensuite, le pourtour méditerranéen présente une orographie marquée ; enfin bien sûr un contexte synoptique favorable permet d'engendrer un flux de basses couches qui transporte de l'air chaud et humide de la mer Méditerranée vers les côtes. La prévision numérique du temps a fait récemment de nombreux progrès, en particulier avec les modèles opérationnels de fine échelle, comme AROME qui a une résolution horizontale de 1.3 km depuis 2015.

Cependant, la prévision des pluies intenses demeure encore trop souvent imprécise tant en localisation qu'en intensité, ceci en raison des échelles caractéristiques mise en jeu et de la complexité des processus impliqués. En effet, la gamme des échelles spatio-temporelles concernées s'étend de l'échelle des systèmes convectifs de méso-échelle ( $\sim 100$  km ; 12 h) à l'échelle de la microphysique du nuage ( $\sim \text{qqs } \mu\text{m} ; \text{qqs } \sim 10^{-3}$  ms).

Une autre difficulté à prévoir précisément la localisation et l'intensité des événements de pluie intense réside dans le nombre de facteurs de l'environnement météorologique influençant le développement et l'évolution de la convection et la difficulté à modéliser correctement les processus fortement non-linéaires et à seuil impliqués dans les systèmes convectifs intenses, comme les processus liés à la microphysique du nuage (condensation, évaporation, sublimation) ou bien encore l' entraînement et le détraînement au sommet et sur les bords du nuage par exemple.

On voit donc la nécessité d'évaluer l'incertitude associée aux prévisions et ainsi de mesurer la prévisibilité à l'échelle convective en évaluant la capacité du modèle à fine échelle à prévoir ces épisodes fortement précipitants. La connaissance de cette incertitude permettra de mieux définir le risque d'occurrence d'un phénomène dangereux en général, son intensité possible, et également les régions susceptibles d'être concernées.

Un autre enjeu majeur concerne cette fois le devenir de ces épisodes de pluie intense méditerranéens dans la perspective du changement climatique. La région Méditerranée apparaît comme l'un des principaux "points chauds" régionaux du changement climatique (Giorgi, 2006). En effet les modèles climatiques globaux et régionaux s'accordent tous pour indiquer un réchauffement plus important en Méditerranée que dans beaucoup d'autres régions, en particulier l'été. Celui-ci s'accompagnerait d'un assèchement en moyenne annuelle, surtout l'été, ainsi que d'une augmentation de la variabilité annuelle. Ces tendances prévues pour le XXI<sup>e</sup> siècle rendent donc la région méditerranéenne particulièrement vulnérable d'un point de vue du changement climatique. De plus, les récentes projections réalisées pour l'Europe dans

le cadre de EURO-CORDEX<sup>1</sup> avec des modèles climatiques régionaux avec une résolution horizontale de 12.5 km montrent que les précipitations intenses pourraient augmenter dans la région, ceci malgré une diminution des précipitations en moyenne (Jacob *et al* 2014). Bien qu'ayant beaucoup progressé au cours des dernières années, tant en résolution qu'en représentation des processus, les modèles de climat ont encore beaucoup de difficultés à rendre compte avec un niveau de réalisme et de confiance suffisant des événements convectifs intenses.

Un programme de recherche international dédié à la Méditerranée a débuté en 2010 et s'étendra jusqu'en 2020. Il a pour objectif de mieux comprendre les différents processus relevant du cycle de l'eau en Méditerranée ainsi que les problématiques de la ressource en eau et la conséquence du changement climatique dans la région. Un volet de ce programme international a été consacré à l'étude des événements à fort impact (fortes précipitations et vents forts). Une vaste campagne de mesures dédiée aux fortes précipitations et aux crues-éclairs a eu lieu à l'automne 2012 (SOP1) sur tout le pourtour méditerranéen Nord-Occidental (Espagne, Italie, France). 16 périodes d'observations intensives (POI) ont été organisées. Des mesures aéroporées, en mer et sur terre ont pu être réalisées au cours de ces POI. La stratégie d'observations mise en place visait notamment à mieux documenter l'écoulement amont et les structures précipitantes. Ce jeu de données est unique et novateur car il va permettre de valider les modèles et confirmer ou infirmer certaines hypothèses.

Ce mémoire fait la synthèse de mes travaux de recherche et est organisé en trois grandes parties. Ma contribution à l'amélioration des connaissances des systèmes fortement précipitants méditerranéens est décrite dans la première partie du manuscrit. La démarche que j'ai utilisée au cours de ces différents travaux repose sur l'utilisation des modèles atmosphériques de méso-échelle comme laboratoire numérique, en s'appuyant sur des expériences réelles et/ou idéalisées, des expériences de sensibilité et des diagnostics adaptés à l'étude de la convection. Ces travaux ont été réalisés en partie dans le cadre de la thèse d'Emilie Bresson que j'ai co-dirigée et de la thèse en cours de Maxime Martinet.

La régionalisation climatique des systèmes précipitants en région méditerranéenne a été un autre axe dans mes activités de recherche. Dans une seconde partie, je résume mes activités de recherche axées sur la question de l'évolution possible des événements de pluie intense touchant les régions voisines de la Méditerranée dans leur fréquence, leur intensité et leur localisation préférentielle. J'ai contribué au développement d'une méthode originale de descente d'échelle statistico-dynamique tirant profit à la fois des connaissances acquises sur les systèmes fortement précipitants et des outils de modélisation à haute résolution. Ces travaux ont été réalisés en partie dans le cadre du séjour post-doctoral de Anne-Lise Beaulant que j'ai co-dirigé.

Enfin dans une troisième et dernière partie sont présentés ma recherche et les travaux exploratoires visant à étudier la prévisibilité à l'échelle convective et à identifier les différentes sources d'incertitude pesant sur les prévisions du modèle AROME. Leur importance est évaluée par des approches en prévision d'ensemble dédiées à l'échelle convective, ceci pour déterminer au mieux la configuration du futur système opérationnel. Ces travaux ont été réalisés en partie dans la cadre de la thèse de Benoît Vié que j'ai co-dirigée.

Ces travaux ont contribué à la définition de la stratégie d'observation de la période d'observation Spéciale (SOP1) de la campagne HyMeX, et celle-ci a fourni en retour le cadre pour le développement et l'évaluation d'outils numériques pour la prévision des pluies intenses et des crues rapides.

---

1. World Climate Research Program Coordinated Regional Downscaling Experiment

## 2.2 Connaissance et modélisation des systèmes précipitants intenses

Dans cette partie, je décrirai les différentes contributions de mes travaux de recherche à la connaissance des systèmes précipitants intenses sur la base de la modélisation numérique. Nous y verrons, dans une première partie, les résultats marquants pour les cyclones tropicaux, puis l'apport en terme de connaissances sur les épisodes de pluie intense en Méditerranée.

### 2.2.1 Connaissance et modélisation à méso-échelle des cyclones tropicaux

#### Une filière d'initialisation pour les cyclones tropicaux

La question de la sensibilité des simulations ainsi que la prescription de l'état initial pour les modèles de méso-échelle sont des problématiques auxquelles je me suis tout d'abord intéressé lors de mon travail de thèse sur la modélisation des cyclones tropicaux avec le modèle Meso-NH. C'est à cette occasion qu'une filière d'initialisation dédiée a été développée pour la modélisation des cyclones tropicaux à méso-échelle.

Les toutes premières simulations de cyclones tropicaux à l'aide de modèles de nuage ont débuté vers les années 1960 avec des modèles 2D simplifiés à symétrie axiale. Anthes (1972) fut le premier à mettre en évidence les structures asymétriques d'un cyclone en utilisant un modèle 3D hydrostatique avec une résolution de 30 km et des paramétrisations sophistiquées pour l'époque de la microphysique, de la turbulence et des flux de surface entre autres. Des modèles à domaines imbriqués (*gridnesting*) permettant de résoudre à la fois la structure du cyclone et son interaction avec l'environnement se sont développés par la suite. Les résultats issus d'une simulation numérique d'un cyclone réel ont été publiés pour la première fois par Liu *et al* (1997). Ils simulaient les structures internes et l'évolution du cyclone Andrew (1992) avec le modèle 3D non-hydrostatique MM5 à 3 domaines imbriqués 54, 18 et 6 km de résolution horizontale. Lorsqu'il s'agit de situations réelles, les modèles 3D de nuage sont initialisés à partir de champs provenant d'analyses de modèles globaux. Si ces analyses de grande échelle sont relativement bien adaptés pour la description du contexte synoptique à l'intérieur duquel évolue le cyclone, leur résolution horizontale (T319 soit environ 60 km avant 2000) ne permettait pas en revanche de représenter correctement la partie la plus active du cyclone. Ces analyses dépeignaient le plus souvent une circulation cyclonique mal localisée, de faible intensité, d'extension horizontale trop importante et de développement vertical limité. Diverses méthodes, basées sur l'assimilation d'un bogus vortex en vent et pression, ont ainsi été proposées dans la littérature afin de corriger le tourbillon cyclonique initial. Cependant, tous les modèles 3D non-hydrostatique à domaines emboités ne disposaient pas d'une méthode variationnelle nécessaire à la minimisation de la fonction coût définie dans ces méthodes assimilant un bogus vortex, comme par exemple le modèle Meso-NH.

Afin de disposer de conditions initiales plus adaptées à la simulation à méso-échelle de cyclones tropicaux, j'ai été donc amené à développer une filière d'initialisation tout à fait originale combinant l'utilisation de données de radars météorologiques Doppler en synergie avec des données dropsondes pour la simulation numérique de cyclones avec le modèle Meso-NH. Cette méthodologie a été nommée RDVC (**Radar Dropwindsonde Vortex Conditioning**) et fait l'objet d'un article publié au *Q. J. R. Meteorol. Soc.* (Nuissier *et al.*, 2005).

La méthode RDVC est constituée d'une procédure de filtrage adapté des analyses de grande échelle (Kurihara *et al.*, 1993 ; Kurihara *et al.*, 1995), d'un pré-traitement analytique de champs cycloniques équilibrés de vent et de température (Roux *et al.*, 2004) à partir d'observations par radar météorologique – pour inclusion dans l'analyse. La Figure 2.1 montre l'application de

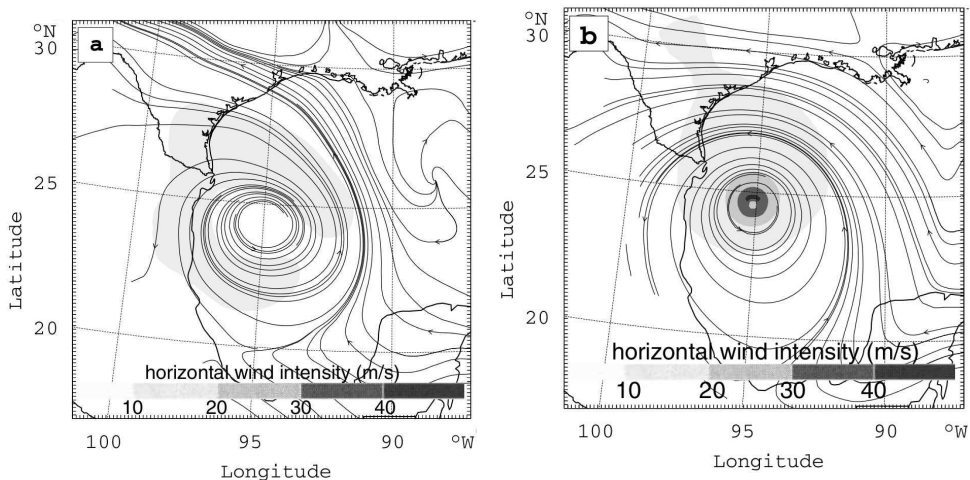


FIGURE 2.1 – a) Module et direction du vent horizontal à 850 hPa (zones grisées et lignes de flux) issus de l’analyse du ECMWF à 0000 UTC le 22/08/1999 ; b) comme a) après inclusion du vortex cyclonique déduit des observations par radar Doppler. D’après Nuissier *et al* (2005).

cette méthode au cas du cyclone Bret (1999) sur le Golfe du Mexique. Le module du vent horizontal à 850 hPa le 22/08/1999 issu de l’analyse du ECMWF à 0000 UTC présente un maximum de l’ordre de  $10\text{--}12 \text{ m s}^{-1}$  et à près de 200 km du centre du cyclone, très inférieur aux valeurs observées (Fig. 2.1a). Après inclusion du vortex cyclonique déduit des observations par radar Doppler (Fig. 2.1b), on obtient une perturbation cyclonique beaucoup plus intense et une structure des vents plus conforme aux observations, avec un vent de l’ordre de  $50 \text{ m s}^{-1}$  localisé à environ 30 km du centre de la circulation. De plus le biais sec présent en moyenne troposphère dans l’analyse du ECMWF à 0000 UTC (Fig. 2.2b) est corrigé grâce aux observations par dropsondes larguées depuis le G-IV de la NOAA dans l’environnement du cyclone Bret (Fig. 2.2a et c).

#### Impact de l’inclusion d’un vortex cyclonique réaliste

Une série de 3 expériences de sensibilité a été menée pour lesquelles le faible vortex analysé a tout d’abord été intégré à une résolution horizontale de 15 km (expérience CTL). Ce test de référence a montré ses limites puisque le cyclone simulé par Meso-NH se déplace rapidement vers l’ouest durant les 6 premières heures de simulation avant que sa trajectoire ne s’infléchisse vers le Nord-Ouest et le dirige vers les terres (Fig. 2.3a). L’erreur de prévision sur le point d’impact est de 140 km au sud de l’observation pour une période de simulation de 18 heures avec une intensité finale n’excédant pas  $20 \text{ m s}^{-1}$ .

En revanche, en incluant un vortex initial plus réaliste (taille et intensité) déduit des observations radar et en conservant une résolution horizontale de 15 km, les caractéristiques du cyclone simulé sont considérablement améliorées (expérience low-RDVC). Les meilleurs résultats sont obtenus en procédant à une simulation imbriquée du vortex cyclonique radar jusqu’à une résolution horizontale de 1.7 km (High-RDVC). Les vents moyens atteignent alors  $70 \text{ m s}^{-1}$  et une pression centrale de 946 hPa le 22/08 à 1800 UTC (non montré), soit des caractéristiques très proches des observations (Fig. 2.3a). Les réflectivités radar simulées par le modèle Meso-NH reproduisent relativement bien la structure précipitante associée à la région centrale

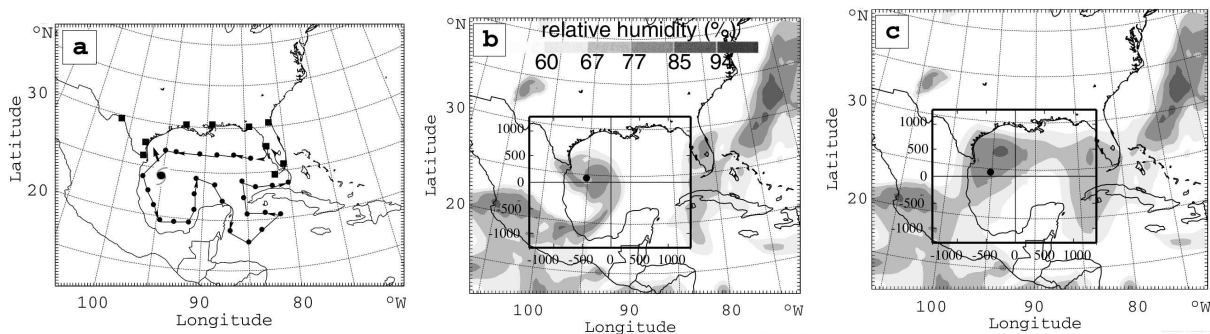


FIGURE 2.2 – **a)** Dropsondes larguées depuis le Gulfstream IV-SP de la NOAA entre 1751 UTC le 21/08/1999 et 2100 UTC le 22/08/1999 (points noirs) et positions des radiosondages (carrés noirs) disponibles à 0000 UTC le 22/08/1999 le long des côtes du golfe du Mexique ; **b)** humidité relative entre 700 et 400 hPa issue de l’analyse du ECMWF à 0000 UTC le 22/08/1999, **c)** la même humidité relative modifiée par une analyse incluant les données dropsondes.

de l’ouragan Bret à son arrivée sur la région de Brownsville (Texas, USA), avec un maximum de 40-50 dBZ associé à de la convection profonde dans le quadrant Sud-Ouest du cyclone (Fig. 2.3b et c).

En raison d’une structure verticale du vortex initial mal définie dans l’expérience CTL, les interactions entre le cyclone et son environnement sont mal appréhendées, ce qui a un impact sur l’évolution et la trajectoire du cyclone. Le fait que des meilleurs résultats soient obtenus avec l’expérience low-RDVC vont tout à fait dans le sens des résultats obtenus par Xiao *et al* (2000) par exemple à partir de simulations numériques du cyclone Fran (1996). Ils montrent que les cyclones avec un grand rayon de vent maximum adoptent préférentiellement une trajectoire plus rapide vers l’Ouest, car étant plus sensibles aux conditions dans les basses couches troposphériques. La comparaison des expériences low-RDVC et high-RDVC révèle également la sensibilité du modèle vis-à-vis de la résolution horizontale. A 1.7 km de résolution (high-RDVC), le modèle est capable de simuler explicitement la convection profonde et les processus diabatiques associés dans la région du mur de l’oeil du cyclone<sup>2</sup> qui jouent un rôle important dans l’intensification et l’évolution du cyclone.

#### Importance des structures asymétriques dans le cyclone

Une analyse détaillée du mouvement asymétrique dans la région du mur de l’oeil du cyclone, a aussi mis en évidence, de manière transitoire, des tourbillons de petite échelle ou “inner gyres”, dont la présence affecte particulièrement l’intensité et la propagation du cyclone. Pour le cas du cyclone Bret (1999), il a été mis en évidence une structure type onde de Rossby d’ordre 2, avec deux paires de tourbillons cycloniques et anticycloniques (Fig. 2.4a). Ces tourbillons résultent probablement de l’interaction entre la convection profonde dans le mur de l’oeil et des instabilités liées à la dynamique interne du cyclone (ondes de Rossby). Ces structures de l’oeil polygonales sont fréquemment observées à l’intérieur des phénomènes cycloniques les plus intenses, comme ce fut lors de l’évolutin du cyclone Isabel (2005) sur l’Atlantique par exemple (Fig. 2.4b). Dans mes travaux de thèse, il a été trouvé que ces “inner gyres”, en plus d’être as-

2. Il s’agit de la zone de vent violent entourant la région de l’oeil du cyclone large de 10 à 100 km et composé d’épais nuages type *cumulonimbus* pouvant atteindre 15 km d’altitude.

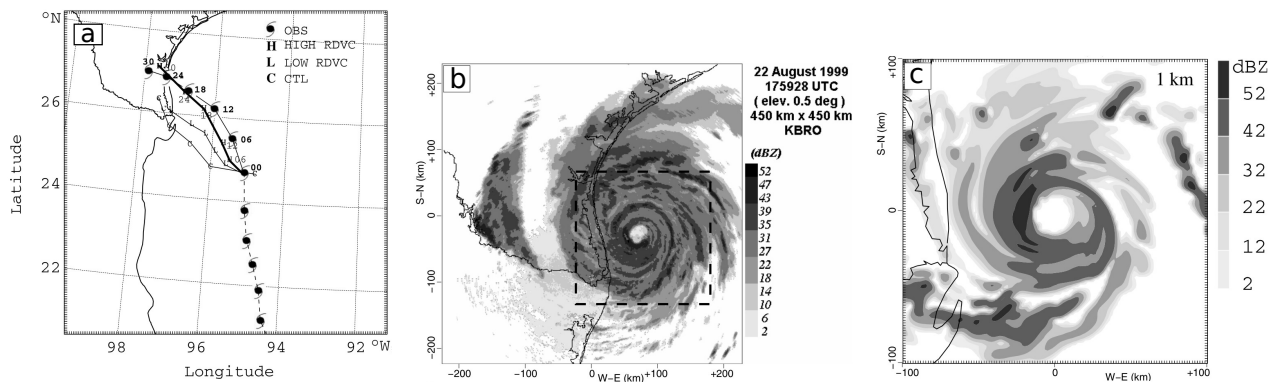


FIGURE 2.3 – a) Analyse “best-track” du cyclone *Bret* (OBS) toutes les 6 h à partir de 1800 UTC le 20/08/1999 et des cyclones simulés pour les expériences CTL (C), Low-RDVC (L), High-RDVC (H) de 0000 UTC le 22/08 à 0600 UTC le 23/08. b) Réflectivités radar à 0.5°d’élévation sur un domaine de 450 km x 450 km observées par le radar du réseau WSR-88D de Brownsville (Texas, USA) à 1759 UTC le 22/08/1999 (les lignes tiretées représentent le domaine de c)) ; c) réflectivités radar simulées à 1 km d’altitude pour l’expérimentation High RDVC sur un domaine de 200 km x 200 km à 1900 UTC le 22/08/1999.

sociés à de significatifs mélanges horizontaux entre le mur de l’œil et l’œil , modulent le flux de grande échelle dans la partie centrale du cyclone. Il semble exister une bonne corrélation entre la présence de ces tourbillons dans la région du mur de l’œil et les écarts observés entre la propagation et le flux de commande<sup>3</sup>. D’autre part, ces tourbillons internes provoquent une intensification locale de la convergence du vent qui favorise la génération de mouvements ascendants et donc de nuages type *cumulonimbus* les plus développés, associé aux vents horizontaux les plus violents susceptibles de créer les dégâts les plus importants. Kossin and Schubert (2004) retrouvent des résultats allant dans ce sens pour le cyclone Isabel (2003) sur l’Atlantique.

Cette étude a montré que la modélisation réaliste des processus associés à la dynamique interne d’un cyclone tropical passe par l’utilisation d’un maillage horizontal proche du kilomètre. Cette forte résolution horizontale permet, *de facto*, de simuler une structure précipitante et une interaction avec son environnement les plus réalistes possible. Cette méthode RDVC semblait également prometteuse, avec même une vocation opérationnelle, notamment grâce à l’exploitation d’observations de cyclones par des radars météorologiques Doppler côtiers. Dernièrement Jolivet *et al* (2013) ont repris et revisité la méthode RDVC afin de l’adapter à l’étude de l’influence de l’île de la Réunion avec le cyclone Dina (2002), qui avait bénéficié pour la première fois d’une couverture radar Doppler sol remarquable lors de son passage à proximité immédiate de l’île. L’élaboration de nouvelles paramétrisations dans le modèle Meso-NH, notamment la prise en compte du couplage avec une couche océanique mélangée, ont aussi grandement contribué à améliorer les résultats obtenus à l’époque. Cette approche d’inclusion d’un vortex cyclonique corrigé dans les analyses de plus grande échelle a été reprise lors d’un séjour post-doctoral à RSMAS/MPO à l’Université de Miami (Floride, USA) en 2004. J’ai travaillé plus précisément sur l’utilisation de données satellite (vents de surface dérivés du sa-

3. La propagation d’un cyclone tropical est conditionnée par le vent moyen entre deux niveaux de troposphère. Bien que les basses couches soient plus influentes, plus un tourbillon cyclonique s’intensifie et plus celui-ci devient sensible à la moyenne et haute troposphère. En première approximation le flux de commande pour un cyclone d’intensité modérée est donné par le vent moyen entre 400 et 850 hPa.

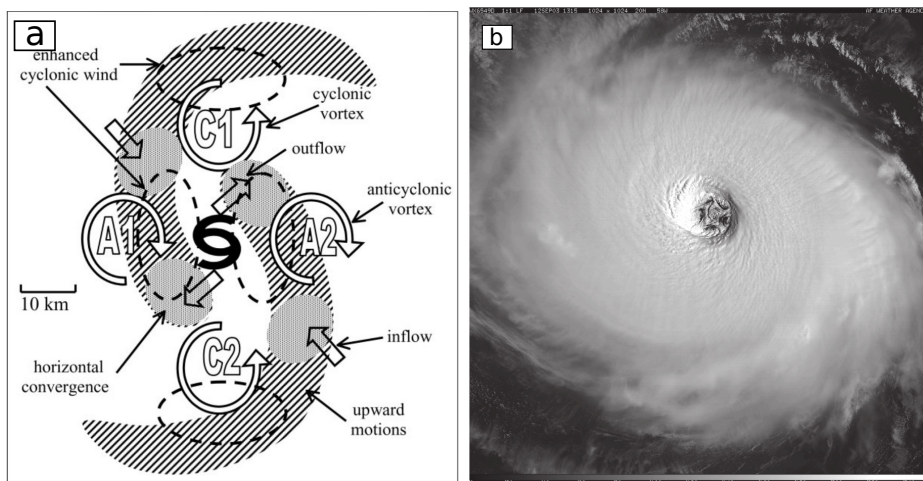


FIGURE 2.4 – a) Représentation schématique des perturbations de vent horizontal et vertical induites par la présence d'une structure type onde de Rossby d'ordre 2 dans la région du mur de l'oeil du cyclone Bret. D'après Nuissier *et al* (2005) ; b) image satellite visible issue de GOES-12 du cyclone Isabel (2003) à 1315 UTC le 12/09/2003.

tellite Quicksat) et de données dropsondes dans le schéma d'assimilation du modèle couplé océan-atmosphère non-hydrostatique à méso-échelle MM5.

Enfin ces résultats obtenus dans le cadre de mes travaux de thèse m'ont fait prendre conscience de la forte sensibilité des perturbations cycloniques tropicales vis-à-vis des conditions initiales à plus fine échelle et de la représentation des processus liés au cycle de l'eau. Cette question de la sensibilité des simulations s'est également retrouvée au coeur des travaux que j'ai par la suite menés sur les épisodes de pluie intense en Méditerranée.

## 2.2.2 Connaissance et modélisation des orages stationnaires des régions méditerranéennes

facteurs

### Simulations non-hydrostatiques de cas réels

Comme pour les cyclones tropicaux, les années 1990 ont vu l'émergence de nouvelles procédures d'initialisation sophistiquées des modèles de nuages pour simuler de manière réaliste des systèmes convectifs en général, à partir de données réelles. Les méthodes utilisant des perturbations académiques types "bulles chaudes ou froides" superposées à un champ initial homogène déduit d'un radiosondage ou utilisant des analyses de grande échelle ont progressivement fait place à des techniques d'initialisation permettant d'introduire des informations utiles pour une meilleure simulation du système convectif. Les travaux de Lin *et al* (1993), Sun and Crook (1997,1998), Bielli and Roux (1999), entre autres, proposent de combiner des variables restituées d'observations par radar Doppler à un état de base issu d'un radiosondage. Bielli and Roux (1999) concluent que, mise à part la structure tridimensionnelle du champ de vent, le paramètre le plus important est la description du champ initial d'humidité. Ducrocq *et al* (2000,2002) vont plus loin et proposent une technique d'initialisation statique basée sur une

analyse par interpolation optimale des données de surface et un ajustement de l'humidité et des variables microphysiques. La pré-analyse des zones nuageuses et précipitantes réalisée grâce aux réflectivités radar et aux températures de brillance infra-rouge permet d'introduire à la fois une information sur la présence d'un système convectif et un environnement de méso-échelle compatible avec ce dernier. Ducrocq *et al* (2002) ont étudié deux cas de systèmes convectifs sur le nord de la France, deux cas de systèmes orageux quasi-stationnaires ancrés sur les contreforts des reliefs du Massif Central et le cas des crues catastrophiques de l'Aude des 12-13 novembre 1999. Pour le cas de la crue-éclair extrême de 1999, les résultats sont améliorés en augmentant la résolution horizontale du modèle de prévision même en partant de conditions initiales issues de modèles de prévisions à l'échelle globale. Par contre, pour les quatre autres cas, l'état de base du modèle doit être impérativement modifié et amélioré via la procédure d'initialisation décrite plus haut. La description du champ d'humidité initial (saturation des tours convectives et quasi-saturation des basses couches) est cruciale.

La méthode d'initialisation statique de Ducrocq *et al* (2000), a été évaluée sur deux cas de systèmes convectifs dans les travaux de thèse de Didier Ricard (Ricard, 2002). Les résultats ont montré que les champs de précipitations simulés par le modèle Meso-NH étaient significativement améliorés par rapport aux prévisions opérationnelles de l'époque. Cette étude a également montré les ingrédients favorables au développement de systèmes quasi-stationnaires sur orographie : (i) la convergence de basses couches associée à un flux de contournement des Alpes et à un flux de sud longeant les côtes espagnoles, amène la saturation des basses couches de l'atmosphère et la formation des premières cellules convectives et (ii) le forçage orographique permet de libérer l'instabilité convective. Les fines structures du relief influent sur l'intensification des cellules, sur leurs trajectoires et la distribution spatio-temporelle des cumuls de précipitations.

La question scientifique importante à mon arrivée en séjour post-doctoral au CNRM de Météo-France, dans le cadre du projet intégré du 6ème Programme Cadre Européen FLOOD-site, était de déterminer ce qui différencie les événements précipitants exceptionnels des cas plus classiques d'un point des ingrédients météorologiques favorables. Il s'agissait alors d'identifier les processus atmosphériques sur un échantillon plus large de situations pluvieuses intenses du pourtour Méditerranéen.

Dans cette optique la modélisation numérique à l'échelle kilométrique et sub-kilométrique a été utilisée comme un laboratoire numérique, dans les travaux de recherche que j'ai ménés ou encadrés, afin d'étudier les ingrédients propices à la formation de systèmes convectifs quasi-stationnaires sur le Sud-Est de la France. La procédure d'initialisation décrite dans Ducrocq *et al* (2002) a été appliquée à différents cas de systèmes convectifs et plus précisément sur des cas de systèmes convectifs quasi-stationnaires méditerranéens : le cas des inondations de l'Aude des 12-13 novembre 1999, la catastrophe du Gard des 8-9 septembre 2002 et un cas moins exceptionnel, mais typique des épisodes Cévenols, le cas des 13-14 octobre 1995. Deux articles publiés au *Q. J. R. Meteorol. Soc.* (**Nuissier et al 2008 ; Ducrocq et al 2008**) font la synthèse des ingrédients météorologiques conduisant au caractère stationnaire de ces trois événements de pluies intenses sur le Sud-Est de la France.

Ces travaux sur la connaissance des systèmes orageux méditerranéens à faible mobilité se sont également inscrits dans le cadre de la thèse d'Emilie Bresson que j'ai co-dirigée (**Bresson, 2011**). L'objectif de cette thèse était, dans une première partie, d'explorer plus systématiquement les relations entre les caractéristiques de l'environnement à méso-échelle et la localisation et l'intensité des systèmes convectifs et les mécanismes de soulèvement et d'entretien de la convection (**Bresson et al 2012**). Dans une seconde partie nous avons voulu confronter ces résultats au cas des pluies exceptionnelles du 15 Juin 2010 sur le Var pour savoir si le système

convectif quasi-stationnaire sur le Var était généré par des mécanismes de soulèvement similaires. J'ai également participé à l'étude des mécanismes impliqués dans le déclenchement et le maintien d'un système convectif sur mer observé le 26 octobre 2012 durant la Période d'Observation Intense 16a (POI16a) de la SOP1 de la campagne HyMeX.

#### Rôle du relief et du dôme froid sous orages

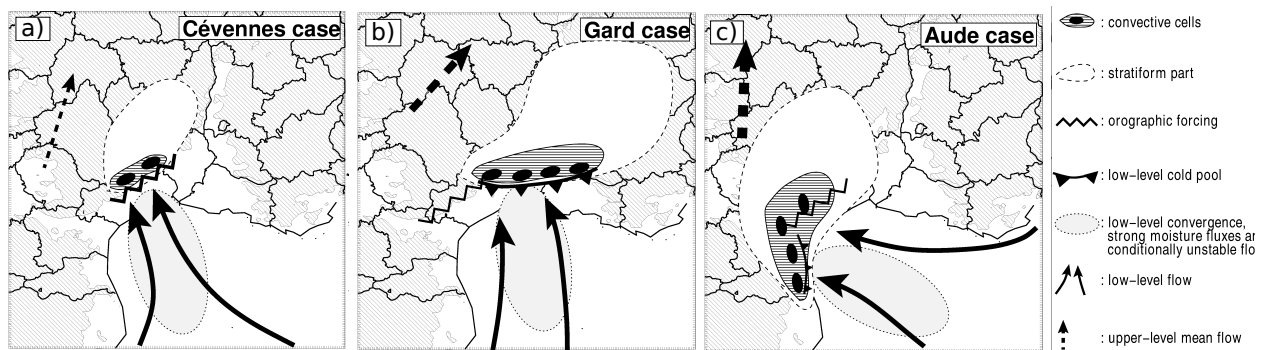


FIGURE 2.5 – Synthèse des ingrédients propices à la formation des systèmes convectifs quasi-stationnaire du a) 13-14 octobre 1995 (cas Cévennes), b) 8-9 septembre 2002 (cas Gard) et c) 12-13 novembre 1999 (cas Aude). D'après Ducrocq et al (2008).

Les facteurs propices à la production de forts cumuls de précipitation, à la fois dans l'environnement d'échelle synoptique et à méso-échelle, ont été mis en évidence pour les trois situations mentionnées plus haut. Ces caractéristiques de l'environnement sont communes à celles décrites par Lin *et al* (2001) pour les situations de pluie intense sur zones montagneuses dans d'autres régions du globe (présence d'un thalweg d'altitude, un flux de basses couches très humide d'intensité modérée à forte venant buter contre la zone de relief, un flux conditionnellement instable en amont des contre-forts des reliefs, une situation évoluant lentement,...).

Sur la base d'expériences de sensibilité et d'outils diagnostiques telles que les rétrotrajectoires de particules lagrangiennes, nous avons mis en évidence les rôles du forçage orographique, de la convergence de basses couches ou encore d'un dôme d'air froid sous orages comme des sources potentielles de soulèvement souvent impliqués dans les événements précipitants en Méditerranée. La Fig. 2.5a illustre que le relief est le principal responsable du soulèvement du flux, par forçage orographique, dans le cas où le système convectif est situé sur les contreforts des Cévennes. Une expérience de sensibilité, dans laquelle le relief du Massif Central a été rasé, nous a permis de montrer que celui-ci jouait un rôle essentiel dans le blocage de la zone d'instabilité convective et sa libération par forçage orographique (Fig. 2.6a).

Lors d'épisodes plus atypiques, comme celui du Gard des 8-9 septembre 2002, le maximum de précipitations se positionne en amont des reliefs. Un dôme froid (ou "cold pool") intense ancré sur les plaines devient un facteur essentiel de stationnarité et de soulèvement de la masse d'air instable. Ce dôme froid est le résultat du refroidissement associé à l'évaporation des précipitations liquides chutant dans les régions sous-saturées de la basse troposphère et dans une moindre mesure de la fonte et de la sublimation d'une partie des précipitations solides. Il implique des chutes de 3 à 4 °C, sur une distance de 10 à 30 km et celui-ci force, à son tour, l'air chaud et humide de basses couches au soulèvement sur son bord d'attaque. En septembre 2002

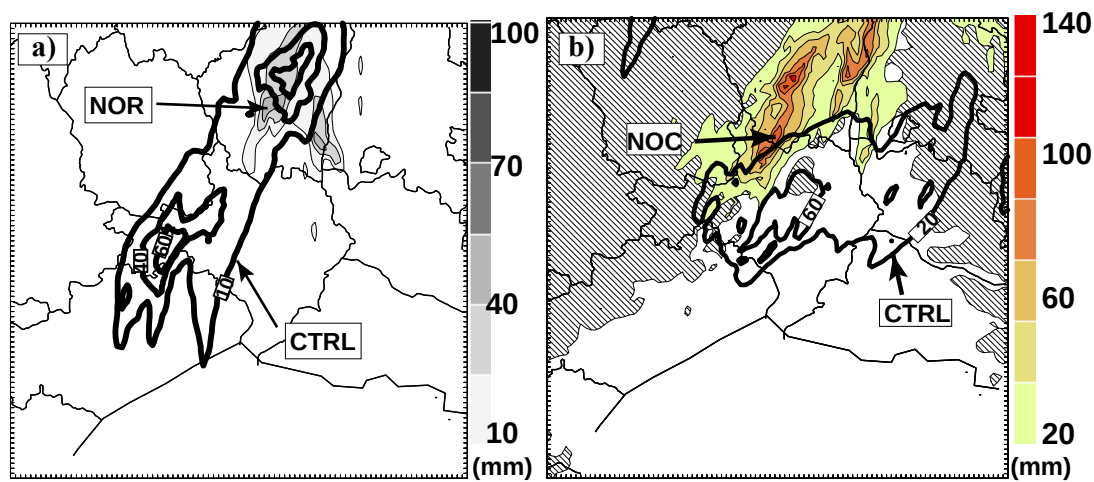


FIGURE 2.6 – a) Précipitations simulées cumulées entre 00 et 06 UTC le 14 oct. 1995 pour l’expérience sans Massif Central (NOR, grisé) et la simulation de contrôle (CTRL, isolignes), b) précipitations simulées cumulées entre 18 et 22 UTC le 8 sept. 2002 pour l’expérience sans le refroidissement associé à l’évaporation des précipitations liquides (NOC, couleurs) et la simulation de contrôle (CTRL, isolignes). D’après Ducrocq et al (2008).

dans le Gard par exemple, les gradients thermiques associés à la plage froide sous orages atteignaient même 5 à 7 °C. D’ailleurs, si on supprime le refroidissement associé à l’évaporation des précipitations liquides dans la simulation numérique (Fig. 2.6b), le système ne se positionne plus durablement sur les plaines gardoises mais sur les contreforts Cévenols. De plus, si les reliefs du Massif Central ou des Alpes sont "rasés" (non montré ici), le dôme froid n’est plus bloqué dans la vallée du Rhône et dérive vers le Nord, et avec lui l’activité pluvio-orageuse.

D’autre part, les reliefs voisins (Alpes, Pyrénées) jouent également un rôle important en déviant et en canalisant le flux de basses couches, produisant ainsi de la convergence de basses couches en amont du Massif Central (Fig. 2.5). Les Alpes ont ainsi tendance à dévier le flux de sud, induisant ainsi de la convergence de basses couches. Ce contournement aux Alpes est exacerbé par un environnement plus sec ou un flux amont plus lent (Bresson et al (2012)). Cette convergence de basses couches peut permettre le déclenchement de la convection en amont du relief, sur plaine voire même sur mer.

Bresson (2011) a montré également dans sa thèse que les inondations lors du cas exceptionnel de Draguignan de juin 2010 étaient conditionnées par deux branches d’alimentation en air marin de basses couches humide et conditionnellement instable de composante est à sud-est convergent vers le Var, favorisant alors la convection sur le littoral et sur mer. Un courant de densité se développe et s’intensifie sous les précipitations du système et aide à la stationnarité du système sur le Var. Le relief moyen des Alpes permet quant à lui de canaliser dans la vallée du Rhône un flux de nord qu’on retrouve sur le Golfe de Lion, et aussi, de dévier le flux d’est dans le Golfe de Gênes. Le courant de densité au nord du Var est également alimenté par ce flux de nord qui franchit les Alpes. Les bas reliefs escarpés des massifs des Maures, et dans une moindre mesure du massif de l’Estérel, déclenchent de la convection. Ces structures orographiques fines bloquent le refroidissement sous orages dans la vallée de l’Argens et le canalisent entre les massifs des Maures et de la Sainte-Baume.

Ces mécanismes de soulèvement soit par dôme froid sous orages ou par la convergence de

basses couches ont également été mis en évidence pour des cas observés durant la SOP1 de la campagne HyMeX, et expliquent notamment le déclenchement et le maintien d'un système convectif sur mer observé le 26 octobre 2012 (POI16a). Lors de cet épisode fortement précipitant, le système convectif était alimenté durant son évolution au-dessus de la Méditerranée par une masse d'air humide et conditionnellement instable, advectée par un jet de basses couches de sud-est. La convergence entre deux flux de basses couches sur mer de composantes sud-est et sud-ouest respectivement est le facteur qui déclenche perpétuellement un train de cellules maintenant le système convectif (Duffourg *et al.*, 2015). Un minimum de pression se formant dans le sillage sous le vent des reliefs espagnols, associé à un thalweg d'altitude plus à l'ouest, contribue à établir et renforcer cette convergence de basses couches.

Les différents mécanismes de soulèvement que sont le relief et le dôme froid sous orages ont été mise en évidence en utilisant principalement une résolution horizontale de 2.5 km. Cependant, des expériences ont été réalisées en augmentant la taille de la grille du modèle à 500 m. Pour certains cas, comme celui de Draguignan de juin 2010 par exemple, l'utilisation d'un domaine à 500 m de résolution améliore sensiblement les simulations car elle apporte une description plus fine des petits reliefs qui sont essentiels dans le déclenchement des premières cellules convectives.

Cependant, pour d'autres cas comme celui du système convectif sur mer lors de la POI16a de HyMeX, les résultats sont plus contrastés et la prévision apparaît même dégradée par rapport à la résolution de 2.5 km. Dans la thèse de Maxime Martinet (démarrée à l'automne 2014) que je co-dirige, nous avons montré que les simulations du système convective de la POI16 est fortement sensible à la représentation de certains paramètres de la turbulence comme la longueur de mélange. Outre un effet des processus turbulents au sein même des nuages orageux, il y a un impact significatif sur le dôme froid sous orages qui se maintient plus difficilement lorsque le mélange turbulent est plus prononcé. Cet impact sur le dôme froid sous orages conduit à des cumuls de précipitations au sol très différents.

#### *Lien entre mécanismes de soulèvement et caractéristiques du flux amont et environnement*

Nous avons vu précédemment le rôle crucial joué par le dôme froid sous orages dans le soulèvement des masses d'air humides et instables. La prévision de l'occurrence d'un dôme froid (et son ancrage éventuel) demeure problématique et anticiper un régime fortement précipitant sur les pentes au vent du relief ou alors plus en amont sur plaine revêt un enjeu particulièrement crucial. Le dôme froid sous orages devient alors un facteur aggravant quant à la mise en place d'un événement fortement précipitant sur les régions de plaine et/ou littorales impactant plus durement les populations.

Pour donner des éléments de réponse quant à l'apparition de tel ou tel type de régime précipitant, une partie de la thèse d'Emilie Bresson a été consacrée à l'étude du comportement d'un flux conditionnellement instable venant buter contre un relief. Il s'agit de déterminer les conditions météorologiques favorisant soit : (i) l'émergence d'un dôme froid sous orages (régions de plaine plus touchées dans ce cas) ou alors (ii) un forçage orographique direct, faisant déplacer les zones précipitantes en aval en direction des contreforts des reliefs.

Parmi les travaux antérieurs à la thèse d'Emilie Bresson, Chu et Lin (2000) puis Chen et Lin (2005a) ont été parmi les premiers à simuler ces régimes précipitants. Sur la base d'expériences numériques et d'hypothèses simplificatrices (relief 2D, écoulement uniforme), ils simulent des régimes précipitants ne dépendant que de l'instabilité convective (CAPE<sup>4</sup>) ou de la vitesse du flux amont et de la hauteur caractéristique du relief (Fig. 2.7a).

4. Convective Available Potential Energy

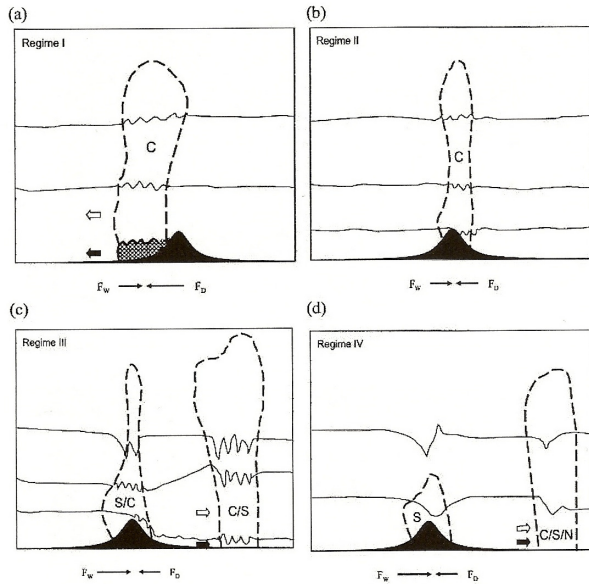


FIGURE 2.7 – Récapitulatif des quatre régimes précipitants, dépendant de deux paramètres de contrôle : le nombre de Froude humide et la CAPE. Les flèches  $F_w$  et  $F_D$  correspondent respectivement à l'intensité du flux amont et celle du courant de densité. Les lettres C, S et N qualifient le type nuageux des système précipitant (C pour convectif, S pour stratiforme, N pour autre type). Les flèches blanches font référence à la direction de propagation du système précipitant, les noires à celle du courant de densité. D'après Chen et Lin (2005a)

Miglietta et Rotunno (2009, 2010) approfondissent ces résultats dans un cadre cette fois tri-dimensionnel dans lequel le relief est représenté par une montagne bi-dimensionnelle. Les auteurs concluent que, outre l'instabilité convective et la vitesse du flux amont, les régimes précipitants étaient également pilotés par l'intensité du forçage orographique, en partie contrôlée par la morphologie du relief et la capacité de ce dernier à soulever les masses d'air au-delà de la couche d'inhibition convective (CIN<sup>5</sup>)

Cependant, les études numériques idéalisées décrites plus haut présentent des limitations. En effet, le relief 2D ou 3D, considéré dans ces travaux est un unique massif idéalisé, qui par conséquent ne rend pas compte de la complexité de l'orographie de la Méditerranée Nord-Ouest avec ses trois chaînes montagneuses principales (Pyrénées, Alpes et Massif Central). De plus, le gradient horizontal d'humidité et de vent n'est pas pris en compte, ni les échanges entre la mer et l'atmosphère ou le transport de l'air chaud et humide par le flux amont marin.

Pour ces différentes raisons, Bresson (2011) a repris et amélioré, dans le cadre de sa thèse, un protocole numérique idéalisé dans lequel on impose un flux humide de basses couches butant contre les Cévennes, mais avec un vent plus lent et plus sec sur son bord (Fig. 2.8a). A cela, nous voulions ajouter la topographie réelle du Sud-Est de la France, avec ses trois massifs principaux et la mer Méditerranée. Ce cadre expérimental avait été développé au CNRM par Bresson *et al* (2009) et De Saint-Aubin (2008). L'objectif de cette partie de la thèse d'Emilie Bresson était d'explorer plus systématiquement les relations entre les caractéristiques de l'environnement

5. Convective INhibition

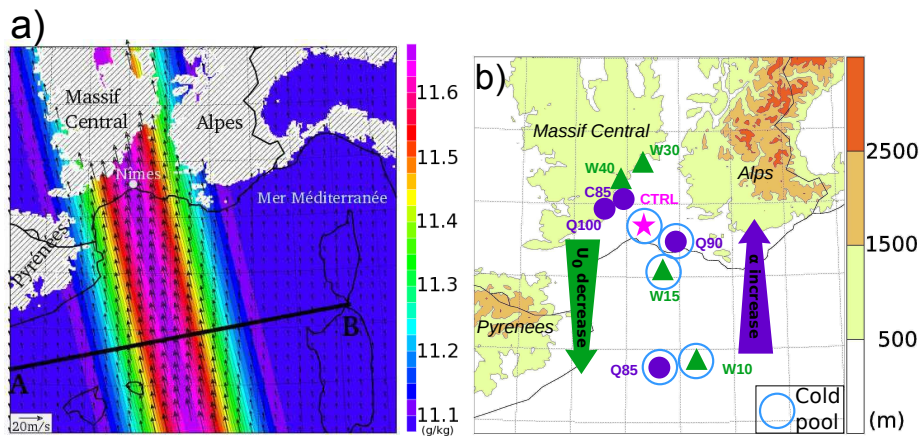


FIGURE 2.8 – a) Conditions initiales pour la simulation de référence (CTRL) en terme de rapport de mélange en vapeur d'eau à 500 m d'altitude (couleurs,  $g\ kg^{-1}$ ) et de vent horizontal à 500 m d'altitude. b) Positions préférentielles des maxima de pluies simulées pour la simulation de référence (étoile), les expériences de sensibilité au vent du flux amont (triangles) et à l'humidité de l'environnement (points). Les cercles indiquent l'occurrence de dôme froid stationnaire dans la simulation. D'après Bresson et al (2012).

et la localisation et l'intensité des systèmes orageux quasi-stationnaires sur la région. Un article publié au *Q. J. R. Meteorol. Soc.* (Bresson et al 2012) fait la synthèse des résultats obtenus.

Deux régimes de systèmes précipitants ressortent de notre étude : (i) les systèmes généralement les plus précipitants, centrés sur les zones de relief et associés à un forçage orographique direct (**régime I**) et (ii) ceux en amont des reliefs (sur plaine ou sur mer), avec un dôme sous orages (**régime II**).

L'analyse de nos différentes expériences de sensibilité au moyen de suivis de particules lagrangiennes, de bilans et de diagnostics fait clairement apparaître un lien fort entre les caractéristiques du système convectif et la vitesse du flux amont de basses couches. Lorsque celui-ci est étroit (*i.e.* un gradient important entre le centre du flux de basses couches et l'environnement) ou lent, l'activité orageuse associée à un dôme froid sous orages a plus de chance de se produire sur les plaines ou plus en amont sur mer (Fig. 2.8b). Ceci s'explique pour deux raisons : premièrement l'air plus sec environnant subit une forte déviation de la part du massif Alpin, augmentant l'effet de convergence dans le golfe de Lion, et deuxièmement cet air plus sec renforce l'évaporation sous l'activité pluvio-orageuse et favorise par conséquent l'occurrence d'un dôme froid (Fig. 2.9b).

L'étude de Bresson et al (2012) confirme par ailleurs la sensibilité de la localisation du système précipitant (plaine ou relief) vis-à-vis de l'intensité du flux amont (Fig. 2.9a). Lorsque ce dernier est rapide, l'advection des cellules orageuses au-dessus des reliefs et une plus faible évaporation des précipitations dans les couches sous le nuage proches de la saturation ne permettent pas l'établissement d'une plage froide. Ces processus se trouvent amplifiés par l'humidification des basses couches par évaporation au-dessus de la mer par vent fort. Les plus forts cumuls seront alors localisés sur les zones de relief.

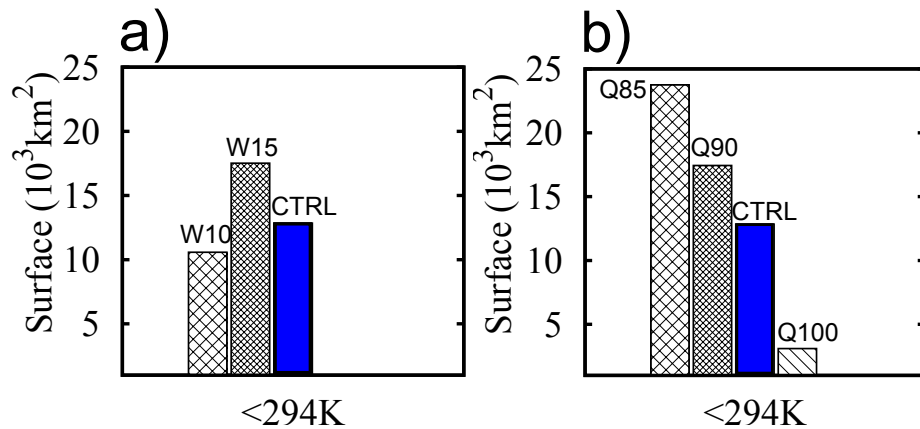


FIGURE 2.9 – Extension spatiale du dôme froid sous orages au bout de 24h de simulation, en fonction de : a) l'intensité du flux de basses couches amont (W10 pour  $10 \text{ m s}^{-1}$ , CTRL pour  $20 \text{ m s}^{-1}$ , etc), et b) de l'humidité de l'environnement (Q85 le plus sec, Q100 le plus humide). D'après Bresson et al (2012).

### 2.2.3 Conclusions

Une partie de mes activités recherche s'est donc articulée autour de l'étude des processus et des mécanismes qui pilotent la dynamique des cyclones tropicaux et les systèmes orageux quasi-stationnaires méditerranéens, ceci sur la base de simulations numériques à méso-échelle. Une première étape est de pouvoir disposer d'une simulation la plus réaliste possible, ce qui confère aux conditions initiales une importance toute particulière. L'introduction dans l'état initial d'un vortex cyclonique plus réaliste (intensité et sa structure verticale) pour les cyclones tropicaux par exemple, ou alors la saturation des zones précipitantes dans les systèmes orageux permet de simuler une évolution la plus proche possible des systèmes précipitants observés. Le modèle est ensuite utilisé comme un laboratoire numérique afin d'identifier les processus importants expliquant les caractéristiques des phénomènes.

L'ingrédient principal et nécessaire à l'occurrence d'un épisode de pluie intense sur le sud-est de la France est la mise en place d'un flux marin de sud-ouest à est humide et conditionnellement instable venant buter contre les reliefs exposés. Ce flux de basses couches est lui-même piloté et contraint par la circulation de plus grande échelle. L'alimentation chaude et humide de basses couches qui en résulte, doit être persistante ( $> 6\text{-}9 \text{ h}$ ) et peu mobile dans l'espace. Cependant, ces conditions ne sont pas suffisantes à elles seules. Pour que se déclenche la convection, il faut un soulèvement de la masse d'air conditionnellement instable au-delà de la couche d'inhibition convective. Le forçage orographique, la convergence de basses couches ou encore un dôme froid sous orages sont les sources de soulèvement souvent impliquées dans les événements précipitants en Méditerranée.

Le cadre expérimental utilisé durant la thèse d'Emilie Bresson (Bresson, 2011) nous permet de disposer dorénavant d'un peu plus d'éléments pour anticiper un régime fortement précipitant plus en amont sur les plaines ou sur les régions côtières, avec une localisation plus inhabituelle et donc potentiellement plus dangereuse. L'apparition d'un dôme froid est principalement liée aux processus d'évaporation des précipitations. Si le flux amont de basses couches n'est pas trop rapide et/ou si l'environnement immédiat est relativement sec, les conditions permettent la mise en place d'un dôme froid bloqué et à un système orageux de se maintenir

en plaine.

En dépit d'un flux marin simplifié, l'étude menée par **Bresson (2011)** a montré que, la prise en compte dans le modèle d'une topographie réelle ainsi qu'une description des caractéristiques à méso-échelle du flux marin au-dessus du bassin Nord-Ouest Méditerranéen sont des éléments clef quant à une bonne prévision de la localisation des systèmes convectifs méditerranéens à faible mobilité.

Il convient cependant de souligner que le cadre expérimental utilisé pourrait être encore amélioré. En effet la prise en compte dans les conditions initiales et aux limites pour le modèle de la variation verticale du vent (cisaillement de vent) peut amener une meilleure prise en compte de l'interaction du système convectif avec son environnement. En effet, lors des épisodes fortement précipitants méditerranéens, le flux s'organise assez souvent en jet avec du cisaillement vertical du vent horizontal produisant du tourbillon renforçant les ascendances. Ce tourbillon peut également interagir avec un dôme froid sous orages et renforcer les vitesses verticales sur le bord d'attaque de ce dernier (Weisman *et al.*, 1988).

Les mécanismes de soulèvement évoqués dans ce chapitre 2.2 sont généralement pilotés par la circulation d'échelle synoptique favorisant la mise en place de l'environnement à méso-échelle propice à la génération de pluies intenses et durables. La partie 2.3 présentera en quoi mes travaux de recherche ont également contribué à la connaissance de ces environnements et à la régionalisation climatique de cet aléa "fortes précipitations en Méditerranée".

## 2.3 Régionalisation climatique des systèmes précipitants en régions méditerranéennes

Il existe au jour d'aujourd'hui une grande incertitude sur l'évolution de la fréquence et l'intensité des événements pluvieux intenses en région méditerranéenne dans le climat futur. La résolution horizontale de la plupart des modèles de climat actuel (d'échelle régionale) ne permet pas la représentation de tels événements et il est nécessaire de développer des approches par régionalisation climatique des sorties des modèles de climat. Un défi consistait donc à détecter, dans ces simulations climatiques, les cas potentiellement les plus propices uniquement à partir des circulations de grande échelle favorables aux épisodes intenses.

Dans ce chapitre, je présenterai mes travaux de recherche en lien avec la caractérisation et la régionalisation climatique des systèmes fortement précipitants méditerranéens, ainsi que la possible évolution de la fréquence et de l'intensité de ces pluies intenses dans la perspective d'un changement climatique. Pour ce faire, je décrirai alors une approche de descente d'échelle 'statistico-dynamique', pour laquelle j'ai participé à la conception, et dont l'objectif était d'extraire des situations d'épisodes méditerranéens d'une projection climatique donnée (scénario A2 en l'occurrence), puis de réaliser des simulations d'échelle kilométrique. Ces travaux de recherche ont été réalisés dans le cadre du projet ANR-CYPRIM<sup>6</sup>.

### 2.3.1 Caractérisation des environnements météorologiques associés aux pluies intenses en Méditerranée

Le lien existant entre les fortes précipitations se produisant sur le bassin méditerranée nord-occidental et les dépressions ou les thalwegs d'échelle synoptique a été bien documenté sur des événements passés. La manière avec laquelle ces précurseurs de plus grande échelle interagissent avec l'orographie complexe du bassin méditerranéen nord-occidental puis favorisent une dynamique favorable à l'occurrence de situations à pluies torrentielles a également été étudiée (Buzzi *et al.*, 1998 ; Doswell *et al.*, 1998 ; Massacand *et al.*, 1998 ; Homar *et al.*, 1999 ; Romero *et al.*, 2000 ; Jansa *et al.*, 2001). Pour trois cas du Sud-Est de la France, Nuissier *et al* (2008) insistent sur la présence de bas géopotentiels à l'ouest immédiat de la France ainsi qu'une dorsale anticyclonique sur l'Europe centrale bloquant la progression vers l'est de ces anomalies d'altitude. Une telle configuration favorise la mise en place d'un flux de sud à sud-est et une advection d'humidité très importante de la Méditerranée vers les régions impactées.

Toutes ces études se sont intéressées et focalisées uniquement sur des cas particuliers. Une question importante a donc été de déterminer si les caractéristiques de ces circulations à plus grande échelle se retrouvaient sur un échantillon plus significatif. Pour y répondre, nous avons cherché à caractériser le contexte de grande échelle de manière objective et systématique. L'approche que j'ai utilisée avec mes collaborateurs s'inspire des nombreuses études en régimes de temps sur le bassin Atlantique (Vautard, 1990) qui permettent de décrire les modes fréquents de la variabilité synoptique de basse fréquence au sein d'un domaine d'intérêt.

Plaut *et al* (2001, PSD01 ci-après) ont été les premiers à initier un tel cadre d'étude afin de donner des éléments de réponse à la question précédente. A partir d'un jeu de jours pour lesquels la précipitation quotidienne a dépassé 40 mm, ils effectuent une classification objective du géopotentiel à 700 hPa associé à ces mêmes jours de pluie. PSD01 déduisent que les pluies se produisant sur la région des Alpes Maritimes sont associées à une configuration d'échelle synoptique dans laquelle des bas géopotentiels se positionnent au sud de l'Irlande, accompa-

---

6. Cyclogénèse et Précipitations Intenses en Méditerranée

gnés d'une forte advection d'humidité par flux de sud-ouest au voisinage sud des Alpes. Les auteurs montrent également que lorsqu'un tel schéma d'échelle synoptique se produit il est associé à la génération de précipitations dans 50 à 75 % des cas.

Les travaux présentés ici élargissent le champ d'étude et vont au-delà de ce qu'ont proposé PSD01 en : (i) combinant des données (ré-analyse et/ou précipitations) sur une plus grande profondeur temporelle, (ii) en considérant une population d'événements précipitants plus intenses et d'autres paramètres utiles pour la description de ces derniers et (iii) en généralisant les phénomènes à tout le Sud-Est de la France (hors Corse). Ces travaux de recherche que j'ai effectués sont résumés dans un article publié au *Q. J. R. Meteorol. Soc.* (**Nuissier et al 2011**)

#### *Deux classes d'environnement prépondérantes pour le Sud-Est de la France*

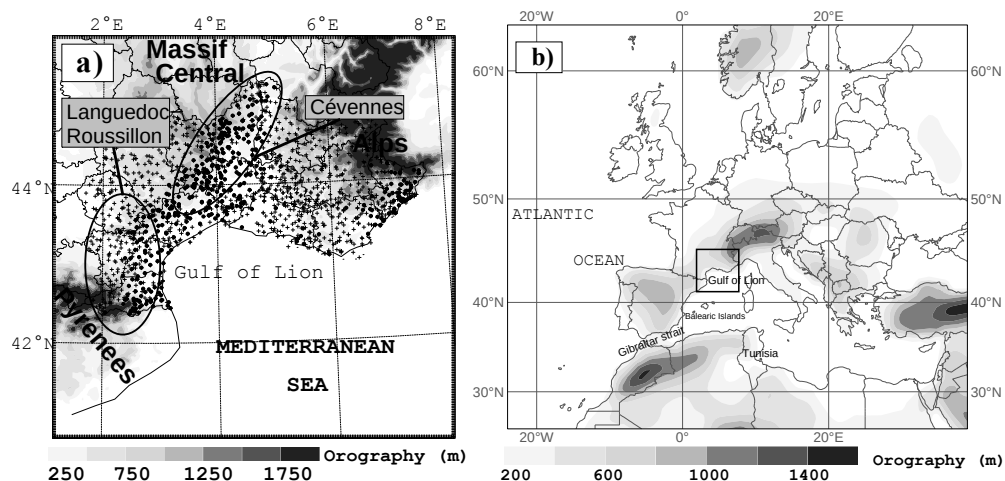


FIGURE 2.10 – a) Cartographie des stations pluviométriques utilisées pour la définition des événements précipitants (cercles noirs); les croix présentent le réseau considéré au départ. b) Domaine géographique utilisé pour la classification en '*type de temps*'. Le relief est grisé et à une résolution de 2.5 km en a) et de 110 km en b). D'après Nuissier et al (2011).

Afin de garantir de la robustesse, de l'objectivité et de la significativité dans la définition des classes d'environnement associées aux pluies intenses méditerranéennes, nous avons employé des outils de classification automatique. Cette classification (ou "*clustering*") a été directement appliquée à un jeu de jours pluvieux caractérisant les événements de pluies intenses sur le sud de la France (hors Corse). Cette approche d'identification systématique a été validée sur la période 1960-2001, en s'appuyant délibérément sur des paramètres observés. L'échantillon était composé des réanalyses ERA-40 pour les paramètres dynamiques et des séries pluviométriques du Réseau climatologique d'Etat géré par Météo-France pour définir les différentes catégories de jours pluvieux.

A partir des 1271 stations du réseau pluviométrique (les croix sur la Fig. 2.10a), il était important dans un premier temps d'isoler la partie extrême de la distribution de chaque série de pluie, de manière à avoir une homogénéité statistique d'un point de vue des fortes précipitations pour l'ensemble des stations. Un critère de dépassement d'un certain quantile de précipitation permet de filtrer et ainsi réduire le jeu à 435 stations (cercles noirs de la Fig. 2.10a). Ainsi un jeu de 1200 événements pluvieux significatifs (SRE dans la suite du texte) a été constitué

## 2.3. RÉGIONALISATION CLIMATIQUE DES SYSTÈMES PRÉCIPITANTS EN RÉGIONS MÉDITERRANÉENNES

pour des valeurs de quantiles dépassant 97 % et un autre jeu a été défini regroupant les 202 cas les plus intenses correspondant à des quantiles au-delà de 99 % (HPE dans la suite du texte).

Comme pour la détermination des régimes de temps, nous avons retenu comme méthode de classification automatique celle des nuées dynamiques (Michelangeli *et al.*, 1995). La réanalyse ERA-40 est utilisée pour l'information synoptique et sous-synoptique, dans sa plus grande profondeur, c'est-à-dire de 1960 à 2001 et pour la période Septembre-Décembre, soit un quarantaine d'automnes au total. Le "clustering" est appliqué au champ de géopotentiel à 500 hPa des 1200 jours identifiés comme SRE. Le champ de géopotentiel de ces SRE se décompose selon une partition de quatre classes. Trois d'entre elles contiennent des épisodes intenses, et surtout deux se trouvent associées aux événements les plus intenses de façon étroite, en contenant plus de 70 %.

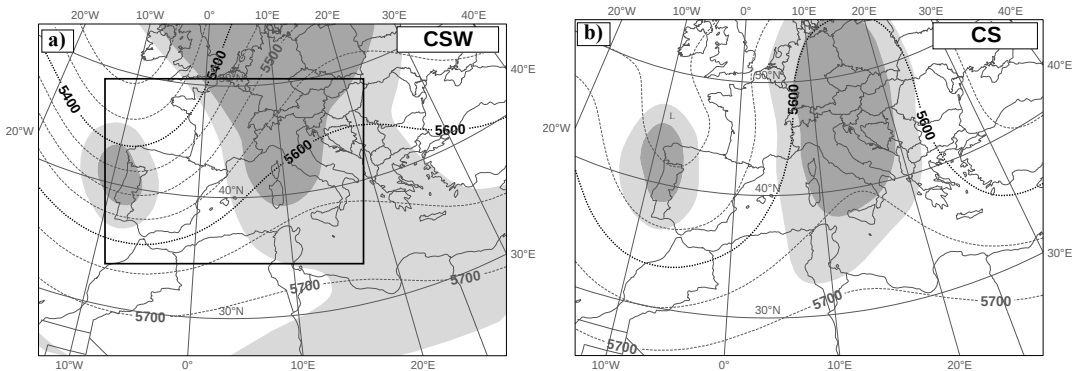


FIGURE 2.11 – Champs composites du géopotentiel à 500 hPa (contour, tous les 25 m) des jours HPE contenus dans les 'types de temps' ou clusters a) CSW et b) CS. Les plages grisées montrent les zones où le composite des jours HPE est significativement différent par rapport à la classe entière, avec un test de Student dont les intervalles de confiance sont respectivement de 90 et 95 %. D'après Nuissier *et al* (2011).

Pour illustrer les caractéristiques communes aux cas d'une même classe, on calcule alors la moyenne (que l'on appelle composite ou *centroïd*) de tous les champs et pour tous les jours de la même classe. On calcule également cette moyenne uniquement pour les jours HPE contenus dans ces classes afin d'examiner les caractéristiques des champs météorologiques des jours les plus intensément pluvieux. La Fig. 2.11 illustre les composites des cas HPE compris dans les deux classes. Le composite de géopotentiel à 500 hPa pour la première de deux classes, que l'on nommera par la suite CSW (pour *Cyclonic Southwesterly*), montre la présence de bas géopotentiels (ou thalweg) assez intenses sur la péninsule Ibérique, suivi en aval du flux par une dorsale de courbure modérée (Fig. 2.11a). Pour la second classe, on remarque également une circulation cyclonique mais qui aboutit cette fois à l'isolement d'une goutte froide d'altitude sur la péninsule Ibérique. En outre, les hauts géopotentiels sur le continent européen se présentent comme nettement plus intenses (Fig. 2.11b). On nommera par la suite cette classe CS pour *Cyclonic Southerly*.

Le géopotentiel à 500 hPa est le champ dont la variabilité est classée initialement. Cependant, on peut toute fois calculer des composites d'autres paramètres pour une même classe. Ainsi, il apparaît remarquable d'obtenir également des composites structurés et bien organisés, signe de l'occurrence de circulations tri-dimensionnelles complexes dotées de vrais liens dynamiques entre les niveaux. Les classes CSW et CS révèlent ainsi la présence d'un fort flux

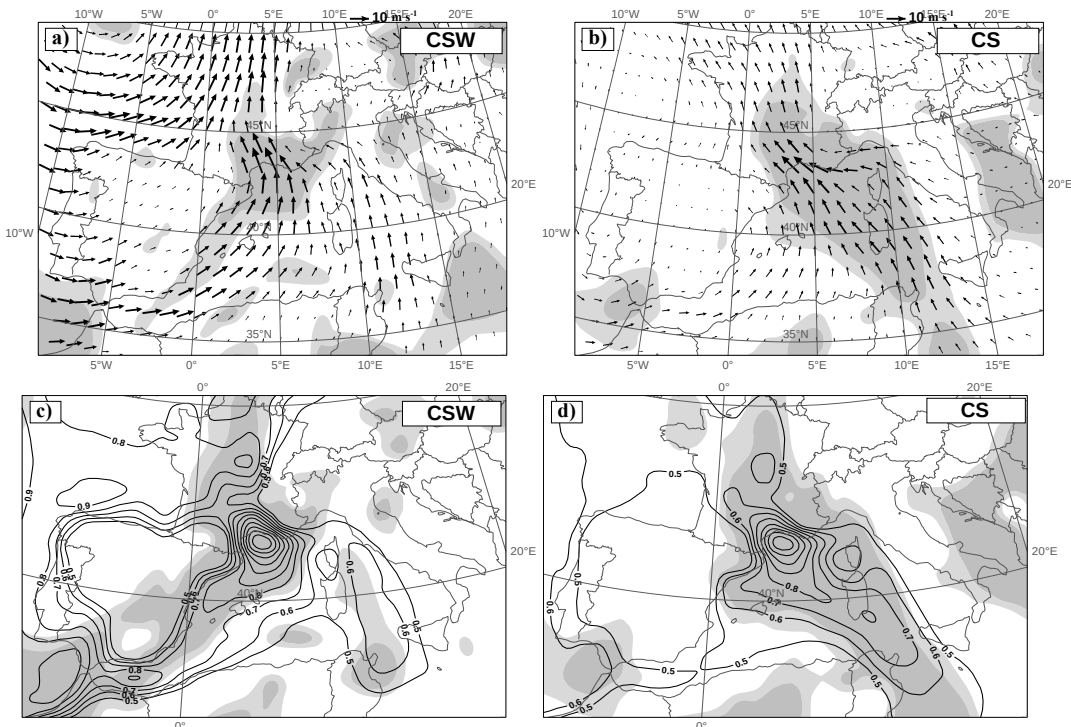


FIGURE 2.12 – Comme la Fig. 2.11 mais pour les paramètres de basses couches : a) et b) le vent horizontal à 925 hPa et c) et d) le flux d'humidité à 925 hPa (isolignes, tous les  $0.1 \text{ kg m s}^{-2}$ ). D'après Nuissier et al (2011).

de basses couches advectant beaucoup d'humidité en Golfe de Lion après son parcours au-dessus de la Méditerranée. Dans le cas de la classe CSW, l'alimentation dominante provient de l'Atlantique puis remonte du détroit de Gibraltar (Fig. 2.12a et c). Pour CS, la puissante dorsale conditionne un flux de basses couches orienté plus au sud-est advectant des masses d'air humides et instables provenant de la partie orientale de la mer Méditerranée (Fig. 2.12b et d).

Les anomalies de bas géopotentiels sur la péninsule Ibérique, la dorsale sur le continent européen et le flux de basses couches humide et instable constituent les structures clés dont le positionnement et l'intensité vont prédéterminer le potentiel pluvieux de la situation.

#### *Conditions suffisantes pour des pluies intenses en Méditerranée : un algorithme de détection pragmatique*

Nous venons de voir que près des trois quarts des épisodes fortement précipitants se produisant sur le Sud-Est de France (hors Corse) peuvent être systématiquement associés à deux classes d'environnement d'échelle synoptique bien différenciées. Nous avons intuitivement effectué la démarche réciproque afin d'examiner si ces environnements, représentés ici uniquement par un seul champ caractéristique de la haute et/ou basse troposphère, fournissaient à eux seuls des ingrédients ou des conditions suffisantes à l'occurrence d'épisodes de pluies exceptionnelles. Autrement dit, est-ce que la seule réalisation de ces configurations d'échelle synoptique implique systématiquement l'occurrence d'une situation de pluies intenses ?

Afin d'examiner cette question, nous sommes repartis non plus des jours de pluies mais du géopotentiel à 500 hPa pour les jours de la période ERA-40. Les dates qui présentent une faible

### 2.3. RÉGIONALISATION CLIMATIQUE DES SYSTÈMES PRÉCIPITANTS EN RÉGIONS MÉDITERRANÉENNES

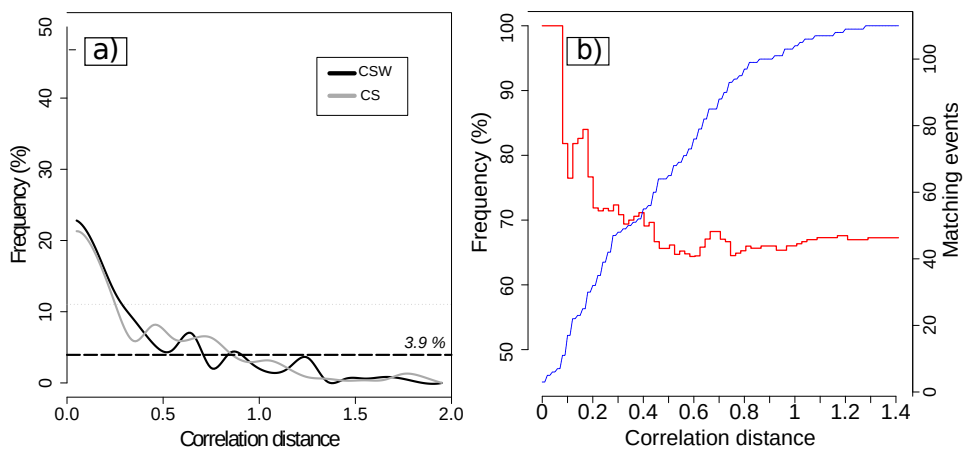


FIGURE 2.13 – a) Fréquence d’occurrence des événements de type HPE en fonction de la distance de corrélation spatiale par rapport aux *centroïds* des classes CSW et CS sur la base du géopotentiel à 500 hPa uniquement. La valeur climatologique est indiquée par la ligne horizontale tiretée. La fréquence montrée en b) (courbe rouge) est calculée en rajoutant les paramètres de basses couches vent et flux d’humidité à 925 hPa et en combinant les deux classes CSW et CS. L’imagette b) montre aussi le nombre de cas cumulés à une distance de corrélation d (courbe bleue). D’après Nuissier et al (2011).

distance de corrélation<sup>7</sup> par rapport aux *centroïds* des classes d’environnements identifiées sont sélectionnées puis on vérifie la pluviométrie associée.

Si plus de la moitié des dates proches des classes CSW et CS sont bien des SRE (non montré), la fréquence chute de manière drastique lorsque l’on augmente les seuils de pluie. En effet si on se base uniquement sur le géopotentiel à 500 hPa, on ne retrouve seulement que 20 % des cas les plus intenses (HPE) (Fig. 2.13a). Si cette fréquence reste supérieure à la climatologie (environ 5 %), ce taux ne suffit pas à qualifier ces configurations synoptiques de suffisantes. Nous décidons alors de compléter le géopotentiel à 500 hPa par d’autres champs représentatifs de la circulation et des structures de basses couches décrites précédemment dans le manuscrit. Nous ajoutons aux environnements favorables le flux d’humidité à 925 hPa. L’étude en distributions montre que ce champ de vecteur possède une orientation et une amplitude préférentielles lors des situations de type HPE. En effet, le flux d’humidité doit posséder une amplitude minimale dans une zone géographique englobant le Golfe de Lion. D’autre part, pour la direction, il doit s’orienter du secteur sud-est à sud (entre 110° et 160°) sur cette région maritime en amont des régions concernées par les fortes pluies.

Avec cette nouvelle combinaison (géopotentiel à 500 hPa et amplitude-orientation du flux d’humidité à 925 hPa), quasiment toutes les dates situées très près de l’une ou l’autre des deux classes d’environnement sont assurément un jour de pluies intenses, avec cependant le bémol d’un taux de détection très(trop) bas (Fig. 2.13b). Se positionner à une distance de corrélation un peu plus importante constitue un compromis acceptable pour lequel un peu moins d’une cinquantaine de situations météorologiques favorables aux épisodes pluvieux serait détectée par mesure de proximité aux composites de référence. Cette fois, près de 75 % d’entre elles

7. La distance de corrélation  $d$  est définie comme  $d = 1 - \text{corr}$ , où  $\text{corr}$  est la corrélation entre le champ et le *centroïd* de la classe. La classe est qualifiée de discriminante vis-à-vis des fortes pluies si on obtient majoritairement pour ces dates des distances de corrélation proches de zéro. Ce critère a été défini par PSD01

correspondent en effet à des événements intenses.

Nous avons donc à ce stade élaboré un algorithme de détection de l'occurrence de fortes pluies basé sur la seule prise en compte de paramètres météorologiques d'altitude et de basses couches. Cet outil ne permet d'explorer qu'une partie de la population des événements intenses (environ un quart), mais dès lors que les conditions synoptiques décrites plus haut sont avérées, nous obtenons presque sûrement de forts cumuls de pluie, en particulier, les plus extrêmes.

### 2.3.2 Evolution des épisodes de pluies intenses dans la perspective d'un changement climatique

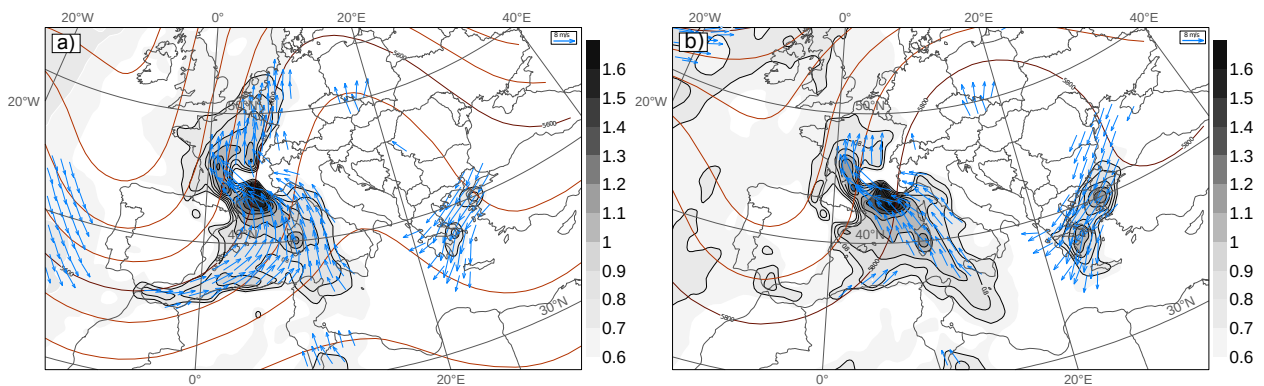


FIGURE 2.14 – Composites de basses couches des cas détectés par la méthode de proximité aux classes CSW et CS fusionnées toutes les deux dans la période climat présent de la simulation climatique ARPEGE-Climat a), et dans la période climat futur b). Les champs représentés sont le géopotentiel à 500 hPa (isolignes rouges, intervalles 40 damgp), le flux d'humidité à 925 hPa (plages grisées, intervalles  $1 \text{ g kg}^{-1} \text{ m s}^{-1}$ ) et le vent à 925 hPa supérieur à  $5 \text{ m s}^{-1}$  (flèches bleues). D'après Beaulant et al (2011).

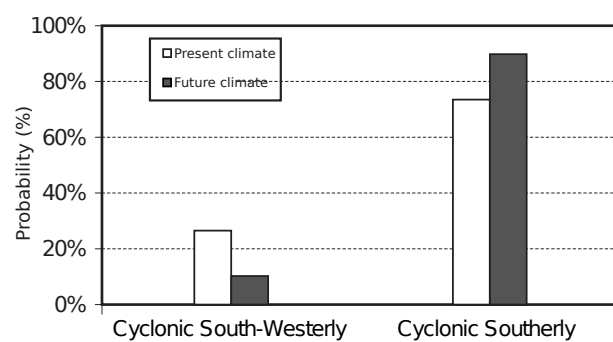


FIGURE 2.15 – Probabilité pour un cas détecté de faire partie de la classe CSW (blanc) ou CS (gris) en climat présent (colonne de gauche) et en climat futur (colonne de droite). D'après Beaulant et al (2011).

Un des objectifs du projet CYPRIM étaient d'apporter des éléments de réponse à cette question difficile de l'évolution des événements de pluies intenses en Méditerranée dans le contexte

## 2.3. RÉGIONALISATION CLIMATIQUE DES SYSTÈMES PRÉCIPITANTS EN RÉGIONS MÉDITERRANÉENNES

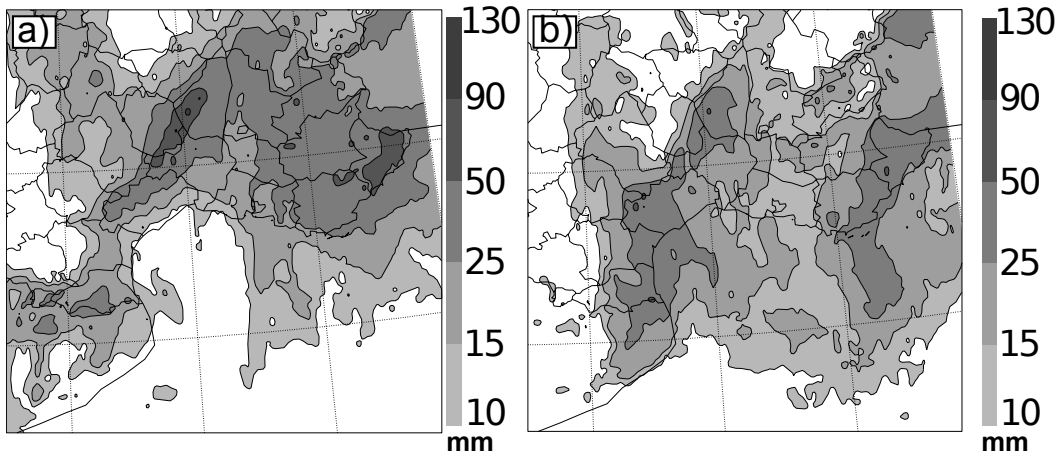


FIGURE 2.16 – Composites des cumuls de pluies (mm/24h) simulés par Meso-NH à 2.5 km de résolution horizontale couplé à ARPEGE-Climat/OPAMED sur les deux séries de situations sélectionnées par la méthode de proximité aux classes d’environnements synoptiques, 10 cas pour le climat présent **a)**, et 10 autres dans le climat futur **b)**. D’après Beaulant et al (2011).

global du changement climatique.

Différentes méthodes dites de *désagrégation* existent et ont pour but de projeter les signaux du changement climatique depuis les échelles résolues par les modèles climatiques jusqu’aux échelles locales. Pour se faire les techniques statistiques présentent une robustesse et une stabilité très intéressantes car elles permettent de relier les paramètres du modèle aux observations par des fonctions de transfert, ceci à différentes échelles (Wilby *et al.*, 1998 ; Plaut et Simonet, 2001 ; Plaut *et al.*, 2001 ; Vrac *et al.*, 2007). Bien que le coût numérique de ces méthodes soit relativement modéré, elles supposent que les liens statistiques établis initialement ne changent pas dans le scénario climatique, ce qui n’est pas nécessairement le cas. Il a même été démontré que ces méthodes statistiques ne sont pas pleinement appropriées à l’étude des précipitations intenses en Méditerranée (Quintana Segui *et al.*, 2010).

On peut aussi réaliser une descente d’échelle dynamique dans laquelle le modèle de climat est couplé à un autre modèle résolvant explicitement les processus convectifs (Trapp *et al.*, 2010). Le gros point fort de cette approche dynamique est de pouvoir résoudre simultanément les circulations de grande échelle induites par le forçage climatique et les processus de petites échelles pilotant les phénomènes convectifs. Cependant et comme on peut s’en douter, ce sont des approches excessivement gourmandes d’un point de vue coût numérique, et il n’était pas réaliste à l’époque de simuler à très haute résolution tous les jours de la période climatique.

La partie de mon travail de recherche décrite dans les précédents paragraphes s'est retrouvée au cœur d'une méthodologie innovante basée sur l'association de ces méthodes de descente en échelle dynamique et statistique. Elle repose sur deux étapes : (i) l'identification puis la sélection de situations dans des classes d'environnements synoptiques potentiellement favorables au déclenchement de pluies intenses dans le climat présent (1961-1990) et dans le climat futur (2070-2099), (ii) la simulation de ces cas à l'aide d'un modèle à haute résolution capable de simuler de façon détaillée les mécanismes conduisant au déclenchement d'événements précipitants. Les simulations climatiques avaient été réalisées avec le modèle régional

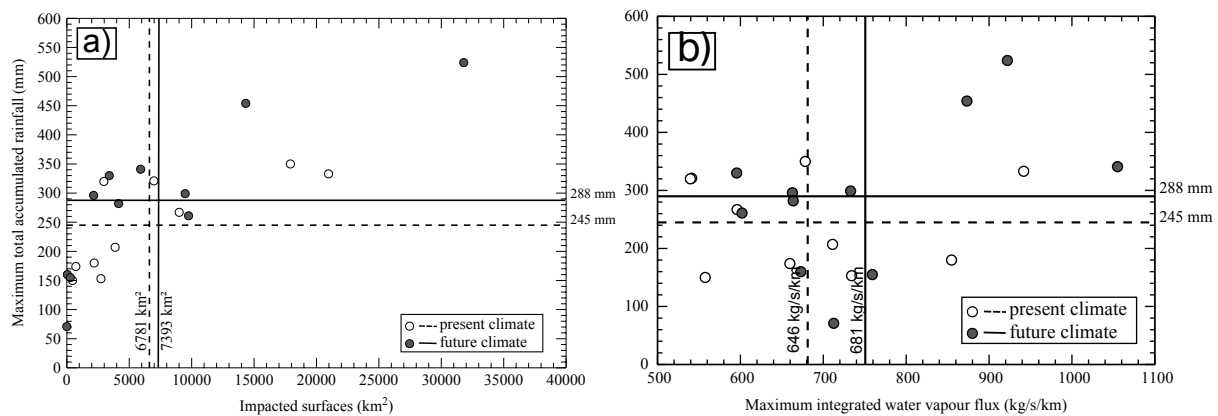


FIGURE 2.17 – Cumuls maximum de précipitations (mm) sur 30 heures pour les 20 cas simulés par Méso-NH à 2.5 km de résolution horizontale en fonction des surfaces impactées par des pluies supérieures à 100 mm a) et pour le flux d’humidité maximum intégré entre 0 et 3 km d’altitude. Le climat présent est représenté par les cercles blancs et le climat futur par les cercles gris. Les lignes tiretées et pleines correspondent aux valeurs moyennes. D’après Beaulant et al (2011).

couplé ARPEGE-Climat/OPAMED selon le scénario A2 du GIEC<sup>8</sup> (Somot et al., 2008). Ces travaux ont été réalisés en partie lors du séjour post-doctoral de Anne-Lise Beaulant que j’ai encadré puis les résultats ont été publiés au *Q. J. R. Meteorol. Soc.* (Beaulant et al., 2011).

#### *Evolution de la fréquence des pluies intenses en Méditerranée*

Avant d’appliquer aux sorties des modèles climatiques l’outil de détection basé sur la recherche d’analogue d’environnements synoptiques, il a été nécessaire de vérifier au préalable dans quelle mesure la simulation du climat présent reproduisait la variabilité des environnements synoptiques obtenus dans la réanalyse ERA-40. Suite à une correction ou un débiaisage appliqué sur les champs du modèle ARPEGE-Climat par rapport à la réanalyse ERA-40, nous avons contrôlé ainsi que le nombre de situations potentielles détectées en climat présent est du même ordre de grandeur que dans la réanalyse ERA-40.

Un premier résultat obtenu concerne le nombre d’événements détectés en climat futur, il augmente de façon notable (45 cas en climat présent et 52 en climat futur, soit +13 %). Concernant la structure spatiale des environnements, le composite des cas obtenus en climat futur montre que, entre les deux branches d’alimentation de basses couches, la branche de sud-est semble devenir prépondérante (Fig. 2.14b). Les événements détectés en climat futur présentent ainsi un jet de basses couches de Sud-est plus marqué mais aussi plus rapide qu’en climat présent. Si l’on détermine parmi les cas détectés par la méthode ceux dont la distance de corrélation est faible par rapport aux classes d’environnement CSW et CS, on note que l’évolution de leur fréquence d’occurrence va dans le même sens que ce qu’on peut voir sur les composites de basses couches. En effet, la configuration CS a une probabilité beaucoup plus importante de se produire dans le climat futur (Fig. 2.15).

8. Groupe d’experts Intergouvernemental sur l’Évolution du Climat

## 2.3. RÉGIONALISATION CLIMATIQUE DES SYSTÈMES PRÉCIPITANTS EN RÉGIONS MÉDITERRANÉENNES

### Régionalisation des fortes précipitations en climat futur

La méthode d'analogues précédente a permis d'identifier une centaine de situations (climat présent et futur confondus) propices à la formation de fortes précipitations dans les sorties du modèle couplé ARPEGE-Climat/OPAMED. Parmi ces situations, les plus proches des *centroïds* de chaque classe (faible distance de corrélation), seulement une vingtaine d'entre elles ont été sélectionnées pour des raisons évidentes de coût de calcul. Ces situations ont été par la suite simulées avec le modèle Meso-NH (Lafore *et al.*, 1998) aux résolutions horizontales de 10 et 2.5 km dans une configuration avec deux domaines imbriqués en utilisant comme conditions initiales et aux limites latérales les sorties du modèle ARPEGE-Climat/OPAMED.

Pour répondre à la deuxième question spécifique de l'évolution de l'intensité de ces événements de pluies intenses dans le climat futur, **Beaulant et al (2011)** ont comparé deux aspects. En premier lieu, les caractéristiques des pluies simulées puis les ingrédients clés pour la formation de pluies intenses (flux d'humidité de basses couches, instabilité convective, etc) ont été examinés dans les deux échantillons.

La comparaison des composites des cumuls de pluies montre une plus grande variabilité spatiale des pluies intenses affectant davantage la région du Languedoc-Roussillon dans le climat futur, avec une baisse relative des précipitations au sud du Massif Central (Fig. 2.16). Les maxima de cumuls atteints en climat futur sont globalement plus élevés qu'en climat présent. De plus les surfaces impactées par les forts cumuls de pluies sont légèrement augmentées en climat futur (Fig. 2.17a). Pour finir, une analyse des ingrédients clés montre que le flux d'humidité de basses couches est plus prononcé de presque 20 % en climat futur.

Ces résultats sur les ingrédients favorables à méso-échelle laisseraient penser que, malgré une diminution de l'instabilité convective disponible (non montrée), les événements orageux en climat futur disposeraient d'une alimentation plus efficace par cette branche de sud-est. Les masses d'air provenant de cette région de la Méditerranée seraient plus chaudes et plus riches en vapeur d'eau ce qui expliquerait le caractère pluvieux plus marqué mis en évidence en climat futur. Cependant, ces résultats doivent être tempérés compte tenu du nombre limité des cas simulés et de l'unique scénario considéré.

### 2.3.3 Conclusions

Une autre partie de mes activités recherche s'est donc articulée autour de la régionalisation climatique des systèmes fortement précipitants dans les régions méditerranéennes et de la délicate question de l'évolution des phénomènes orageux intenses dans la perspective du changement climatique.

Je me suis tout d'abord penché sur les éléments météorologiques précurseurs caractéristiques d'événements de pluies intenses sur les régions méditerranéennes. Une approche en régimes de temps et l'utilisation combinée de données pluviométriques et de la ré-analyse ERA-40 permettent de résumer les trois quarts des cas les plus intenses en deux classes d'environnements d'échelle synoptique. Outre des anomalies de bas géopotentiels sur la péninsule Ibérique, les deux classes CSW et CS montrent la présence d'un fort flux de basses couches advectant beaucoup d'humidité dans le Golfe de Lion après son parcours au-dessus de la Méditerranée. Dans le cas de la classe CSW, l'alimentation dominante provient de l'Atlantique via la région de Gibraltar. Pour la classe CS, des hauts géopotentiels sur l'Europe centrale conditionnent un flux de basses couches orienté plus au sud-est advectant des masses d'air humides provenant de la partie orientale de la mer Méditerranée.

Nous avons également démontré que ces classes d'environnement, à condition de combi-

ner des paramètres d'altitude et de basses couches (géopotentiel à 500 hpa et flux d'humidité à 925 hPa), sont des ingrédients ou des conditions suffisantes à l'occurrence d'épisodes de pluies exceptionnelles. Cela nous a permis dans un deuxième temps de développer un outil de détection de l'occurrence des pluies fortes pour lequel le taux de fausse alarme est relativement bas. Pour ces cas de fausse alarme, il se peut que les processus mis en jeu soient d'échelle plus fine et soient de ce fait hors d'atteinte dans la réanalyse ERA-40 de résolution trop lâche.

Même si de nombreuses incertitudes persistent concernant la robustesse des résultats, la méthode de descente d'échelle statistico-dynamique, mise en oeuvre dans le cadre du projet CYPRIM et appliquée au scénario A2 simulé avec le modèle ARPEGE-Climat/OPAMED, semble indiquer pour la fin du 21<sup>ème</sup> siècle une diminution des précipitations sur le Massif Central et les Alpes au profit de la région du Languedoc-Roussillon. La variabilité de la localisation des zones impactées par les fortes précipitations augmente clairement dans le climat futur. Cette évolution, bien que basée sur un nombre restreint de cas, est cohérent avec l'évolution des conditions synoptiques associées aux événements fortement précipitants. Le climat futur tend à augmenter et à privilégier les événements associés à la classe CS affectant préférentiellement la région du Languedoc-Roussillon.

Afin d'examiner l'importance de la résolution dans les modèles de climat, l'approche développée dans le cadre du projet CYPRIM a été reprise dans les travaux de thèse de Jeanne Colin (Colin, 2011). Cette étude a montré que l'emploi de la haute résolution (12 km) dans le modèle régional ALADIN-Climat permettait de reproduire plus d'événements fortement précipitants qu'avec le modèle global ARPEGE-Climat (50 km), ceci avec un taux de fausse alerte équivalent à celui de l'outil de détection de l'occurrence des pluies fortes. En d'autres termes, l'utilisation de la haute résolution dans le modèle de climat permet une meilleure représentation des processus physiques pilotant la convection et par conséquent la proportion de HPE pour lesquels l'état de l'atmosphère à l'échelle synoptique constitue une condition suffisante à l'occurrence de ces événements dépasse donc le pourcentage détectable par l'outil mise en œuvre dans le projet CYPRIM.

## 2.4 Prévisibilité à l'échelle convective des pluies intenses en Méditerranée

Dans cette dernière partie, je décrirai les différentes contributions de mes travaux de recherche sur l'étude de la prévisibilité à l'échelle convective des systèmes précipitants intenses avec le modèle de prévision AROME. Nous y verrons en quoi ces travaux préparatoires ont permis de mieux cerner la prévisibilité des situations prévues par le modèle AROME, ceci en élaborant une méthode de génération de prévision d'ensemble à l'échelle convective. Ces résultats ont également servi de fondations au futur système de prévision d'ensemble AROME, dont la phase opérationnelle est prévue en 2016.

Ces travaux de recherche ont été réalisés dans le cadre du projet ANR-MEDUP<sup>9</sup> et du programme international HyMeX.

### 2.4.1 Quantification des incertitudes de prévision : une approche en prévision d'ensemble (PE)

Les travaux de modélisation à l'échelle convective mentionnés dans la section 2.2 ont permis de progresser dans deux domaines : (i) la connaissance des événements eux-mêmes en utilisant le modèle comme laboratoire numérique et (ii) la prévisibilité à l'échelle convective, en évaluant les capacités d'un modèle à fine échelle à prévoir ces épisodes fortement précipitants, grâce à des conditions initiales appropriées (Ducrocq *et al.*, 2000, 2002). Les résultats de ces travaux ont également conforté les orientations prises par Météo-France en terme de prévision numérique du temps avec le développement de la nouvelle génération du modèle non-hydrostatique AROME (opérationnel depuis 2008) à quelques kilomètres de résolution horizontale et aussi doté de son propre système d'assimilation de données à méso-échelle<sup>10</sup>.

Ceci étant, ces différentes études ont montré également une très grande sensibilité vis-à-vis des conditions initiales et des forçages aux interfaces. Par exemple, il a été montré dans la section 2.2 que les résultats numériques obtenus, pour une expérience dans laquelle des observations de surface à méso-échelle supplémentaires sont assimilées, sont beaucoup plus réalistes que ceux issus d'une simulation initialisée à partir d'une analyse issue de modèle de grande échelle. La prévisibilité d'une situation météorologique appréhendée par le modèle va dépendre de : (i) la nature intrinsèque du phénomène atmosphérique lui-même, puis (ii) de la capacité du modèle à prévoir cet événement atmosphérique. Par exemple, il est admis que les orages isolés en plaine ont une prévisibilité intrinsèque plus faible que les systèmes convectifs à méso-échelle organisés sur les régions montagneuses de la Méditerranée, qui sont eux-mêmes sans doute moins prévisibles que les perturbations d'échelle synoptique. De même un modèle numérique à haute résolution comme AROME a par ailleurs une meilleure capacité à représenter ces phénomènes atmosphérique de petite échelle que le modèle ARPEGE. Il a donc été important de bien connaître et documenter la sensibilité du modèle et de cerner la prévisibilité des phénomènes prévus par celui-ci.

Il existe des approches probabilistes qui permettent de quantifier la prévisibilité des situations météorologiques à l'échelle synoptique. La prévision d'ensemble (PE) est une technique stochastique qui a montré son efficacité pour quantifier une part des incertitudes dans les prévisions, en particulier pour évaluer la variance associée aux erreurs des prévisions qui demeure

9. Forecast and projection in climate scenario of Mediterranean intense events : Uncertainties and Propagation on environment

10. Depuis 2015 le modèle de prévision AROME est opéré à 1.3 km de résolution horizontale et avec une assimilation des données en cycle horaire.

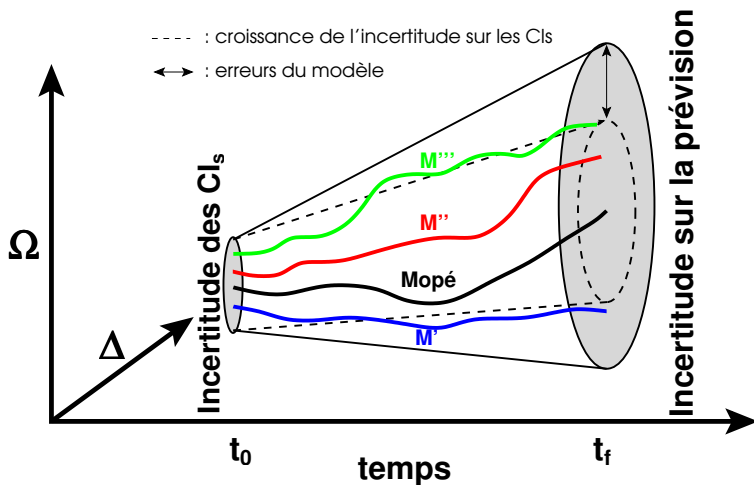


FIGURE 2.18 – Espace des phases simplifié à deux dimensions de l'état de l'écoulement atmosphérique. Le disque grisé représente l'incertitude sur la prévision qui grandit en raison de la croissance de l'incertitude sur les conditions initiales et des erreurs associées au modèle.

un bon indicateur de prévisibilité.

L'idée de la prévision stochastique est de remplacer, dans la prévision, l'état initial unique (analyse) par une fonction de densité de probabilité qui représente l'erreur d'analyse (cette incertitude sur l'état initial est symbolisée par le disque grisé au temps  $t_0$  de la Fig.2.18). Mais les états atmosphériques modélisés possèdent un très grand nombre de degrés de liberté (de l'ordre de  $10^6$ ), ne permettant pas une véritable évolution stochastique. Dans la pratique, on est donc contraint de construire un échantillon d'états initiaux, constituant un ensemble, et dont la dispersion reflète l'incertitude sur l'état initial (Leith, 1974). Ces nouvelles conditions initiales sont obtenues par ajout à l'analyse de perturbations d'amplitudes faibles, compatibles avec l'erreur d'analyse. Chaque élément de l'ensemble est ensuite pris comme condition initiale pour le modèle que l'on intègre autant de fois qu'il y a de constituants dans l'ensemble. La Fig.2.18 montre, dans l'espace des phases de Lorenz (1963), les différentes "trajectoires"  $M$  issues des différents éléments de l'ensemble et comment l'incertitude sur la prévision croît dans le temps en raison de la croissance de l'incertitude sur les conditions initiales et des erreurs associées au modèle. Le choix de la structure des perturbations initiales est donc crucial et les techniques actuelles reposent sur l'identification d'un petit nombre de perturbations qui croissent les plus vite et qui assurent à l'ensemble de représenter le plus large éventail de solutions différentes, représentant l'incertitude de la prévision. Des méthodes de PE destinées aux échelles synoptiques qui considèrent les modes singuliers linéaires (Mureau *et al.*, 1993), les "bred-modes" (Toth et Kalnay, 1997) et l'ensemble Kalman filter (Houtekamer *et al.*, 1996), sont utilisées respectivement de manière opérationnelle dans le modèle du CEPMMT (Buizza et Palmer, 1995), du NCEP (Toth et Kalnay, 1997) et du Centre Météorologique du Canada.

#### 2.4.2 Méthodes dédiées de prévisions d'ensemble pour l'échelle convective

Avec la mise en opérationnel des nouvelles générations de modèles atmosphériques non-hydrostatiques à des résolutions kilométriques résolvant explicitement la convection, comme le modèle AROME de Météo-France, le réalisme des prévisions de précipitations a été signifi-

cativement amélioré, grâce notamment à une meilleure représentation du cycle de l'eau et une résolution explicite de la convection profonde. L'augmentation du réalisme ne s'accompagne cependant pas toujours d'un gain en terme de prévision quantitative des précipitations. Il est donc d'autant plus essentiel que la prévision apparaît réaliste, de pouvoir quantifier l'incertitude associée à cette prévision, et plus généralement la prévisibilité à l'échelle convective. Les systèmes de PE pré-citées s'intéressent principalement à la prévision des transitions entre régimes de temps par exemple, ou des trajectoires de cyclones tropicaux ou de dépressions des moyennes latitudes. Les perturbations générées par les "bred-modes" ou les vecteurs singuliers, de nature principalement linéaire, sont bien adaptées à l'instabilité barocline de l'atmosphère, mais sont par contre moins pertinentes à l'échelle kilométrique, où les processus fortement non-linéaires et à seuil dominent.

Les modèles à convection explicite sont très utiles à la prévision d'événements extrêmes et dangereux de petite échelle spatiale et temporelle, comme par exemple les orages et les fortes précipitations. Cependant, la prévisibilité de ces situations météorologiques dans les modèles à échelle convective se retrouve limitée par la très forte sensibilité aux conditions initiales d'une part, et par les instabilités convectives non-linéaires d'autre part. Enfin, les CRMs souffrent également d'une source d'erreur supplémentaire, par rapport aux modèles globaux. Ils ont besoin de conditions aux limites, fournies à une résolution spatiale et temporelle insuffisante par un modèle de plus grande échelle, lui-même entaché d'erreurs. Ces différences importantes, ainsi que le coût numérique très important des prévisions à haute résolution, obligent donc à se contenter d'un nombre de membres réduit dans l'ensemble et expliquent le besoin de mettre au point des méthodes de génération de PE dédiées à l'échelle convective, échantillonnant au mieux la densité de probabilité des solutions possibles pour la prévision.

La PE à échelle convective est ainsi devenue un axe de recherche prioritaire des grands centres de prévision météorologique, d'abord sous forme d'études de sensibilité et de prévisibilité des événements extrêmes. Il est important également de souligner que, lorsque j'ai débuté mes travaux de recherche sur la prévisibilité et la PE, peu de travaux existaient sur ce sujet notamment à plus fine échelle, i.-e. à l'échelle convective. C'est dans ce contexte que mes travaux de recherche présentés ici ont proposé l'esquisse d'une méthodologie d'un système de PE à l'échelle convective avec le modèle AROME, qui reposera sur l'utilisation de la technique d'assimilation pour perturber et générer des états initiaux du modèle. Cette recherche s'est principalement focalisée sur les événements intenses méditerranéens.

Ces travaux sur la prévisibilité à l'échelle convective avec le modèle AROME se sont également inscrits dans la cadre de la thèse de Benoit Vié que j'ai co-dirigée (Vié, 2012). Cette thèse était un travail exploratoire, visant à identifier les différentes sources d'incertitude pesant sur les prévisions AROME et évaluer leur importance, pour permettre de choisir au mieux la configuration du futur système opérationnel. D'autre part, la SOP1 de la campagne expérimentale HyMeX (Ducrocq *et al.*, 2014) a été une opportunité unique durant laquelle un prototype de PE avec le modèle AROME a été mis en place et a fourni des prévisions en temps quasi-réel. Même si ces prévisions n'étaient pas systématiquement intégrées dans les bulletins des prévisionnistes de la campagne, elles ont néanmoins permis d'affiner la variabilité spatio-temporelle de la convection prévue par le modèle AROME déterministe, et ainsi optimiser les plans de vol avion. Enfin, nous le verrons plus loin que la PE avec le modèle AROME a permis d'étudier la prévisibilité des événements fortement précipitants observés durant la SOP1 HyMeX.

### *La méthodologie de travail utilisée : quantification de chaque source d'incertitude*

Nous avons choisi d'explorer séparément les différentes sources d'incertitude pesant sur la prévision du modèle AROME à l'aide de simulations d'ensemble. Le choix des méthodes de génération d'ensemble que l'on retiendra découlera donc à la fois de l'identification des différentes sources d'incertitude ainsi que de l'étude de sensibilité des événements fortement précipitants.

Nous avons discuté dans la partie 2.2 et 2.3 de l'importance du forçage d'échelle synoptique d'une part, et des conditions de basses couches à méso-échelle d'autre part, pour le déclenchement de systèmes convectifs, leur évolution et leur stationnarité. Les ensembles avec le modèle AROME présentés ci-après ont été construits afin d'évaluer la prévisibilité de ces événements au regard de ces deux sources d'incertitudes. D'autre part, nous avons été amenés également à nous questionner sur les autres sensibilités des événements de fortes précipitations. L'importance de processus physiques tels que l'évaporation des précipitations et la mise en place de plages froides sous orages, a motivé la mise en place de simulations d'ensemble représentant l'incertitude liée à la paramétrisation de la microphysique en phase chaude. De même, la sensibilité aux flux de surface, notamment à la température de surface de la mer, nous a conduit à mettre en place différentes perturbations des conditions de surface.

Plusieurs types d'évaluation des ensembles de prévision AROME ont été conduits. En plus des scores probabilistes classiquement utilisés pour évaluer les prévisions d'ensemble, d'autres méthodes d'évaluation ont été conçues et appliquées aux prévisions d'ensemble. Tout d'abord, une évaluation de type « modèle vers satellite » a été appliquée (non montrée dans le mémoire). La propagation de l'incertitude sur la prévision de pluie dans la modélisation hydrologique a ensuite été étudiée en utilisant en particulier les ensembles de prévisions AROME en entrée du modèle hydrologique ISBA-TOPMODEL.

Trois articles publiés respectivement au *Mon. Wea. Rev.* et au *Nat. Hazards Earth Syst. Sci.* (**Vié et al 2011 ; Vié et al 2012 et Nuissier et al 2012**) quantifient l'impact des différentes sources d'incertitude pesant sur la prévision du modèle AROME et examinent leur propagation jusqu'aux échelles hydrologiques.

### *Incertitudes issues des conditions initiales et aux limites : impact des conditions synoptiques*

Dans le cadre de sa thèse, Benoit Vié a dans un premier temps évalué de manière séparée l'impact de l'incertitude provenant de l'échelle synoptique à travers les conditions aux limites, et l'incertitude de méso-échelle sur les conditions initiales (**Vié et al, 2011**). Les ensembles avec le modèle AROME réalisés dans cette partie l'ont été avec la version opérationnelle de 2008 à 2.5 km de résolution et l'incertitude provenant des conditions aux limites a été étudiée en utilisant les membres de la prévision d'ensemble globales de Météo-France, la PEARP, également dans sa configuration opérationnelle en 2008. Cela signifie que l'ensemble PEARP ne disposaient à l'époque que de 11 membres pour ces travaux.

Dans une première expérience (AROME-PEARP), chaque membre de la PEARP (d'une résolution de 23 km sur la France à l'époque) sert de conditions aux limites latérales à un cycle d'assimilation tri-horaire AROME semblable à la configuration opérationnelle. Pour éviter un trop grand saut de résolution entre PEARP et AROME, un cycle d'assimilation ALADIN est intercalé entre les deux composantes. Ensuite, dans une seconde expérience (AROME-PERTOBS), l'incertitude provenant des conditions initiales à méso-échelle est évaluée par la méthode d'assimilation d'observations perturbées (Houtekamer *et al.*, 1996 ; Berre *et al.*, 2006), tirant parti du système d'assimilation à méso-échelle 3D-Var du modèle AROME. Les conditions aux limites latérales, identiques pour chaque membre, sont fournies par le modèle ALADIN. Ces deux

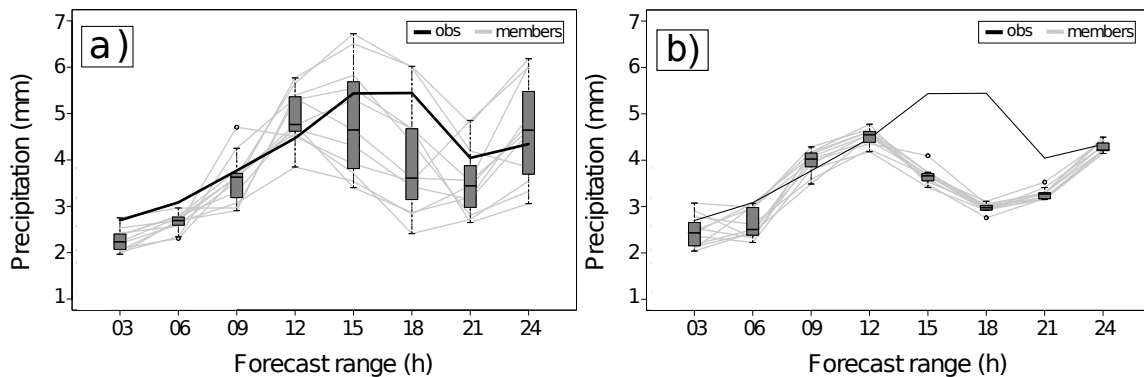


FIGURE 2.19 – Séries temporelles des précipitations cumulées sur 3h et moyennées dans une boîte de 400 km de côté, pour l’ensemble AROME-PEARP **a)** et AROME-PERTOBS **b)**, du 1<sup>er</sup> au 2 nov. 2008 à 12 UTC. La ligne épaisse noire représente les observations par pluviomètres, tandis que les lignes fines et grises représentent chaque membre de l’ensemble. Les boîtes à moustaches indiquent, toutes les 3h, la médiane, les premiers et derniers quartiles ainsi que les minima et maxima de chaque ensemble. D’après Vié et al (2011).

ensembles sont évalués sur une période continue d'un mois, du 6 oct. au 5 nov. 2008 et leur comportement est aussi analysé pour deux cas de fortes pluies méditerranéens le 20 oct. 2008 et les 1-2 nov. 2008.

Autant l'étude statistique que l'analyse des deux cas d'étude révèlent les différences d'impact de perturbations des conditions initiales à méso-échelle ou des conditions aux limites. Il apparaît essentiel de tenir compte des incertitudes sur les conditions initiales à méso-échelle pour les premières heures de simulation. Après quelques heures (environ 12h dans nos expériences), l'incertitude provenant des conditions aux limites domine. La part de chaque source dans l'incertitude de la prévision varie aussi selon les conditions synoptiques : lorsque la circulation d'échelle synoptique est prononcée (ce qui était le cas du 1-2 nov. 2008), l'incertitude est plus largement dominée par les conditions aux limites (Fig. 2.19). Les diagrammes de rang de la Figure 2.20, calculé pour le vent en basses couches, montrent une forme en U caractéristique d'une sous-dispersion des ensembles à 12h d'échéance de la prévision (la dispersion est plus faible que l'erreur de prévision). Ce caractère sous-dispersif augmente avec l'échéance de prévision si l'incertitude venant des limites latérales n'est pas prise en compte et si en plus la dynamique d'échelle synoptique est marquée. Les premières échéances de la prévision sont dominées principalement par les erreurs sur les conditions initiales à méso-échelle.

Nous voyons donc que l'incertitude sur les conditions aux limites latérales a un impact à des échéances plus lointaines que l'incertitude venant des conditions initiales à méso-échelle (typiquement au-delà de 12 heures), à mesure que la dispersion augmente dans l'ensemble global coupleur. De plus, la vitesse avec laquelle se propage cette incertitude venant des conditions aux limites est étroitement liée aux conditions d'échelle synoptique. L'étude de Gebhardt *et al* (2011), qui se focalise sur des méthodes de perturbation dans le modèle COSMO-DE à 2.8 km de résolution horizontale, adopte une approche de séparation des sources d'incertitude similaire à celle utilisée dans Vié *et al* (2011). Ils trouvent eux aussi que les erreurs modèles dominent principalement les premières heures de prévision, et que les variations des conditions aux limites prennent le dessus les heures suivantes.

L'incertitude provenant des conditions aux limites latérales peut être prise en compte en

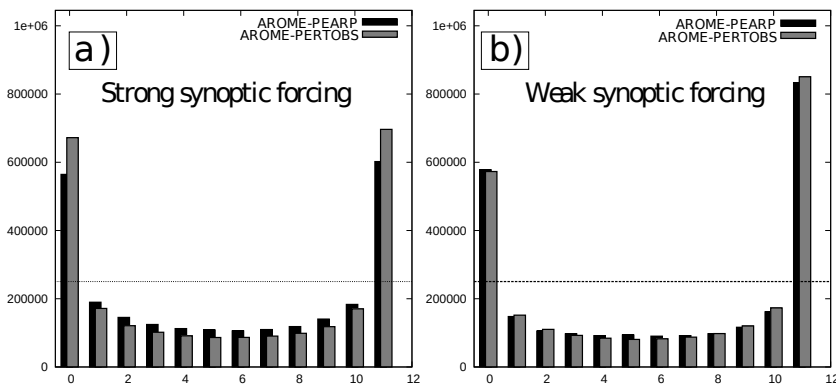


FIGURE 2.20 – Diagramme de rang pour la prévision du module du vent à 925 hPa à 12h d'échéance, calculé pour les jours avec un forçage d'échelle synoptique fort a) et pour les jours avec un forçage d'échelle synoptique faible b). D'après Vié et al (2011).

couplant chaque prévision à haute résolution avec un membre d'une PE à l'échelle globale. Néanmoins, l'ensemble à l'échelle convective doit englober l'ensemble des sources d'incertitude susceptibles d'impacter la prévision à cette échelle. A première vue, l'approche consisterait à combiner  $N$  membres d'une PE d'échelle globale comme conditions aux limites latérales à  $M$  autres membres représentant des perturbations supplémentaires générées dans le modèle à convection explicite, conduisant ainsi à la réalisation de  $N \times M$  prévisions dans cette configuration. Si la taille des PE d'échelle globale varie typiquement autour de 35-50 membres, le coût numérique très important des prévisions à haute résolution obligent, au contraire, à se contenter d'un nombre de membres réduit dans l'ensemble, avec des tailles cibles autour de 8 à 20 membres. Nous avons donc été amenés à nous poser la question du choix des membres coupleurs en amont pour un ensemble à échelle convective.

#### Incertitudes provenant des conditions aux limites latérales : une méthode de sélection

Pour se faire j'ai évalué deux méthodes dans lesquelles les membres de la PE globales sont sélectionnés soit : (i) de manière simplement aléatoire (expériences nommées RAND dans le mémoire) ou (ii) en s'attachant à minimiser, dans le sous-jeu de membres retenus, les erreurs d'échantillonnage de la distribution complète de tous les membres de la PE globale. Dans cette deuxième méthode, les structures météorologiques de plus grande échelle sont regroupées en classes via un algorithme de "clustering" dynamique de certains champs atmosphériques issus des membres de la PE globale. Pour chaque classe, un membre est identifié comme élément représentatif de son "cluster" et fourni les conditions aux limites latérales au modèle AROME. La méthodologie de classification utilisée de cette étude (expériences nommées CLUST-REF) est proche de celle adaptée pour le système COSMO-LEPS (Molteni et al., 2001 ; Marsigli et al., 2001 ; Montani et al., 2003 ; Marsigli et al., 2005 ; Federico et al., 2007 ; Montani et al., 2011).

Les champs météorologiques sont la hauteur du géopotentiel  $Z$ , les deux composantes du vent horizontal  $U$  et  $V$  et l'humidité spécifique  $Q$  aux niveaux 500, 700 et 850 hPa. Sur la base de la connaissance des environnements météorologiques de plus grande échelle favorables aux fortes précipitations en Méditerranée, qui ont été décrits dans la partie 2.3, nous avons raffiné la classification en introduisant, dans une expérience nommée CLUST-MOIST, des prédicteurs statistiques associés aux fortes pluies sur notre région d'intérêt (e.g. la hauteur du géopoten-

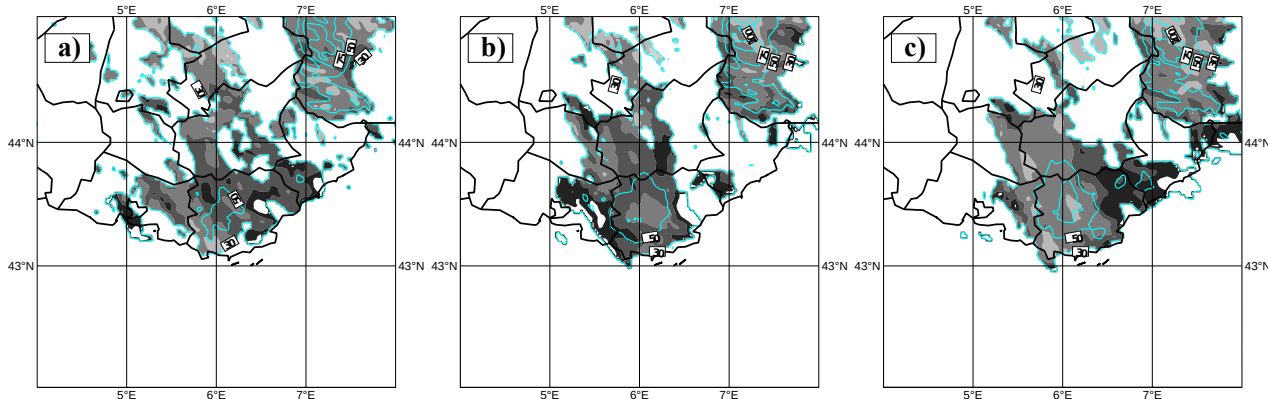


FIGURE 2.21 – Moyenne de l'ensemble AROME (isolignes turquoises) et dispersion (plages grisées) pour les précipitations simulées cumulées entre 06 UTC le 15 Juin 2010 et 06 UTC le 16 Juin 2010, pour des conditions aux limites latérales choisies : a) de manière aléatoire (RAND), b) sur la base d'une classification de champs météorologiques "classiques" (CLUST-REF) et c) sur la base d'une classification de champs météorologiques "spécifiques" aux fortes pluies (CLUST-MOIST). D'après Nuissier et al (2012).

tiel à 500 hPa ainsi que le flux d'humidité à 925 hPa). L'approche aléatoire et la classification standard ou "orientée" sont illustrée sur le cas des inondations de Draguignan dans le Var le 15 Juin 2010. Ces travaux font l'objet d'un article publié dans la revue Natural Hazards and Earth System Sciences (NHESS), (Nuissier et al (2012)). Ce cas dans le département du Var en Juin 2010 (présenté dans la partie 2.2) était une situation avec une prévisibilité limitée dans laquelle la variabilité à fine échelle des fortes précipitations observées était étroitement liée au positionnement précis d'un ligne convective quasi-stationnaire sur le Var et la mer Méditerranée. Cette ligne convective était elle-même pilotée par une dépression de surface sur le golfe de Lion, drainant une très forte advection d'humidité en basses couches vers les côtes varoises. La prévisibilité limitée de cette situation se caractérisait également par une forte variabilité dans la PE globale traduisant une forte incertitude sur la prévision de ce cas.

La Figure 2.21 montre que, dans ce cas d'étude, la variabilité des conditions aux limites latérales est bien mieux conservée suite à une classification des membres de la PEARP qu'en effectuant une sélection aléatoire. L'ensemble CLUST-REF semble plus clairement cibler les plus fortes précipitations en moyenne sur le département du Var. Si on va plus loin en considérant cette fois dans la classification des prédicteurs spécifiques aux événements convectifs dans la région d'intérêt (e.g. la hauteur du géopotentiel à 500 hPa et le flux d'humidité horizontal à 925 hPa), les plus fortes précipitations sont encore mieux ciblées sur le Var, avec un écart-type normalisé ou dispersion qui devient plus faible sur la région.

L'analyse de ces résultats à travers les fréquences de dépassement de seuil des précipitations en surface confirme que, dans les situations de fortes pluies avec une faible prévisibilité, une classification objective de certains champs météorologiques prévus, comme méthode de sélection des membres d'une PE globale, a clairement un impact très important sur la qualité de la PE à l'échelle convective en aval. En effet, sur la Figure 2.22 les probabilités les plus fortes de dépasser le seuil de 50 mm en 24h sont obtenus à partir d'une classification. Cependant, il est important de souligner que cette méthode de classification perd nettement de son intérêt lorsque la situation météorologique gagne en prévisibilité (lors de certains événements

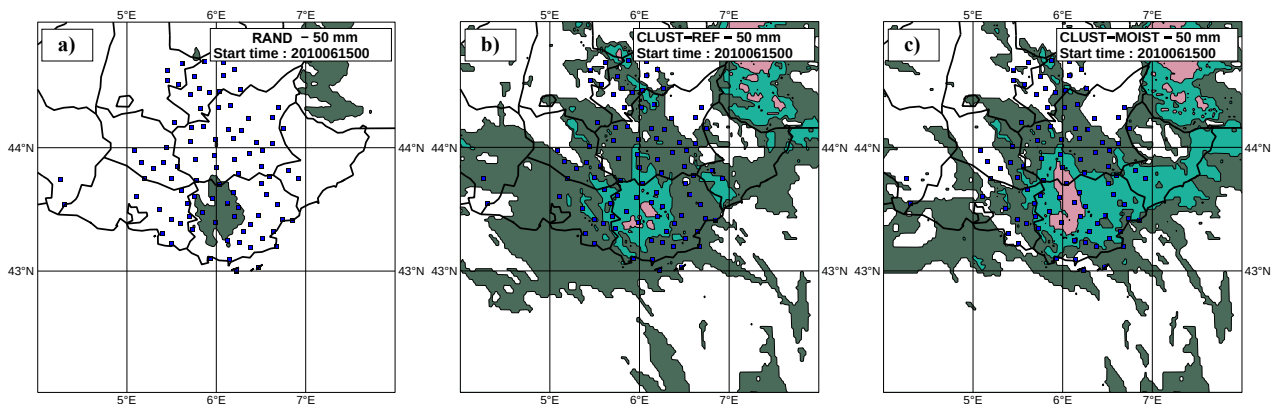


FIGURE 2.22 – Distribution spatiale des probabilités de dépassement du seuil de 50 mm pour les précipitations simulées cumulées entre 06 UTC le Juin 2010 et 06 UTC le 16 Juin 2010, pour des conditions aux limites latérales choisies : a) de manière aléatoire (RAND), b) sur la base d'une classification de champs météorologiques "classiques" (CLUST-REF) et c) sur la base d'une classification de champs météorologiques "spécifiques" aux fortes pluies (CLUST-MOIST). D'après Nuissier et al (2012).

convectifs plus pilotés par les reliefs des Cévennes par exemple), c'est-à-dire lorsque la variabilité demeure faible dans la PE globale. Dans ces cas de figures, un choix aléatoire des membres de la PE globale devient équivalent à la classification objective.

#### *Combinaison des sources d'incertitude et impact des processus microphysiques et de surface*

Si la quantification séparée de chaque source d'incertitude est une étape nécessaire, la sous-dispersion des ensembles présentés jusqu'ici peut s'expliquer par le fait que chacun des ensembles ne prend en compte qu'une seule source d'incertitude. Nous avons donc cherché à combiner les sources d'incertitude et à prendre en compte aussi les erreurs de modélisation.

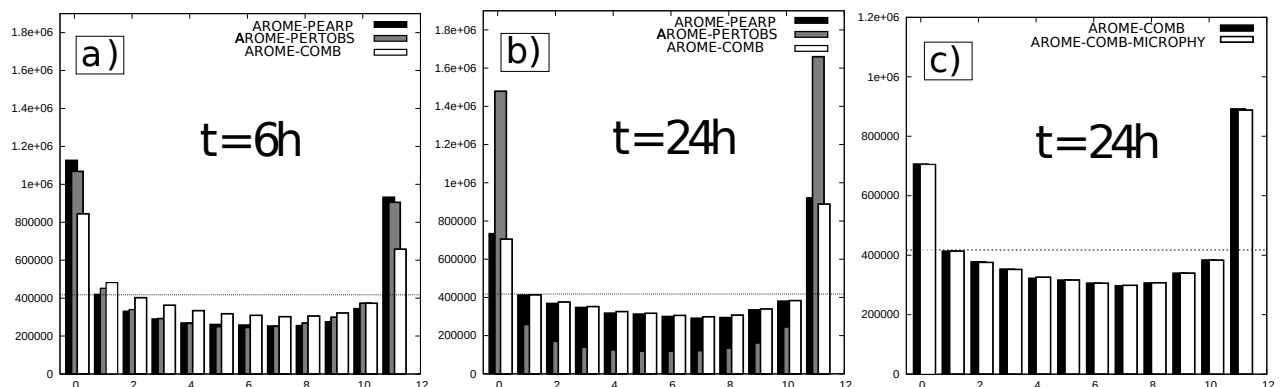


FIGURE 2.23 – Diagramme de rang pour la prévision du module du vent à 925 hPa, calculé pour la période du 15 oct. au 1er nov. 2008 et ceci pour l'échéance 6h a) et 24h b) et c). D'après Vié et al (2012).

Dans un article publié dans la revue *Natural Hazards and Earth System Sciences* (NHESS), Benoît Vié montre l'impact de la prise en compte simultanée des différentes sources d'incertitude présentées précédemment (Vié et al., 2012). La période continue allant du 15 oct. au 1 nov. 2008 ainsi que les deux cas de fortes pluies méditerranéens le 20 oct. 2008 et les 1-2 nov. 2008 sont considérés. Les ensembles précédemment nommés AROME-PEARP et AROME-PERTOBS dans Vié et al (2011) servent de référence. Un autre ensemble (AROME-COMB) tient compte simultanément des incertitudes provenant des conditions initiales et aux limites latérales, en combinant les techniques utilisées pour élaborer AROME-PEARP et AROME-PERTOBS.

L'évaluation statistique de AROME-COMB sur la période d'un mois montre une nette amélioration de la dispersion entre AROME-PEARP et AROME-PERTOBS (Fig. 2.23a et b). Il est donc bénéfique de prendre en compte simultanément les incertitudes provenant des conditions initiales et aux limites latérales. L'amélioration est significative à courte échéance (6 à 12h), pour laquelle l'ensemble AROME-PERTOBS a déjà perdu une grande partie de sa dispersion, et l'ensemble AROME-PEARP n'en a pas encore suffisamment. Pour les échéances plus longues, l'impact plus important des conditions aux limites latérales fait que AROME-COMB et AROME-PEARP ont le même comportement (Fig. 2.23b).

Pour échantillonner au mieux l'incertitude sur la prévision, il est nécessaire de tenir compte également des erreurs de modélisation, en complément des incertitudes sur les conditions initiales et aux limites latérales. Les sources d'erreur de modélisation sont nombreuses. Les approximations utilisées dans les systèmes d'équations implémentés dans les modèles, la discréétion numérique de ces équations, ou encore l'utilisation de paramétrisations pour représenter les processus sous-maille sont autant de sources d'erreur.

Les travaux présentés dans la partie 2.2 ont montré le rôle important que jouent les processus physiques de basses couches à méso-échelle dans l'entretien et la stationnarité des systèmes convectifs. Le mécanisme de soulèvement identifié, mettant en jeu l'évaporation des précipitations et le refroidissement associé des basses couches dans la formation d'une plage froide sous orages, favorise à son tour le déclenchement de nouvelles cellules convectives.

Dans le cadre de sa thèse, Benoît Vié a également examiné l'impact de perturbations appliquées aux paramétrisations des processus impliqués dans la génération et l'évolution de la pluie dans le modèle, ceci afin d'étudier l'impact de cette source d'incertitude la prévisibilité des systèmes précipitants. Benoît Vié a repris la même approche de perturbation du schéma de la microphysique chaude proposé par Fresnay et al (2012) pour le modèle Meso-NH, qu'il a implémentée dans le modèle AROME. Dans le schéma de la microphysique chaude, les tendances d'autoconversion des goutelettes nuageuses en eau précipitante, l'accrétion des gouttelettes nuageuses sur les particules d'eau précipitante, ainsi que l'évaporation de l'eau précipitante sont perturbées en leur appliquant un coefficient multiplicatif constant dans l'espace et dans le temps.

Un ensemble avec le modèle AROME a été réalisé, prenant de surcroît une partie de l'erreur de modélisation, associée au schéma de la microphysique chaude, on nomme ainsi cet ensemble AROME-COMB-MICROPHY. Aucune différence statistique ne peut être mise en évidence entre AROME-COMB et AROME-COMB-MICROPHY. Les perturbations microphysiques appliquées, ne jouant que sur les fortes précipitations, leur effet n'est pas visible en moyenne sur notre période (Fig. 2.23c). Cependant, pour certains des cas d'étude où le contexte météorologique est moins piloté par le forçage synoptique et l'orographie, il existe une sensibilité plus marquée quant à la localisation et l'intensité des précipitations due aux perturbations sur les processus microphysiques. Dans ce type de situations, l'incertitude de la prévision associée aux erreurs de modélisation de la microphysique chaude est donc importante pour les mécanismes d'initiation de la convection et de régénération des systèmes convectifs par déclen-

chement de nouvelles cellules, et donc pour la stationnarité des systèmes précipitants.

Bien évidemment, la perturbation des tendances de la microphysique chaude n'est pas suffisante. Même en ce qui concerne les épisodes fortement précipitants, il est indispensable de s'intéresser également, *a minima*, aux processus impliquant les espèces microphysiques glacées. L'incertitude provenant d'autres paramétrisations du modèle (turbulence, rayonnement,...) doit aussi être prise en compte. Afin d'englober une grande part de l'erreur de modélisation, la technique de perturbation stochastique des tendances physiques (SPPT) a été adaptée au modèle AROME puis implantée dans ce dernier par Boutrier *et al* (2012). Les résultats de cette étude montrent que la qualité de l'ensemble est fortement améliorée, notamment dans les basses couches de l'atmosphère.

### 2.4.3 Evaluation de systèmes de PE à l'échelle convective dédiés à la campagne HyMeX

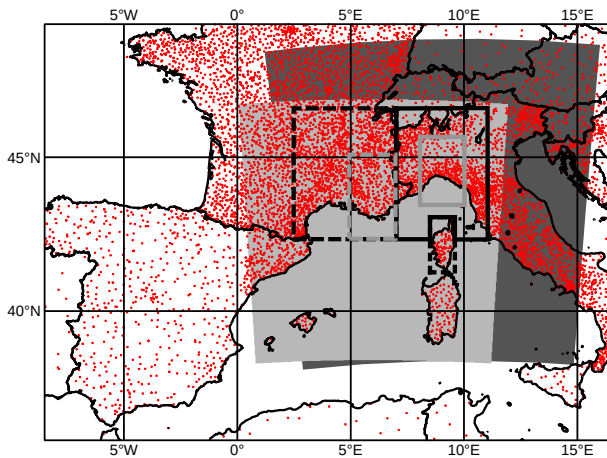


FIGURE 2.24 – Domaines géographiques des ensembles PE AROME (gris clair) et COSMO-H2-EPS (gris foncé). Les points rouges matérialisent le réseau de stations de pluviomètres avec une densité renforcée pour les besoins de la campagne sur la France, l'Italie et la Catalogne. D'après Nuissier *et al* (2016).

Sur la base de ces premiers travaux s'attachant à quantifier l'importance de chaque source d'incertitude impactant la prévision du modèle AROME, j'ai contribué par la suite à la mise en place d'un prototype de PE avec le modèle AROME qui a fourni des prévisions en temps quasi-réel lors de la SOP1 HyMeX. Ce système de PE intégrait l'ensemble des avancées scientifiques réalisées jusqu'alors, à savoir : (i) la prise en compte de l'incertitude issue des conditions aux limites via une classification objective des membres de la PEARP, (ii) une assimilation d'ensemble (assimilation d'observations perturbées) fournissant les conditions initiales à méso-échelle et (iii) les erreurs de modélisation décrites par la SPPT.

La PE AROME, avec ses 8 membres, a été comparée à un autre système de PE à l'échelle convective (COSMO-H2-EPS) dédié à la campagne HyMeX. COSMO-H2-EPS est basé sur le modèle COSMO avec une résolution horizontale de 2.8 km. Les conditions initiales et aux limites latérales proviennent des 10 premiers membres de l'ensemble régional COSMO-LEPS. COSMO-LEPS quant à lui avec une résolution horizontale de 7 km, est initialisé et forcé par une sélection objective de 16 membres de l'ensemble global ECMWF EPS. Les deux ensembles

PE AROME et COSMO-H2-EPS sont évalués sur la période SOP1 (6 sep. - 5 nov 2012) et sur un domaine de vérification centré sur le Sud-Est de la France et sur la région Ligure-Toscane.

#### *Performance globale des ensembles sur la période SOP1*

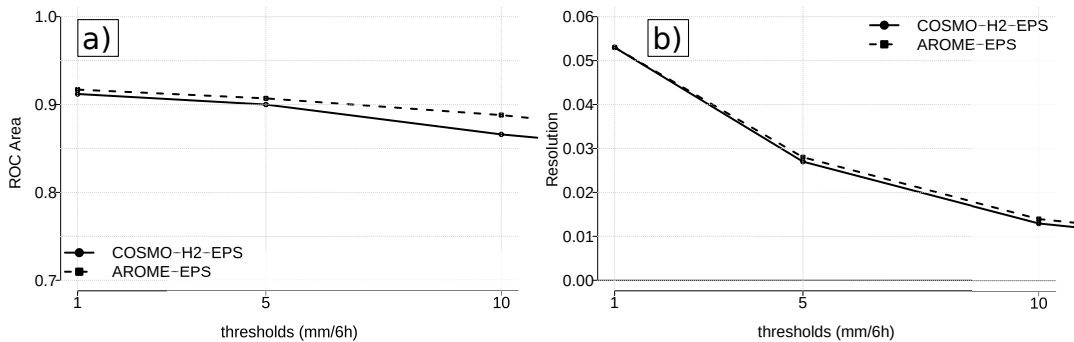


FIGURE 2.25 – Résolution et aire sous la courbe ROC (ROCA) pour les ensembles PE AROME et COSMO-H2-EPS sur le domaine de validation italien Ligure-Toscane (LT). D'après Nuissier et al (2016).

La Figure 2.25a montre que, sur la période SOP1, la PE AROME a une meilleure discrimination des événements précipitants (pluies sur 6h supérieures aux seuils définis) que COSMO-H2-EPS, en particulier sur le domaine de vérification Ligure-Toscane où la variabilité des précipitations a été plus importante. Cependant, les résolutions statistiques sont équivalentes pour les deux systèmes.

#### *Prévisibilité hydrométéorologique d'épisodes précipitants observés durant la POI 16a*

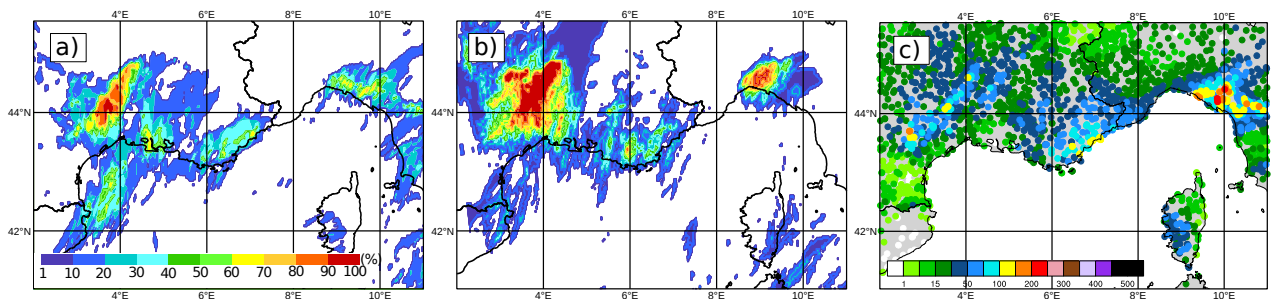


FIGURE 2.26 – Distribution spatiale des probabilités de dépassement du seuil de 50 mm pour les précipitations simulées cumulées entre 00UTC le 26 Octobre 2012 et 00 UTC le 27 Octobre 2012 pour a) la PE AROME et b) COSMO-H2-EPS. La vignette c) représente les observations de précipitations cumulées sur la même période. D'après Nuissier et al (2016).

Dans un second temps, nous nous sommes intéressés à l'analyse de la prévisibilité de deux situations fortement précipitantes observées durant la période d'observation intensive 16a le 26 Octobre 2012 sur le bassin Méditerranée Nord-Occidental. Dans la matinée du 26 Octobre

2012, les conditions météorologiques étaient très favorables à la génération d'événements fortement pluvieux, à savoir un flux en altitude orienté de sud à sud-ouest et une puissante advection d'humidité en basses couches. Un premier Système Convectif de Méso-échelle (MCS) au-dessus de la Méditerranée et a traversé le département du Var dans l'après-midi du 26 en causant deux morts sur Toulon. Un autre système quant à lui a touché la région de Ligure-Toscane avec des cumuls très importants de l'ordre de 250 mm en 24h.

Les ensembles PE AROME et COSMO-H2-EPS permettent de bien anticiper le risque de fortes précipitations à partir des cartes de probabilités de dépassement du seuil de 50 mm en 24h présentées en Figure 2.26. En effet, les risques de fortes pluies est bien cerné sur la région des Cévennes, du Var et Ligure-Toscane comparativement aux observations. Cependant, la PE AROME semble un peu mieux englober l'incertitude spatiale associée aux précipitations les plus fortes concernant le Var et la Ligure-Toscane.

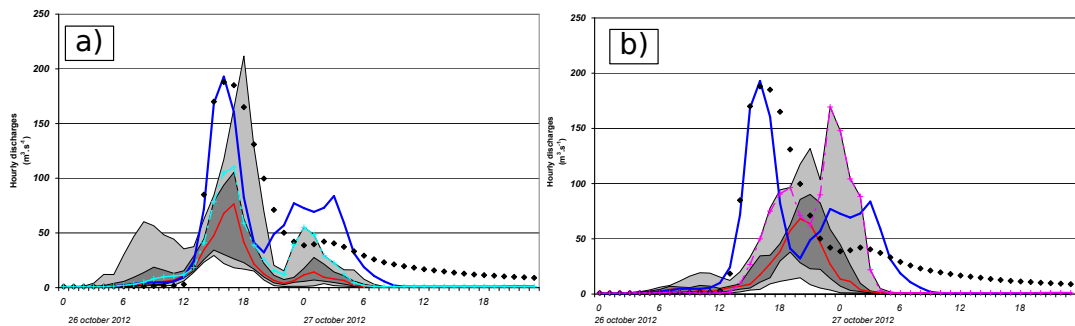


FIGURE 2.27 – Prévisions d’ensemble de débits pour la rivière du Gapeau à Hyères pour a) la PEAROME et b) COSMO-H2-EPS : les losanges noirs représentent les observations. Les débits obtenus en forçant le modèle ISBA-TOP avec des données radar sont représentés par ligne bleue. La plage grisée indique l’intervalle interquartile avec la médiane en ligne rouge. D’après Nuissier et al (2016).

En plus de l’évaluation météorologique classique, cette étude met également en place un processus innovant d’évaluation hydro-météorologique de ces prévisions d’ensemble de cas de fortes pluies. Chaque prévision de précipitations a alors été utilisée en entrée du modèle hydrologique ISBA-TOP (Vincendon *et al.*, 2011), pour ainsi constituer un ensemble de débits pour des bassins versants de la rivière du Gapeau à Hyères et de Magra à Améglio.

Les résultats pour le département du Var sur la Figure 2.27 montrent que les deux systèmes d’ensemble indiquent un risque de dépasser un premier seuil d’alerte, qui est de  $130 \text{ m}^3 \text{s}^{-1}$  à Hyères. Cependant, la PERAOME représente mieux la dynamique de la crue, avec une médiane de l’ensemble reproduit les deux pics de débit observés. L’ensemble COSMO-H2-EPS propose quant à lui des scénarii avec des pics de crues décalés temporellement par rapport aux observations (Fig. 2.27b). Cette approche en prévision d’ensemble hydrométéorologique permet d’évaluer les ensembles atmosphériques en terme de chronologie et de localisation précise des fortes précipitations, qui sont elles mêmes pilotées par la bonne représentation de certains ingrédients météorologiques que nous avons vus dans la partie 2.2.

Duffourg *et al* (2015) ont montré que le creusement d’une dépression de surface au sud du golfe du Lion et la convergence de basses couches associée étaient les éléments clés favorisant la régénération continue de cellules convectives sur mer constituant le MCS qui a ensuite affecté le Var dans la journée du 26 Octobre 2012. Si l’on examine de manière “ensembliste” ces ingrédients favorables, ils sont mieux représenter en moyenne dans la PE AROME, ce qui explique

un meilleur ciblage de fortes précipitations sur le département du Var.

La meilleure capacité de la PE AROME à pouvoir mieux discriminer les événements précipitants vient probablement du fait que ce dernier a son propre système d'assimilation et tire bénéfice de perturbations construites à l'échelle kilométrique, aidant ainsi à mieux capturer la variabilité à cette échelle. Les résultats de cette étude viennent en tout cas conforter notre stratégie et nos choix quant à la représentation des principales sources d'incertitudes inhérentes à la prévision du modèle AROME.

#### 2.4.4 Conclusions

Une troisième et dernière partie de mes activités de recherche s'est donc focalisée sur l'étude de la prévisibilité à l'échelle convective des systèmes précipitants avec le modèle AROME. Dans cette partie, j'ai contribué donc à mieux quantifier la prévisibilité de ces événements et à estimer l'incertitude associée à leur prévision dans les modèles numériques à haute résolution. Ces résultats ont été à la base du futur système de prévision d'ensemble AROME, dont la première version exploitée en mode opérationnelle verra le jour en fin d'année 2016. Une partie de ces travaux ont été également réalisée dans le cadre de la thèse Benoit Vié (**Vié, 2012**) que j'ai co-dirigée.

Pour répondre à la question de l'identification des sources d'incertitude, nous avons adopté une approche dans laquelle nous avons étudié séparément les sources d'incertitude essentielles à considérer (conditions aux limites latérales, conditions initiales et erreurs de modélisation) à l'aide de simulations d'ensemble. La grande difficulté pour la définition d'une prévision d'ensemble aux échelles du modèle AROME est le petit nombre de membres de l'ensemble qui est contraint par la puissance de calcul. Le challenge est donc de concevoir des méthodes de perturbation qui permettent d'échantillonner les principales erreurs en un dizaine de solutions. D'autre part, la campagne HyMeX a fourni un cadre pour le développement de la prévision d'ensemble à la résolution kilométrique et une opportunité unique pour son évaluation dans le contexte de la prévision des pluies intenses et des crues rapides.

Concernant les incertitudes issues des conditions aux limites latérales, j'ai mis au point une technique de classification automatique, sur la base de critères objectifs, qui permet de ne retenir que quelques membres de la prévision d'ensemble globale tout en minimisant l'erreur d'échantillonnage de la distribution complète de la PEARP utilisée en conditions latérales pour le modèle AROME. Cette approche a un impact significatif, par rapport à un choix aléatoire, surtout si la situation météorologique présente une forte variabilité c'est-à-dire une faible prévisibilité.

Benoit Vié a ensuite montré, au moyen d'une méthode de perturbation initiales par assimilation d'ensemble, qu'il était aussi nécessaire de perturber les conditions initiales en particulier pour améliorer la dispersion de l'ensemble dans les 12 premières heures (**Vié et al., 2012**).

Un système de prévision d'ensemble basé sur ces méthodes de perturbation (conditions initiales, conditions aux limites et erreurs de modélisation) et pour un domaine AROME couvrant la Méditerranée nord-occidentale a été mis en œuvre en temps réel pendant la SOP1. Ce système a été comparé au système italien de prévision d'ensemble à la résolution kilométrique (COSMO-H2-EPS) sur la période de la SOP1, avec des scores globalement meilleurs pour la prévision d'ensemble AROME (Nuissier et al., 2015).

Une mise en exploitation opérationnelle du système de prévision d'ensemble avec le modèle AROME sera effective d'ici fin 2016. Cependant, pour des raisons de complexité de mise en œuvre opérationnelle de l'assimilation d'ensemble, la technique d'assimilation d'ensemble est remplacée par l'application des perturbations de la PEARP à l'analyse AROME pour cette

première version opérationnelle de la PE AROME. Cette technique est moins performante dans les premières 9 heures de prévision. Néanmoins, il a été montré la supériorité de la PE AROME par rapport à la PEARP et à AROME-France déterministe pour la prévision des fortes précipitations.

## Chapitre 3

# Synthèse et perspectives

La Méditerranée nord-occidentale est régulièrement touchée, principalement durant l'automne, par des épisodes de pluie intense. La région connaît un cas à très forts enjeux, en moyenne une fois par an, à une fois tous les deux ans. Parmi ces événements, les cas de convection stationnaires ou peu mobiles sont très nombreux. La prévision de la localisation et de l'intensité précises de ces intempéries demeure délicate et difficile en raison de processus et mécanisme impliqués complexes, et pouvant être assez variables spatialement.

Mes travaux de recherche effectués entre 2005 et 2016 sont résumés dans ce mémoire. Ils ont porté sur 3 principaux axes thématiques : (i) l'amélioration des connaissances et la modélisation, (ii) la régionalisation climatique et (iii) la prévisibilité à l'échelle convective des systèmes précipitants des régions méditerranéennes. Je vais, dans un premier temps, faire une synthèse de ma contribution pour chacune des thématiques, puis je présenterai les principales orientations que je souhaiterais donner à mes recherches pour les 4 ou 5 prochaines années.

Lors de mes travaux sur la modélisation des systèmes fortement précipitants méditerranéens, j'ai cherché à identifier les processus atmosphériques associés aux situations météorologiques de précipitations intenses conduisant à la formation de crues rapides sur le pourtour méditerranéen, à partir de simulations numériques issues du modèle Meso-NH. Des études de sensibilité ont permis de mettre en évidence les liens étroits qui existent entre la localisation et la structure spatiale de ces système fortement précipitants d'une part, et la structure du relief à fine échelle et le flux amont de basses couches humide et instable d'autre part. Un des résultats importants a été de mieux comprendre notamment les conditions favorisant un régime fortement précipitant plus en amont sur les plaines ou les régions côtières plus vulnérables, conduisant donc à une situation potentiellement plus dangereuse.

Ces études sur la modélisation des épisodes fortement pluvieux méditerranéens nous ont montré également que l'utilisation d'une résolution horizontale de 500 m n'améliorait pas systématiquement la prévision quantitative des précipitations, avec des résultats spatialement différents et parfois mitigés, dégradant la prévision de certaines situations. Parmi les processus clés, la microphysique et la turbulence ont une influence importante sur la localisation et la production des fortes précipitations dans les systèmes précipitants. Pour améliorer la prévision de ces événements extrêmes, il reste des progrès à faire dans l'identification des mécanismes et leurs interactions multi-échelles, ainsi que dans leurs représentations dans les modèles avec des mailles d'échelle sub-kilométrique.

Pour l'amélioration des paramétrisations physiques clés dans les modèles d'échelle sub-kilométrique deux axes importants pour la recherche au cours des prochaines années sont identifiés et concernent : (i) la modélisation des processus microphysiques, qui sont des sources importantes d'erreur dans la prévision et (ii) la modélisation de la turbulence dans la couche

limite et la représentation de la turbulence dans et à proximité des nuages convectifs. Pour la paramétrisation des processus microphysiques de nouveaux schémas à 2 moments, représentant explicitement l'effet des particules d'aérosols, ont été développés. Un schéma comme LIMA<sup>1</sup> par exemple, développé pour le modèle Meso-NH, permettra de mieux comprendre le rôle des particules d'aérosols dans la production des précipitations intenses. En ce qui concerne la turbulence, des schémas plus adaptés permettront de mieux représenter le mélange turbulent qui reste actuellement insuffisant pour des gammes de résolution allant de 500 m à 2 km.

Mes activités de recherche sur cette thématique de la modélisation des systèmes fortement précipitants aux échelles sub-kilométriques s'inscriront en partie dans la suite de la thèse de Maxime Martinet. Les simulations déjà réalisées à 500 m de résolution avec les paramétrisations actuelles dans le modèle Meso-NH ont été une première étape. Dans la suite de ce travail de thèse, des simulations sur des grands domaines et une résolution horizontale de 150 m seront réalisées, afin de simuler explicitement une grande partie de la turbulence et de représenter pleinement les interactions multi-échelles des mécanismes générant la convection. Une analyse des processus à cette échelle sera réalisée et les résultats obtenus pour ces simulations dites de références seront confrontés à de nouvelles simulations réalisées avec les nouvelles paramétrisations développées dans le modèle Meso-NH pour la turbulence et/ou la microphysique. Les données de la campagne HyMeX permettront de valider les processus mis en évidence dans les simulations numériques. Ces travaux de recherche seront réalisés en partie dans la cadre du projet ANR MUSIC<sup>2</sup> (2015-2018).

Une autre partie de mes travaux de recherche a contribué à quantifier les incertitudes et à mieux cerner la prévisibilité des situations prévues par le modèle AROME. Nous avons adopté une approche en prévision d'ensemble. Une des caractéristiques et difficultés pour la définition d'une prévision d'ensemble à la résolution kilométrique est le petit nombre de membres de l'ensemble contraint par la puissance de calcul. La question était donc d'identifier les sources d'incertitudes essentielles à considérer (conditions initiales, conditions aux limites latérales, erreurs de modélisation) et de concevoir des méthodes de perturbation qui permettent d'échantillonner les principales erreurs en une dizaine de réalisations. Pour se faire, nous avons évalué les différents facteurs limitant la prévisibilité des événements fortement méditerranéens.

Ces méthodes de perturbation sur les conditions initiales, conditions aux limites et erreurs de modélisation, dédiés à l'échelle convective, ont été développées puis évaluées dans le cadre de la SOP1 de la campagne HyMeX et pour un domaine AROME couvrant la Méditerranée nord-occidentale. Ce prototype de prévision d'ensemble AROME sur la France, qui devrait être opérationnelle d'ici fin 2016, a bénéficié pour son évaluation de la haute densité des observations en Italie et Espagne disponibles sur la période SOP1.

Cependant, il comporte encore des marges d'amélioration : d'une part, certaines faiblesses connues du système ne sont pas encore représentées sous forme de perturbations d'erreur de modélisation (dynamique du modèle, couche limite, couplage océan-atmosphère) ; d'autre part, le système actuel a été validé en termes de performances moyennes, mais pas de manière systématique sur d'autres événements à enjeux, on sait donc encore peu de choses sur leurs limites de prévisibilité.

Dans le cadre de la phase d'exploitation de la SOP1 HyMeX, mes travaux de recherche continueront autour de l'étude des processus impliqués dans les systèmes précipitants méditerranéens à partir de la prévision d'ensemble AROME. L'objectif sera d'examiner si la variabilité des champs prévus correspond à des processus et mécanismes déclencheurs de la convection différents ou alors communs, mais simplement variables temporellement et géographiquement.

---

1. Liquid Ice and Multiple Aerosol

2. Multiscale process studies of intense convective precipitation events in Mediterranean

ment. Pour répondre à cette question, différentes simulations avec le modèle Meso-NH seront réalisées à partir de conditions initiales et aux limites latérales fournies par différents ensembles AROME dans lesquelles les sources d'incertitude auront été isolées. Les diagnostics développés dans le modèle Meso-NH permettront d'analyser en détails les mécanismes déclencheurs de la convection.

Pour terminer cette synthèse, un autre partie de mes travaux de recherche s'est articulée autour de la thématique de la régionalisation climatique des épisodes fortement précipitants méditerranéens et de la question de l'évolution des événements extrêmes dans la perspective du changement climatique. Pour répondre à cette question nous avons mis en œuvre une méthode de descente d'échelle statistico-dynamique dans laquelle les potentiels événements fortement précipitants sont détectés uniquement par leurs contextes météorologiques de plus grande échelle puis simuler à haute résolution avec le modèle Meso-NH. Même si de nombreuses incertitudes persistent concernant la robustesse des résultats, la variabilité de la localisation des zones impactées par les fortes précipitations augmente clairement dans le climat futur. Ce dernier tend à augmenter et à privilégier les événements affectant préférentiellement la région du Languedoc-Roussillon.

Une perspective d'amélioration de l'outil de sélection serait de considérer d'autres paramètres importants pour la génération de fortes pluies, en partant cette fois d'une réanalyse de résolution plus fine (ERA-Interim par exemple). Cela permettrait d'accéder à une part plus importante de la population des événements intenses. Une autre piste d'amélioration de la méthode pourrait être d'intégrer le caractère de stationnarité de ces conditions d'échelle synoptique dans la méthode, ce qui contribuerait grandement à ne conserver que les situations pluvieuses durables, soit celles aboutissant aux cas potentiellement les plus intenses.

La démarche méthodologique utilisée dans le cadre du projet CYPRIM demande malgré tout à être généralisée en considérant différents scénarios climatiques, en améliorant l'outil d'identification des situations météorologiques favorables aux événements de fortes pluies et en augmentant le nombre de simulations à haute résolution, seules capables de représenter de manière réaliste les processus associés aux événements fortement précipitants. Le modèle de prévision à fine échelle AROME permettrait de multiplier aisément le nombre de simulations à réaliser à haute résolution.

Cependant, ces approches statistico-dynamiques reposent sur l'hypothèse forte que les environnements et circulations météorologiques associés aux événements de fortes pluies ne changent pas entre le climat présent et futur, ce qui n'est nécessairement pas le cas. D'autre part les processus physiques qui interagissent et pilotent la convection (interaction avec le relief ou plages froides sous orages par exemple) sont souvent mal représentés dans les modèles de climat de type régional ou global de résolution horizontale trop lâche, ce qui induit des sources d'incertitude importantes.

L'utilisation du modèle AROME à la résolution horizontale de 2.5 km apparaît comme une perspective naturelle de progrès dans l'étude des événements fortement précipitants méditerranéens aux échelles climatiques. Ce type de modèle, appelé modèle de climat à échelle convective, commence à être utilisé dans des études de climat en Europe (Kendon *et al.*, 2014). Il faut signaler que dans le cadre de MED-CORDEX et EURO-CORDEX<sup>3</sup> seront réalisées de longues simulations climatiques à partir de modèles à convection explicite sur un domaine Europe englobant les Alpes et centré sur la Méditerranée Nord-Occidentale. Cette étude visera à examiner l'impact du changement climatique sur les événements météorologiques extrêmes sur la région. Au CNRM plus particulièrement des simulations seront réalisées avec le modèle

---

3. Downscaling Experiment - European Domain

**AROME.**

J'envisage de m'investir dans cette recherche dont l'objectif sera donc d'utiliser le modèle AROME dans de longues simulations du climat présent et d'un potentiel climat futur, afin de régionaliser plus finement l'évolution des événements précipitants méditerranéens, tant en fréquence qu'en intensité. On pourrait se placer à une échelle infra journalière et se focaliser dans un premier temps sur les pluies horaires et mesurer la valeur d'ajoutée d'un modèle AROME climat (résolution 2.5 km) par rapport aux modèles climatiques régionaux (résolution > 10 km). Un objectif ambitieux serait d'aller plus loin et de déterminer si une évolution dans les intensités et la distribution spatiale est corrélée à des modifications des environnements météorologiques favorables voire même des modifications dans les processus physiques pilotant le déclenchement et le maintien de ces épisodes convectives.

Mes perspectives de recherche pour ces prochaines années seront donc organisées autour de la connaissance et la prévisibilité des systèmes fortement précipitants et de leurs simulations climatiques. Des études en processus seront réalisées en synergie avec l'exploitation du jeu de données de la campagne de mesures HyMeX.

# Références bibliographiques

- Anthes, R. (1972). The development of asymmetries in three-dimensional numerical model of tropical cyclone. *Mon.*, 100 :461–476.
- Beaulant, A.-L., Joly, B., Nuissier, O., Somot, S., Ducrocq, V., Joly, A., Sevault, F., Déqué, M., et Ricard, D. (2011). Statistico-dynamical downscaling for mediterranean heavy precipitation. *Quart. J. Roy. Meteor. Soc.*, 137 :736–748.
- Berre, L., Stefanescou, S., et Belo Pereira, M. (2006). The representation of the analysis effect in three error simulation techniques. *Tellus*, 58A :196–209.
- Bielli, S. et Roux, F. (1999). Initialization of a cloud-resolving model with airborne doppler radar observations of an oceanic tropical convective system. *Mon. Wea. Rev.*, 127 :1038–1055.
- Bouttier, F., Vié, B., Nuissier, O., et Raynaud, L. (2012). Impact of stochastic physics in a convection-permitting ensemble. *Mon. Wea. Rev.*, 140 :3706–3721.
- Bresson, E. (2011). *Mécanismes de formation des systèmes convectifs quasi-stationnaires en Méditerranée nord-occidentale. Application au cas du 15 Juin 2010 sur le Var.* PhD thesis, Université Toulouse III Paul Sabatier.
- Bresson, E., Ducrocq, V., Nuissier, O., Ricard, D., et de Saint-Aubin, C. (2012). Idealised numerical simulations of quasi-stationary convective systems over the northwestern mediterranean complex terrain. *qjrms*.
- Bresson, R., Ricard, D., et Ducrocq, V. (2009). Idealized mesoscale numerical study of mediterranean heavy precipitating convective systems. *Meteor. Atmos. Phys.*, 103 :45–56.
- Buizza, R. et Palmer, T. N. (1995). The singular vector of the atmosphere global circulation. *J. Atmos. Sci.*, 52(1434–1456).
- Buzzi, A., Tartaglione, N., et Malguzzi, P. (1998). Numerical simulations of the 1994 piedmont flood : Role of orography and moist processes. *Mon. Wea. Rev.*, 126 :2369–2383.
- Chen, C. et Lin, Y. (2005). Orographic effects on a conditionally unstable flow over an idealized three-dimensional mesoscale mountain. *J. Atmos. Sci.*, 62 :331–350.
- Chu, C. et Lin, Y. (2000). Effects of orography on the generation and propagation of mesoscale convective systems in a two-dimensional unstable flow. *J. Atmos. Sci.*, 57 :3817–3837.
- Colin, J. (2011). *Etude des évènements précipitants intenses en Méditerranée : approche par la modélisation climatique régionale.* PhD thesis, Université Toulouse III Paul Sabatier.
- Doswell, C. A., I., Ramis, C., Romero, R., et Alonso, S. (1998). A diagnostic study of three heavy precipitation episodes in the western mediterranean region. *Weather and Forecasting*, 13 :102–124.
- Ducrocq, V., Braud, I., Davolio, S., Ferretti, R., Flamant, C., Jansa, A., Kalthoff, N., Richard, E., Taupier-Letage, I., Ayral, P.-A., Belamari, S., Berne, A., Borga, M., Boudevillain, B., Bock,

- O., Boichard, J.-L., Bouin, M.-N., Bousquet, O., Bouvier, C., Chiggiato, J., Cimini, D., Corsmeier, U., Coppola, L., Cocquerez, P., Defer, E., Delanoë, J., Di Girolamo, P., Doerenbecher, A., Drobinski, P., Dufournet, Y., Fourrié, N., Gourley, J., Labatut, L., Lambert, D., Le Coz, J., Marzano, F., Molinié, G., Montani, A., Nord, G., Nuret, M., Ramage, K., Rison, W., Rousset, O., Said, F., Schwarzenboeck, A., Testor, P., Van Baelen, J., Vincendon, B., Aran, M., et Tamayo, J. (2014). Hymex-sop1 : The field campaign dedicated to heavy precipitation and flash flooding in the northwestern mediterranean. *Bull. Amer. Meteor. Soc.*, 95 :1083–1100.
- Ducrocq, V., Lafore, J.-P., Redelsperger, J.-L., et Orain, F. (2000). Initialization of a fine-scale model for convective-system prediction : A case study. *Q. J. Roy. Meteor. Soc.*, 126 :3041–3065.
- Ducrocq, V., Nuissier, O., Ricard, D., Lebeaupin, C., et Thouvenin, T. (2008). A numerical study of three catastrophic precipitating events over southern france. ii : Mesoscale triggering and stationarity factors. *Quart. J. Roy. Meteor. Soc.*, 134 :131–145.
- Ducrocq, V., Ricard, D., Lafore, J.-P., et Orain, F. (2002). Storm-scale numerical rainfall prediction for five precipitating events over france : On the importance of the initial humidity field. *Wea. Forecasting*, 17 :1236–1256.
- Duffourg, F., Nuissier, O., Ducrocq, V., Bock, O., Chazette, P., Delanoë, J., Doerenbecher, A., Flamant, C., Fourrié, N., di Girolamo, P., Lac, C., Martinet, M., et Said, F. (2015). Offshore deep convection initiation and maintenance during hymex iop 16a heavy precipitation event. *Q. J. Roy. Meteor. Soc.*, page Submitted.
- Federico, S., Avolio, E., Bellecci, C., Lavagnini, A., et Walko, R. (2007). Predictability of intense rain storms in the central mediterranean basin : sensitivity to upper-level forcing. *Adv. Geosci.*, 12 :5–18.
- Fresnay, S., Hally, A., Garnaud, C., Richard, E., et Lambert, D. (2012). Heavy precipitation events in the mediterranean : sensitivity to cloud physics parameterisation uncertainties. *Nat. Hazards Earth Syst. Sci.*, 12 :2671–2688.
- Gebhardt, C., Theis, S., Paulat, M., et Ben Bouallègue, Z. (2011). Uncertainties in cosmo-de precipitation forecasts introduced by model perturbations and variation of lateral boundaries. *Atmos. Res.*, 100 :168–177.
- Giorgi, G. (2006). Climate change hot-spots. *Geophys. Res. Lett.*, 33.
- Homar, V., Romero, R., Ramis, C., et Alonso, S. (1999). A case of convection development over the western mediterranean sea : a study through numerical simulations. *Meteor. Atmos. Phys.*, 71 :169–188.
- Houtekamer, P. L., Lefavre, L., Derome, J., Ritchie, H., et Mitchell, H. L. (1996). A system simulation approach to ensemble prediction. *Mon. Wea. Rev.*, 124(1225–1242).
- Jacob, D. et CoAuthors (2014). Euro-cordex : new high-resolution climate change projections for european impact research. *Reg Environ Change*, 14 :563–578.
- Jansa, A., Genoves, A., Angeles Picornell, M., Campins, J., Riosalido, R., et Carretero, O. (2001). Western mediterranean cyclones and heavy rain. part 2 : Statistical approach. *Meteorol. Appl.*, 8 :43–56.
- Jolivet, S., Chane-Ming, F., Barbary, D., et Roux, F. (2013). A numerical study of orographic forcing on tc dina (2002) in south west indian ocean. *Ann. Geophys.*, 31 :107–125.
- Kendon, E. J., Roberts, N. M., Fowler, H. J., Roberts, M. J., Chan, S. C., et Senior, C. A. (2014). Heavier summer downpours with climate change revealed by weather forecast resolution model. *Nature Climate Change*, 4(7) :570–576.

- Kossin, J. P. et Schubert, W. (2004). Mesovortices in hurricane isabel. *Bull. Amer. Meteor. Soc.*, 85 :151–153.
- Kurihara, Y., Bender, M., et Ross, R. (1993). An initialization scheme of hurricane models by vortex specification. *Mon. Wea. Rev.*, 121 :2030–2045.
- Kurihara, Y., Bender, M., Tuleya, R., et Ross, R. (1995). Improvements in the gfdl hurricane prediction system. *Mon. Wea. Rev.*, 123 :2791–2801.
- Lafore, J.-P., Stein, J., Ascencio, N., Bougeault, P., Ducrocq, V., Duron, J., Fisher, C., Hereil, P., Mascart, P., Pinty, J.-P., Redelsperger, J.-L., Richard, E., et Vila-Guerau de Arellano, J. (1998). The meso-nh atmospheric simulation system. part i : Adiabatic formulation and control simulations. *Ann. Geophys.*, 16 :90–109.
- Leith, C. (1974). Theoretical skill of monte carlo forecasts. *Mon. Wea. Rev.*, 102(6) :409–418.
- Lin, Y., Chiao, S., Wang, T., Kaplan, M., et Weglarz, R. (2001). Some common ingredients for heavy orographic rainfall. *Weather and Forecasting*, 16 :633–659.
- Lin, Y., Ray, P., et Johnson, K. (1993). Initialization of a modelled convective storm using doppler radar derived fields. *Mon. Wea. Rev.*, 121 :2757–2775.
- Liu, Y., Zhang, D., et Yau, M. (1997). A multiscale numerical study of hurricane andrew (1992). part i : explicit simulation and verification. *Mon. Wea. Rev.*, 125 :3073–3093.
- Marsigli, C., Bocanera, F., Montani, A., et Paccagnella, T. (2005). The cosmo-leps mesoscale ensemble system : validation of the methodology and verification. *Nonlin. Proc. Geophys.*, 12 :527–536.
- Marsigli, C., Montani, A., Nerozzi, F., Paccagnella, T., Tibaldi, S., Molteni, F., et Buizza, R. (2001). A strategy for high resolution ensemble prediction. ii : Limited-area experiments in four alpine flood events. *Quart. J. Roy. Meteor. Soc.*, 127 :2095—2115.
- Massacand, A., Wernli, H., et Davies, H. (1998). Heavy precipitation on the alpine south side : An upper-level precursor. *Geophys. Res. Lett.*, 25 :1435–1438.
- Michelangeli, P., Vautard, R., et Legras, B. (1995). Weather regimes : recurrence and quasi-stationarity. *J. Atmos. Sci.*, 52 :1237–1256.
- Miglietta, M. et Rotunno, R. (2009). Numerical simulations of conditionally unstable flows over a mountain ridge. *J. Atmos. Sci.*, 66 :1865–1885.
- Miglietta, M. et Rotunno, R. (2010). Numerical simulations of low-cape flows over a mountain ridge. *J. Atmos. Sci.*, 67 :2391–2401.
- Molteni, F., Buizza, R., Marsigli, C., Montani, A., Nerozzi, F., et Paccagnella, T. (2001). A strategy for high resolution ensemble prediction. i : Definition of representative numbers and global-model experiments. *Quart. J. Roy. Meteor. Soc.*, 127 :2069—2094.
- Montani, A., Cesari, D., Marsigli, C., et Paccagnella, T. (2011). Seven years of activity in the field of mesoscale ensemble forecasting by the cosmo-leps system : main achievements and open challenges. *Tellus A*, 63 :605—624.
- Montani, A., Marsigli, C., Nerozzi, F., Paccagnella, T., Tibaldi, S., et Buizza, R. (2003). The soverato flood in southern italy : performance of global and limited-area ensemble forecasts. *Nonlin. Proc. Geophys.*, 10 :261–274.
- Mureau, R., Molteni, F., et Palmer, T. (1993). Ensemble predicting using dynamically conditioned perturbations. *Q. J. Roy. Meteor. Soc.*, 119 :299–323.

- Nuissier, O., Ducrocq, V., Ricard, D., Lebeaupin, C., et Anquetin, S. (2008). A numerical study of three catastrophic precipitating events over southern france. i : Numerical framework and synoptic ingredients. *Quart. J. Roy. Meteor. Soc.*, 134 :111–130.
- Nuissier, O., Joly, B., Joly, A., Ducrocq, V., et Arbogast, P. (2011). A statistical downscaling to identify the large-scale circulation patterns associated with heavy precipitation events over southern france. *Quart. J. Roy. Meteor. Soc.*, 137 :1812—1827.
- Nuissier, O., Joly, B., Vié, B., et Ducrocq, V. (2012). Uncertainty of lateral boundary conditions in a convection-permitting ensemble : a strategy of selection for mediterranean heavy precipitation events. *Nat. Hazards Earth Syst. Sci.*, 12 :2993–3011.
- Nuissier, O., Rogers, R. F., et Roux, F. (2005). A numerical simulation of hurricane bret on 22–23 august 1999 initialized with airborne doppler radar and dropsonde data. *Quart. J. Roy. Meteor. Soc.*, 131 :155—194.
- Plaut, G., Schuepbach, E., et Doctor, M. (2001). Heavy precipitation events over a few alpine sub-regions and the links with large-scale circulation. *Clim. Res.*, 17 :285–302.
- Plaut, G. et Simonet, E. (2001). Large-scale circulation classification, weather regimes, and local climate over france, the alps and western europe. *Clim. Res.*, 17 :303–324.
- Quintana Segui, P., Ribes, A., Martin, E., Habets, F., et Boé, J. (2010). Comparison of three downscaling methods in simulating the impact of climate change on the hydrology of mediterranean basins. *J. Hydrometeorol.*, 383 :111–124.
- Ricard, D. (2002). *Initialisation et assimilation de données à méso-échelle pour la prévision à haute résolution des pluies intenses de la région Cévennes-Vivarais*. PhD thesis, Université Toulouse III Paul Sabatier.
- Romero, R., Doswell, C. I., et Ramis, C. (2000). Mesoscale numerical study of two cases of long-lived quasi-stationary convective systems over easter spain. *Mon. Wea. Rev.*, 128 :3731–3751.
- Roux, F., Chane-Ming, F., Lasserre-Bigorry, A., et Nuissier, O. (2004). Structure and evolution of intense tropical cyclone dina near la réunion on 22 january 2002 : Gb-evtd analysis of single doppler radar observations. *J. Atmos. Oceanic Technol.*, 21 :1501—1518.
- Somot, S., Sevault, F., Déqué, M., et Crépon, M. (2008). 21st century climate change scenario for the mediterranean using a coupled atmosphere-ocean regional climate model. *Global and Planetary change*, 63 :112–126.
- Sun, J. et Crook, N. (1997). Dynamical and microphysical retrieval from doppler radar observations using a cloud model and its adjoint. part i : Model development and simulated data experiments. *J. Atmos. Sci.*, 54 :1642–1661.
- Sun, J. et Crook, N. (1998). Dynamical and microphysical retrieval from doppler radar observations using a cloud model and its adjoint. part ii : Retrieval experiments of an observed florida convective storm. *J. Atmos. Sci.*, 55 :835–852.
- Toth, Z. et Kalnay, E. (1997). Ensemble forecasting at ncep and the breeding method. *Mon. Wea. Rev.*, 125 :3297–3319.
- Trapp, R., Robinson, E., Baldwin, M., Diffenbaugh, N., et Schedler, B. (2010). Regional climate of hazardous convective weather through high-resolution dynamical downscaling. *Clim. Dyn.*, 37 :677–688.
- Vautard, R. (1990). Multiple weather regimes over the north atlantic : Analysis of precursors and successors. *Mon. Wea. Rev.*, 118 :2056–2081.

- Vié, B., Nuissier, O., et Ducrocq, V. (2011). Cloud-resolving ensemble simulations of mediterranean heavy precipitating events : uncertainty on initial conditions and lateral boundary conditions. *Mon. Wea. Rev.*, 139 :403–423.
- Vincendon, B., Ducrocq, V., Nuissier, O., et Vié, B. (2011). Perturbation of convection-permitting nwp forecasts for flash-flood ensemble forecasting. *Nat. Hazards Earth Syst. Sci.*, 11 :1529–1544.
- Vié, B. (2012). *Méthodes de prévision d'ensemble pour l'étude de la prévisibilité à l'échelle convective des épisodes de pluies intenses en Méditerranée*. PhD thesis, Université Paris-Est.
- Vié, B., Molinié, G., Nuissier, O., Vincendon, B., Ducrocq, V., Bouttier, F., et Richard, E. (2012). Hydro-meteorological evaluation of a convection-permitting ensemble prediction system for mediterranean heavy precipitating events. *Nat. Hazards Earth Syst. Sci.*, 12 :2631–2645.
- Vrac, M., Stein, M., et Hayhoe, K. (2007). Statistical downscaling of precipitation through non-homogeneous stochastic weather typing. *Clim. Res.*, 34 :169–184.
- Weisman, M. L., Klemp, J. B., et Rotunno, R. (1988). Structure and evolution of numerically simulated squall lines. *J. Atmos. Sci.*, 45 :1990–2013.
- Wilby, R., Wigley, T., Conway, D., Jones, P., Hewitson, B., et Main, J., W. D. (1998). Statistical downscaling of general circulation model output : A comparison of methods. *Water Resour. Res.*, 34 :2995–3008.
- Xiao, Q., Zou, X., et Wang, B. (2000). Initialization and simulation of a landfalling hurricane using a variational bogus-data assimilation scheme. *Mon. Wea. Rev.*, 128 :2252–2269.